# Plasma-assisted ignition and combustion in pulverised fuel burners

Von der Fakultät Energie-, Verfahrens- und Biotechnik der Universität Stuttgart zur Erlangung der Würde eines Doktors der Ingenieurwissenschaften (Dr.-Ing.) genehmigte Abhandlung

Vorgelegt von

Reyhane Youssefi

aus Tehran

| | |
|---|---|
| Hauptberichter: | Univ.-Prof. Dr. techn. Günter Scheffknecht |
| Mitberichter: | Prof. Dr. Emmanuel Kakaras<br>National Technical University of Athens NTUA |

Tag der mündlichen Prüfung: 28.10.2022

Institut für Feuerungs- und Kraftwerkstechnik der Universität Stuttgart

2022

# Acknowledgement

This work has been performed from 2017 until 2021 during my employment as research scientist at the Institute of Combustion and Power Plant Technology (IFK) of University of Stuttgart. The main experimental investigations of this work were conducted in the frame of the research project FlexIgnite that received funding from the German Federal Ministry of Economic Affairs and Energy (03ET7076A). I acknowledge with appreciation FlexIgnite project partners, Lausitz Energie Kraftwerke AG, Mitsubishi Power Europe GmbH, PlasmaAir AG and the Institute of Interfacial Process Engineering and Plasma Technology (IGVP) of University of Stuttgart, Dr. Stefan Merli and Dr. Andreas Schulz, who supported the pilot-scale experimental campaigns by performing optical measurements.
For the CFD simulations performed within this work, I acknowledge that Ansys Student version is used. Permission is given by Ansys inc. as an exception.
I also would like to thank the Explosion Safety Group of Adinex N.V. for the bilateral cooperation on the determination of dust explosion characteristics, in particular, Frederik Norman and Tom Segers.
I express my deepest appreciation to Prof. Dr. techn. Günter Scheffknecht, for his supervision of this thesis and his support and advice during this work, as well as for creating the opportunity to perform research at IFK. My gratitude goes to Jörg Maier, the head of Firing System Department, for his guidance, inspiration, support and all the technical discussions.
I am grateful to my colleagues from the Firing System Department, Manoj Paneru, Simon Grathwohl, Thomas Matthies, Aaron Fuller, Ioannis Papandreou, Francisco Carrasco, Selahattin Babat, Timo Wagner, Cynthia Kroumian and Alexander Mack for their support in experimental campaigns, scientific publications and constructive discussions. I would also like to thank the students who supported me during this work, Mirza Hammad Baig, Patrick Reich, Sai Kiran Nunna, Pedro Kasmirski, Christopher Roth and Mohammad El Wajeh. I thank Wolfgang Ross and his colleagues in the Laboratory for Fuels and Ashes as well as the workshop and administrative teams of IFK.
I warmly thank my family, my mother Azar, my father Reza and my sister Ramina, which without their support and inspiration I could not stand here today. Special thanks to my supportive friend and colleague, Ida, for being the best companion during my time in IFK

and to Sepide, Pantea, Sahar and Niloufar who have been always supported me emotionally with their love and sympathy even from far distances. My greatest thank goes to my husband, Mohamad, who inspired me with his courage and patience within these years.

Stuttgart, November 2021
Reyhane Youssefi

# Contents

**Acknowledgement** **i**

**Contents** **iii**

**List of Figures** **vi**

**List of Tables** **ix**

**Nomenclature** **x**

**Abstract** **xvi**

**Kurzfassung** **xviii**

**1 Introduction** **1**

1.1 Energy system and the need for flexibility . . . . . 1

1.2 Motivation and objectives . . . . . 3

1.3 Approach and outline . . . . . 4

1.4 Previously published results . . . . . 5

**2 Background** **7**

2.1 Fundamentals of ignition and combustion in pulverised fuel (PF) systems . . 7

2.1.1 PF ignition and combustion . . . . . 7

2.1.1.1 $NO_x$ formation and reduction . . . . . 12

2.1.1.2 Assessment of ignitability and explosibility of dusts . . . . . 13

2.1.2 PF Flames in swirl burners . . . . . 18

2.2 Plasma-assisted ignition and combustion for PF systems . . . . . 25

2.2.1 Fundamentals and the application of plasma-assisted ignition and combustion . . . . . 25

2.2.2 Power plant flexibility and plasma-coal firing systems . . . . . 29

2.2.3 An overview of commercially available systems . . . . . 33

**3 Material and Method** **38**
3.1 Fuel properties . . . 38
3.1.1 Chemical properties . . . 38
3.1.2 Physical properties . . . 40
3.1.2.1 Particle size distributions of milled/sieved wood . . . 42
3.2 Lab-scale investigations of dust ignition characteristics . . . 43
3.2.1 Laboratory dust explosion tests . . . 43
3.2.1.1 Dust explosibility screening and determination of minimum ignition energy (MIE) . . . 43
3.2.1.2 Determination of minimum cloud ignition temperature (MCIT) 44
3.2.1.3 Determination of explosion characteristic parameters . . . 45
3.2.2 Ignitability characteristic number . . . 46
3.3 Pilot-scale experiments on the plasma ignition system . . . 47
3.3.1 400 kW combustion test facility . . . 47
3.3.2 Plasma-integrated swirl burner . . . 48
3.3.3 Atmospheric plasma torch . . . 52
3.3.4 Experimental procedures . . . 53
3.3.5 Measurement techniques . . . 55
3.3.5.1 Optical measurement . . . 55
3.3.5.2 Gas measurements . . . 56
3.3.6 Evaluation methods . . . 57
3.3.6.1 Combustion Class (CC) . . . 57
3.3.6.2 Combustion Degree (CD) and equivalent flue gas temperature 59
3.3.6.3 Flame brightness and fluctuation . . . 60
3.3.7 Isothermal CFD simulations . . . 61

**4 Investigations of solid fuel ignition characteristics** **62**
4.1 Explosibility and minimum ignition energy . . . 62
4.2 Minimum cloud ignition temperature . . . 63
4.3 Explosion characteristic parameters . . . 67
4.3.1 The rate of pressure rise . . . 67
4.3.2 Maximum explosion pressure . . . 68
4.3.3 Deflagration index . . . 69
4.4 Modified ignitability characteristic number . . . 71
4.5 Conclusion . . . 74

**5 Investigations of the plasma ignition system for cold start-ups** **75**
5.1 Interpretation of the ignition process and system validation . . . 75
5.1.1 Ignition and flame formation process in the plasma ignition system . 75

5.1.2 System validation . . . 77
5.2 Investigations of lignite qualities . . . 78
5.2.1 The effect of the thermal load and air ratio on the ignition behaviour 79
5.2.2 The effect of the thermal load and air ratio on the combustion behaviour 81
5.2.3 Characterisation of the performance of lignites in the plasma ignition system . . . 86
5.3 The role of the plasma torch . . . 89
5.3.1 The effect of the plasma power . . . 89
5.3.2 The effect of the plasma system . . . 95
5.4 Investigations of the burner design and aerodynamics . . . 100
5.4.1 The effect of swirling . . . 100
5.4.1.1 The effect of secondary air swirling . . . 101
5.4.1.2 The effect of primary air swirling at different plasma positions 102
5.4.2 The effect of the plasma position . . . 111
5.4.3 The effect of the primary air nozzle design . . . 118
5.4.4 The effect of the primary air velocity . . . 121
5.5 Investigations of the influence of particle size using milled wood pellet . . . 122
5.5.1 Ignition boundary conditions . . . 123
5.5.2 Ignition and combustion behaviour . . . 124
5.6 Theoretical and experimental considerations on plasma-assisted ignition . . . 128
5.6.1 Correlation to fuel properties . . . 128
5.6.2 Correlation to ignitability parameters . . . 131
5.7 Some remarks on burner design parameters . . . 132

**6 Investigations of plasma-assisted combustion during part-load operation 135**
6.1 Part-load operation with plasma-assisted combustion . . . 135
6.1.1 In-flame measurements . . . 135
6.1.2 Flue gas emissions . . . 140
6.2 The impact of the plasma position on plasma-assisted combustion . . . 142
6.3 The impact of the air ratio on plasma-assisted combustion . . . 144

**7 Conclusion and outlook 148**

**References 155**

# List of Figures


2.1 Parameters related to ignition in swirl burners . . . . . 23
2.2 Sketch of the Plasma-Fuel System . . . . . 34

3.1 Cumulative volumetric particle size distribution . . . . . 40
3.2 Cumulative gravimetric particle size distribution for sieved and mixed wood pellets . . . . . 42
3.3 Schematic diagram of the 400 kW combustion facility . . . . . 47
3.4 Cross section view of the plasma-integrated swirl burner . . . . . 49
3.5 Primary air nozzle design . . . . . 49
3.6 Cross section view of the movable block swirl generator . . . . . 50
3.7 Spectral emissions of the plasma systems PS I and PS II . . . . . 53
3.8 The procedure of the cold start-up with plasma-assisted ignition . . . . . 54
3.9 The mean brightness profile over time . . . . . 56
3.10 Mean brightness profile for different CC values . . . . . 58

4.1 MCIT of lignite qualities in ascending order . . . . . 64
4.2 The rate of pressure rise versus equivalence ratio . . . . . 67
4.3 Explosion pressure versus equivalence ratio . . . . . 68
4.4 $K_{st}$-value in descending order . . . . . 69
4.5 Devolatilisation degree and ignition potential of lignites, hard coal and biomass 72
4.6 The modified ignitability characteristic number in descending order . . . . . 73

5.1 Ignition and flame formation with Lignite B with plasma-assisted ignition . . 76
5.2 CC versus air ratio for Lignite A and WP 2 . . . . . 77
5.3 CC versus air ratio for Lignite B, Lignite C and Lignite D at different thermal loads . . . . . 79
5.4 CC versus air ratio for Lignite E, Lignite F, Lignite G and Lignite H at different thermal loads . . . . . 81
5.5 CD and equivalent flue gas temperature versus air ratio for Lignite B at different thermal loads . . . . . 82

5.6 CD and equivalent flue gas temperature versus air ratio for Lignite C at different thermal loads . . . . . 83
5.7 CD and equivalent flue gas temperature versus air ratio for Lignite D at different thermal loads . . . . . 84
5.8 CD versus air ratio for Lignite E, Lignite F, Lignite G and Lignite H at different thermal loads . . . . . 86
5.9 CC and CD for Lignite B with 4.2 kW and 7 kW plasma power . . . . . 90
5.10 CC and CD for Lignite C and Lignite D with 4.2 kW and 7 kW plasma power 91
5.11 CC and CD for Lignite E with 4.2 kW and 7 kW plasma power . . . . . 92
5.12 CC for Lignite G with 4.2 kW and 7 kW plasma power . . . . . 92
5.13 Flame brightness and brightness fluctuation for Lignite B, Lignite C and Lignite D with 4.2 kW and 7 kW plasma power . . . . . 94
5.14 CC and CD for Lignite D with PS I and PS II . . . . . 96
5.15 CC and CD for Lignite E with PS I and PS II . . . . . 97
5.16 CC for Lignite G and Lignite H with PS I and PS II . . . . . 97
5.17 Flame brightness and brightness fluctuation for Lignite D and Lignite E with PS I and PS II . . . . . 98
5.18 CC and CD for Lignite D versus secondary air swirl number . . . . . 102
5.19 Axial velocity fields for swirling and non-swirling primary air at different plasma positions . . . . . 103
5.20 Particle trajectories for the swirling and non-swirling primary air at different plasma positions . . . . . 105
5.21 CC, CD, flame brightness and brightness fluctuation for swirling and non-swirling primary air with Lignite B at 25 % thermal load . . . . . 107
5.22 CC, CD, flame brightness and brightness fluctuation for swirling and non-swirling primary air with Lignite B at 38 % thermal load . . . . . 109
5.23 Flame shape with swirling and non-swirling primary air . . . . . 110
5.24 CC and CD for Lignite B, Lignite D and Lignite E at plasma positions 0 and -40 . . . . . 112
5.25 CC for Lignite G at plasma positions 0 and -40 . . . . . 113
5.26 Flame brightness and brightness fluctuation for Lignite B, Lignite D and Lignite E at plasma positions 0 and -40 . . . . . 115
5.27 Flame evolution at positions 0 and -40 for Lignite B, Lignite D and Lignite E 117
5.28 The comparison of Nozzle 1 and Nozzle 2 for Lignite E . . . . . 119
5.29 The comparison of Nozzle 1 and Nozzle 3 for Lignite B . . . . . 120
5.30 CC and CD for WP 1 for high and low primary air velocities . . . . . 121
5.31 CC for Lignite G with high and low primary air velocities . . . . . 122
5.32 CC and CD for different WP size distributions at the air ratio of 0.5 and 0.7 125

5.33 CC and CD for different WP size distributions at the air ratio of 0.9 and 1.1 126
5.34 The correlation of fuel properties to the ignition performance . . . . . 129
5.35 Modified ignitability characteristic number and deflagration index versus median particle size . . . . . 132

6.1 In-flame measurement of temperature and $O_2$ at several thermal loads . . . . 136
6.2 In-flame measurement of $NO_x$ and CO at several thermal loads . . . . . 139
6.3 The average $O_2$ volume fraction in furnace end flue gas at several thermal loads 141
6.4 Emissions of $NO_x$ and CO at several thermal loads . . . . . 141
6.5 In-flame measurement of temperature and $O_2$ at plasma positions 0 and -40 . 143
6.6 In-flame measurement of $NO_x$ and CO at plasma positions 0 and -40 . . . . 143
6.7 In-flame measurement of temperature and $O_2$ at different burner air ratios . 145
6.8 In-flame measurement of $NO_x$ and CO versus burner air ratio . . . . . 145
6.9 Emissions of NOx and CO versus burner air ratio . . . . . 146

# List of Tables


3.1 Chemical analysis of fuels . . . . . 39
3.2 Physical properties . . . . . 41
3.3 Characteristic particle sizes and cumulative gravimetric distribution of individual fractions . . . . . 43
3.4 Theoretical swirl numbers of the movable block swirler . . . . . 51
3.5 Operational parameters of plasma systems . . . . . 52
3.6 Technical details of the gas analysers . . . . . 56
3.7 Definition of Combustion Classes . . . . . 57

4.1 Explosibility of dust . . . . . 62
4.2 Minimum ignition energy . . . . . 63
4.3 Minimum cloud ignition temperature . . . . . 66
4.4 $K_{\mathrm{st}}$-value and $ZWZ_{\mathrm{mod.}}$ of different fuel types . . . . . 70

5.1 Ignition boundary conditions for different milled wood particle size distributions 123
5.2 Burner parameters . . . . . 134

6.1 Furnace wall temperature at 33 cm from the burner during part-load operation 137

# Nomenclature

## List of Acronyms

| Acronym | Definition |
|---|---|
| af | As fired |
| CC | Combustion Class |
| CD | Combustion Degree |
| CFD | Computational fluid dynamics |
| CTRZ | Central toroidal recirculation zone |
| FD | Forced draught |
| H | Hard coal |
| IFRF | International Flame Research Foundation |
| ID | Induced draught |
| LEAG | Lausitz Energie Power Plant AG |
| L-A | Lignite A |
| L-B | Lignite B |
| L-C | Lignite C |
| L-D | Lignite D |
| L-E | Lignite E |
| L-F | Lignite F |
| L-G | Lignite G |
| L-H | Lignite H |
| MIE | Minimum ignition energy |
| MCIT | Minimum cloud ignition temperature |
| PS I | Plasma system I |
| PS II | Plasma system II |
| PSD | Particle size distribution |
| PF | Pulverised fuel |

(continued)

| Acronym | Definition |
|---|---|
| PFS | Plasma-Fuel System |
| PICS | Plasma Ignition and Combustion Stabilising System |
| SOFIS-PIT | Solid Fuel Ignition and Combustion Stabilisation System with Plasma at Intermediary Temperature Support |
| STP | Standard temperature and pressure (273.15 K and 101 325 Pa) |
| TL | Thermal load |
| WP | Wood pellet |

# List of symbols

| Symbol | Unit | Definition |
|---|---|---|
| $a$ | $m^2/g$ | Specific surface area |
| $\alpha$ | ° | Vane angle of the axial vane swirler |
| $\alpha$ | ° | Inclination angle of the block surface in the movable-block swirler |
| $B$ | m | The width of the channels in the movable-block swirler |
| $B$ | % | Flame brightness |
| $B_i$ | - | Grey level of pixel $i$ |
| $B_t$ | - | Mean brightness of an image at the time $t$ |
| $\bar{B}$ | - | Average flame brightness |
| $B_{\text{fl.}}$ | % | Brightness fluctuation |
| $c_i$ | $mg/m^3$ | Mass concentration of the constituent $i$ |
| $\bar{c}_{p,\text{G}}$ | kJ/kg K | Integral specific heat capacity of the flue gas based on 0 °C |
| $dp/dt$ | bar/s | Maximum rate of pressure rise over the pressure time history |
| $(dp/dt)_{\max}$ | bar/s | Maximum rate of pressure rise over the entire tested concentrations |
| $DL$ | kg/kg | Dust loading (the ratio of fuel to the primary air) |
| $DL_i$ | g/kg | Dust loading of the particle sizes below $i$ |
| $D10$ | µm | The particle diameter at which 10 % of the cumulative distribution has a smaller particle size |
| $D50$ | µm | The particle diameter at which 50 % of the cumulative distribution has a smaller particle size (median particle size) |
| $D90$ | µm | The particle diameter at which 90 % of the cumulative distribution has a smaller particle size |
| $\eta$ | % | Combustion Degree |
| $\eta_{\text{devol}}$ | % | Devolatilisation degree |
| $\vartheta$ | °C | Equivalent flue gas temperature |
| $E$ | V | Voltage |
| $\gamma_i$ | kg/kg | Mass fraction of the substance $i$ in fuel |

(continued)

| Symbol | Unit | Definition |
|---|---|---|
| $\gamma_{i,\mathrm{ch}}$ | kg/kg | Mass fraction of the substance $i$ in char after devolatilisation |
| $G_x$ | $\mathrm{kg\,m/s^2}$ | Axial flux of the axial momentum |
| $G_\phi$ | $\mathrm{kg\,m^2/s^2}$ | Axial flux of the tangential momentum |
| $h_{\mathrm{LT}}$ | kJ/kg | Specific enthalpy of the dry combustion air |
| $H_u$ | MJ/kg | Net calorific value |
| $I$ | A | Electric current |
| $K_{\mathrm{st}}$-value | $\mathrm{bar\,m/s}$ | Deflagration index |
| $\mu_{\mathrm{G}}$ | kg/kg | Specific wet amount of flue gas with respect to fuel mass |
| $\mu_{\mathrm{LT}}$ | kg/kg | Specific dry combustion air amount with respect to the fuel mass |
| $\mu_{\mathrm{LoT}}$ | kg/kg | Specific dry combustion air amount for the stoichiometric condition with respect to the fuel mass |
| $\dot{M}_{\mathrm{f}}$ | kg/s | Mass flow rate of fuel |
| $n$ | - | Air ratio (ratio of the actual combustion air amount to the stoichiometric combustion air amount ) |
| $n$ | - | Equivalence ratio (ratio of the actual dust concentration to the stoichiometric dust concentration) |
| $n_{\mathrm{VM}}$ | - | Air ratio with respect to the volatile matter |
| $n_{\mathrm{PA}}$ | - | Air ratio with respect to the primary air |
| $n_{\mathrm{PA,VM}}$ | - | Air ratio with respect to volatile matter in the primary air |
| $n$ | - | Number of fixed and movable blocks |
| $N$ | - | Number of images |
| $N_{\mathrm{Z500}}$ | MJ/kg | Ignition potential with respect to dried fuel |
| $N_{\mathrm{Z500,\,af}}$ | MJ/kg | Ignition potential with respect to as fired fuel |
| $NCV_{\mathrm{VM}}$ | MJ/kg | Net calorific value of released volatile matter |
| $P_{\mathrm{el.}}$ | kW | Electric power consumption of the plasma system |
| $p_{\mathrm{m}}$ | bar | Maximum explosion pressure over the pressure time history |
| $p_{\mathrm{max}}$ | bar | Maximum explosion pressure over the entire tested concentrations |
| $Q_i$ | % | Cumulative particle size distribution at the particle size of $i$ |

(continued)

| Symbol | Unit | Definition |
|---|---|---|
| $Q_{63}$ | % | The cumulative distribution of particles smaller than 63 µm |
| $Q_{90}$ | % | The cumulative distribution of particles smaller than 90 µm |
| $Q_{200}$ | % | The cumulative distribution of particles smaller than 200 µm |
| $Q_{500}$ | % | The cumulative distribution of particles smaller than 500 µm |
| $R$ | m | Primary air tube radius |
| $R$ | m | Outer radius of the secondary air annulus |
| $R$ | - | The ratio of primary air momentum to secondary air momentum |
| $R_h$ | m | Vane hub radius of the axial vane swirler |
| $R_h$ | m | Inner radius of the secondary air annulus |
| $Re$ | - | Reynolds number |
| $\sigma$ | - | Coefficient of the movable-block swirl generator |
| $S$ | - | Swirl number |
| $t$ | s | Time |
| $V$ | m3 | Volume of the explosion chamber |
| $\dot{V}$ | $m^3/h$ $(STP)$ | Volume flow rate at standard temperature and pressure |
| $\xi$ | ° | The aperture angle of the tangential channel in the movable-block swirler |
| $\xi_m$ | ° | The maximum aperture angle of the tangential channel in the movable-block swirler |
| $w_{\mathrm{PA}}$ | m/s | Velocity of the primary air |
| $w_{\mathrm{PG}}$ | m/s | Velocity of the plasma gas |
| $w_{\mathrm{SA}}$ | m/s | Velocity of the secondary air |
| $x$ | µm | Particle size |
| $y_i$ | $m^3/m^3$ | Volume fraction of the constituent $i$ |
| $ZWZ$ | kJ/kg °C | Ignitability characteristic number |
| $ZWZ_{\mathrm{mod.}}$ | kJ/kg °C | Modified ignitability characteristic number |

# List of indices

| Index | Definition |
|---|---|
| A | Referring to ash |
| C | Referring to carbon |
| $C_{fix}$ | Referring to fixed carbon |
| ch | Referring to the remaining char after devolatilisation |
| CO | Referring to carbon monoxide |
| el. | Referring to electrical power |
| f | Referring to fuel |
| H | Referring to hydrogen |
| $H_2O$ | Referring to moisture in fuel |
| N | Referring to nitrogen |
| $NO_x$ | Referring to nitrogen oxides (NO and $NO_2$) |
| O | Referring to oxygen |
| S | Referring to sulphur |
| VM | Referring to volatile matter |

# Abstract

This work focuses on the application of plasma-assisted ignition and combustion in pulverised fuel burners. Plasma-assisted ignition of pulverised fuel as an alternative technology for the start-up of pulverised fuel furnaces is investigated in a 400 kW pilot-scale facility using various qualities of lignite as well as woody biomass with distinct ignition characteristics. Short-time plasma-supported ignition under the cold furnace condition was demonstrated with parametric studies regarding the required power of plasma torch, air swirling, torch positioning, particle size distribution, etc. to identify the influence of different burner design parameters. The knowledge and experience obtained during this work are expected to support the development of such systems under the condition that plasma is only used as an ignition source rather than a continuous flame stabilisation method. Experiments are also performed to investigate the potential of plasma-assisted combustion during part-load and low-load operation.

Analyses on the fuel ignition characteristics showed that the ignitability characteristic number and deflagration index represent the most pronounced influence regarding the fuel properties and could be related to the ignition performance of fuels observed in the pilot-scale experiments, to a good extent. Plasma-assisted ignition tests showed that lignites with a moisture content up to 15 % form attached self-sustained flames under cold burner conditions with short-time plasma assistance and an increase in the moisture content up to around 20 % does not hinder the formation of this self-sustained flame, though flame lift-off was observed and the operational range, e.g. the burner load and air ratio, was restricted. These lignite qualities all had a median particle size of below 450 µm and an ash content lower than 12 %. Lignites with a median diameter above 500 µm were also ignited with the used 4.2 kW to 7 kW plasma torch but did not form a self-sustained flame in the absence of plasma.

Variations in the ignition boundary conditions, i.e. burner parameters, displayed more prominent effects on the fuels with lower ignitability. Increasing the plasma power expanded the ignition limit, mostly for the less ignitable fuels, where ignition was accomplished over a broader range of operational parameters, though no improvement was observed with respect to the formation of self-sustained flame. Moreover, comparisons between two plasma systems, differing mainly in the size of the plasma jet, suggested that the extent of plasma-

particle contact plays a significant role in ignition initiation.
Parametric studies also highlighted the importance of the secondary air swirling not only for flame stabilisation but also the ignition initiation. Swirling of the primary air showed a detrimental effect on ignition and flame stability when the plasma torch was retracted from the burner head inside the primary air annulus. On the contrary, plasma retraction showed promising results in the case of non-swirling primary air owing to a reduced velocity at the burner outlet and improved plasma-particle contact.
Plasma-assisted combustion during part-load operation showed slight improvements in combustion performance up to 50 % thermal load. Further reductions in the load deteriorated the combustion behaviour due to excessive heat loss and possibly improper burner aerodynamics, where plasma-assisted combustion could not contribute in a notable enhancement. Although an increase in CO and $NO_x$ concentrations was observed close to the burner zone at low thermal loads, e.g. thermal load of 38 %, flue gas $NO_x$ emission was even slightly reduced by decreasing the thermal load. Plasma-assisted combustion was also associated with higher $NO_x$ emissions compared with standard combustion, due to thermal NO formation by high-temperature plasma. This incremented $NO_x$ level was overcome successfully with the air-staging technique, where similar $NO_x$ levels were obtained for plasma-assisted combustion and normal combustion with a burner air ratio of 0.8 and 1.2, respectively.

# Kurzfassung

Diese Arbeit konzentriert sich auf die Anwendung der plasmaunterstützten Zündung und Verbrennung in Staubbrennern. Die plasmaunterstützte Zündung von staubförmigem Brennstoff als alternative Technologie zum Anfahren von staubgefeuerten Kraftwerken wird in einer 400 kW Pilotanlage unter Verwendung verschiedener Qualitäten von Braunkohle sowie holzartiger Biomasse mit unterschiedlichen Zündeigenschaften untersucht. Die kurzzeitige plasmaunterstützte Zündung unter kalten Kesselbedingungen wird anhand von Parameterstudien bezüglich der erforderlichen Leistung des Plasmabrenners, des Luftdralls, der Plasmabrennerpositionierung, der Partikelgrößenverteilung usw. demonstriert, um den Einfluss verschiedener Brennerparameter zu identifizieren. Die während dieser Arbeit gewonnenen Erkenntnisse und Erfahrungen sollen die Entwicklung solcher Systeme unterstützen, bei denen Plasma nur als Zündquelle und nicht als kontinuierliche Flammenstabilisierungsmethode verwendet wird. Darüber hinaus werden Versuche durchgeführt, um das Potenzial der plasmaunterstützten Verbrennung im Teillast- und Mindeslastbetrieb zu untersuchen.
Untersuchungen der Zündeigenschaften von Brennstoffen zeigen, dass die Zündwilligkeitskennzahl und der Deflagrationsindex den stärksten Einfluss auf die Brennstoffeigenschaften zeigen und in gutem Maße mit dem in den Pilotversuchen beobachteten Zündverhalten von Brennstoffen übereinstimmen. Die plasmaunterstützten Zündversuche haben gezeigt, dass Braunkohlequalitäten mit einem Wassergehalt bis zu 15 % unter kalten Kesselbedingungen mit kurzzeitiger Plasmaunterstützung und 4.2 kW Leistung eine Flamme am Brennermund bilden. Eine Erhöhung des Wassergehalts auf etwa 20 % behindert nicht die Bildung dieser selbsterhaltenden Flamme, obwohl ein Abheben der Flamme beobachtet wurde und der Betriebsbereich, bzw. die Brennerlast und die Luftzahl begrenzt wurde. Diese Braunkohlequalitäten hatten alle eine mittlere Korngröße von unter 450 µm und einen Aschegehalt von unter 12 %. Braunkohlequalitäten mit einer mittleren Korngröße größer als 500 µm wurden mit einem Plasmabrenner mit bis zu 7 kW Leistung gezündet, bildeten aber keine selbsterhaltende Flamme ohne Plasmaunterstützung.
Die Variation der Zündrandbedingungen, d. h. der Brennerparameter, hatten einen stärkeren Einfluss auf die Brennstoffe mit geringerer Zündfähigkeit. Eine Erhöhung der Plasmaleistung erweiterte die Zündgrenze, vor allem bei den weniger zündfähigen Brennstoffen, wo die

Zündung über einen breiteren Bereich von Betriebsparametern durchgeführt wurde, obwohl keine Verbesserung bezüglich der Bildung von selbsterhaltenden Flammen beobachtet wurde. Darüber hinaus legten Vergleiche zwischen zwei Plasmasystemen, die sich hauptsächlich in der Größe der Plasmaflamme unterscheiden, nahe, dass das Ausmaß des Plasma-Partikel-Kontakts eine bedeutende Rolle bei der Zündung spielt.
Parameterstudien haben auch die Bedeutung des Sekundärluftdralls bekräftigt, und zwar nicht nur für die Flammenstabilisierung, sondern auch für die Zündung. Ein Drall der Primärluft zeigte eine nachteilige Wirkung auf die Zündung und die Flammenstabilität, wenn der Plasmabrenner vom Brennerkopf in den Primärluftring zurückgezogen wurde. Im Gegensatz dazu zeigte der Rückzug des Plasmabrenners bei drallfreier Primärluft aufgrund einer reduzierten Geschwindigkeit am Brenneraustritt und eines verbesserten Plasma-Partikel-Kontaktes vielversprechende Ergebnisse.
Die plasmaunterstützte Verbrennung im Teillastbetrieb zeigte eine leichte Verbesserung des Verbrennungsverhaltens bis zum Erreichen von 50 % Teillast. Bei weiterer Verringerung der Last verschlechterte sich das Verbrennungsverhalten aufgrund von übermäßigem Wärmeverlust und möglicherweise ungeeigneter Brenneraerodynamik, dabei konnte auch die plasmaunterstützte Verbrennung nicht zu einer bemerkenswerten Verbesserung beitragen. Obwohl es einen Anstieg der CO und $NO_x$-Emissionen in der Nähe der Brennerzone bei niedriger Last gab, z. B. Teillast von 38 %, wurden die Emissionen des Rauchgases durch die Verringerung der Last sogar leicht reduziert. Aufgrund der thermischen NO-Bildung durch Hochtemperaturplasma war die plasmaunterstützte Verbrennung, im Vergleich zur Standardverbrennung, mit höheren $NO_x$-Emissionen verbunden. Dieses erhöhte $NO_x$-Niveau wurde mit der gestuften Verbrennung erfolgreich überwunden, wo ähnliche $NO_x$-Niveaus bei der plasmaunterstützten Verbrennung wie bei der normalen Verbrennung mit einer brennernahen Luftzahl von 0,8 bzw. 1,2 erreicht wurden.

# 1 Introduction

## 1.1 Energy system and the need for flexibility

To reach the ambitious emission targets of the 1.5 °C scenario [1], new strategies and frameworks have been introduced by the involved countries. This has led to a dramatic growth in the renewable energy production and a considerable reduction in fossil fuel-related $CO_2$ emissions. The European Green Deal promotes the EU's climate ambition to reach climate neutrality by 2050 and sets the goal for 2030 to cut the greenhouse gas emissions by 55 % compared with the values from 1990 [2]. A further increase in the share of renewable energy sources is foreseen to meet these climate objectives [3]. In Germany, the electricity production by renewable sources from around 40 % in 2021 is targeted to reach 100 % by 2050 [4, 5]. The major share of renewable energy is supplied by intermittent wind and solar power. Due to the high volatility of $CO_2$-free renewable energies, the thermal power plants are still responsible to respond to the fluctuating power supply and demand. Providing this residual load has changed the operational regimes of these thermal power plants that were originally designed for base-load operation and are now subjected to more frequent load changes and eventually an increasing number of start-ups and shutdowns. This is associated with higher operational costs, hampering the overall plant efficiency and a reduced lifetime [6]. To alleviate these drawbacks, the power plants need to be operated with higher flexibility, where cost- and energy-efficient solutions are required. The flexible operation of thermal power plants, in particular pulverised fuel firing plants, is mainly limited by the minimum technical load and the start-up process. Beside the losses that a plant suffers from each shutdown and start-up, increased expenses of the start-up process are largely related to the costly start-up fuels, e.g. natural gas and fuel oil. Alternative start-up methods can to a certain extent compensate for the reduced efficiency and can increase the overall flexibility of the plant [6, 7].

Electrical ignition systems using plasma for the start-up have recently drawn special attention, in which pulverised fuel particles are directly ignited with the support of a plasma jet. Within this scenario, the oil and gas as start-up fuels are completely or partially removed

and instead the inexpensive pulverised fuel is used.
This is not only related to the coal-fired power plants but also the growing biomass-fired plants. With a view towards long-term climate objectives, biomass as a sustainable solid fuel, has high potentials to contribute to the supply of the residual load. The retrofitting of existing coal-fired stations to co-combustion plants and even further to 100 % biomass-fired plants will promote a more efficient energy transition. The utilization of existing infrastructures provides a cost-effective solution with a short-time deployment prospect [8]. Similar to the current situation of coal power stations regarding the flexibility, future biomass-fired plants need to ensure flexible operation. The increasing trend of the power production using intermittent sources of energy in the past few years has highlighted the necessity of a highly flexible and $CO_2$-neutral residual load supplier in the near future, to balance out the fluctuations [9]. Even for the existing coal-fired plants, biomass can be used as the start-up fuel, where the cost and concurrently the $CO_2$ emissions during start-ups are minimized.
Plasma-assisted ignition and combustion of coal has been implemented in several power plants in Russia, China, Kazakhstan and other countries in Asia and the Middle East, where inefficient combustion related to low-quality fuels and the reduction in the cost of start-ups were the driving forces [10–13]. The technology has been used for fuel ignition and combustion during the plant start-up as well as for supporting firing during the low-load operation. As the need for plant flexibility has emerged in Europe, plasma-assisted solid fuel ignition has drawn great attention. The prosperity of a highly flexible start-up process motivates the plant operators to consider the possibility of such modifications. The technology of plasma-assisted ignition and combustion for solid fuels needs to be adopted for each plant depending on the plant's requirements and fuel characteristics. The application of this technology under certain start-up conditions, cold, warm or hot start-ups, differs in system boundaries which necessitates detailed investigations on the burner optimization depending on the target fuel. Under warm and hot start-up conditions, where an adequate amount of heat is available inside the plant, the selectivity of fuel for plasma ignition becomes less significant. Nevertheless, for a cold start-up, the fuel ignition potentials are of high interest and play the main role in the burner design.
Although this technology brings economic benefits, the operational limitations can curb its implementation. The lifetime of the plasma system and its scalability parameters may lower the system's robustness and the availability. For an optimized operation, it is highly strived to minimize the operation time and costs of the plasma system. Considering the minimized plasma power and the operation time, up to present, pre-dried lignite dust has been successfully used for cold start-ups, where only 20 s plasma-assisted combustion was sufficient to stabilize the lignite flame. However, implementation of the system with lower quality fuels did not show satisfactory results [14–16].
There is a lack of sufficient investigations to identify the underlying parameters and the suit-

able fuel qualities for this application. Hence, there is an incentive to study the potentials of different fuel qualities and the critical parameters for the application of plasma-assisted ignition and combustion.

## 1.2 Motivation and objectives

The development of plasma-assisted ignition and combustion of solid fuels have been so far mostly focused on prolonged plasma assistance during the start-up and implementing relatively high plasma powers to treat a large amount of the solid fuel stream to initiate the ignition [10–13]. Using fuels with high ignitability has shown promising results to reduce the plasma support time for ignition below to few seconds and concurrently lowering the required plasma power [14–16]. The latter scenario reduces the capital and operational costs and concurrently improves the system robustness significantly.
For the above-introduced concept with short-time plasma support under extreme ignition conditions, i.e. the cold start-up, not much information is available with respect to the fuel properties and the burner design. There is a lack of experimental studies on the effect of operational parameters and the required boundary conditions for various fuel qualities. A better understanding of the plasma-assisted ignition and combustion process supports the technology providers for the design and development of such burner systems. This dissertation aims to investigate plasma-assisted ignition and combustion of pulverised fuel for industrial burners with the following objectives:

- Analysis of the ignition properties of dedicated fuel qualities
- Testing the applicability of plasma-assisted ignition for cold start-ups using different lignite qualities
- Investigating individual burner design parameters and fuel properties for ignition and the flame formation under the cold start-up condition with a focus on
  - Plasma torch power and system
  - Primary air and secondary air swirling
  - Plasma torch positioning
  - Primary air nozzle and velocity
  - Particle size distribution for a high volatile fuel

- Correlating the fuel ignitability to its performance in the developed system
- Assessing the impact of plasma-assisted combustion on the combustion and emissions behaviour during part-load operation

## 1.3 Approach and outline

The dissertation is formulated in seven chapters. Chapter 1 and chapter 7 are dedicated to the **Introduction** and **Conclusion** of the work, respectively.
Chapter 2 on **Background** is divided into two parts. The first part reviews the fundamentals of ignition and combustion of pulverised fuel, in particular in swirl burners, as well as the parameters evaluating the fuel ignitability. The second part focuses on the research and commercials activities related to the plasma-assisted ignition and combustion system and its role in increasing the power plant flexibility.
Chapter 3, **Material and Method**, first reports the characteristics and properties of the investigated fuel qualities and then describes the test equipment and facilities, measurement devices, the test procedures and evaluation approaches. The methodology of this work consists of the lab-scale investigations of the fuel ignitability and the pilot-scale investigations of plasma-assisted ignition and combustion, where the main focus of the work is concentrated on the latter.
Chapter 4, **Investigations of solid fuel ignition characteristics**, explains the results of the lab-scale tests on fuel ignition properties with dedicated fuel qualities. This assessment includes determination of dust explosibility, the minimum ignition energy, the minimum ignition temperature, explosion characteristic parameters (explosion pressure and the rate of pressure rise) and the ignitability characteristic number. For selected parameters, the behaviours are discussed in correlation with the fuel properties such as the moisture content, the volatile content, the ash content and the median particle size. Finally, among the investigated parameters the ones that represent the fuel ignitability to a better degree, are identified to be correlated to the fuel performance in pilot-scale experiments in Chapter 5.
The main objectives of this work are focused on the experimental investigations performed in Chapter 5 with the title of **Investigations of the plasma ignition system for cold start-ups**. The chapter is divided into five sections. First, the developed plasma ignition system is validated using two high-quality fuels (pre-dried lignite and pulverised wood pellet) and the ignition process with plasma is explained with more details to provide a better understanding of the ignition and flame formation and stabilisation process in the system. Second, seven lignite qualities are tested in the plasma ignition system over several burner

thermal loads and air ratios to evaluate the ignition behaviour and self-sustained flame formation, where eventually the fuels are categorized into different groups according to their performance. Third, the role of the plasma torch on ignition and flame formation is examined using a higher plasma power of 7 kW, compared with the reference power of 4.2 kW, and also a second plasma system. Next, parametric studies are performed to analyse the role of burner design parameters related to the flow and particle profiles. These studies include swirling of the primary air and secondary air, the plasma torch positioning, the primary air nozzle design and the primary air velocity. Afterwards, the influence of particle size distribution of milled wood pellets is studied to determine the fineness required for ignition and flame formation under cold start-up conditions. Finally, the performance of the investigated fuels is correlated to their properties as well as to the lab-scale ignition characteristic parameters from chapter 4 to identify the suitable fuel qualities for the application of plasma ignition system and to evaluate if these ignition parameters can be used as indicative criteria to predict the fuel potential for this application. The optimized system parameters with respect to the performed studies are then summarized for future design considerations.
Chapter 6, **Investigations of plasma-assisted combustion during part-load operation**, explores the impact of part-load operation on the combustion and emissions behaviour of one hard coal and aims to determine to what extent the plasma-assisted combustion influences the combustion process and the emissions formation during part-load operation. Further experiments are performed to investigate the influence of plasma position and the air ratio during plasma-assisted combustion at part-load operation.

## 1.4 Previously published results

Parts of the results presented in this dissertation have been published in several conferences and journals during the course of this work. Some of the experimental data that have been published previously may deviate slightly from the ones reported here, as those experimental data have been re-evaluated to ensure the accuracy and consistency between all the results presented here. A part of the results in section 5.4.1.2 on the influence of primary air swirling at different plasma positions is incorporated in this work from a conference paper [17]. Some of the results of the pilot-scale investigation on one fuel quality (Lignite D) were published in a conference proceeding [18]. Moreover, the experimental results related to one wood pellet quality (WP 1) from the previous publications [19, 20] are included here. Another publication in which the author of this dissertation was involved as a co-author [21] is not directly discussed here but it is referenced in section 4.3.3. Parts of the texts in Material and Method chapter as well as Introduction and Background chapters were obtained from

these conference publications that were submitted by the author of this dissertation [18–20]. It should be highlighted that the results presented in the above-mentioned publications were re-plotted in this work. Parts of the text and results in sections 4.2, 4.3, 4.4, 5.1.2, 5.2 and 5.6 are embedded in this dissertation from two research papers, published by the author as the main author [22, 23].

Furthermore, several master theses and student research projects were carried out in the frame of this work under the direct supervision of the author [24–27]. The students supported the execution of experiments and simulations and contributed to data analysis. However, the data that were derived from those theses were re-analysed and re-evaluated by the author of this dissertation.

# 2 Background

## 2.1 Fundamentals of ignition and combustion in pulverised fuel (PF) systems

### 2.1.1 PF ignition and combustion

Among different firing systems, pulverised fuel firing has been widely implemented in steam power plants. In the PF system, finely milled solid fuel, i.e. coal, lignite and biomass, are transported with the primary air and are mixed with the combustion air at the burner outlet, inside the furnace. In large PF furnaces, the coal particles are heated with a considerably high heating rate of ($10^4$ to $10^6$) K/s via convection and radiation. The particles undergo several processes from drying to ignition and combustion of volatiles and the residual char [28]. Each step and its influencing parameters are explained in detail as follows.

**Drying:** Water in coal exists in different forms as surface-bound water, hygroscopic-bound water in large pores and capillary-bound water in small pores. The fuel particles are partially dried during the milling process, where the water in the large pores and surface-bound water is first released. The rest of water is evaporated in the furnace, as the particle temperature exceeds 100 °C. The drying time in the furnace depends on the heating rate, the fuel moisture content and the particle size [29].

**Devolatilisation (pyrolysis):** At temperatures above approximately 300 °C, a part of organic compounds, i.e. volatile matter, are decomposed and are released in the form of light gaseous products, tars (condensible hydrocarbons) and pyrolysis water. The degree of devolatilisation, volatile yield and the product composition are related to the devolatilisation temperature, the fuel type, the heating rate and fuel physical characteristics such as the surface area and the particle size.

*Temperature*: The decomposition of the coal organic substances starts at temperatures above 300 °C, where light volatile compounds of $CO_2$, CO, $CH_4$, $H_2$ and other light hydrocarbons ($C_2H_2$, $C_2H_6$ and $C_3H_6$) are formed. The evolution of tars begins at temperatures above 450 °C and reaches its maximum value at approximately 650 °C. Based on the elemental composition, it is evident that tars are complex hydrocarbons that have organic structures similar to that of original coal [30]. During the heating process, the coal particles may swell due to the escape of gases, resulting in a more porous residual char. At higher temperatures, above 600 °C, tars and the residual char are involved in the secondary reactions such as cracking, producing CO, $H_2$ and soot [31]. The volatile yield grows dramatically with the temperature. Fundamental investigations of devolatilisation at a heating rate of 1000 K/s and a residence time of 2 s showed that the volatile yield rises steeply up to a temperature range of (600 to 700) °C, followed by a gradual rise, as the temperature rises subsequently [32]. Kobayashi [33] observed that at high heating rates, corresponding to that in PF furnaces ($1 \cdot 10^4$ to $2 \cdot 10^4$) K/s, the weight loss of the char is increased from around 30 % at 1260 K to around 70 % at 2100 K at residence times in the ms order. The trend was found similar for both, bituminous coal and lignite.

*Fuel type*: Not only the devolatilisation yield and the distribution of products but also the composition of devolatilised gas are in accordance with the coalification degree of coal. As the volatile content increases from bituminous coal to lignite and biomass, the devolatilisation yield and correspondingly the volatile gases grow [29]. The tar formation is promoted stronger in hard coals than in lignites, whereas the product distribution is shifted more towards light volatile gases, in particular CO, in lower rank coals [30]. The composition of the volatile gas produced is directly influenced by the fuel type. As the coalification degree increases, less oxygen exists in the fuel, which therefore, results in the formation of high-calorific gases including $H_2$, $CH_4$ and other light hydrocarbons ($C_mH_n$) on a larger degree than CO and $CO_2$. This means fuels with a higher volatile content produce volatile gases with a lower calorific content than fuels with a higher coalification degree [29].

*Heating rate*: Investigations of the devolatilisation behaviour at high heating rates, corresponding to those at PF furnaces, showed more than 100 % volatile yield compared with volatile matter determined by the fuel analysis [28, 29]. Increasing the heating rate shows an increment in the devolatilisation products, where the increase is mainly related to an intensified tar yield via tar formation processes at higher temperatures [34]. However, there are discrepancies in literature on whether the observed effect is the result of heating rate or the final devolatilisation temperature [31, 34]. The residual char produced during pyrolysis with a higher heating rate is expected to be more porous and to have a larger surface area. This effect was more pronounced for lignites than higher rank coals [32].

*Particle size and shape*: The influence of particle size on the devolatilisation process is related to the process control mechanism. For particles smaller than a certain size, where

the devolatilisation process is chemically controlled, the particles size has no influence on the devolatilisation rate. In a chemically controlled devolatilisation, the product is only a function of the final temperature. For larger particles, the process is governed by the heat and mass transfer within the particle. Hence, the temperature at the centre of the particle differs considerably from its surface temperature. Under such circumstances, the devolatilisation rate increases by reducing the particle size. The reason is associated with the surface-to-volume ratio of particles that decreases with the particle diameter. Therefore, in larger particles, due to a smaller specific surface area, it takes longer for the heat to be transferred from the surface of particle to its centre [31, 35]. The critical particle size at which the controlling regime of the devolatilisation process changes, depends largely on the heating rate. As the heating rate[1] reduces, the critical diameter moves towards larger sizes. The results of a modelling from experimental data predicted this transition particle size as 200 µm at a heating rate of $10^4$ K/s [31].
There are contrary findings with regard to the influence of particle size on the devolatilisation rate which seem related to the investigated size range and the fuel type. Howard et al. [35] showed that for bituminous coal with a typical pulverised fuels particle size (below 200 µm) no relation between the particle size and the devolatilisation is found and the final temperature is the only decisive parameter. Experimental investigations by Anthony et al. [36] on lignite and bituminous coals with a particle size range between (50 to 1000) µm showed no influence of lignite particle size on the volatile yield, whereas in the case of bituminous coal the yield was dependant on the particle size. In another study [37] on fast pyrolysis of single woody biomass particles at temperatures up to 500 °C, the particle size below which the devolatilisation process is only controlled by the final temperature was found to be 500 µm. For biomass particles with irregular shapes, the particle shape also plays an important role in the mass and heat transfer process. The flake-like and cylinder-like particles have a larger surface-to-volume ratio than spherical shape particles, which leads to an enhanced heat and mass transfer within the particles and consequently a higher volatile yield [38].

**Ignition:** Ignition can be described as the transition from no oxidation to self-sustaining combustion. Ignition happens when the heat generation rate from the oxidation reaction exceeds the heat dissipation rate to the surrounding. The exothermic combustion reactions proceed independently afterwards [39, 40]. The temperature at which ignition occurs is denoted as the ignition temperature. However, under different boundary conditions, distinct definitions for the ignition temperature are identified [29].
To better understand the ignition process, the temperature of fuel can be correlated to the ratio of the heat release to the heat loss, corresponding to the air-fuel mixture temperature. The temperature increases gradually as the fuel is heated and respectively the heat release

[1] At a constant final temperature

to heat loss ratio rises. When the temperature reaches the ignition temperature, the combustion reactions initiate, generating a significant amount of heat. Under *critical ignition conditions*, if the heat loss increases or the heat release reduces slightly, the temperature sinks consequently. As the temperature goes below the critical ignition temperature, the combustion reactions terminate. On the other hand, if the heat release well exceeds the heat loss, the temperature rises exponentially and the self-sustained flame proceeds [29].
The ignition of solid fuels is accomplished by the ignition of released volatile gases and the residual char. The homogeneous ignition mechanism describes the ignition of volatile matter components when the evolution of gases in the vicinity of the particle reaches the lower ignition limit, at the ignition temperature. The heterogeneous ignition mechanism is related to the ignition of char particles by direct oxygen attack to the surface at the required particle temperature. The ignition mechanism is governed by a combination of several factors such as the fuel composition, the particle size and the heating rate [28, 29].
*Fuel composition*: A high-volatile coal promotes homogeneous ignition due to significant volatile evolution, whereas heterogeneous ignition is more prone in higher rank fuels with a low volatile content [28]. Experimental investigations by Khatami et al. [41] on single particle ignition of the same size, (79 to 90) µm, high-volatile bituminous coal and lignite showed that lignite particles are ignited heterogeneously due to fragmentation and formation of several finer particles, while the bituminous coal ignites homogeneously.
*Particle size*: In PF firing systems with particle sizes of mainly below 1 mm and very high heating rates, a mixture of different ignition mechanisms can be found within the flame. Extremely fine particles are heated rapidly, where the particles reach the char ignition temperature and consequently ignite instantly before a combustible mixture is formed (heterogeneous ignition). The mass flux of volatile gases increases proportionally with the particle size. Hence, in coarse particles, a volatile cloud is formed around the particle that reduces the oxygen partial pressure in the particle boundary layer and ultimately prevents oxygen to reach the char surface. When this critical mass flux, above which volatile gases hinder the oxygen diffusion to the char surface, is reached, volatile ignition arises (homogenous ignition), where the reaction front is farther from the particle surface. Consequently, the char ignition happens only after complete oxidation of the volatile cloud. At particle sizes below which this critical mass flux is not reached, the ignition occurs concurrently by heterogeneous ignition on the char surface and homogeneous ignition of volatiles around the particle (hetero-homogeneous ignition). Under this condition, the volatile flux is not high enough to prevent the oxygen diffusion to the particle. Howard and Essenhigh [42] calculated the critical particle size of 65 µm for bituminous coal above which only homogenous ignition and below which hetero-homogeneous ignition occurs.
*Heating rate*: In addition to the particle size, the heating rate of particles governs the volatile evolution and the particle temperature. Jüntgen and Heek [43] investigated the effect of the

heating rate on low-volatile anthracite and high-volatile bituminous coal with a particle size range of 50 µm and 250 µm and showed that at low heating rates the coarse particles ignite homogeneously, while fine particles ignite heterogeneously. As the heating rate increases, the particle size at which heterogeneous ignition occurs shifts to finer sizes and the limit for homogeneous ignition moves towards larger sizes. At the highest tested heating rate of approximately 800 K/s, particles smaller than 50 µm demonstrated heterogeneous ignition, whereas particles up to around 220 µm showed hetero-homogeneous ignition [43]. Although the quantitative accuracy of the critical particle sizes could be argued and the values change for lower rank coals, the trend lines provided a structured basis to understand the ignition regimes [44]. The influencing parameters on the ignitability of dust will be thoroughly discussed in section 2.1.1.2.

**Combustion of volatiles:** The volatile concentration drops with the distance from the particle surface, while the temperature rises. Therefore, the combustion front is displaced to a point where the minimum flammable concentration of volatile is reached and the temperature exceeds the minimum ignition temperature. The combustion rate of volatiles is mainly governed by the temperature, volatile evolution and the oxygen concentration in the mixture. Therefore, the influencing factors on devolatilisation have also a direct impact on volatile combustion. At high temperatures, where the chemical reaction is fast, the mixing rate of oxygen with the combustible gas limits the volatile combustion process [29].

**Combustion of char:** The char combustion consists of several processes including the oxygen diffusion to the particle surface, chemical reaction on the surface and oxygen diffusion within the particle pores. The overall rate of char oxidation is governed by the rate-limiting step. At low temperatures, the chemical reaction is the rate limiting step, whereas at higher temperatures the mixing of the fuel and the oxidant, i.e. the oxygen diffusion to the boundary layer around the particles, controls the reaction rate. The rate of char oxidation is proportional to the oxygen partial pressure, the available surface area and the reaction velocity that is defined by the velocity of the above rate-limiting processes [28].

**Ignition of a cloud of particles:** The ignition of a cloud of dust is realised by the ignition of single particles within the cloud, forming a coherent flame. The knowledge on the mechanism of single particle ignition is, therefore, necessary to better understand the mechanism of dust cloud ignition and the influencing parameters. The chemical and physical characteristics of the fuel, e.g the volatile content, the moisture content, the particle size, etc. are the main governing parameters defining the ignitability of the fuel and respectively the ignition of the dust cloud. Particle size is particularly of high importance for the ignition of coal dust clouds with a broad particle size distribution, where the fine fraction of fuel

initiates the ignition and produces the heat required for the ignition of larger particles. In addition to fuel-related parameters, the boundary conditions inside the furnace control the mass and heat transfer between the fuel and oxidiser and correspondingly govern the ignition process. A successful ignition requires adjustments of all influencing parameters [29].

#### 2.1.1.1 $NO_x$ formation and reduction

$NO_x$ emissions are regarded as the sum of NO and $NO_2$ emissions, while in coal power plants NO accounts for 95 % of the total $NO_x$ emissions. $NO_x$ is produced via three pathways during combustion: (I) thermal $NO_x$, (II) fuel-$NO_x$ and (III) prompt $NO_x$.
*Thermal $NO_x$*: Thermal $NO_x$ is formed by the reactions of $N_2$ molecules from the air (combustion air) with atomic oxygen at temperatures above 1300 °C according to the Zeldovich mechanism. The reaction rate increases exponentially with the temperature and is proportional to the radical O concentration. The N radicals formed in the first reaction further reacts with $O_2$ in the second reaction [45]. In PF burners the thermal $NO_x$ contribution accounts for around 20 % of the total emission [28].

$$N_2 + O \longrightarrow NO + N \tag{2.1}$$

$$N + O_2 \longrightarrow NO + O \tag{2.2}$$

*Fuel-$NO_x$*: These $NO_x$ emissions are formed from organic nitrogen in the fuel. During the devolatilisation, a part of nitrogen is released by volatiles in the form of HCN and $NH_3$ species that are either oxidised to $NO_x$ or decomposed to $N_2$, through a series of reaction pathways. The rest of nitrogen stays in the char and is subsequently converted to $NO_x$, with a low conversion rate of around (10 to 25) %, and $N_2$. Fuel $NO_x$ emissions are influenced by the fuel nitrogen content and the operational conditions. They account for approximately (75 to 80) % of the total $NO_x$ emissions in typical PF firing plants. The fuel $NO_x$ formation is predominantly related to volatile-bound nitrogen, which can be modified to a large extent by combustion conditions, e.g. air temperature, air ratio, mixing of primary and secondary air, etc.
The conversion of volatile-related nitrogen to $NO_x$ can be controlled by techniques, such as air staging (substoichiometric combustion at the burner zone followed by the injection of over-fire air in the furnace to complete the combustion). This has the potential to reach a nitrogen to $NO_x$ conversion rate of around 5 % (from approximately 30 %), where the remaining fuel-$NO_x$ emissions are associated only with char-related $NO_x$ [28, 46, 47].
The initial nitrogen-containing precursor (HCN and $NH_3$) are converted to $NH_i$. Under abundant oxygen conditions, $NH_i$ reacts with $O_2$ and produces NO, while under oxygen-lean

atmosphere, $NH_i$ reacts with an already produced NO, forming molecular nitrogen. Furthermore, the hydrocarbon radicals ($CH_i$) can decompose NO molecules to HCN, recycling NO molecules back to the loop and subsequently further reducing to $N_2$. This reaction is 10 to 100 times faster than the conversion of HCN to $NH_i$ [28, 48].
*Prompt $NO_x$*: These $NO_x$ molecules are formed quickly by the reaction of hydrocarbon radicals ($CH_i$) with $N_2$, producing atomic nitrogen and further react with $O_2$ to form NO. However, the quantity of the prompt $NO_x$ in pulverised fuel systems is negligible [45, 49].

#### 2.1.1.2 Assessment of ignitability and explosibility of dusts

Several laboratory methods describe the explosibility and the ignitabilty of combustible dust. The ignitability refers to the susceptibility of the dust mixture to be ignited and the explosibility refers to the ability of the dust and oxidizer mixture to be propagated after ignition. There are laboratory equipment and test methods that assess the explosibility and the ignitability of dust. Dust explosion parameters are usually determined to support the design of safety systems in the industrial processes and to minimize the explosion hazard. These explosion parameters are also relevant for characterizing the ignition requirement and the intensity of dust ignition and flame propagation. In the following, several parameters are introduced and their influencing factors are explained.

**Minimum ignition temperature:** The minimum ignition temperature is the temperature from which ignition initiates. There are different test equipment and criteria to determine the minimum ignition temperature of a layer of dust or a cloud of dust. The minimum ignition temperature rises by increasing the moisture content, the ash content and the particle size, whereas it falls as the volatile content and the oxygen concentration increase [50].
Cheng et al. [51] predicted the ignition temperature of coal powder using neural network models, where the data from proximate and ultimate fuel analysis was used for the model input. It was concluded that the ignition temperature is more relevant to the moisture content, the volatile content, the oxygen content and the calorific value of fuel.
Numerous investigations have been conducted on the effect of the volatile content and the particle size on the ignition temperature. In a study [29], the ignition temperature of a bituminous coal was compared with its devolatilised char to investigate the ignition temperature associated with volatile and char ignition. It was specified that the fuel ignition temperature of 775 °C increased by 125 °C as the fuel was devolatilised (char ignition temperature). The influence of the volatile content and the particle size on the cloud ignition temperature was further investigated, where the ignition temperature was determined 150 ms after the sample dispersion inside the oven. The ignition temperature of four fuel types with a volatile content

between 9 % and 55 % were determined at different particle sizes from 10 µm to 150 µm. The results showed a direct relationship between the volatile content and the ignition temperature, where the ignition temperature rises from 600 °C to 950 °C as the volatile content of the fuel reduces. The ignition temperature of the fuel with 9 % volatile content showed a strong dependency on the particle size, whereas the ignition temperature of fuels with a volatile content between 33 % and 55 % was independent of the particle size within the investigated size range (up to 150 µm). The results shed some light on the ignition mechanism of a flame cloud. The ignition temperature of high volatile fuels was governed by homogeneous ignition and therefore the particle size did not play a significant role in the ignition temperature. However, for low-volatile fuels, the concentration of volatiles stays below the ignition limit and therefore ignition occurs via the heterogeneous char ignition mechanism, where particle size influences the ignition temperature [29].

In another study similar observations were obtained, in which an investigation showed that particle sizes in the range of (74 to 125) µm and (125 to 212) µm have similar ignition temperatures, whereas for the particle size range of smaller than 75 µm, the ignition temperature drops by 15 °C. It was concluded that for larger particles the ignition temperature was governed by the homogeneous ignition and therefore it was independent of the particle size, while for smaller particles the heterogeneous ignition played a role and hence the ignition was facilitated as the particle size was reduced [52]. A study on the ignition of six coal qualities with a volatile content ranging from 15 % to 60 % and three particle size ranges (40 µm, 140 µm and 250 µm) demonstrated that the ignition temperature rises with the char content (i.e. decreasing fuel reactivity) and with the particle size, where the effect of particle size on the ignition delay time is minimised as the oven temperature rises [53]. Weiguo et al. [54] demonstrated that the ignition temperature of a coal dust cloud does not have a linear correlation with the particle size. The ignition temperature of a coal dust with 800 °C grows sharply by 60 °C as the particle size is increased from 25 µm to 75 µm, followed by a gradual increase of around 55 °C by increasing the particle size from 75 µm to 500 µm.

Moreover, coal ash or any inert material increases the ignition temperature by absorbing the heat and worsening the radiative and convective heat transfer. In fact, ash creates a shielding effect that hinders the heat transfer and consequently the flame propagation between particles. The addition of coal fly ash to a dust cloud increases the ignition temperature linearly, where the inhibition effect is more prominent for a lignite coal rather than a bituminous coal. The reason is associated with a highly volatile flame of the lignite, compared with the bituminous coal [55, 56]. The heat adsorption by ash suppresses the ignition process more pronouncedly in a flame with high volatiles. Yu et al. [55] observed that depending on the fuel type, each 10 % of fly ash, increases the ignition temperature by (4 to 6) °C. A clear correlation between the ignition temperature of a dust layer and the ash content was found by another group [56], where a 10 % increase in the ash content corresponded to a 10 °C rise

in the ignition temperature.
Moisture in coal is also expected to increase the ignition temperature, mainly due to additional heat that is required for the water vaporisation. The effect of moisture on the ignition inhibition and the flame propagation will be later discussed together with its effect on explosion characteristics parameters. A (10 to 20) °C reduction in the minimum ignition temperature was reported when the moisture content was reduced from 10 % to 3 % [57].
In addition to intrinsic parameters, the ignition temperature is influenced by the gas composition. Increasing the oxygen partial pressure, enhances the oxygen diffusion rate and its access to the particle surface and facilitates the combustion reaction rate, resulting in lower ignition temperatures [58]. In an $O_2/CO_2$ atmosphere, the ignition temperature rises, which is associated with a higher $CO_2$ heat capacity and also lower oxygen diffusivity in a $CO_2$ atmosphere compared with $N_2$ [57, 59].

**Minimum ignition energy:** The minimum ignition energy (MIE) is defined as the lowest amount of energy stored on a capacitor that can ignite a readily ignitable dust mixture [60]. The MIE falls with increasing the volatile content and with decreasing the particle size, the moisture content and the ash content of dust [56, 60]. Beside dust properties, the MIE also changes with the operating parameters of the measurement equipment. By changing the time between the dust dispersion and spark ignition (ignition delay time) and also the concentration of dust in the test equipment, the MIE changes accordingly. The optimum ignition delay time and the dust concentration need to be determined for each fuel quality to find the MIE [60].

**Explosion characteristic parameters:** The maximum explosion pressure, $p_{max}$, and the maximum rate of pressure rise, $(dp/dt)_{max}$, describe the severity of explosion. These maximum values correspond to the largest explosion pressure and the rate of pressure rise, respectively, which is achieved over the entire explosive dust concentrations. The explosion pressure is associated with the amount of heat release, i.e. the temperature in the explosion vessel, whereas the rate of pressure rise is related to the combustion kinetics and the rate of heat release, i.e. the rate of flame propagation [50, 61]. The explosion characteristic parameters, similar to previously described parameters, are influenced by fuel properties (e.g. moisture, ash and volatile contents as well as the particle size and the surface area) together with operational parameters, namely the dust concentration and the oxygen concentration [50].
Ignition occurs within the ignitable dust concentrations. The minimum amount of dust required to create a combustible mixture and to sustain the flame determines the lower limit. A further increase in the dust concentration increments the explosion pressure and the rate of pressure rise until the maximum values are reached, above which the trends may level

off and eventually drop, due to an excessive amount of dust that can not contribute to the ignition and combustion process which consequently cools the flame down. The upper limit of the dust concentration is related to a fuel-rich condition, where lack of oxygen prevents the ignition. Moreover, as the dust concentration increases, there is a high probability that the dust can not be properly dispersed in the combustion vessel, which additionally contributes to reduce the explosion characteristic parameters [50, 62].

Cashdollar [62, 63] investigated the influence of the particle size on explosion characteristic parameters using a high-volatile bituminous coal. The results showed that the maximum rate of pressure rise declines steeply from 70 bar/s to 20 bar/s as the median particle size from several narrow size distributions increases from around 3 µm to 60 µm, while the trend continues to fall very gently to 10 bar/s at the median particle size of 100 µm until it is completely suppressed at 250 µm. Indeed, the maximum rate of pressure rise and the particle size showed a logarithmic trend line. The maximum explosion pressure dropped accordingly with the particle size but to a lower degree compared with the rate of pressure rise. Further investigations of the effect of particle size by combining the narrow particle size distributions and creating a broad one, demonstrated that the ignition is mostly governed by the finer size fractions.

Beside the particle size, explosion characteristic parameters are expected to be influenced by the available surface area. A comparison between two comparable fuel qualities showed a considerable difference in $p_{\max}$ and $(dp/dt)_{\max}$ that was correlated to a notable variation in the available surface area, resulting in an enhanced volatile release and char combustion. It was then concluded that for high-volatile bituminous coal with fine particle sizes, heterogeneous ignition plays an important role in the flame propagation [64].

An increase in both explosion characteristic parameters with the volatile content, for fuels with similar particle sizes, has been reported by several studies. The volatile release and the formation of a combustible mixture is considered as the main ignition initiation mechanism for fuels with medium to high volatile contents [50, 62, 65].

Moisture consumes the heat not only from the particle surface during the heating but also during the combustion. In addition to the main inhibition mechanism of moisture, which is the heat absorption in the form of latent and also sensible heat, moisture strengthens certain types of inner-particle bonds that lead to particle agglomeration and correspondingly inefficient particle dispersion inside the explosion sphere [66]. The particle agglomeration vastly reduces the effective surface area and curbs the combustion reaction. Additionally, a high moisture content lowers the oxygen partial pressure in the vicinity of solid particles and further inhibits the mass transfer and reduces the reaction rate [61, 67]. Investigations by Yuan et al. [61] on the influence of fuel moisture on the explosion characteristics showed a dependency between the limiting moisture content and the fuel particle size. The explosion pressure and the rate of pressure rise over defined dust concentrations showed that ignition is

completely suppressed at the moisture content of 15 % when particles sizes are below 125 µm and this limiting moisture level drops to 7 % when particle size is increased to a range of (125 to 500) µm. Moreover, it was concluded that the impact of moisture content on the rate of pressure rise is larger than its impact on the explosion pressure.
Adding inert material to combustible dust has been used as a measure to lower the ignition susceptibility of dust. Inherent fuel ash, as an inert material, lowers the explosibility of the dust via several pathways. First, it consumes the heat from the surrounding and even after the ignition from the already combusting particles, which consequently reduces the heating rate of the unburned particle [55, 68–70]. Second, as the combustion on the particle surface proceeds, a growing ash layer is deposited on the particle surface, which hinders the oxygen access to the surface and also the volatile release from the particle [28]. Similar to the effect that ash poses on the ignition temperature, beside the heat sink effect, the dispersion of inert material impairs the flame propagation within the dust cloud. These effects lead to a reduction in the maximum explosion pressure and the maximum rate of pressure rise [55, 68]. The impact of ash on reducing the explosion characteristic parameters also depends on the ignition mechanism. Du et al. [68] showed that maximum rate of pressure rise and the maximum explosion pressure of a bituminous coal with homogenous ignition drops dramatically by 60 bar/s with 20 % addition of inert material, while for anthracite with heterogeneous ignition the drop was by around 30 bar/s. This finding is in line with the effect of ash on the ignition temperature of different rank fuels observed by others [55].
It needs to be highlighted that moisture represents a stronger inhibiting effect than ash. Moisture has a considerably larger heat demand that is associated with a higher degree to the latent heat of evaporation and with a lower degree to a higher specific heat capacity of water compared with ash [61, 68]. Considering an ignition temperature of 600 °C, the heat demand for 1 kg of moisture is around 6 times higher than that for 1 kg of ash [61].

**Dust explosibility:** Torrent et al. [71] developed a correlation between the explosibility of coal dust and the fuel composition. However, in that study, no physical properties were taken into account. An explosibility index was derived by correlating not only the proximate fuel analysis but also the ultimate analysis to several ignition and explosion parameters including minimum ignition temperature, minimum explosible concentration, maximum explosion pressure and maximum rate of pressure rise. The model was developed using a data bank to identify the individual variables for fuel composition parameters as input in order to predict the explosibility of dust. The model showed a large dependency on the volatile content [71, 72]. Later the group developed another methodology to assess the explosibility of dust using the activation energy and oxidation temperature obtained from a thermogravimetric analysis [73–75].

**Ignitability characteristic number:** A parameter developed by Zelkowski [29] correlates the energy released by devolatilised material to the ignition temperature, called "Zündwilligkeitskennzahl ($ZWZ$)", in this work translated as the ignitability characteristic number. Zelkowski showed that the ignitability characteristic number, ranging from (1 to 20) kJ/kg °C, promisingly describes the ignitability of various hard coal and lignite qualities. For different types of hard coal, $ZWZ$ number showed an increasing trend with the volatile content. For lignites, the $ZWZ$ behaved differently, where a linear trend was not observed. This was related to different shares of inert material such as ash, moisture and sulphur that reduced the ignitability [29]. The ignition characteristic number was generally successful to distinguish the ignition behaviour between solid fuel types such as hard coal, lignite, etc. However, the $ZWZ$ number was not highly effective in differentiating the ignitability of one fuel type's distinct grades because the effect of these inert components was not integrated in the number.

### 2.1.2 PF Flames in swirl burners

In swirl burners, the combustion air is swirled to form a recirculation zone and to intensify the ignition and combustion process. Depending on the burner design, the combustion air can be divided into different streams to control the swirling degree of each stream separately. In some designs, the pulverised fuel and primary air stream are also swirled to further improve the flame stabilisation. The design target of a swirl burner is to reach a suitable condition in which a continuous source of heat and a proper mixing is ensured to guarantee the ignition and flame stability. Heat in swirl burners is mainly supplied by the recirculation of hot flue gas products and the mixing of fuel and oxidiser is assured via a suitable mixing time [76].

**Flow characteristics in swirl burners:**
The flow in swirl burners is characterised by a toroidal recirculation zone in the centre of the burner known as the central toroidal recirculation zone (CTRZ). The CTRZ is formed when the ratio of the swirl momentum to the axial momentum is sufficiently high. The CTRZ is formed due to the pressure gradient. Large radial pressure gradients are formed as the result of centrifugal forces which in consequence produce a sub-atmospheric low pressure zone in the centre. As the flow moves farther from the burner outlet, the axial and swirl velocities as well as the sub-atmospheric pressure decay due to the mixing and entrainment of surroundings. The reduction in the pressure gradient with the distance forms a negative axial pressure gradient towards the burner, which sucks the flow backwards. A certain degree of the axial pressure gradient is required to form the recirculation, which depends on the swirl

degree. As the swirl degree increases, the jet width, the rate of entrainment and velocity decay rise. The swirl degree is represented by the swirl number, which is defined as the axial flux of the swirl momentum to the axial flux of the axial momentum divided by the nozzle radius.

At swirl numbers equal or smaller than 0.2, very weak swirl motions are formed where the pressure gradients are ignored. In week swirl with swirl numbers of equal or smaller than 0.5, the recirculation zone is still not created. However, the pressure gradient is formed which increases the width of the flow field, the entrainment rate and the rate of velocity decay, leading to a wider and shorter flame.

As the swirl degree is increased to the swirl numbers above 0.6, large axial and radial pressure gradients are formed. Under this strong swirl, CTRZ is created, the flow field gets wider and slower. The size of the CTRZ depends on several parameters such as the swirl number, the type of swirl generator, quarl exit, etc. As the swirl number increases, the ratio of the recirculated mass flow to the total mass flow rises accordingly. This means at a sufficiently high Reynolds number, a constant flow recirculation rate is obtained at a given swirl number and dedicated burner design. For swirl numbers above 0.6, disturbance in the recirculation and mixing can occur at Re below 18000. Hence, to ensure a stable CTRZ, the Reynolds number needs to be kept above this lower limit. As the swirl number is increased, the recirculation zone enlarges accordingly, improving the flame stability and combustion performance. Additionally, a high turbulence intensity is associated with strong swirling flows, which correspondingly improves combustion and flame stability. Extensive turbulence intensity at very high swirl numbers should be however avoided to prevent any flame extinction.

Furthermore, in confined combustion systems, under very high swirl numbers where the entrainment rate is also significantly large, an external recirculation zone is formed between the flow boundaries and the furnace wall, known as the corner recirculation zone [77–79].

**Flame stabilisation in swirl burners:**

Flame is defined as a self-sustained propagation of a localised combustion area. The flame comprises two zones: a preheating zone, where fuel and combustion air are heated up and a reaction zone where the chemical reactions occur. The diffusion of heat and radicals from the reaction zone to the preheating zone sustains the flame propagation. The flame propagates in the direction of unburned reactants and is considered stable when the flame keeps propagating without extinguishing or a flashback within a range of operational parameters. The toroidal vortex in the swirl flow recirculates the devolatilised gas during ignition and the hot flues gas products during the combustion back to the preheating and the reaction zone. This brings an additional heat source from the hot combustion products to the critical ignition zone. Hence, the flame is stabilised where a well-mixed zone is formed in which the

critical heat amount and the combustible concentration are reached [77, 80].
A flame *flashback* occurs when the flame propagates into the burner port and it happens when the velocity of the unreacted fuel stream is lower than the flame propagation velocity. When the flow velocity stays lower than the flame propagation velocity over a certain width and the heat supply to the preheating zone is sufficient for the ignition, the flame anchors at the burner outlet. As the flow velocity exceeds the flame propagation velocity at every point along the flame area, *flame lift-off* occurs, where the flame is lifted above the burner to a new position at which the flow velocity matches the flame propagation velocity at a point along the width of the flame area. In swirl burners, the CTRZ is of high importance for the flame stability by creating a reduced velocity zone inside the recirculation bubbles and also recirculating the heat from hot combustion products to the reactants. Therefore, a point in the recirculation zone can be found where the flame velocity matches the flow velocity, stabilizing the flame base. As the flow velocity is increased, once the flame is lifted, the lift-off distance between the flame base and the burner port increases until the blowout velocity is reached. *Blowout* occurs when the flow velocity is considerably higher than the flame propagation velocity at every points, where a matching velocity cannot be found downstream [77, 80–82].
Another method for the flame stabilisation in industrial burners is a bluff body system. Recirculation eddies are formed behind the bluff body, which serves as a continuous source of heat. Similar to the stabilisation mechanism in swirl burners, the formation of a recirculation zone behind the bluff body stabilizes the flame [77].

**$NO_x$ formation and particle trajectories in swirl burners:**
In swirl burners, the $NO_x$ production depends on the burner aerodynamic configurations. Swirling flows impact the $NO_x$ production in several ways. An increased swirl on one hand enhances the combustion intensity, increasing the temperature and correspondingly the thermal $NO_x$ and on the other hand intensifies the mixing of the secondary air with the hot combustion products, reducing the hot spots and consequently reducing the thermal $NO_x$. The effect of swirl on fuel $NO_x$ production is strongly governed by the aerodynamic boundary conditions at the burner outlet. $NO_x$ formation is reinforced when ignition occurs under oxygen abundance conditions in the vicinity of the secondary air stream, whereas $NO_x$ production is suppressed when the particles are ignited within the internal recirculation zone where the oxygen is deficient [77, 78].
As fuel $NO_x$ has the major contribution in pulverised fuel systems, particle trajectories within the flame region define the overall $NO_x$ emissions. When the fuel particles have a large axial momentum, they penetrate completely or partly within the internal recirculation zone. The larger is the relative particle velocity inside the recirculation zone and the bigger is the particle size, the penetration length becomes longer. Under these conditions, the de-

volatilisation and ignition under an oxygen-lean atmosphere prevents the formation of fuel $NO_x$. If the particles do not have sufficient axial momentum, they are dragged early into the secondary air stream either before entering the recirculation zone or after a very short penetration length. Under such circumstances, the ignition occurs on the oxygen-rich side, advancing the formation of fuel $NO_x$ [83–85].

$NO_x$ formation was investigated in the International Flame Research Foundation (IFRF) movable block swirl generator, where the particle trajectories were modified by the position of the annular coal injection channel. The results showed a decreased $NO_x$ level by around 60 %, when the particles were directed more inside the recirculation zone and their mixing with the secondary air was delayed [83]. Another technique to reduce the $NO_x$ emissions at the burner is low-$NO_x$ swirl burners. Within this design, air staging is realised at the burner outlet, where the secondary air is introduced via several stages, resulting in the initial devolatilisation and ignition in an oxygen-lean atmosphere. This delayed mixing of the fuel and combustion air, which may deteriorate the combustion efficiency, needs to be compensated by enhanced mixing between the fuel and the oxidizer afterwards [86].

Hence, $NO_x$ formation and reduction mechanisms are evidently influenced by the aerodynamics and particle trajectories in the swirling flow as well as the air ratio at the burner outlet. Several experimental and simulation studies validated that the $NO_x$ level increases when the air ratio and swirl number at the burner are increased. A higher air ratio provides an enhanced oxygen availability, which supports the $NO_x$ formation. Similarly, the $NO_x$ level first decreases as the swirl number is increased from the weak swirl number to above the critical swirl number, where the CTRZ is enlarged and the particle residence time within the recirculation zone is expanded, reaching an optimum swirl number at which the $NO_x$ emissions are minimised. A further increase in the swirl intensity strongly promotes the early mixing of the fuel and oxidizer, leading to less penetration in the central reducing zone, meaning shorter residence time within the CTRZ, and correspondingly higher $NO_x$ levels [85, 87, 88].

The optimised near burner aerodynamics and accordingly the $NO_x$ emissions are affected particularly when the burner load is reduced to a level at which the burner air ratio is increased and/or the recirculation zone is disrupted. Experimental studies in a 400 kW test facility signified that the $NO_x$ emission increases when the burner load is reduced from 70 % to around 30 %. The behaviour was related to a reduced velocity of the secondary air and a disruption in the designed flow profile [89]. Operational experiences from a 500 MW unit showed relatively stable $NO_x$ emission values, as the turbine load was reduced from full load to around 200 MW, while by a further load reduction to around 75 MW, the $NO_x$ emission increased significantly [86].

**Burner operating and design parameters:**
The ignition is accomplished when the evolution of volatiles within the flammable limit reaches the sufficient temperature. This condition is directly related to the boundary conditions at the burner outlet. Thus, the ignition process is governed by fuel-related and burner-related parameters. The rates of heating, devolatilisation and ignition of particles are associated with chemical and physical characteristics of the fuel as discussed earlier. The velocity and swirling intensity of the primary air and secondary air determines the intensity of the mixing of the particles with recirculated flue gas products and the combustion air, which ultimately defines the ignition point. Figure 2.1 shows an overview of the influencing parameters relevant for the ignition in a swirl burner.
Under typical furnace conditions, particles are heated up via radiation and convection. To reach the particle ignition temperature, the rate of heating and the residence time of particles within the heating zone are decisive. Smaller particles are heated up relatively fast and start the ignition process. For larger particles, the residence time required to reach the ignition temperature increases and the ignition process is delayed. The boundary conditions of a burner at low-load or during start-up differs from the typical design conditions. The burner load and correspondingly the ratio of pulverised fuel to the primary air, known as the dust loading, is decreased. Consequently, less heat is liberated by the combustion and subsequently the furnace temperature drops. The heating rate falls accordingly and the ignition becomes unstable. The minimum burner load is then restricted by the ignition and flame stability [90].
The air ratio, the ratio of actual combustion air to the stoichiometric air demand, of the burner governs the oxygen availability. The air ratio for hard coal and lignite burners under normal operation is adjusted to 1.15 to 1.3. However, at low burner loads, the air ratio increases, as the minimum amount of air entering the burner is limited. Increasing the air ratio, on one hand, increases the oxygen availability, on the other hand, can inhibit the ignition process due to excessive cooling [76, 90]. Moreover, by increasing the air ratio, the amount of secondary air and accordingly its velocity increases. As a result, the tangential and axial momentum of the secondary air rise, leading to an amplified swirl intensity and accordingly an enlarged amount of reverse flow in the CTRZ [91].
The aerodynamic profile at the burner outlet is the net effect of the primary air and secondary air axial and tangential momentums. If the forward momentum of the primary air carrying the fuel is comparatively high, the flow penetrates inside the formed CTRZ and depending on the intensity of the recirculated flow the particles may be stagnated inside the CTRZ from where they are either recirculated back or are spread away towards the secondary air flow. The particle size is a critical parameter that defines the particle trajectories. Within a broad particle size distribution, the larger particles have stronger forward momentum and penetrate further inside the CTRZ, whereas the smaller particles are sooner dragged out-

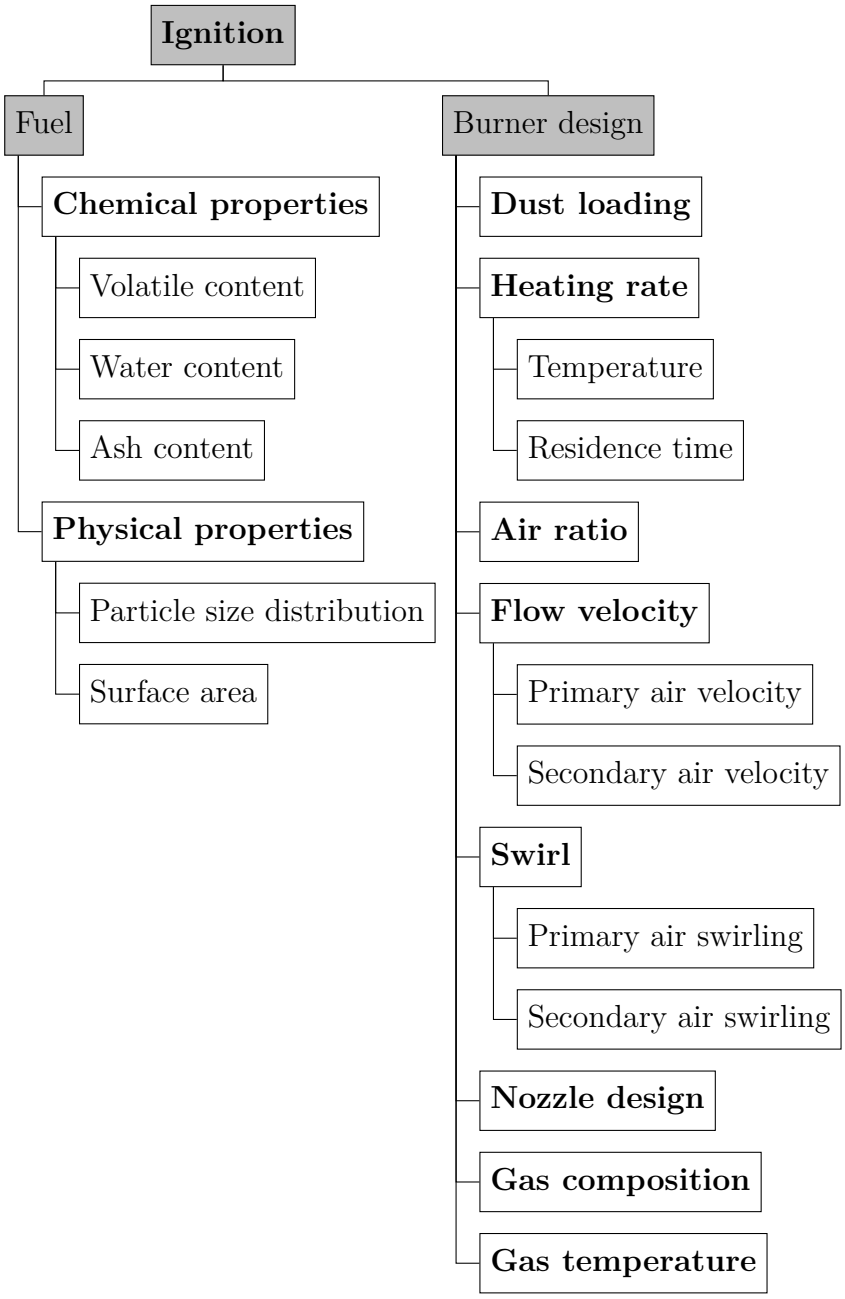


Figure 2.1: Parameters related to ignition in swirl burners

wards and mixed with the secondary air. When the forward momentum of the primary air is significantly high, it completely penetrates to the CTRZ. As a result, the central reverse flow region is disrupted and the recirculation zone is formed around the primary air flow, which in return isolates the primary air stream from the secondary air stream. Under such circumstances, the ignition and combustion process can be hindered by oxygen depletion and an insufficient residence time within the critical ignition zone. On the other hand, high primary air forward momentum can be compensated by increasing the secondary air tangential momentum. If the tangential momentum is extensively increased by increasing the

swirl degree, the primary air stream is initially mixed with the secondary air and it merely enters the CTRZ. This scenario can also be detrimental for the ignition, as the particles are mixed with the cold secondary air before they are properly heated up by the recirculated combustion products and the already released volatiles will be diluted. The optimised burner aerodynamics is found within a momentum range, where the primary air partially enters the CTRZ and then is extended towards the secondary air for complete combustion. Depending on the fuel ignitability and the devolatilisation rate, the suitable penetration length changes [91, 92].

The velocity of the primary air is related to the fuel ignitability and the velocity of the secondary air is dependant on the primary air penetration length, the required mixing rate and the combustion process. An easily ignitable fuel requires a shorter residence time within the ignition zone and should be transported with a higher velocity to avoid any flash back to the burner owing to their larger flame propagation velocity. Easily ignitable fuels do not require long penetration within the CTRZ, as fast ignition necessitates earlier mixing with the oxidizer for complete combustion. Correspondingly, at a low secondary air velocity, the primary air momentum greatly exceeds the secondary air momentum and at extremely high secondary air velocities, the mixed particles have a short residence time and are rapidly moved away from the ignition zone. For typical PF swirl burners, the primary air velocity stays within a range of (20 to 26) m/s for hard coal and lignite and the secondary air velocity rises from (25 to 35) m/s for lignite to (30 to 40) m/s for hard coal fired burners [76].

The quantity of the primary air depends on several parameters such as the fuel ignitability, the fuel transportation in the pipes, the type of firing (direct/indirect) and the milling system. To specify the lower limit of the primary air ratio, uniform fuel transportation and avoidance of any particle sedimentation in the pipes have to be ensured. The quantity of the primary air defines the local air ratio in the primary air, which is more relevant for the volatiles combustion. At low ratios, lack of oxygen hampers the ignition process, while at high ratios local cooling and short residence time exacerbate the ignition. Furthermore, the share of the primary air to the total combustion air and also its velocity depend not only on the fuel ignitability but also on the gas composition. This is more relevant for the direct firing in lignite-fired burners, where the fuel in the milling system is dried by a mixture of air and flue gas and transported to the burner with a gas containing lower $O_2$ content than air. For typical lignite burners with flue gas drying in the mill, depending on the heat demand for the drying, the share of the primary air is (20 to 45) %. When air is used for the fuel transport, the primary air ratio in hard coal burners is (20 to 40) % [28, 76]. In case of indirect firing, where the fuel is already pretreated, the amount of primary air is only limited to ensure a proper transportation in the pipes. Therefore the dust loading in the primary air can be increased significantly, and accordingly the air ratio is reduced, which both are beneficial for the ignition [93].

Primary air swirling intensifies the mixing of the particles, resulting in earlier ignition for high-volatile fuels and ignition inhibition due to very early mixing with the cold secondary air in case of low ignitable fuels. This intensified mixing further reduces the flame length [91].
The flow field and particle trajectories at the burner outlet can be as well modified by the burner nozzle. Employing a toothed nozzle or a divergent nozzle outlet for the primary air and PF is expected to enhance the mixing at the burner throat [86, 91].
The primary air and secondary air temperature also have a significant influence on solid fuel ignition. Preheating of the combustion air via available heat from the flue gas improves the ignition and combustion performance and increases the flame temperature. In PF furnaces, the secondary air is preheated to (350 to 400) °C. In hard coal-fired furnaces the primary air can also be heated to the required temperature for the coal drying via the flue gas air pre-heater, whereas in lignite-fired plants the flue gas is used to adjust the required milling temperature [28].

## 2.2 Plasma-assisted ignition and combustion for PF systems

### 2.2.1 Fundamentals and the application of plasma-assisted ignition and combustion

**Fundamentals:** Plasma is produced when a gas is ionised by receiving energy. It consists of electrons, ions of various charge states, neutral molecules and atoms. Plasma has a broad range of applications in industrial processes such as coating, thermal treatment, etc. For these applications, thermal plasma, also known as equilibrium plasma, or cold plasma (non-equilibrium) have been implemented. The plasma can be generated via different electrical sources including DC, AC, microwave and radio frequency [94]. An example of plasma application in the energy sector is plasma gasification of waste. This technology is particularly interesting for hazardous waste, where toxic substances are destructed at high temperatures [94, 95].
Plasma-assisted combustion for liquid and gaseous fuels has been extensively investigated to improve the ignition limits, the flame stability, the combustion performance and to control emissions in gas turbines, turbo machines and internal combustion engines [96, 97]. For in-

stance, Kim et al. [98] investigated the effect of non-thermal plasma on the lean flammable limit in a model gas turbine and concluded that plasma assistance extends the minimum flammable limit to smaller equivalence ratios. In another study [99], the stability of lean premixed methane-air flame in a swirl burner was improved by a non-thermal plasma. The role of plasma for $NO_x$ reduction was studied by Lee et al. [100], where plasma-assisted combustion of liquefied natural gas was performed in a two-stage industrial burner. A reduction in $NO_x$ levels by more than half compared with the levels in one-stage reference burner was reported.

Plasma improves the combustion process via three mechanisms: (I) thermal, (II) kinetic and (III) transport. The thermal enhancement pathway is related to facilitating the combustion reaction due to a high temperature. The kinetic mechanism addresses the radical pool, where ions and electrons produce excited species and active radicals of O, OH and H that accelerate low temperature oxidation reactions. The transport mechanism is associated with the fragmentation of large fuel molecules to smaller sizes. These three mechanisms have a combined effect on the combustion enhancement, while depending on the plasma type and the operational conditions one effect may dominate the other.

The presence of OH, H and more importantly O radicals in plasma creates new kinetic pathways that facilitate the chain branching reactions. During normal combustion, the chain initiation reaction requires a certain amount of heat to proceed and to subsequently trigger the chain branching reactions, producing more radicals that are required for the ignition initiation. Plasma assisted combustion provides the radicals that are required for the chain branching reactions and therefore bypasses the slow chain initiation reactions. Hence the ignition can be accomplished at a lower temperature. Moreover, the availability of excited species such as $O_3$ and excited atomic O enable new branching reaction pathways that take place at temperatures lower than the conventional chain branching reactions. These are in particular relevant for ignition at low temperatures because as the temperature rises, the rate of the conventional branching reaction increases rapidly and it becomes the dominant radical production pathway. At temperatures above 1100 K, the plasma-assisted ignition is mainly due to the thermal effect and the kinetic mechanism plays a negligible role. Similarly, the enhancement in the flame propagation relies to a larger degree on the thermal mechanism, where the kinetic mechanism represents a modest effect [96, 101].

Experimental studies on the particle heating with thermal plasma showed a significantly large heating rate for solid particles. Aluminium oxides particles of 100 µm reached a surface temperature of more than 1200 K in around 0.1 ms in $N_2$ plasma with a temperature of 10 000 K. This corresponds to a particle heating rate in the order of $(10^6$ to $10^7)$ K/s [102].

The fundamentals of plasma-assisted solid fuel ignition and combustion have not been investigated as extensively as gaseous and liquid fuels. Zhao et al. [103] examined the mechanism of plasma-assisted ignition of pulverised lignite in a conventional Hencken burner equipped

with a plasma system. A pin-to-pin electrode powered by a DC source generated plasma within a voltage range up to 20 kV. As the voltage was increased in the range of 0 kV (no plasma) to below 3 kV, no impact on the ignition delay time was observed, whereas a sudden drop of around 1.5 ms in ignition delay time was detected at 3 kV. Further increases of the voltage to 10 kV and 20 kV resulted in an ignition delay time decrement by 2.5 ms and 2.9 ms, respectively. It was concluded that the sudden drop at 3 kV was attributed to the chemical effect, as soon as the complete discharge created a radical pool, while the thermal effect was gradually promoted as the voltage was increased to 20 kV.

**Applications:** Other studies have investigated the application of plasma assistance for solid fuel gasification and combustion and do not look into the underlying mechanisms.

Plasma gasification of pulverised coal was carried out experimentally in a plasma reactor fed by three-phase electric power. Gasification of coal in a plasma-reactor produced a high gasification degree of (90 to 95) % and altered the gas composition, as contrary to conventional gasification, no $CO_2$ was found in the product gas. The experimental data were further used to validate the numerical modelling. The developed model showed good agreement with the experimental data using different oxidizing mediums [104–106]. In a study by Pang et al. [107] plasma-assisted gasification of biomass was investigated using a non-thermal plasma. The results showed an enhanced gasification yield by 10 % compared with thermal gasification for wood powder. It was also observed that the positive effect of plasma-enhanced gasification diminishes with the temperature when compared with the conventional gasification method.

Ignition and combustion of solid fuels with plasma in PF burners of thermal power plants have been developed as an alternative technology for the start-up and supporting firing. Most of the research activities on plasma-assisted ignition and combustion of PF investigate the applicability of the system developed via experiments and mathematical modelling. Only limited information could be extracted from the available literature concerning the critical influencing parameters and the required boundary conditions for the system design.

Plasma-assisted ignition of pulverised coal was demonstrated in a small-scale 1 m reactor using a microwave plasma, where no heat was supplied by the secondary air or from the reactor wall to the system. Ignition of low-rank coal with 30 % ash content and a fine particle size distribution ($Q_{90}$ of 75 %) within a burner thermal power of 40 kW to 150 kW was accomplished with 3.7 kW plasma power. However, flame extinction was observed when the plasma was turned off. The coal conversion was reduced from 41 % to 28 % as the burner air ratio was decreased from an overstoichiometric to a substoichimetric condition with increasing the burner load. Moreover, higher $NO_x$ levels compared with those during the conventional firing were reported [108].

In another study, the ignition and flame stabilisation of three types of pulverised coal with low, medium and high volatile content was accomplished in an experimental apparatus with

a 10 kW plasma torch. A higher temperature, correspondingly a longer stabilisation time, was required for the low volatile fuel to reach a good degree of devolatilisation. A plasma power corresponding to 10 % of the coal flame was specified as the required power amount for the ignition [109]. However, due to the scale of the experimental facility, this power demand seems extremely overestimated. Experimental data from large-scale test facilities have showed considerably lower ratios (see section 2.2.3).

Messerle and Gorokhovski et al. [11, 12, 110] introduced the concept of thermochemical preparation of coal by gasification of a portion of the coal stream with plasma under extreme substoichiometric conditions. Plasma gasification of coal with a plasma torch under an air ratio of less than 0.5 produces a combustible gas (syngas) with a high concentration of CO and $H_2$ together with partially oxidised char. This burning combustible solid-gas stream is subsequently mixed with a non-treated fuel stream and the secondary air in the furnace, resulting in rapid ignition and combustion of the entire fuel flow [12]. The coal particles exposed to high temperatures of plasma jet undergo instant devolatilisation and ignition that cannot be otherwise achieved. Besides, the high heating rate experienced by particles induces a heat shock that leads to particle fragmentation and ultimately an enhanced devolatilisation. The system features low $NO_x$ levels, owing to a two-stage burner design, where fuel-N is released under substoichiometric conditions, suppressing the fuel $NO_x$ formation mechanism [11, 12]. Messerle et al. [12, 111, 112] also developed and verified numerical simulations of plasma-assisted combustion in plasma fuel systems. Two numerical approaches were deployed: one-dimensional simulation containing the detailed chemical mechanism predicting the products of plasma-assisted coal devolatilisation and gasification inside the plasma fuel system, and three-dimensional simulation based on the fast chemistry mechanism, accounting for the plasma-coal interaction and the burner geometry. Satisfactory results were obtained by combining the two approaches, where the results of one-dimensional simulation were used as initial parameters for the full three-dimensional simulation of the burner. In both approaches, plasma was only considered as a heat source and the models did not include any additional reaction pathway related to the plasma kinetics.

Several numerical investigations of plasma-coal systems highlighted the importance of the mass flow rate and the velocity of the primary air. An increment in the primary air velocity increases the ignition distance and also reduces the peak temperature of the plasma-treated coal stream [113, 114]. When the amount of cold primary air flow is increased, flame blowout may occur due to excessive cooling of the hot flame region [114, 115]. Moreover, the plasma power and fuel's volatile content are other influencing parameters for the ignition. A higher plasma power produces a plasma jet with higher temperature fields, which correspondingly enhances the ignition performance. The results of numerical simulations showed reductions in the coal flame temperature by reducing the volatile content [114].

Katzer et al. [116] investigated the ignition of a finely milled pulverised lignite ($Q_{90}$ of 60 %)

with a 3 kW microwave plasma torch installed inside the pre-combustion chamber of a 400 kW burner. The results showed improvements in the ignition stability by the burner thermal load, i.e. dust concentration, and a reduced primary air velocity. The ignition was achieved at a lower thermal load when the primary air was decreased. Further optimisations to reduce the lower ignition limit (i.e. thermal load) were accomplished by increasing the swirl degree of the secondary air, via swirl number and an altered air distribution ratio of the swirled secondary air and the non-swirled tertiary air [116]. Another lignite quality with a coarser particle size distribution was also tested and it was concluded that a higher thermal load is required to initiate the ignition [117]. Trials with this coarser fuel showed unsuccessful ignition in the 400 kW facility [118].
An investigation of plasma-assisted ignition at a larger scale was performed by a research group [119] in a 5 MW facility, equipped with a chamber in which the fuel was pretreated with a 10 kW AC-powered plasma arc at an air ratio of 0.5. The temperature of the furnace wall was started to rise after around 7 min operation at a burner thermal load of 20 %.
The development of pulverised fuel firing systems with plasma support has led to its deployment in thermal power plants which will be reviewed in section 2.2.3.

### 2.2.2 Power plant flexibility and plasma-coal firing systems

A flexible power plant operation is described by three parameters: (I) start-up, (II) minimum load and (III) ramp rate. Since power plants are designed for base-load operation (operation at nominal design values), a flexible operation of these plants with more frequent start-ups and quick load variations brings about deteriorated performance and reduced plant's lifetime as well as increased expenditure. Optimisations are aimed to reduce the minimum load as well as the start-up time and to increase the ramp rate, while a trade-off between the costs and performance is required to optimize the plant for this new operational scheme [6, 120].
*Start-up*: Power plants have three start-up regimes, hot start-up: the plant is out-of-operation for maximum 8 h, warm start-up: the plant is out of operation for 8 h to 48 h and cold start-up: the plant is out of operation for more than 48 h. For a typical base-load plant, hot start-ups occur for example due to less power demand at night and a warm start-up could be related to a power demand reduction during weekends, while cold start-ups do not happen regularly. However, with the increasing penetration of intermittent renewable energies, the start-up regimes have changed significantly. The average overall start-ups for 49 hard coal power plants in Germany has increased from around 30 start-ups in 2009 to roughly 60 start-ups in 2014 [6].

The time between the start of operation and the minimum load is regarded as the start-up time, which is directly related to the type of the start-up. The colder is the furnace, the longer becomes the start-up time and more expensive auxiliary fuels need to be consumed. For a typical lignite plant, the start-up time for a hot and cold start-up is (4 to 6) h and (8 to 10) h, respectively. A shorter start-up time and an earlier start of the turbine operation reduces the auxiliary fuel consumption and waste heat loss and correspondingly the costs during the start-up process. Besides, a fast start-up allows the plant operator to respond quickly to the market requirements. Special attention needs to be given to the thermal and mechanical stress on the plant component when reducing the start-up time. As the number of start-ups and shutdowns has been increased over the past years and is expected to further rise in the coming years, the cost associated with the start-up process has become a growing concern [6, 7, 28, 120].
*Minimum load*: The lowest burner load at which pulverised fuel ignition is stable without the co-combustion of a supporting fuel is regarded as the minimum load. A low minimum load may prevent a shutdown and consecutively a start-up. This not only reduces the losses during the low price hours but also prevents additional costs and losses associated with a start-up and as well offers higher flexibility with regard to the synchronisation to the power grid [6]. The minimum load is often limited by the combustion stability. For a typical lignite power plant, the minimum load is (50 to 60) %, while for a state-of-the-art plant the value reaches (35 to 50) % [120].
*Ramp rate*: The rate at which the output load changes is regarded as the ramp rate. A high ramp rate provides a faster response to the market need and therefore improves the flexible operation. Here again, thermal and mechanical stresses are the main limiting factor in increasing the ramp rate. For a typical lignite power plant, the average ramp rate is (1 to 2) % per min, which can be increased up to (2 to 6) % per min in a state-of-the-art plant [6, 120].

In PF systems, stable ignition, particularly when low amount of heat is available in the furnace, e.g. during start-up and low load operation, is ensured by auxiliary fuels. The power plant start-up is performed with fuel oil or natural gas and a dedicated igniter. These highly flammable gaseous and liquid fuels are prone to ignition at low temperatures, which makes them a suitable option for ignition under low heat conditions. The igniters are typically gas or oil-fired spark igniters, which are available in various capacities. During the start-up, the furnace is warmed up with an auxiliary fuel until the conditions for PF ignition are reached. The rate of auxiliary fuel reduces and accordingly that of pulverised fuel increases until the burner reaches a stable operation without any supporting combustion. Low heat available in the furnace and also from the secondary air reduces the combustion efficiency and increases the emissions of carbon monoxide and hydrocarbons due to incomplete combustion. Thus,

to improve the combustion performance at the minimum load, auxiliary fuels may still be co-combusted [121].
Ignition of PF with plasma substitutes the conventional start-up systems, where instead of an auxiliary fuel, the PF is ignited even under cold start-up conditions. Depending on the plant and burner configurations, the conventional plant start-up is realised either by a dedicated start-up burner or the main PF burner contains a lance for the auxiliary fuel. Swirl burners are usually arranged with the latter configuration. Plasma-supported combustion for the start-up can also be arranged in both configurations, where the plasma system is either integrated into the main burner design or the plasma-coal system serves as a separate start-up and supporting burner, where direct or indirect firing mode can be arranged for both configurations. In case of direct firing, an external air preheating system is required to enable the operation of the milling system [10, 15].
Contrary to the direct firing, where the solid fuel is directly transported from the milling system to the burner, the indirect firing mode decouples the burners from the mill via a separate storage silo. The indirect firing is an additional flexibility measure, which allows a faster response to the load changing and a secure fuel supply to the burner at the low and minimum burner load. Moreover, in indirect firing, mill operation is independent of the burner thermal load, meaning the mills can run closer to the design values during part-load and minimum load operation [6, 7, 120].
The implementation of the plasma-coal firing system in power plants for start-up and also for supporting combustion not only improves the flexible operation of the plant but also allows for the utilisation of more diverse fuel qualities, offering fuel flexibility. Replacing the expensive gas and oil fuel with a comparably cheaper solid fuel saves a considerable amount of expenses not only related to the fuel cost but also the additional costs associated with dedicated infrastructure and safety measures required for these gaseous and liquid fuels.
A techno-economic study [122] on the deployment of a plasma ignition system in a 800 MW hard coal power plant showed only a fuel cost reduction by around 13.000 EURO for each warm start-up and 25.000 EURO for each cold start-up. Given the CAPEX and OPEX for retrofitting of 16 burners with the plasma ignition system and a total of 50 warm and cold start-ups and an additional ten hot start-ups per year, a payback period of less than four years is expected. The calculations considered the costs of the plasma system and the burner modification efforts, as well as the electricity consumption by the plasma system and the associated maintenance costs. The payback period reduces correspondingly by an increasing number of plant start-ups in the next years. General Electric [123] predicted a payback period of two to three years, depending on the site-specific conditions. Yantai Longyuan Ltd [13] estimated the expenditure saving of 3 Mio. USD during the commissioning of a 600 MW boiler with four burners with an additional 1.5 Mio. USD saving related to the oil system infrastructure. Messerle et al. and Gorokhovski et al. [12, 124] observed from the industrial

trials that the start-up time with the plasma system is shorter than a conventional start-up. They made an economic comparison for a conventional start-up with oil and plasma-assisted start-up using experimental data from retrofitted power plants in Kazakhstan and Russia and estimated a payback period of 12 to 18 months [12, 124]. However, within the provided data, no information regarding the cost of the pulverised fuel as well as the number and the type of start-ups is given.

In addition to the start-up process, plasma-assisted ignition can be employed as a supporting firing system during unstable firing. The unstable firing conditions may occur during the minimum load, part-load and ramping operation. As one of the major limiting factors in reducing the minimum load is the combustion performance and the flame stability, plasma-supported combustion can effectively boost the firing and reduces the emissions related to incomplete combustion.

The economic feasibility of plasma-assisted combustion was investigated for a 200 MW power station, where the analysis considered only the costs that were cut due to the reduction of the minimum load from 60 % to 30 % and assuming that this load reduction avoided 20 start-ups within a year. The results proved the economic viability of the application by only considering the benefits of reducing minimum load and showed that the investment cost of the plasma torch has a minor influence on the return period [125].

In Block F of Jänschwalde Power Plant, Germany (500 $MW_{el.}$ with 2 boilers), the implementation of dry lignite plasma burners in one boiler enabled the reduction of the minimum load from 180 $MW_{el.}$ to 100 $MW_{el.}$ using additional four dry lignite plasma burners accounting for total 120 $MW_{th}$. Pre-dried lignite was fed to the dry lignite plasma ignition burner via indirect firing and therefore its operation was decoupled from the milling system, which brought more flexibility to the plant by additionally supporting the minimum load operation, where the milling performance does not affect the firing [16]. Trials in GKM Power Plant, Germany, showed a clear improvement in the flame stability, where the flame blowout at 25 % burner load was prevented [123].

Ensuring the flame stability during the ramping by plasma-assisted combustion improves the ramping capability. Based on the operational data reported by Yantai Longyuan Ltd, the ramp rate was increased from 2 % per min during conventional operation to 5 % per min with plasma-assisted combustion [13].

Besides, the implementation of the plasma system for start-ups and low-load operations reduces the plant emissions compared with oil firing. This is because the ESP systems are incompatible with regard to the unburned oil particles and therefore they are out of operation during the start-up. In the case of no other dust removal system, the power plant releases a significant amount of dust and particles to the environment during the oil firing start-up. This can be avoided when plasma systems are deployed [13].

### 2.2.3 An overview of commercially available systems

The development of plasma-assisted ignition and combustion systems has been matured to the commercial demonstration. The design of each system can be different based on the type of the existing burners, the configuration of burners, the firing mode (direct/indirect) and more importantly the fuel quality.
Two principles have been generally employed for plasma-assisted combustion of solid fuels:

- Thermochemical preparation of an entire or a part of the fuel stream, via gasification and partial oxidation of fuel particles in a highly reducing atmosphere inside the burner, followed by full combustion in the second stage of the burner via secondary air at the burner throat [12, 13, 123, 126],
- Direct ignition and combustion of fuel particles at the burner throat under reducing or oxidizing atmospheres [14, 16].

Although the burner design, the plasma type and the operational and boundary conditions differ in each system, they all share a similar underlying principle: pulverised fuel particles are exposed to high-density energy of the plasma jet, experiencing extremely large heating rates and undergo instant devolatilisation and ignition. In the first concept, a large portion of the coal stream is treated with plasma to produce a sufficient amount of solid-gas reactive stream that ignites the rest of the coal flow. Therefore the plasma power is proportional to the amount of fuel that needs thermochemical preparation. On the contrary, in the second concept, the plasma works as an ignition source from which the combustion propagates through the entire dust cloud. As a result, plasma power is not directly related to the fuel quantity, but it is more dependent on the fuel quality.

Messerle and Karpenko et al. [10, 12, 127] developed the so-called Plasma-Fuel System (PFS). The PFS was designed based on the thermochemical preparation of fuel. More than 70 PFS were installed in 27 pulverised fuel boilers on different types of burners (swirl-burner and jet burner) for direct and indirect firing configurations in several Asian and East European countries by 2007 [10, 12, 127]. In this design, a DC plasma torch, in a power range of 50 kW to 200 kW, is integrated into the main burner, where it is located inside the fuel channel and perpendicular to the stream as shown in Figure 2.2.
PFS has a two-stage design that results in an initial flame formation at understoichiometric conditions and consequently lower $NO_x$ emissions. Moreover, reduced CO emissions and less unburned ash were observed after retrofitting the plant with PFS. PFS has been applied for cold start-ups without preheating of the primary air, where different fuel ranks from an-

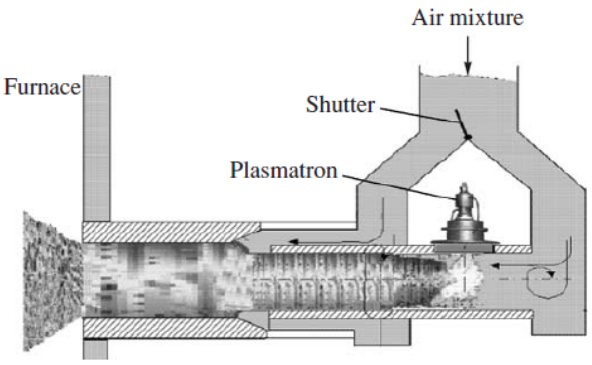


Figure 2.2: Sketch of the Plasma-Fuel System (PFS) obtained from [127]

thracite to lignite with particle sizes of mainly below 200 µm have been tested. Data obtained during commissioning showed ignition initiation within (3 to 5) s. The plasma system was turned off after stable operation was reached, depending on the plant and the fuel characteristics, the stabilisation time was reported between 35 min and 4 h [128–130]. Experimental data collected from different trials determined that the relative electric power of plasma[1] changes from 2.5 % for a fuel with 5 % volatile content to 0.25 % for a fuel with 50 % volatile content. The minimum load for the plant start-up and correspondingly the required number of the PFS for each plant was also found proportional to the fuel volatile content and could be calculated from an empirical equation [12, 128]. Further evaluations of the experimental data showed an optimised range of the dust loading (ratio of fuel to the primary air) for PFS stays between (0.5 to 1) kg/kg. In addition, the relative power consumption of plasma was, beside the volatile content, governed by the particle size, the dust loading, the temperature of the primary air and the length of the first stage burner chamber [131].

Yantai Longyuan Power Technology Co., Ltd developed a similar system, called Plasma Ignition and Combustion Stabilising System (PICS). In 2000, the first PICS installation was undertaken at Yantai power plant, China. By 2016, PICS had been massively deployed in almost 800 power plants in China, among them 52 plants operated completely oil-free start-ups. PICS generally follows a similar principle as that of PFS. Plasma-assisted ignition occurs in the first burner stage with the plasma torch positioned laterally in the fuel channel. The products of the first stage ignition respectively ignite the coal stream introduced in the second burner stage. A DC plasma torch is integrated into the main coal burner, where PICS acts as a normal PF burner after the start-up is completed and the plasma system is turned off. The system is also equipped with a steam-air pre-heater to provide the hot air required for the milling during cold start-ups [13].

Plasma ignition for dry lignite was developed by Babcock Borsig Steinmüller GmbH and was

[1] $\frac{P_{el.}}{\dot{M}_f H_u}$

installed in one of the boilers of Jänschwalde Power Plant (LEAG), Germany. Contrary to the above-introduced systems, this plasma system was designed based on the direct ignition of fuel particles at the burner tip. Within this concept, fuel itself serves as the main heat source and plasma only assists the ignition initiation and is in contact with only a small part of fuel particles. The plasma system is not responsible to support the combustion and therefore it is turned off shortly after the flame is formed. During the trial, ignition was achieved within few seconds and the plasma system was turned off approximately 20 s after. For this concept, the fuel needs to be ignitable enough to sustain the flame after a short period of plasma-supported combustion. All eight oil burners were replaced with eight 30 MW dry lignite plasma ignition burners featured with 3 kW microwave plasma [14–16]. This is equivalent to a relative plasma power consumption of 0.01 %, which is considerably smaller than the values reported by others [12, 128]. This is because, within this concept, flame formation is accomplished owing to a high-volatile fuel when ignition of a small portion of it with plasma assistance provides sufficient energy to devolatilise and to ignite the entire fuel stream. The microwave plasma lance is positioned laterally in an inner burner channel, where the coal particles are transported in an outer annulus and come into contact with the plasma jet at the burner tip. A separate fuel feeding system was considered for the dry lignite plasma ignition burners and therefore the system was not limited by the mill operation. The cold start-up of the boiler was performed successfully and the combustion of dry lignite was stopped after the start of main raw lignite burners and reaching the minimum load. In this configuration, the dry lignite plasma ignition burners offer an additional thermal power of 240 MW to the boiler, which can be deployed as a booster mode to increase the total power output of the plant and temporarily supporting the grid [14–16]. Since this concept strongly relies on the coal flame as the continuous heating source, only specific fuel qualities with high ignitability (e.g. high volatile content, low moisture content and small particle sizes) are suitable for this application [16].

Another system based on the thermochemical preparation of fuel was developed by General Electric, called Solid Fuel Ignition and Combustion Stabilisation System with Plasma at Intermediary Temperature Support (SOFIS-PIT). SOFIS-PIT consists of a multi-stage ignition system, which can be implemented for all types of fuels and combustion systems using an AC plasma torch. The system can be retrofitted to the plant's existing burner, where the PIT is positioned at the PF pipe elbow and a nozzle is integrated inside the PF pipe that divides the coal flow into two streams, creating multi-stage ignition. For cold start-ups and direct firing from the mill, a separate pre-heater is considered to provide the required heat for the start-up of the first mill. Based on plant-specifics, different types of pre-heaters such as a steam-air heat exchanger, a gas or liquid fuel duct burner and an electrical system can be utilized [123, 132]. SOFIS-PIT was installed in GKM Power Plant in Mannheim, Germany, on two hard coal tangentially fired burners of one level. The ignition was achieved

85 s after the start at the burner load of 25 % [123]. However, no information with regard to the required time for the flame stabilisation with plasma in the SOFIS-PIT is available.

Within the developed commercial systems, plasma torches of three types, DC, AC and microwave generators, have been mainly used. In DC arc plasma torches, direct current is used to draw an arc discharge between a cathode and an anode, where the plasma gas is ionised, extending the arc and forming the plasma jet. The commonly used plasma carrier gases are air, nitrogen, argon and helium but other gases such as water vapour can also be used. These torches can be found in the form of a transferred arc, the arc is transferred from a cathode to an external anode which serves the workpiece, and non-transferred arc, the anode is in a form of a nozzle and the electrodes are not involved in the process. Non-transferred torches are used for pulverised fuel burners, while plasma reactors can be also featured with transferred torches. DC arc plasma torches are equilibrium plasma and the temperature of the plasma jet is in the range of 10 000 K and can go up to 20 000 K. The temperature of the jet drops from the core towards the jet envelope. DC plasma torches have a high level of maturity and are available in a wide power range of 1 kW to 6 MW, which make them a suitable candidate for small and large-scale applications. DC systems offer an enhanced arc stability compared to AC plasma arcs [94, 102, 133]. However, a major drawback of electrode-based torches is the electrode erosion, which restraints the electrode lifetime. The common electrode material are copper, tungsten and graphite. Various parameters influence the erosion rate, such as the electrode material, the type of plasma carrier gas, the velocity of the carrier gas, etc. The electrodes need to be replaced regularly and frequent maintenance increases the operational cost and curtails the system robustness [102, 134, 135].
In AC plasma torches, the arc is produced by alternating current. At low frequencies, e.g. (50 to 60) Hz, plasma jet characteristics are comparable to DC plasma jets [102]. In AC systems developed for solid fuel applications, the plasma temperature is lower than microwave and DC plasma torches, which minimizes the heat loss by radiation and convection and correspondingly has a higher efficiency than the other torches. Each electrode serves consecutively as an anode and a cathode, resulting in less electrode erosion. This less erosion and longer electrode lifetime accordingly is expected to reduce the operational cost and maintenance efforts. Moreover, contrary to DC plasma torches, AC systems do not require any AC-DC convertor, and this lowers the system cost [134, 136]. Plasma at intermediate temperature is formed with a three-phase AC system, in which the temperature of plasma reaches the maximum of (2500 to 3000) °C [123, 137] The AC plasma system design offers the coexistence of several arcs, creating a large discharge volume. This configuration due to an unconfined form of the plasma jet allows the fuel particles to transport within the plasma volume, which intensifies the plasma-particle interaction [123]. However, the number of required electrodes increases, which can potentially increase the system capital cost.

In microwave plasma torches, the microwave is generated by a magnetron and is transferred through a waveguide to the discharge lance, where, normally with the help of an igniter, the plasma gas is ionised and the gas discharge is created. Microwave generators typically are operated at a frequency of 2.45 GHz providing a power range of up to a few kW. The up-scaling of microwave torches to 100 kW can be realised by generators operating at 915 MHz. Although microwave plasma is an electrode-free system and has a considerably longer lifetime than electrode-based systems, its application can be restricted by the power range and the equipment size and geometry [135, 138]. The temperature of a 3 kW microwave plasma torch was reported approximately 3500 °C [139].

# 3 Material and Method

## 3.1 Fuel properties

### 3.1.1 Chemical properties

Eight types of pre-dried lignite originating from Germany were investigated for the application of the plasma ignition system under cold furnace conditions with short-time plasma support. To study a variety of fuel properties for this application, lignites with distinct chemical and physical characteristics were selected. The lignites were provided by Lausitz Energie Power Plant AG (LEAG). Lignite A was dried brown coal from the Lusatia region that was dried to 10 % moisture by a tabular drier. This lignite, which had similar properties as the one used in the commercial-scale implementation of the dry lignite plasma burners in the Jänschwalde Power Plant [14], served as the reference fuel for this study due to its high reactivity and ignitability. Lignite B and lignite C also originated from the Lusatia region and were dried to 15 % and 20 % moisture, respectively, via a pressurised steam fluidised bed drier. The lignites from the Lusatia region were low in the ash and sulphur content. Lignite D and Lignite F derived from a mine in East Saxony, containing high ash, sulphur, moisture, and correspondingly low heating values. Lignite E, Lignite G and Lignite H were lignites from Central Germany with a high ash and sulphur content but high heating values. The Lignites from East Saxony and Central Germany were all treated and pre-dried to a moisture content between 12 % to 30 %. It should be noted that the "af" in Table 3.1 refers to the composition "as fired", the composition used for the ignition and combustion tests. The South African hard coal, as a medium-volatile hard coal was used for plasma-assisted combustion in part-load experiments. WP 1 was a wood pellet quality with a small ash content and a moisture content of about 11 % which slightly differs from WP 2 with almost no ash and a lower moisture content of 6 %. WP 2 had a quality corresponding to A1 classification of the wood according to ISO 17225-2 [140]. For each fuel, chemical analysis was performed after the fuel delivery, after the fuel sieving, before and after the measurement

Table 3.1: Chemical analysis of fuels

| Fuel | $H_u$ | $\gamma_{H_2O}$ | $\gamma_A$ | $\gamma_{VM}$ | $\gamma_C$ | $\gamma_H$ | $\gamma_N$ | $\gamma_S$ | $\gamma_O$ |
|---|---|---|---|---|---|---|---|---|---|
| | as fired (af) | | | | dry and ash free | | | | |
| | MJ/kg | $10^{-2}$ kg/kg (%) | | | | | | | |
| Lignite A | 20.8 | 10.5 | 5.0 | 48.5 | 66.3 | 4.9 | 0.8 | 1.2 | 26.9 |
| Lignite B | 20.2 | 14.5 | 4.7 | 46.4 | 66.4 | 5.0 | 0.8 | 0.7 | 27.2 |
| Lignite C | 18.8 | 19.4 | 4.0 | 43.8 | 66.7 | 5.2 | 0.8 | 0.9 | 26.5 |
| Lignite D | 15.8 | 20.2 | 12.5 | 42.6 | 63.3 | 4.9 | 0.8 | 5.5 | 25.5 |
| Lignite E | 18.2 | 21.3 | 10.5 | 41.3 | 71.0 | 5.7 | 0.7 | 4.3 | 18.3 |
| Lignite F | 12.2 | 29.3 | 19.6 | 32.5 | 67.3 | 5.4 | 0.9 | 6.5 | 20.0 |
| Lignite G | 19.6 | 12.6 | 15.5 | 44.7 | 70.1 | 5.8 | 0.7 | 4.7 | 18.8 |
| Lignite H | 15.8 | 26.6 | 14.9 | 36.4 | 69.7 | 5.8 | 0.7 | 7.9 | 15.8 |
| Hard coal | 25.9 | 2.6 | 15.3 | 26.3 | 83.4 | 4.9 | 1.8 | 0.6 | 9.3 |
| WP 1 | 16.3 | 11.0 | 1.75 | 69.7 | 50.6 | 6.1 | 0.2 | 0 | 42.1 |
| WP 2 | 17.4 | 5.8 | 0.3 | 77.3 | 50.6 | 5.9 | 0.3 | 0 | 43.2 |

campaign to verify the consistency in the composition.

The chemical analysis of coals was performed according to the following standards, DIN 51718 determination of the water content at 106 °C in $N_2$ atmosphere until the steady-state condition [141], DIN 51720 determination of the volatile content at 900 °C in $N_2$ atmosphere for 7 min [142], DIN 51719 determination of the ash content at 815 °C in $O_2$ atmosphere until steady-state [143], DIN 51734 determination of fixed carbon calculated by the difference [144], DIN 51732 determination of carbon, hydrogen and nitrogen contents in $O_2$-He atmosphere by thermal conductivity detection of combustion gases [145], DIN 51724-1 determination of the sulphur content by ion chromatography of a sulfate-containing solution [146] and DIN 51900-1 determination of calorific value by adiabatic combustion in a calorimeter [147].

For biogenic solid fuels, the analysis methods are adopted accordingly. For wood pellets the chemical analyses were performed according to the standards of solid biofuels based on ISO 18134-3 determination of the moisture content [148], ISO 18123 determination of the volatile content [149], ISO 18122 determination of the ash content at 550 °C [150], ISO 16948 determination of carbon, hydrogen and nitrogen [151], ISO 16994 determination of the sulphur content [152] and ISO 18125 determination of calorific value [153].

### 3.1.2 Physical properties

Fuels are prepared in two particle size series for pilot-scale experiments in Chapter 5 and dust explosion tests in Chapter 4. Excluding Lignite A that is a finely milled dust with a median diameter of 45 µm, other lignites used for pilot-scale experiments were sieved with a mesh size of 2 mm to eliminate operational and technical problems related to fuel dosing. The South African hard coal was milled with an impact classifier mill to a fineness of 32 µm median diameter. The hard coal was finer than typical hard coal particle sizes with 15 % to 20 % of material above the 90 µm size. The wood pellets were milled in a hammer mill with a sieve size of 1 mm. The fuels that were investigated by lab-scale dust tests were further sieved with a mesh size of 0.5 mm.

Figure 3.1 illustrates the cumulative volumetric particle size distribution of lignites sieved with 2 mm mesh size and wood pellets milled with 1 mm size used for the pilot-scale experiments.

Table 3.2 summarizes characteristic particle sizes of *D10*, *D50*, and *D90* for the coarse and fine material and cumulative volumetric distributions of particles below 500 µm, $Q_{500}$, and below 63 µm, $Q_{63}$. Lignite B, Lignite C and Lignite D had a median diameter below 450 µm, where *D50* of Lignite F, G and H stayed between 550 µm and 900 µm. Lignite E with a median diameter of 1048 µm has the largest particle sizes. It should be mentioned that the characteristic diameter of the pre-dried lignites used in this study were relatively coarser compared with typical fineness of lignites with 57 % to 63 % volatile content, milled in power plants that comprise less than 1 % particles larger than 1000 µm size and around 40 % to 50 % particles below 90 µm [45]. However, these coarse particle sizes were of interest to determine if plasma-assisted ignition has potential to shift the ignition to coarser particle sizes

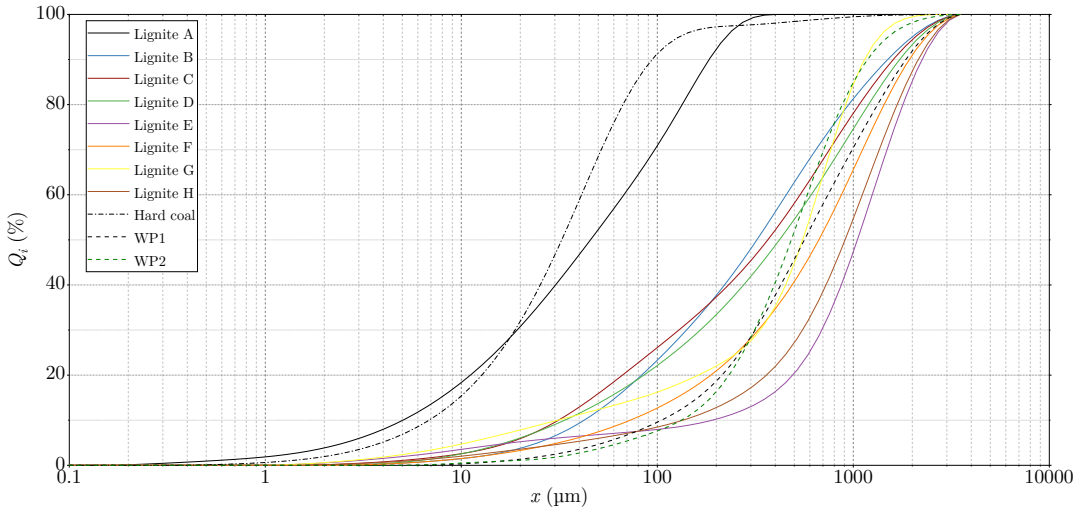


Figure 3.1: Cumulative volumetric particle size distribution measured by laser diffraction

Table 3.2: Physical properties

| Fuel | *D10* | *D50* | *D90* | $Q_{500}$ | $Q_{63}$ | *D10* | *D50* | *D90* | $Q_{63}$ | *a* |
|---|---|---|---|---|---|---|---|---|---|---|
| | 2 mm sieved/milled | | | | | 0.5 mm sieved | | | | |
| | µm | | | % | | µm | | | % | $m^2/g$ |
| Lignite A | 5 | 45 | 184 | 100 | 58 | 5 | 45 | 184 | 66 | 0.56 |
| Lignite B | 42 | 320 | 1500 | 65 | 16 | 19 | 83 | 225 | 40 | |
| Lignite C | 31 | 366 | 1600 | 59 | 19 | 22 | 149 | 402 | 31 | 1.79 |
| Lignite D | 34 | 420 | 1726 | 54 | 16 | 15 | 128 | 503 | 37 | 19.80 |
| Lignite E | 190 | 1048 | 2247 | 20 | 7 | | | | | |
| Lignite F | 73 | 667 | 1935 | 41 | 9 | 18 | 173 | 520 | 26 | 5.00 |
| Lignite G | 31 | 551 | 1143 | 45 | 13 | 8 | 80 | 337 | 46 | 15.50 |
| Lignite H | 134 | 907 | 2147 | 26 | 7 | | | | | |
| Hard coal | 7 | 32 | 94 | 98 | 77 | 5 | 40 | 158 | 76 | |
| WP 1 | 105 | 563 | 1854 | 56 | 6 | | | | | |
| WP 2 | 132 | 482 | 1184 | 51 | 5 | 44 | 237 | 676 | 15 | |

and consequently to reduce the milling operating costs.

The particle sizes in Table 3.2 represent volumetric distribution measured by the laser diffraction principle using Malvern Mastersize 3000 analyser and Horiba LA-950 analyser for samples used in pilot-scale experiments and lab-scale tests, respectively. Based on the laser diffraction method, also known as the light scattering method, the light scattering pattern is a function of the particle size. The intensity and the angle of the light scattered by the dispersed particles in a measurement cell are detected and translated into particle size using the Mie and Fraunhofer theory. The Fraunhofer theory is only applicable for particles that are larger than the light wavelength of 0.63 µm, while the Mie theory also accounts for particles as small as 0.01 µm size [154, 155].

In addition to particle size characteristics, selected lignites sieved to 0.5 mm, were further analysed for the determination of specific surface area, *a*. The specific surface area was determined based on the BET method according to DIN ISO 9277. Within this method, $N_2$ gas at 77 K is passed through the sample at several relative pressures and the amount of adsorbed gas on the surface is determined. The specific surface area is then calculated from a linear regression of BET equation on the relative pressure [156]. As can be seen from Table 3.2, the powders represent large variations in the specific surface area ranging from 0.56 $m^2/g$ to 19.8 $m^2/g$.

#### 3.1.2.1 Particle size distributions of milled/sieved wood

To explore the role of particle size on performance of the plasma ignition system, 1 mm milled wood pellet (WP 2) was used. WP 2 was prepared in different particle sizes with finer and coarser distributions. The original milled WP 2 was sieved with 100 µm, 212 µm and 315 µm mesh size producing S1, S2 and S3 size distributions, respectively. The fine shares separated by the sieving were mixed proportionally with the original material to produce M3, M2 and M1 size distribution with an increased share of fine particles below 315 µm, 212 µm and 100 µm, respectively.

Since wood particles are not completely spherical, the standard sieve analysis for the determination of particle size is a more representative approach. The gravimetric particle size analysis was performed in a vibrating sieving machine according to ISO 17827 [157]. However, the sieve mesh size was selected with regard to the information required for the sample particle sizes. Figure 3.2 shows the cumulative gravimetric particle size distribution of the prepared biomass material.

The characteristic particle sizes and cumulative gravimetric distribution of sieved and mixed wood pellets are summarised in Table 3.3. The volume distribution is comparable to the mass distribution when the density is constant. The volumetric distribution measurements slightly overestimated the particle sizes of WP 2 compared with the gravimetric measurement [27]. This corresponds to a *D50* of 482 µm by laser diffraction and 391 µm by the sieve analysis.

The particle size distribution shifts to coarser particles from M3 to S3. Although *D50* for WP 2, S1 and S2 stayed constant, more attention should be given to *D10* to distinguish

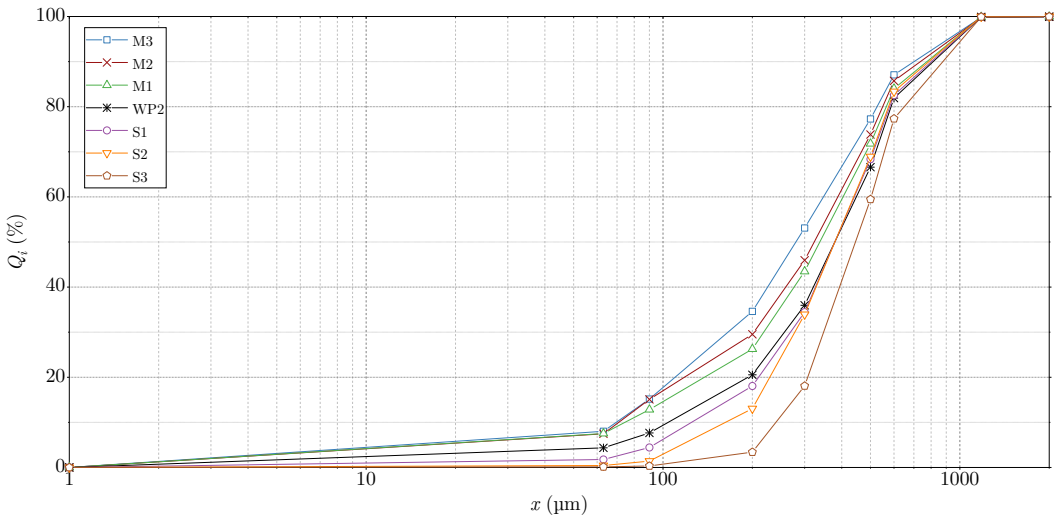


Figure 3.2: Cumulative gravimetric particle size distribution for sieved and mixed wood pellets

Table 3.3: Characteristic particle sizes and cumulative gravimetric distribution of individual fractions

| Fuel | *D10* | *D50* | *D90* | $Q_{500}$ | $Q_{200}$ | $Q_{90}$ | $Q_{63}$ |
|---|---|---|---|---|---|---|---|
| | µm | | | % | | | |
| M3 | 70 | 283 | 733 | 77.3 | 34.6 | 15.2 | 8.0 |
| M2 | 72 | 329 | 776 | 73.8 | 29.5 | 15.1 | 7.5 |
| M1 | 76 | 346 | 819 | 71.8 | 26.3 | 12.8 | 7.5 |
| WP 2 | 110 | 391 | 860 | 66.6 | 20.5 | 7.7 | 4.4 |
| S1 | 135 | 392 | 848 | 68.4 | 18.1 | 4.4 | 1.8 |
| S2 | 171 | 392 | 832 | 68.9 | 13.1 | 1.4 | 0.4 |
| S3 | 245 | 454 | 925 | 59.5 | 3.4 | 0.3 | 0.1 |

the differences in the fine fraction. A better overview of the representative numbers can be given by the cumulative distribution of critical particle fractions. As can be seen, the share of particles below 63 µm was doubled in the M-series and more than halved in the S1 distribution compared with the original material. Similarly, the share of particles below 90 µm was increased from around 8 % in WP 2 to an average of 14 % in the M-series, while it reduced to 4 % in S1 and almost to 0 in S2 and S3 distributions.
S1 and WP 2 demonstrated comparable $Q_{200}$ numbers, 18 % and 20.5 %, respectively, while it increases notably to 26 %, 29 % and 34 % in M1, M2 and M3 series, respectively. These numbers are of high importance for evaluating the results in section 5.5.

# 3.2 Lab-scale investigations of dust ignition characteristics

## 3.2.1 Laboratory dust explosion tests

### 3.2.1.1 Dust explosibility screening and determination of minimum ignition energy (MIE)

**Dust explosibility screening:**
The dust explosibility was determined, based on DIN EN 80079-20-2, in a so-called modified Hartmann apparatus. It comprised of a 1.2 L vertical glass tube with a diameter of 68 mm

(a height of 300 mm), in which a specific quantity of powder was dispersed with a blast of pressurised air from the bottom of the glass and it was ignited via an ignition source located 100 mm above the dust dispenser. The ignition source was a high voltage continuous spark, created by standardised electrodes and a high voltage transformer. The spark discharge represented an energy equivalent to 10 J. However, the energy provided by spark discharge was not a discrete value. Therefore dust that was not ignited with continuous spark was categorised with a minimum ignition energy larger than 1 J. When the ignition was not accomplished with the continuous spark, a glowing coil with a corresponding energy of 10 J was used to assess the explosibility. For the dusts that were not ignited with the glowing coil, a minimum ignition energy larger than 10 J was assigned [158, 159]. The glass tube had a pressure relief cover on its top, where the visual observation of the tube lid at the course of ignition was translated into indications. In case of flame propagation in the glass tube, three indications were defined to describe the intensity of the flame propagation as following: "0" no opening or lift of the cover, "1" small lift or opening of the cover and "2" complete opening of the cover. Powders that reached a maximum indication of "0" and "1" were categorised in the explosion class of "St 1" (weak explosion with $K_{st}$-value<200 bar m/s) [160]. The screening tests were performed over a wide range of dust concentrations and when no ignition was observed within three repetitions, the dust was considered not explosive under the respective boundary conditions.

**Determination of MIE:**

The MIE was similarly determined in the modified Hartmann apparatus based on DIN EN 13821. The spark discharge of a defined energy content was generated by a discharge circuit, containing a capacitor and a 1 mH inductance. Discharge values of (1, 3, 10, 30, 100, 300 and 1000) mJ were adjusted by charging the capacitor with a known voltage. The ignition energy was tested in descending order at several dust concentrations and ignition delay times. The ignition delay time was defined as the time gap between the spark discharge and the dust dispersion.

The MIE is specified within a range, where the lower limit represents the energy at which no ignition occurred within 10 repetitions and the upper limit stands for the minimum energy at which ignition took place [161].

#### 3.2.1.2 Determination of minimum cloud ignition temperature (MCIT)

MCIT was determined according to the standard procedure described in VDI 2263-1 [159]. The dust sample was dispersed with air in a 170 mm horizontal oven, known as the BAM furnace, against an impact plate located in the oven centre, where the temperature was

measured. The electrically heated oven was heated up to its maximum temperature of 600 °C and tests were performed at 10 K descending intervals. The test was demonstrated for three dust concentrations. The lowest temperature at which ignition occurred within a 10 s delay time was considered the minimum cloud ignition temperature. However, the ignition was normally accomplished in less than one second. According to the DIN EN 80079-20-2, the MCIT is defined as the lowest temperature at which ignition occurs, reduced by 20 K for temperatures above 300 °C and by 10 K for temperatures below 300 °C [158, 159]. The MCITs reported in this work are per DIN EN 80079-20-2.
According to the standards, it is recommended to use samples with particle sizes smaller than 63 µm. Even though, since the results need to eventually be correlated with pilot-scale experiments, samples with coarser particle sizes (smaller than 500 µm), more similar to those used in the pilot-scale experiments, were considered.

#### 3.2.1.3 Determination of explosion characteristic parameters

The explosion characteristics of dust clouds were determined according to the standards of VDI 2263-1 [159], DIN EN 14034-1 [162] and DIN EN 14034-2 [163]. The Siwek 20 L sphere was used, in which the dust sample was dispersed and ignited via two chemical (pyrotechnical) igniters of 5 kJ each, located in the centre of the sphere. The pressure was measured and recorded continuously in the course of the explosion tests, using two piezoelectric pressure sensors. $p_{\mathrm{m}}$ is the corrected value of the maximum explosion pressure obtained from the pressure time history at each dust concentration, measured by the online pressure sensor. A correction is applied, which takes into account the cooling effect from the sphere wall when the pressure is above 5.5 bar and the pressure effect of the chemical igniter when the maximum pressure is below 5.5 bar. The corrections are applied to harmonize the results obtained in the 20 L sphere and the 1 $\mathrm{m}^3$ vessel, which is another test apparatus for the determination of explosion parameters. The rate of pressure rise, $dp/dt$, was calculated from the slope of the tangent point in the pressure time history for each dust concentration. The explosion tests were performed at several dust concentrations in the range of (125 to 1500) $\mathrm{g/m}^3$. The maximum value of the corrected explosion pressure and the maximum rate of pressure rise, over the dust concentrations tested, were identified as $p_{\mathrm{max}}$ and $(dp/dt)_{\mathrm{max}}$, respectively.
To compare the explosibility at different size chambers, a volume-independent parameter was derived, known as the dust deflagration index, $K_{\mathrm{st}}$-value. The dust deflagration index was calculated as

$$K_{\mathrm{st}}\text{-value} = (\frac{dp}{dt})_{\mathrm{max}} V^{1/3} \tag{3.1}$$

, where $V$ stands for the volume of the explosion chamber [162, 163].

### 3.2.2 Ignitability characteristic number

The original ignitability characteristic number ($ZWZ$) was defined as the ratio of ignition potential, $N_{\mathrm{Z500}}$, to the ignition temperature. The ignition potential of a solid fuel was described as the energy of volatile matter, released from a water-free state through the pyrolysis process up to the temperature of 500 °C. The ignition temperature in the above definition was specified as the minimum temperature at which a dust cloud of particles below 63 µm ignites within 150 ms [29]. The application of ignition potential on a water-free basis is more relevant for comparing the ignitability between different coal ranks, which mainly differ in their degree of coalification and correspondingly the volatile content. However, when fuels have similar ranks but differences in the moisture content, the calorific value differs significantly between the raw and water-free states. Therefore, the ignition potential determined on the as fired (af) fuel basis was found more relevant in this work when lignites with distinct water contents were concerned. The modified ignitability characteristic number, $ZWZ_{\mathrm{mod.}}$, developed in this study was defined as the ratio of ignition potential on the as fired fuel basis, $N_{\mathrm{Z500,\ af}}$, to MCIT measured in accordance to the DIN EN 80079 standard.

$$ZWZ_{\mathrm{mod.}} = \frac{N_{\mathrm{Z500,\ af}}}{\mathrm{MCIT}} \tag{3.2}$$

To determine $N_{\mathrm{Z500,\ af}}$, samples sieved by 500 µm mesh size were heated up in the presence of $N_2$ to 500 °C, with a heating rate of 30 K/min, until the steady-state condition was reached. The calorific value and major composition of the remaining char was determined, which allowed to solve a mass and energy balance based on fixed carbon as the tracer and to determine the devolatilisation degree (the share of released volatile matter), $\eta_{\mathrm{devol}}$, the calorific value of the released volatile matter, $NCV_{\mathrm{VM}}$, and the ignition potential, according to Eq. 3.3 to 3.5

$$\eta_{\mathrm{devol}} = \frac{\gamma_{\mathrm{VM}}\gamma_{\mathrm{c_{fix,ch}}} - \gamma_{\mathrm{VM,ch}}\gamma_{\mathrm{c_{fix}}}}{\gamma_{\mathrm{VM}}\gamma_{\mathrm{c_{fix,ch}}}} \tag{3.3}$$

$$NCV_{\mathrm{VM}} = \frac{H_u\gamma_{\mathrm{c_{fix,ch}}} - H_{u,\mathrm{ch}}\gamma_{\mathrm{c_{fix}}}}{\gamma_{\mathrm{VM}}\gamma_{\mathrm{c_{fix,ch}}} - \gamma_{\mathrm{VM,ch}}\gamma_{\mathrm{c_{fix}}}} \tag{3.4}$$

$$N_{\mathrm{Z500,\ af}} = \frac{H_u\gamma_{\mathrm{c_{fix,ch}}} - H_{u,\mathrm{ch}}\gamma_{\mathrm{c_{fix}}}}{\gamma_{\mathrm{c_{fix,ch}}}} \tag{3.5}$$

, where $\gamma_{\mathrm{c_{fix,ch}}}$ and $\gamma_{\mathrm{VM,ch}}$ denote the mass fraction of fixed carbon and volatile matter in the remaining char sample and $H_{u,\mathrm{ch}}$ refers to the net calorific value of the char.

# 3.3 Pilot-scale experiments on the plasma ignition system

## 3.3.1 400 kW combustion test facility

Figure 3.3 shows the 400 kW combustion test facility that was used for pilot-scale experiments on cold start-up ignition tests and plasma-assisted combustion experiments. The down-fired combustion chamber consisted of six segments with an inner diameter of 0.85 m for segments one to four, where each segment was 1 m in length, and 0.75 m for segments five and six with a total length of 3 m. The 7 m reactor was cooled by a water jacket, where the cooling water ran in bottom-top direction.
The first three segments and the top plate of the reactor were covered with a refractory lining. The temperature at the furnace wall was measured via thermocouples at several distances from the burner outlet. The reactor was featured with several measurement ports along its

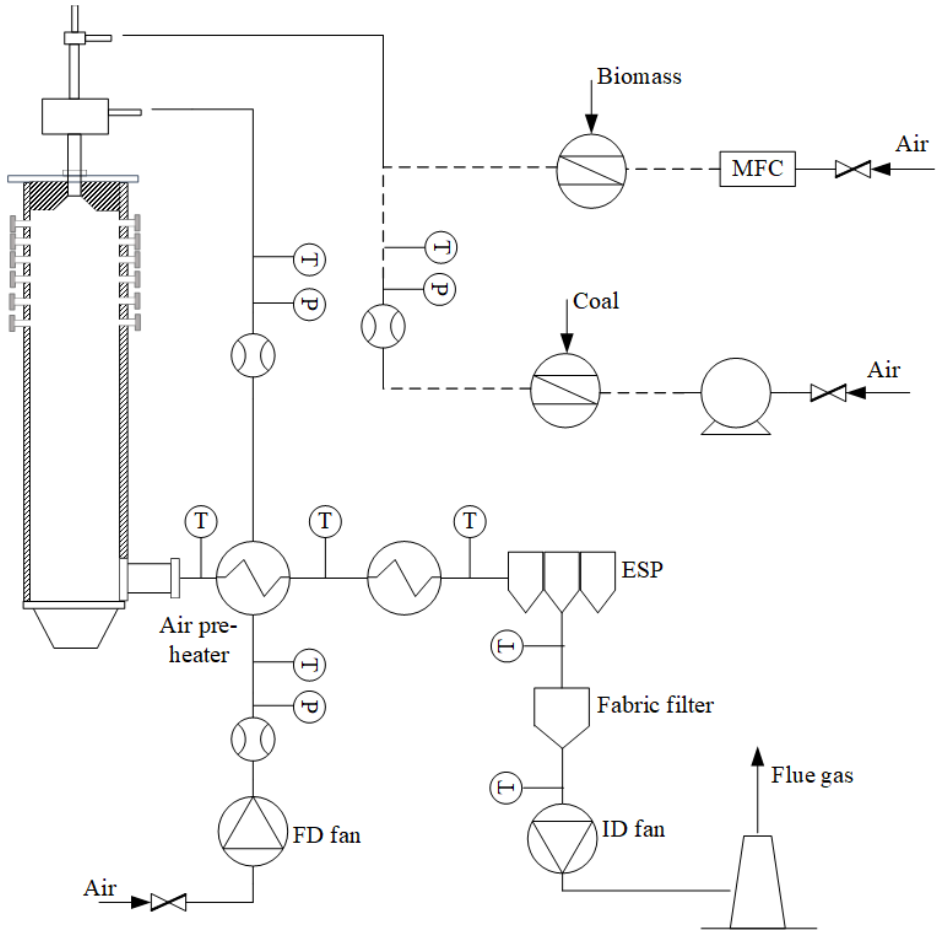


Figure 3.3: Schematic diagram of the 400 kW combustion facility

length, allowing optical and in-flame measurements. The combustion reactor was followed by a flue gas cleaning line, including an air pre-heater, a heat exchanger and particle removal systems, e.g. an electrostatic precipitator and a fabric filter. The flue gas temperature was monitored via thermocouples along its path. An induced draught (ID) fan sucked out the flue gas from the reactor to the stack. The combustion air was supplied to the burner with a forced draught (FD) fan and was passed through the air pre-heater. Before the burner, the combustion air was distributed into two ducts, controlled by vortex flowmeters. The ducts were connected to the two inlets of the burner's windbox. The vortex flowmeters require a minimum Reynolds number of 4000 for an accurate measurement [164]. The minimum amount of combustion air supplied to the burner was hence restricted by the lower limit of the flowmeters. The facility was equipped with gravimetric feeding systems, a fluidised bed system for coal and a double screw feeder for biomass and alternative fuels. The fluidised bed feeding system was featured with a perforated rotating disk. The feeding rate was adjusted with the rotation frequency of the disk. The fluidised materials were distributed in the hollow space of the perforated disk and transported with a carrier gas to the burner. In the double screw feeding system, the feeding rate was proportional to the screw's rotation speed. The screws conveyed the materials to a compartment from where the primary air transported them to the burner. Since the ignition tests had a short period, both feeding systems were calibrated before the experiments for each fuel tested. The calibration was performed with three repetitions to ensure the accuracy and reproducibility of data.

### 3.3.2 Plasma-integrated swirl burner

A movable block swirl burner was modified and integrated with a DC-arc plasma torch. The burner was mounted centrally on the burner plate, see Figure 3.4. The burner outlet was followed by a 0.1 m built-in quarl of the burner plate. The plasma lance was positioned coaxially in the central channel of the burner, which originally was designed for a natural gas lance or oil gun. The plasma lance was movable in forwards or backwards directions, allowing variable vertical lance positioning in the burner. Figure 3.4 shows three plasma lance positions. Plasma "position 0" indicates the lance positioning at the burner throat. The lance was retracted inside the primary air nozzle by 40 mm and 80 mm, denoted as "position -40" and "position -80", respectively. The plasma retraction inside the burner created a fuel-rich pre-combustion section, before mixing the fuel stream with the secondary air. This pre-combustion zone was expected to support the ignition, where a reduced air ratio favours a staged ignition.

The fuel particles were directed towards the plasma jet via a contraction at the outlet of the

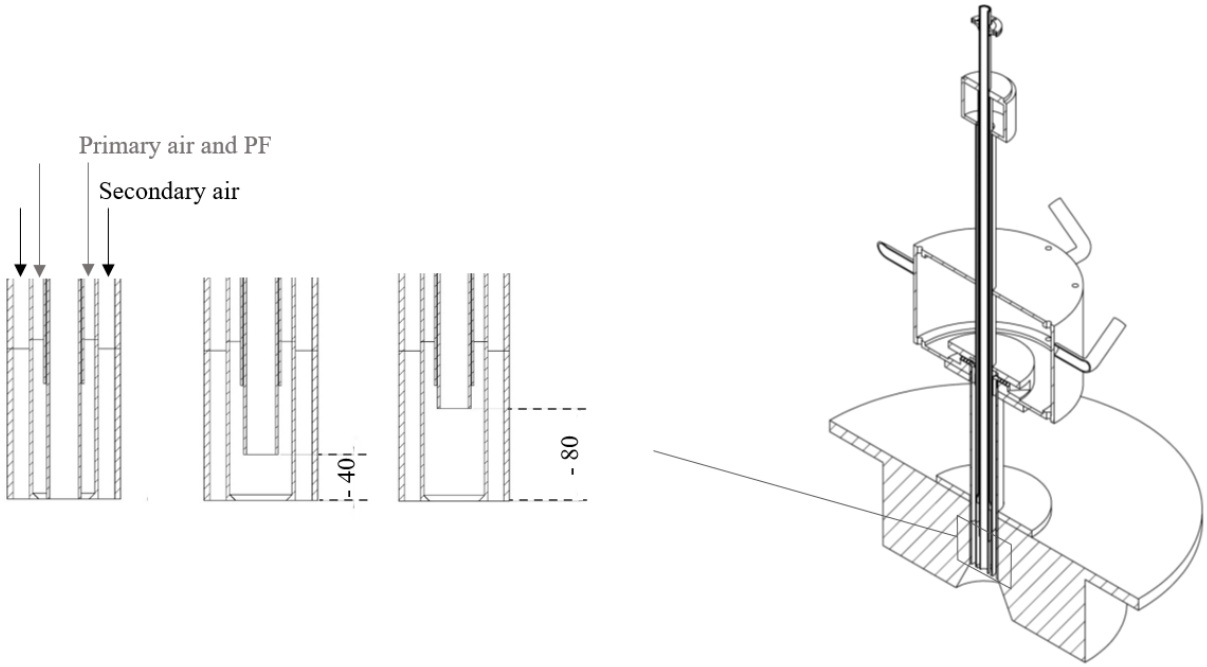


Figure 3.4: Left: sketch of the burner outlet with plasma position 0, -40 and -80, right: cross section view of the plasma-integrated swirl burner

primary air nozzle. Figure 3.5 shows the three designs considered for the primary air nozzle outlet. The standard design, denoted as Nozzle 1, had a contraction ring with 45° inclination angle. Nozzle 2 had a contraction with 90° edge ring to increase the particles' residence time at the burner outlet. Nozzle 3 with a 30° contraction was featured with evenly distributed grooves of 4 mm in depth. This toothed nozzle had a design similar to that of DS® burner of the Company Mitsubishi Power that showed promising results in flame stabilisation and early ignition of particles at the nozzle outlet [86, 165]. Since, primary air swirling concentrated the particles at the inner circumference of the fuel channel, the nozzle rings were dedicated to reduce the particles' velocity and consequently increasing the residence time within the critical ignition zone and also to direct the particles towards the centre, where the plasma

Figure 3.5: Primary air nozzle design, from left to right: Nozzle 1, Nozzle 2 and Nozzle 3

flame was located.

The fuel and primary air in the middle annulus of the burner were swirled by axial vanes for a better mixing of the pulverised fuel and the secondary air flow. Under the assumption of thin vanes, Equation 3.6 gives the swirl number of an annular swirler, where $\alpha$ is the vane angle and $R_h$ and $R$ are the vane hub and the primary air tube radius, respectively [79].

$$S = \frac{2}{3}\left(\frac{1-(R_h/R)^3}{1-(R_h/R)^2}\right)\tan\alpha \tag{3.6}$$

For vanes with 45°, the above equation yields $S = 0.9$ for the primary air after the swirl vanes. It should be noted that the vanes were located 0.12 m upstream from the burner outlet and the theoretical swirl number does not account for the swirl decay from the swirler to the burner outlet.

The modular design of the burner allowed for easy disassembling of the burner's parts. For dedicated tests, the axial vane swirler module was replaced with a vane-free module, producing non-swirled primary air flow.

The velocity of the primary air was adjusted by altering the volume flow rate. The primary air had a volumetric flow rate of 40 $m^3$/h ($STP$) and 30 $m^3$/h ($STP$), depending on the fuel quality, which was equivalent to a velocity of 15.5 m/s and 11.5 m/s, respectively.

The secondary air passed through a movable block swirl generator. The movable-block swirl consisted of fixed and movable blocks, which generated varied swirl degrees by flow distribution between the tangential and radial channels. The tangential channels were created by an oblique surface of each block, where the inclination angle of the block surface, $\alpha$, is the angle between the radial direction and tangential channel axis, see Figure 3.6. The aperture angle of the tangential channel, $\xi$, is defined as the angle of the channel opening in

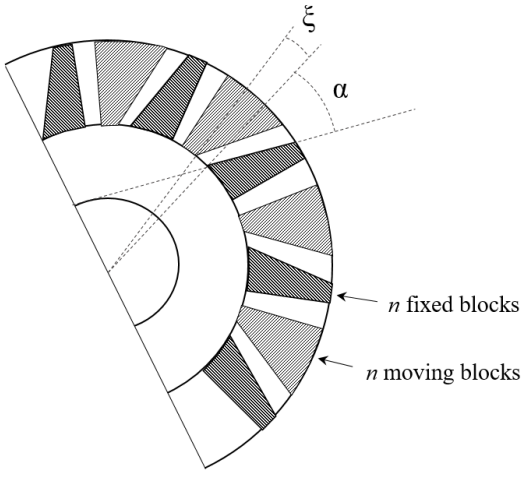


Figure 3.6: Cross section view of the movable block swirl generator

the radial direction, where $\xi_m$ is the maximum aperture angle at which the flow only passes through the tangential channels. The swirl adjustment of $\xi/\xi_m$ defines the swirl intensity by distributing the flow in radial and tangential openings. The theoretical swirl number of the movable block swirler, calculated from the axial flux of the axial momentum $G_x$ and the axial flux of the tangential momentum $G_\phi$, is given as

$$S = \frac{G_\phi}{G_x R} = \sigma \frac{R}{2B} \left[ 1 - \left( \frac{R_h}{R} \right)^2 \right] \tag{3.7}$$

, where $R_h$ and $R$ are the inner and outer radius of the secondary air annulus, respectively and $B$ is the width of the radial and tangential channels. The coefficient $\sigma$ is defined as

$$\sigma = \frac{2\pi}{n\xi_m} \sin\alpha \frac{\cos\alpha(\xi/\xi_m)}{[1-(1-\cos\alpha)\xi/\xi_m]^2} \tag{3.8}$$

, where $n$ is the number of radial and tangential channels, i.e. number of fixed and movable blocks [79, 166]. Eq. 3.7 and Eq. 3.8 are valid under the following assumptions:

- uniform axial velocity distribution in the secondary air duct (plug flow velocity profile)
- uniform velocity profile within the radial and tangential channels of the swirler
- negligible decay in the swirl velocity between the swirler and the burner outlet [166].

The movable block swirler employed had 12 fixed and movable blocks, the maximum aperture angle of $\xi_m = 8°$, the inclination angle of $\alpha = 50°$ and the channel width of $B = 60\,\text{mm}$. This resulted in a maximum swirl number of $S = 0.9$, assuming no loss in the tangential momentum within the 0.6 m distance from the movable-block swirler and the burner outlet. The maximum swirl number of 0.9 was the default setting used for the experiments in chapters 5 and 6, unless otherwise is mentioned. Table 3.4 shows the swirl number calculated at different adjustment ratios. A comparison between experimental data and numerical simulations showed slightly lower values by the theoretical calculations. It was mainly related to the simplifications assumptions made, which neglected the loss of tangential momentum related to the wall friction between the swirler and the burner outlet [166, 167].

Table 3.4: Theoretical swirl numbers of the movable block swirler

| $\xi/\xi_m$ | $S$ |
|---|---|
| 0.25 | 0.1 |
| 0.5 | 0.3 |
| 0.75 | 0.5 |
| 1 | 0.9 |

### 3.3.3 Atmospheric plasma torch

Non-transferred DC arc plasma torches are used in this study. An arc discharge was formed between the cathode located in the centre of the lance and the anode located around the lance. The electrodes were water-cooled. Plasma system I (PS I) was a DC-arc plasma torch with a power range of (3 to 7) kW. Air was used as the medium gas and plasma power was adjusted with the electric current and the flow rate of the plasma medium gas. Copper electrodes were used for both anode and cathode. The plasma jet produced had a length of (70 to 100) mm, and a width of 12 mm at the plasma nozzle outlet and a maximum width of 25 mm, determined by visual measurements.

A second DC-arc plasma system, plasma system II (PS II) was used for dedicated experiments to compare the systems and their performance for the cold-start-up ignition application. PS II used a mix of air (92 %) and argon (8 %) as the medium gas. Argon was aimed to protect the coating and increase the lifetime of electrodes. PS II consisted of copper and tungsten electrodes. It produced a less volumetric plasma jet than PS I with (40 to 65) mm length and a width of 16 mm at the plasma nozzle outlet up to 22 mm.

The operational parameters of PS I and PS II are presented in Table 3.5. The velocity of plasma medium gas for each power was calculated by the average volume flow rate of the gas at the temperature of 25 °C over the nozzle outlet area.

For PS I two power ranges of approximately 4 kW and 7 kW were adjusted. The 4.2 kW power was considered as the default setting for the cold ignition tests and plasma-assisted combustion during part-load operation. PS II was only operated with one power range of around 7 kW and was considered comparable with the higher power of PS I. PS II had a relatively higher range of current and correspondingly lower voltage compared with PS I. It also had a lower gas flow rate and considerably a slower medium gas velocity compared with PS I even at the lower power of 4.2 kW. Both plasma system manufacturers claimed a thermal efficiency of approximately 70 %, which was equivalent to a thermal plasma power of around 3 kW and 5 kW.

Investigations on the plasma jet properties performed by the Institute of Interfacial Process

Table 3.5: Operational parameters of plasma systems

| Plasma system | $I$ | $E$ | $P_{\text{el.}}$ | $\dot{V}$ | $w_{\text{PG}}$ |
|---|---|---|---|---|---|
| | A | V | kW | l/min ($STP$) | m/s |
| PS I | 30-31 | 140-150 | 4.2-4.5 | 25-30 | 4.0-4.8 |
| | 45-47 | 150-155 | 7.0-7.3 | 30-35 | 4.8-5.6 |
| PS II | 55-60 | 115-120 | 6.6-7.2 | 22 | 1.8 |

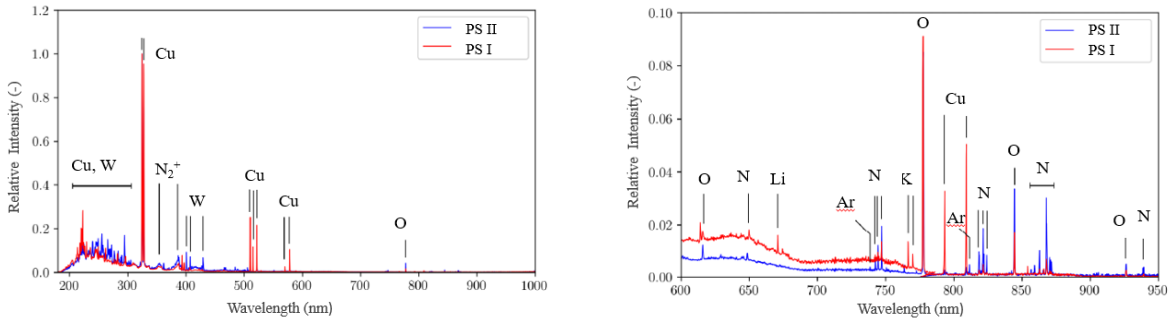


Figure 3.7: Spectral emissions of PS I and PS II obtained from [168], left: spectral emissions over the entire wavelength, right: spectral emissions in the IR region

Engineering and Plasma Technology of the University of Stuttgart indicated similar plasma jet properties for both systems [168]. Figure 3.7 shows the optical emission spectroscopy measurement at the plasma flame root, where comparable spectral emissions by the two systems were observed. The emissions are most pronounced in the UV range (wavelengths between 100 nm and 380 nm). Significant peaks from the Cu emission line at 324.86 nm and 327.53 nm were detected for both systems. It should be noted that small differences in the spectral emissions between PS II and PS I were observed, where PS I signified more prominent radiation of Cu in the range of 510 nm to 520 nm and 570 nm to 580 nm. More significant emission lines were also detected from W by PS II, which was related to tungsten in the electrode. Within the IR range, PS II showed emissions from Ar, associated with its plasma medium gas and also more dominant emissions of atomic N and O [168].
The temperature of the plasma jet was analysed by the Boltzmann plot method and the Cu emission lines. The plasma jet temperature at the plasma nozzle outlet determined for both systems were relatively comparable. The calculated temperature for PS II was 9500 $\pm$1500 K and for PS I was 9700 $\pm$ 3500 K at the root of the plasma jet [169].

## 3.3.4 Experimental procedures

**Cold start-up ignition:**
Cold start-up ignition tests were aimed to investigate the plasma ignition system as a start-up burner for cold start-ups. To emulate the cold start-up condition, ignition tests were performed without preheating the combustion chamber and the secondary air. Consequently, no heat was available in the pre-heater section and the temperature of the secondary air during the ignition tests stayed between 30 °C to 40 °C. A wall temperature of 90 °C at close to the burner zone was a prerequisite for the test initiation to eliminate the impact of existing heat inside the furnace that was generated from the previous experiments, on

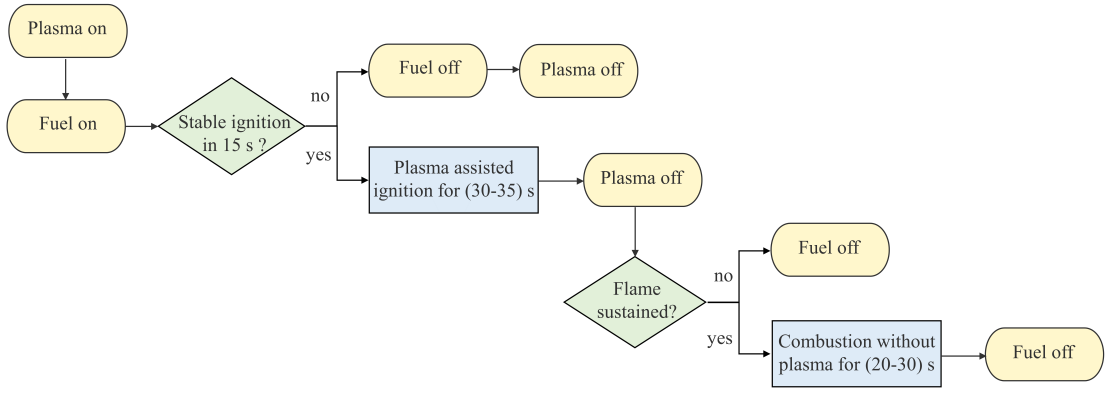


Figure 3.8: The procedure of the cold start-up with plasma-assisted ignition

the following ignition test. The ignition tests were carried out with a maximum duration of 60 s. Figure 3.8 shows the schematic diagram of the test procedure. The plasma jet was started prior to the fuel dosing; when no ignition occurred within (15 to 20) s, both systems were stopped due to safety reasons. In cases where ignition occurred, the plasma system was turned off within (30 to 35) s after the start, depending on the flame stability. In cases where there was a self-sustained flame after plasma turn-off, the fuel dosing was continued for another (20 to 30) s.

It should be emphasised that the ignition test consisted of two parts: the first part that evaluated the ignition and coherent flame formation with plasma support and the second part that assessed the flame self-sustainability under the cold furnace condition after short-time plasma support. Hence, the plasma jet served as the ignition source, where short-time plasma-assisted ignition and combustion concept was applied. The plasma was therefore not used to stabilize the flame and was only applied for ignition initiation. The required heat for flame stabilisation was considered to be supplied by the heat produced from the flame within the short time combustion with plasma support.

**Plasma-assisted combustion during part-load operation:**

To investigate the effect of plasma-assisted combustion on emissions and combustion behaviour during part-load operation, plasma-assisted combustion tests were performed. For this investigation, the 400 kW combustion rig was pre-heated with natural gas, over a duration of 8 h, to reach the sufficiently high temperature required for coal ignition and combustion. At several part-load configurations, plasma assisted combustion was performed for a duration of 30 min to 45 min, where in-flame measurements were carried out.

## 3.3.5 Measurement techniques

Ignition tests were monitored with an optical measurement system at close to the burner zone. The flue gas was analysed continuously at the end of the combustion chamber during the cold start-up ignition tests and plasma-assisted combustion experiments. Additionally, in-flame gas and temperature measurements were performed during plasma-assisted combustion. The measurement techniques are explained in detail in the following.

### 3.3.5.1 Optical measurement

The ignition process was monitored with a high-speed camera, Photron Fastcam SA5 model 775K-M1. The camera was installed out of the furnace and had an access to the flame via a transparent port at 18 cm from the burner outlet. The visual port with a diameter of 10 cm and a length of 35 cm, provided a visual access to the flame root of a length of around 20 cm. The 8bit camera with a resolution of $512 \times 512$ pixels and a frame rate of 250 fps provided a recording time of 32.7 s. The aperture of f/16 and f/22 were used for measurements, where the aperture was adjusted according to the radiation intensity of the flame depending on each fuel quality. The shutter speed was kept constant as 1/fps for all the measurements.
The luminous radiation of the flame reaches the camera sensor and the corresponding greyscale image is created. The brightness intensity of a pixel is represented by a grey level. For an 8bit camera, the minimum and maximum grey level are 0 and 255, respectively. For individual images recorded, the brightness is calculated as the mean grey level according to Eq. 3.9

$$B_t = \frac{1}{512 \times 512} \sum_{i=1}^{512 \times 512} B_i \tag{3.9}$$

, where $B_i$ is the grey level of pixel $i$ and $B_t$ is the mean brightness of an image at the time $t$. The profile of $B_t$ over time was used to monitor the ignition process, as shown in Figure 3.9. The ignition and the flame formation were detected, where ignition was implied by a sudden jump of brightness.
The dynamic brightness profile was subsequently analysed to obtain parameters on the flame luminous radiation. These parameters are introduced in section 3.3.6.3.

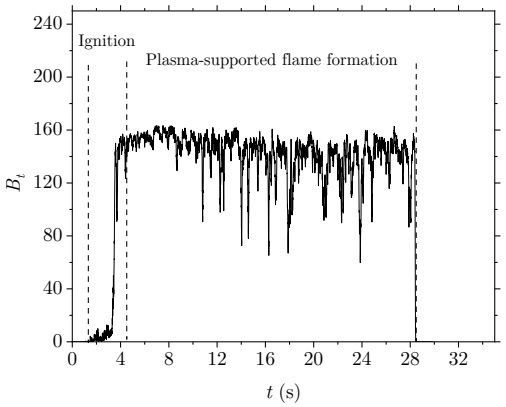


Figure 3.9: The profile of mean flame brightness over time

#### 3.3.5.2 Gas measurements

To monitor the combustion process, the flue gas emissions were measured at the end of the combustion chamber, at a 5.25 m distance from the burner outlet. For in-flame measurements, a portable probe was introduced to the furnace via the measurement ports. The gas was carried via a heated tube, where it passed a particle filter and a cooler before entering the analysers. The particle removal filter was cleaned regularly during the measurements. Table 3.6 summarizes the technical details of the gas analysers and measurement principles. The analysers were calibrated before and during the experimental campaigns to ensure the measurement accuracy.

Table 3.6: Technical details of the gas analysers

| Instrument | Species | Measurement range | Principle |
|---|---|---|---|
| Furnace outlet measurements | | | |
| Servomex Xentra4900 | $O_2$ | 0-25 ($10^{-2}m^3/m^3$) | Paramagnetism |
| ABB Uras26 | $CO_2$<br>CO | 0-100 ($10^{-2}m^3/m^3$)<br>0-10000 ($10^{-6}m^3/m^3$) | Non-dispersive infrared |
| EcoPhysics CLD 700EL ht | $NO_x$ | 0-1000 ($10^{-6}m^3/m^3$) | Chemiluminescence |
| In-flame measurements | | | |
| ABB Magnos206 | $O_2$ | 0-25 ($10^{-2}m^3/m^3$) | Paramagnetism |
| ABB Uras26 | $CO_2$<br>CO | 0-100 ($10^{-2}m^3/m^3$)<br>0-10000 ($10^{-6}m^3/m^3$) | Non-dispersive infrared |
| ABB Limas11 UV | $NO_x$ | 0-5000 ($10^{-6}m^3/m^3$) | UV absorption |

### 3.3.6 Evaluation methods

In chapter 5 quantitative and qualitative evaluation methods are used to assess the cold start-up ignition tests. Two parameters are introduced in this thesis to encompass different aspects of the ignition and combustion process. All ignition tests were allocated with a Combustion Class (CC) that defines the status of the ignition test qualitatively. To further analyse the combustion process quantitatively, Combustion Degree (CD) was introduced and for dedicated configurations, an equivalent flue gas temperature was calculated. The flame luminous radiation and stability of the flame during cold-start-up ignition tests were analysed with the help of information derived from the high-speed camera.
Following in chapter 6, in-flame measurements of gas composition and temperature are mainly used to compare the influence of plasma-assisted combustion on combustion performance and pollutant concentration within the flame zone. The flue gas emissions at the end of the furnace were also evaluated to identify the impact of plasma-assisted combustion on the emissions after the complete burnout.

#### 3.3.6.1 Combustion Class (CC)

An evaluation method was developed to reveal the ignition and flame behaviour, which is explained in Table 3.7. A criterion named Combustion Class (CC) was defined, which represents the visual observations on cold start-up ignition tests. CC 1 stands for no ignition, where CC 3 denotes ignition and flame formation with plasma support. A self-sustained flame after the plasma turn-off is denoted by CC 5 when a lifted flame detached from the burner outlet is formed, and by CC 6 when a self-sustained attached flame is formed at the burner outlet.

Table 3.7: Definition of Combustion Classes

| CC | Definition |
|---|---|
| 0 | No ignition |
| 1 | Ignition and fast extinction (only spark) |
| 2 | Ignition and unstable flame with plasma |
| 3 | Ignition and stable flame with plasma |
| 4 | Ignition and flame blowout in few seconds after plasma turn-off |
| 5 | Ignition and detached self-sustained flame after plasma turn-off |
| 6 | Ignition and attached self-sustained flame after plasma turn-off |

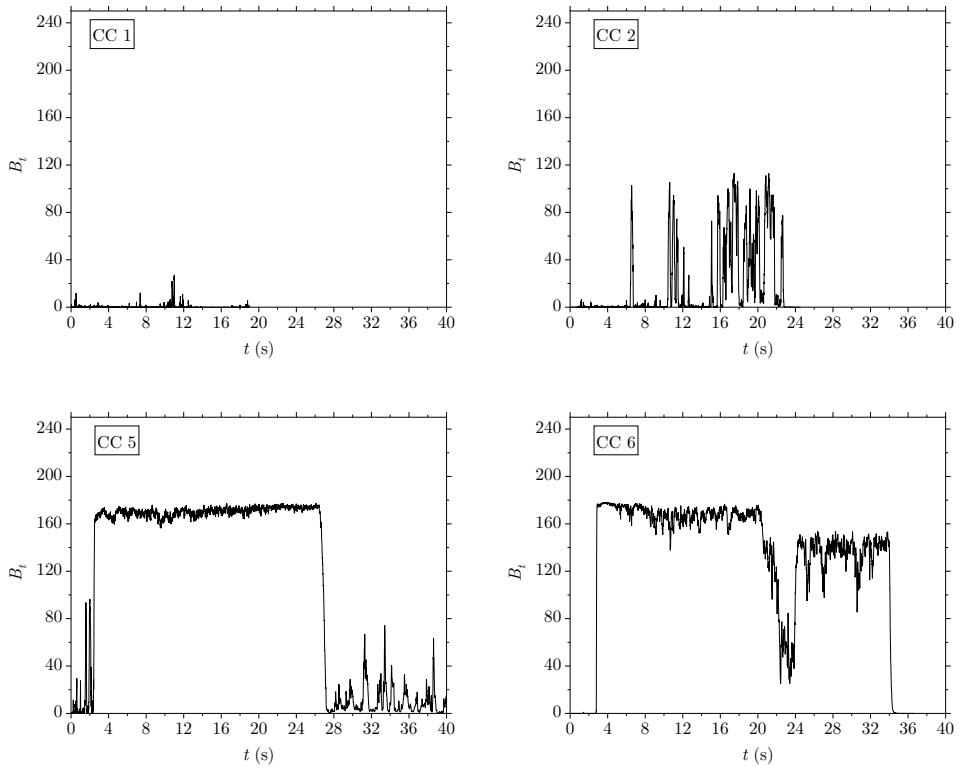


Figure 3.10: Mean brightness profile for different CC values

The CC for each ignition test was determined with the help of the mean brightness profile and observation from the optical ports along the furnace length. Figure 3.10 shows the mean brightness profile at close to the burner zone. For CC 1, almost no brightness was detected, where only sparks were observed. The mean brightness profile for CC 2 showed unstable ignition with large fluctuations between 0 and 120. CC 5 was characterised by a stable flame formation and as the plasma is turned off at 27 s, the flame was lifted downstream from the burner, where it was out of the optical access of the high-speed camera and only a small fluctuating part of the flame was registered. CC 5 was additionally validated with other optical ports along the furnace length. For CC 6, the plasma turn-off at 20 s was associated with a transition zone to reach a stable flame without plasma support while attached to the burner throat. Although the brightness level of the flame was reduced as the plasma support was removed, the flame propagated with slight fluctuations until the stop of the fuel feeding at 34 s.

#### 3.3.6.2 Combustion Degree (CD) and equivalent flue gas temperature

Execution of ignition tests within short time frames in a pilot-scale facility did not allow fly ash samplings to determine the unburnt carbon and consequently combustion efficiency. Hence, to evaluate the combustion process, a criterion was developed to provide information on the combustion process. This parameter indicates the improvements or deteriorations in the combustion process as it implies how much fuel is combusted within a specific time after the ignition initiation. Combustion Degree (CD) was defined as the ratio of burned fuel at a specific time after ignition to the total amount of fuel. For each ignition test, CD was calculated according to Eq. 3.10

$$\eta = \frac{(0.21 - y_{O_2})\mu_{LT}}{0.21\mu_{LoT}} \tag{3.10}$$

, where $\mu_{LT}$ is the specific dry combustion air amount (related to fuel mass) for the operated air ratio, $\mu_{LoT}$ denotes the specific dry combustion air amount for the stoichiometric condition and $y_{O_2}$ stands for the volume fraction of $O_2$ in the flue gas at the specific time after the ignition. The start of ignition was specified as the point from which $y_{O_2}$ starts to drop. For cold ignition tests using lignite, the plasma torch is turned off 30 s after the start and therefore $y_{O_2}$ at 30 s after the ignition initiation was implemented in Eq. 3.10. For the tests using WP 2, the value at 20 s after the ignition initiation was used.

It should be noted that the amount of burned fuel was determined under the assumption of complete combustion, where carbon is completely oxidised to $CO_2$. In case of incomplete combustion, CO and $H_2$ are also produced via incomplete oxidation, with the CO being the major incomplete combustion product [76]. Calculations showed small deviations in the CD value under the complete and incomplete combustion assumptions. Assuming $10000 \cdot 10^{-6}\mathrm{m}^3/\mathrm{m}^3$ CO in the flue gas, corresponded to 4.5 % error in CD. However, during the ignition tests using Lignite the maximum CO volume fraction of $8000 \cdot 10^{-6}\mathrm{m}^3/\mathrm{m}^3$ was reached under a number of operational conditions. During the WP 2 ignition tests, CO values above the analyser measurement range of $10000 \cdot 10^{-6}\mathrm{m}^3/\mathrm{m}^3$ were observed under few test points, which was related to substoichiometric conditions and the high volatile content of the biomass. Thus, to minimize the error associated with the complete combustion assumption, the CD for WP 2 ignition tests was defined at 20 s after the ignition, where the CO volume fraction was below $10000 \cdot 10^{-6}\mathrm{m}^3/\mathrm{m}^3$ .

To have a better understanding of the combustion process and the available heat, an equivalent flue gas temperature was calculated based on the $y_{O_2}$ value used for the CD determination. The flue gas composition at the corresponding $y_{O_2}$ was determined with the help of combustion calculations, under the assumption of complete combustion and the specific heat capacity of the flue gas was calculated accordingly. For the sake of simplicity, the specific

heat capacity of flue gas species at the constant temperature of 1500 °C was considered for the calculation, where $\bar{c}_{p,\mathrm{G}}$ denotes the integral specific heat capacity of the flue gas based on 0 °C. The equivalent flue gas temperature was calculated based on the following equation

$$\vartheta = \frac{10^3 H_u \eta + h_{\mathrm{LT}} \mu_{\mathrm{LT}}}{\mu_{\mathrm{G}} \bar{c}_{p,\mathrm{G}}} \tag{3.11}$$

, where $h_{\mathrm{LT}}$ is the specific enthalpy of the dry combustion air and $\mu_{\mathrm{G}}$ is the specific wet amount of flue gas with respect to fuel mass.
The equivalent flue gas temperature was only determined for selected ignition tests to further analyse the boundary conditions of the flame at the time of plasma turn-off.

#### 3.3.6.3 Flame brightness and fluctuation

The luminous radiation of pulverised fuel flames is mainly attributed to black-body emission from particles (e.g. char, ash and soot particles) in the visible spectral range, while chemiluminescence emissions of excited radicals (such as $CH^*$ and $C_2^*$) can be considered negligible [170]. The flame luminous characteristics have been used to evaluate the ignition and combustion process and to extract information related to the flame length, ignition point, flame geometry, stability, etc. [171–174]. These luminous characteristics have been also employed as a measure to optimize the boiler operation via online flame monitoring systems, where the pollutant emissions were reduced and concurrently combustion efficiency and flame stability were ensured [175, 176].
The luminous characteristics of the flame root region for this study were described by two parameters; flame brightness and brightness fluctuation. According to Eq. 3.12, the average flame brightness, $\bar{B}$, is defined as a 10-s average of the mean brightness value of images (calculated from Eq. 3.9), where $N$ is the number of images within the defined period.

$$\bar{B} = \frac{1}{N} \sum_{t=1}^{N} B_t \tag{3.12}$$

The flame brightness $B$ is represented as the average flame brightness normalised to the maximum brightness value of 255.

$$B = \frac{\bar{B}}{255} \tag{3.13}$$

The flame brightness indicated the flame luminous region, i.e. two dimensional flame area, within the view field of the camera system. Since the registration of the light intensity to the camera was adjusted by the digital system parameters and no additional light absorption filter was used, pixel saturation was observed within the core region of the flame. Hence,

to a good extent, a greater $B$ value corresponded to a larger luminous region. In Eq. 3.14, the brightness fluctuations $B_{\text{fl.}}$ is calculated by the standard deviation of flame brightness normalised to the average flame brightness. The brightness fluctuation describes the fluctuations of the luminous region and is an indication of the flame stability at its root region.

$$B_{\text{fl.}} = \frac{1}{\bar{B}} \sqrt{\frac{1}{N} \sum_{t=1}^{N} (\bar{B} - B_t)^2} \tag{3.14}$$

To analyse the flame at its most stable condition within the short ignition test, the 10 s averaging period was started with a time lag after the ignition initiation. For most of the cases, the stable condition was captured by a 10 -s gap. However, for few cases, the gap was varied between 5 s to 15 s to minimize the instabilities associated with the initial stage of the ignition process.

### 3.3.7 Isothermal CFD simulations

CFD simulations were deployed to visualize the fluid flow and particle trajectories only within the primary air stream to provide a better understanding of the changes in the flow field at different plasma positions and the plasma-particle interaction within the swirling and non-swirling flows. The simulation results are mainly used to better clarify the experimental observations.

ANSYS® FLUENT 2020 R2 [177] was used for two dimensional isothermal simulations of the primary air and coal stream in Nozzle 1 at different plasma lance positions. The pressure-based steady solver setting was used for the simulations. For non-swirling air $k - \epsilon$ model was employed to solve the turbulent terms. In case of swirling flow, the axisymmetric swirl modelling was employed in combination with the Reynolds Stress Model (RSM). To solve the Reynolds Averaged Navier Stokes equations, ANSYS® Fluent recommends the Reynolds Stress Model as a more accurate prediction for simulating swirling flows with a swirl number of above 0.5 [178]. The particle trajectories were realised with the discrete phase model via the uncoupled approach, where the discrete phase was calculated according to the solved continuous phase. Particles were injected with a particle size distribution created by the Rosin-Rammler-logarithmic function with a mean diameter of 453 µm which was equivalent to the PSD of Lignite B. The data obtained from the plotted particle trajectories showed however a larger proportion of fine particles below 100 µm compared with that of Lignite B. The discrete phase boundary condition was adjusted in a way that the particles colliding the wall are reflected, while they lose their normal momentum and only retain their tangential momentum.

# 4 Investigations of solid fuel ignition characteristics

## 4.1 Explosibility and minimum ignition energy

**Dust explosibility screening:**
Explosibility screening tests were performed for selected fuels. Table 4.1 summarizes the results of the maximum indication achieved, the dust explosion class and the minimum dust concentration at which ignition with at least an indication of "0" was observed. The results suggest that all dust qualities are explosive with an explosion class of 1. The "*" shows that the ignition was accomplished with the glowing coil ignition source instead of the continuous spark. WP 2 and Lignite A with an indication of "1" and the lowest explosive concentration than other fuels represent the highest explosibility, respectively. Following, the explosibility is reduced in Lignite C, Lignite D and Lignite G with a maximum indication of "0", where the lowest explosive concentration increases, successively. The least explosive dust qualities are Lignite F and Hard coal, where the ignition was achieved with the glowing coil as the ignition source. Therefore the lowest explosive concentration is not comparable to those ignition obtained by the spark ignition.

**Minimum ignition energy:**

Table 4.1: Explosibility of dust

| Fuel | WP 2 | L-A | L-C | L-D | L-G | L-F | H |
|---|---|---|---|---|---|---|---|
| Max. indication ( - ) | 1 | 1 | 0 | 0 | 0 | 0* | 0* |
| Explosion class ( - ) | 1 | 1 | 1 | 1 | 1 | 1 | 1 |
| Min. dust concentration ($g/m^3$) | 250 | 500 | 500 | 1000 | 1250 | 500 | 1500 |

Table 4.2: Minimum ignition energy

| Fuel | MIE (mJ) |
|---|---|
| L-A | $30 < \text{MIE} < 100$ |
| WP 2 | $100 < \text{MIE} < 300$ |
| L-C | $\text{MIE} > 1000$ |
| L-D | $\text{MIE} > 1000$ |
| L-G | $\text{MIE} > 1000$ |

The minimum ignition energy, MIE, was determined for dedicated Lignite qualities that were ignited with continuous spark in the screening test. Table 4.2 represents the MIE values for the investigated lignites, where representative values of 30 mJ to 100 mJ was specified for Lignite A followed by $100 < \text{MIE} < 300$ for WP 2. Lignite C, Lignite D and Lignite G demonstrated MIE of above 1000 mJ and therefore the actual MIE could not be identified. This higher MIE is perhaps related to a higher moisture content and less combustibles in these fuel qualities.
Classification of dust qualities with ignition energy above 1000 mJ is not plausible with the MIE parameter. This parameter is more relevant for highly explosive dusts with small MIE values.

**Summary:**
Dust explosibility screening and MIE tests were performed for selected fuels. Although dust explosibility screening sheds some light on the explosibility of different dust qualities by comparing the maximum ignition indication and the minimum ignitable concentration, the test results cannot be used as a representative and universal parameter to characterize the ignitability of different dust qualities. In addition, MIE is a limited parameter and hence not applicable for such characterisations.

## 4.2 Minimum cloud ignition temperature

**MCIT of different lignite qualities:**
Figure 4.1 illustrates the MCIT of lignites in ascending order. On the left axis, the MCIT and on the right axis, the moisture content, ash content and the median particle size of sieved samples are shown. It is noteworthy to mention that except Lignite F with 32 % volatile content, the other five lignite qualities have a comparable volatile content of 43 % to 48 %. It can be seen that Lignite A and Lignite F, representing the smallest and largest median

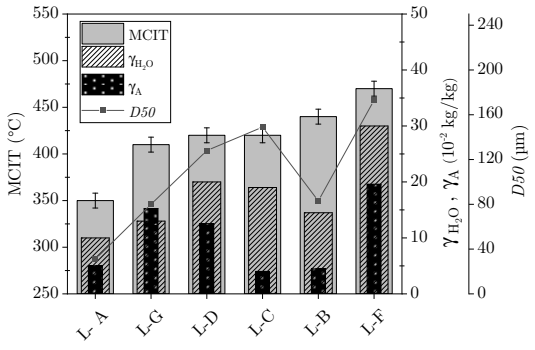


Figure 4.1: MCIT of lignite qualities in ascending order, first right axis: moisture and ash content, second right axis: median particle size

particle size and the lowest and the highest moisture and ash content respectively, stand for the minimum and maximum MCIT of 350 °C and 470 °C among the tested lignites.
Lignite G has the second-lowest MCIT of 410 °C, as the physical and chemical properties concerning ignitability are exacerbated with regard to Lignite A. Comparing Lignite G with Lignite C and Lignite D, despite increases in the median particle size from 83 µm to around 130 µm and in the moisture content from 15 % to 20 %, only a 10 °C rise in MCIT is observed. Lignite C and D with similar median particle sizes, volatile and moisture contents represent a cloud ignition temperature of 420 °C. Although these two lignites have distinct ash contents, the result indicates that this 8 % variation in the ash content does not reflect any impact on the MCIT for Lignite C and Lignite D.
Surprisingly, Lignite B with properties more susceptible to ignition (*D50* of 83 mm, ash content of 5 % and the moisture content of 15 %) compared to Lignite C and D has a higher MCIT of 440 °C. Considering that Lignite B and Lignite C are derived from the same mine and only have different drying degrees, a decrease in the median particle size from 150 µm to 80 µm and a 5 % reduction in moisture content does not show any trend towards a lower MCIT.
Given this finding that a 5 % difference in moisture content between 15 % to 20 % does not show a notable effect on the cloud ignition temperature and considering a comparable volatile content for the lignites, it can be concluded that the low MCIT of Lignite A (350 °C) is most likely related to its high share of fine particles, when compared with other lignites with MCIT of 410 °C to 440 °C. This highlights the importance of fine particles below 63 µm that are considered the critical particle share responsible for ignition [29]. The effect can be related to a change in the ignition mechanism, where it can be assumed that in larger particles homogeneous mechanism controls the ignition, while as the share of small particles below 63 µm are increased, hetero-homogeneous ignition prevails, enhancing the ignition and reducing the ignition temperature. A similar behaviour regarding the drop of ignition temperature below a specific size was observed by others [52].

To better understand the influence of ash on the MCIT, Lignite A was mixed with pure combustion-derived ash to produce dust with similar properties but a higher ash content of 15 %. Table 4.3 specifies that diluting Lignite A with a 10 % rise in the ash content increases the MCIT by 30 °C, which is well above the reported values by others [55, 56]. This larger inhibition effect observed here by Lignite A, compared with the values reported in literature, can be related to the type of fuel. According to [55], a fuel quality that ignites largely through volatiles is more susceptible to ignition inhibition by addition of ash. By having a closer look to this finding, a clear inhibiting effect of ash material on the MCIT of lignite A contradicts with the results obtained by Lignite C and Lignite D.

It is important to mention that there are several aspects that need to be considered when interpreting these results. First, the individual properties of two lignite qualities should be highlighted. Contrary to similar chemical compositions (except the ash content) and comparable median particle sizes, the particle shape, the porosity and the surface area of Lignite C and Lignite D differ, where the net effect may eventually result in a similar ignition temperature. Table 3.2 shows that Lignite D has a specific surface area 11 times larger than that of Lignite C. A larger surface area facilitates the combustion reaction, by enhancing the volatile release from and oxygen diffusion to the surface of particles [63]. This effect may compensate for the inhibition effect associated with a higher ash content.

The second aspect refers to the point that the inhibition mechanism of combustion-derived admixed ash on ignition differs from that of the inherent ash of coal. In general, inert materials are considered as a heat sink source during the ignition. The heat sink occurred by ash hinders the ignition process via various pathways. The single admixed ash particles directly absorb the convective heat from the surrounding in the combustion reactor. Consequently, the temperature in the vicinity of coal particles is reduced which impairs the heating process of particles. In addition to convective heat absorption, ash particles dissipate the heat produced via the initial exothermic combustion reactions, which in return limits the volatile release by the remaining unburned particles and hamper the ignition process [68–70].

Beside the heat dissipation, ash particles can play a blocking role in homogeneous ignition by hindering the mass and heat transfer in the dust cloud. In addition to the blockage and heat sink inhibiting effect of inert material, ash particles may interfere with the heterogeneous ignition process. The deposition of $Al_2O_3$-containing ash material on the surface of coal particles can further curb the solid-gas heat and mass transfer via the formation of a coating film on the surface of coal particles. Hence, it limits the oxygen attack to and volatile release from the solid surface [55].

On the contrary, inherent ash in coal does not have a strong inhibiting effect as admixed ash, because the ash material is not dispersed as individual and separate particles in the dust cloud. Thus, the available heat is directly absorbed from the surface of coal particles, leading to the volatile release and ignition initiation. A small portion of ash material on the

Table 4.3: Minimum cloud ignition temperature

| Fuel | Admixed L-A | H | WP 2 |
|---|---|---|---|
| MCIT (°C) | 380 | 540 | 450 |

particle's outer surface consumes the heat during the particle heating and devolatilisation process and an ash layer on the surface of the particle will grow as the combustion proceeds. The major portion of ash is then partially released from the char surface and contributes in a larger heat consumption, once the ignition is initiated. Under such circumstances, the degree of heat loss associated with ash is insignificant compared to the heat produced by combustion.

**MCIT of different fuel types:**
Table 4.3 also shows the MCIT of H and WP 2. The result shows an approximately 160 °C increment in the MCIT to 540 °C when the volatile content reduces from 48 % in lignite A to 26 % in hard coal. However, WP 2 with 77 % volatiles has a MCIT of 450 °C, which is 100 °C higher than that of Lignite A. This increase in the MCIT of wood pellets material, despite a considerably higher volatile content, is associated with its coarse particle size. Table 3.2 shows similar median diameters for Lignite A and H with a *D50* of around 50 µm, whereas it rises to around 230 µm for WP 2. In fact, 50 µm size corresponds to the *D10* of WP 2.

**Summary:**
Comparing six lignite qualities, one hard coal and one wood pellet sample shows no clear influence on the MCIT when the moisture and ash content varies in a small range of 5 % to 10 %. However, a strong relationship is observed between the ignition temperature and the volatile content as well as particle sizes. The MCIT increases considerably from Lignite A to hard coal, where both fuels have comparable particle sizes. Differences in the median particle size in the range of 80 µm to 150 µm does not show any clear impact on the MCIT of different lignite qualities. Once the median particle size is decreased to 30 µm, the MCIT is considerably reduced and once it is increased to 230 µm in WP 2 with a very low share of fine particles (with a $Q_{63}$ of 15 %), the detrimental effect of the lack of fine particles is alleviated by the high volatile content, resulting in comparable MCIT for the biomass and lignites. The findings highlight that MCIT is more susceptible to a broad variation in the particle size and the fuel's volatile content, whereas it is not significantly impacted by variations within a narrow range of moisture and ash contents.

# 4.3 Explosion characteristic parameters

## 4.3.1 The rate of pressure rise

Figure 4.2a illustrates the rate of pressure rise versus the equivalence ratio, $n$, the ratio of actual dust concentration to the stoichiometric dust concentration, for six lignite qualities, hard coal and WP 2. Between lignites, the rate of pressure rise for Lignite A and Lignite F are the highest and lowest, respectively, under all dust concentrations among those tested. This behaviour agrees with the trend observed by MCIT and suggests that Lignite A and Lignite F has the highest and lowest ignitability according to both criteria. Lignite A reaches a maximum rate of pressure rise of about 520 bar/s at the equivalence ratio of 4, and the maximum value for Lignite F with 115 bar/s is reached at the equivalence ratio of 2.
The $dp/dt$ values of Lignite B stay below those of Lignite A. The $dp/dt$ trend of Lignite B reaches its maximum of 400 bar/s at the equivalence ratio of 2.5. The values corresponding to Lignite G are lower than those of Lignite B when the latter has an ascending trend, reaching a maximum rate of pressure rise of 378 bar/s at a high equivalence ratio of 5.
The $dp/dt$ values for Lignite C are lower than those for Lignite D until the equivalence ratio of appropriately 3 and then become comparable within an equivalence ratio range of 3 to 6, where both dusts reach their maximum rate of pressure rise. Lignite D reaches a slightly higher $(dp/dt)_{\max}$ value of 322 bar/s at the equivalence ratio of 5.3, while Lignite C reaches almost 300 bar/s at the equivalence ratio of 5.
The trends of $dp/dt$ for Lignite C and Lignite D are overall considered comparable, suggest-

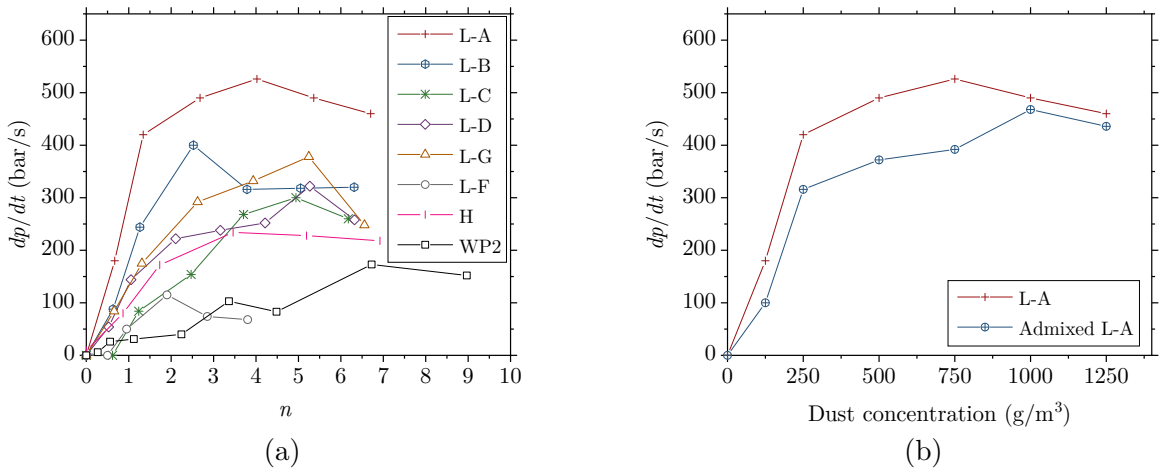


Figure 4.2: (a) The rate of pressure rise versus equivalence ratio for lignites, hard coal and WP 2 and (b) the rate of pressure rise for Lignite A and ash admixed Lignite A

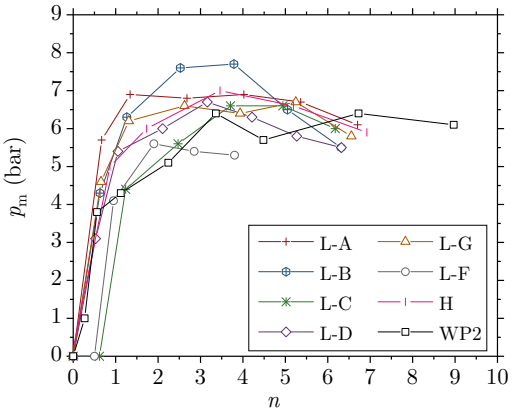


Figure 4.3: Explosion pressure versus equivalence ratio

ing that these two coal qualities have relatively similar heat release rates and reaction rates, despite their difference in the ash content and the specific surface area. To precisely assess the influence of ash and inert materials on the combustion kinetics and the heat release rate, Figure 4.2b compares the $dp/dt$ of Lignite A with the admixed dust at different dust concentrations. Lignite A with 5 % ash shows a higher $dp/dt$ over all tested dust concentrations with a $(dp/dt)_{max}$ of 525 bar/s compared with 470 bar/s for the dust with 15 % ash content. The inert ash's inhibiting effect on the combustion kinetics and heat release rate is clearly observed and is consistent with the literature [68, 69, 74]. Thus, it can be speculated that for Lignite D, a larger surface area alleviates the adverse effects of high ash content on the combustion rate and oxygen diffusion.

The $dp/dt$ trend of hard coal lies between the trends of lignites, where it reaches its maximum of 234 bar/s at the equivalence ratio of 3.5. This indicates that when ignition occurs, the hard coal's heat release rate is comparable to those of certain lignite qualities. On the contrary, WP 2 has surprisingly low $dp/dt$ values, even below those of Lignite F up to the equivalence ratio of 3. The trend of WP 2 rises steadily, reaching a $(dp/dt)_{max}$ of 173 bar/s at a large equivalence ratio of 6.7.

The $K_{st}$-value are compared in subsection 4.3.3 and the values are correlated to the dust characteristics.

## 4.3.2 Maximum explosion pressure

The $p_m$ trends of different lignite qualities, hard coal and WP 2 do not follow that of $dp/dt$. As shown in Figure 4.3, Lignite B has the highest $p_{max}$ of 7.7 bar and Lignite F has the lowest $p_{max}$ value of 5.6 bar. The graphs of the rest of dust samples, including the hard coal,

overlap to a large degree, reaching $p_{max}$ values between 6.6 bar to 6.9 bar. The $p_{max}$ of WP 2 drops slightly to 6.4 bar. Slight variations of $p_{max}$ for lignites and also different fuel types with distinct characteristics suggest that this parameter is not sufficiently sensitive to the changes of physical and chemical properties of the investigated dusts.

### 4.3.3 Deflagration index

**$K_{st}$-value of different lignites qualities**:
To correlate the lignite properties to the maximum rate of pressure rise, Figure 4.4 shows the deflagration index, $K_{st}$-value, in descending order. The trend of $K_{st}$-value for different lignites is similar to that observed by $(dp/dt)_{max}$ trends. It is evident that coals with similar moisture contents and median particle sizes demonstrate comparable $K_{st}$-values and the deflagration index sinks as the median particle size and the moisture content rise. Since within the tested samples, the moisture and particle size vary concurrently, it is challenging to differentiate their contribution to the $K_{st}$-value.
According to [21], where a similar lignite quality was used, sieving with 63 µm and 500 µm mesh sizes, producing a particle size distribution with a median diameters of 28 µm and 137 µm respectively, showed no considerable impact on the $K_{st}$-value. From the above study, it is deduced that mainly the fine particles account for the initial ignition and govern the $K_{st}$-value, where the coarser particles have limited contribution in the combustion process within the 20-litre sphere chamber. The study indicated that when a sufficient amount of fine particles is available, the $K_{st}$-value is independent of the amount of fine particles, as the samples with $Q_{63}$ of 91 %, 36 % and 22 % showed comparable $K_{st}$-values [21]. However, more experiments are required to validate this hypothesis and ultimately determine the suf-

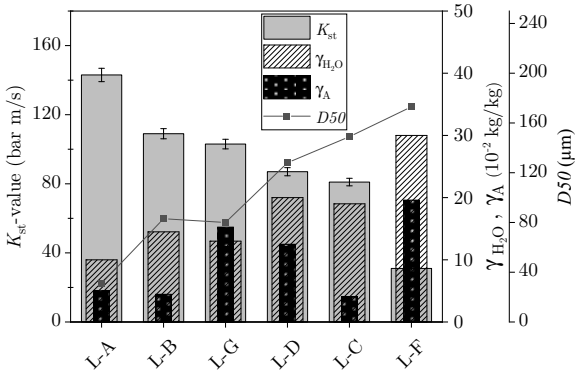


Figure 4.4: $K_{st}$-value in descending order, first right axis: moisture and ash content, second right axis: median particle size

ficient share of fine particles required to produce comparable $K_{st}$-values. This controlling of $K_{st}$-value by the fine particles was also highlighted in literature [62, 63]. Under the assumption of particles below 63 µm, a sample with a finer median diameter may lead to a higher deflagration index, as finer particles ignite faster due to their higher surface to volume ratio. Therefore, it can be concluded that the impact of the median particle size on the deflagration index is less significant when the median diameter changes within the coarse particle share, namely above the critical particle share of 63 µm.

For the lignites investigated, the moisture content demonstrates a decisive factor influencing the heat release rate to a larger degree than the median particle size. A direct comparison between Lignite B and C with distinctive drying degrees, neglecting the difference in the median particle size, shows a reduction of around 30 bar m/s in the $K_{st}$-value when the moisture is increased from 15 % to 20 %. Similarly, the $K_{st}$-value of lignites with comparable moisture content, Lignite B and G compared with Lignite D and C, stay very close.

Although the moisture inhibition behaviour is consistent to the observations by others, a stronger effect was reported by other studies [61]. Heat consumption for endothermic water evaporation is determined as the main inhibition mechanism. Beside this, particle agglomeration at high moisture contents and reducing the oxygen partial pressure in the boundary layer around the particles are expected to reduce the explosibility [61, 66, 67].

The $K_{st}$-value shows no clear correlation to the ash content between different lignite qualities. Although a lower $K_{st}$-value is observed by admixed Lignite A than original Lignite A (see Figure 4.2b), no concrete conclusion can be found when comparing the lignite qualities investigated. Like other criteria, Lignite F with the highest moisture and ash content and the largest median diameter exhibits the lowest $K_{st}$-value.

**$K_{st}$-value of different fuel types**:

Table 4.4 compares the $K_{st}$-value for Lignite A, hard coal and WP 2. Lignite A with a volatile content of around 50 % shows a $K_{st}$-value of 143 bar m/s, where for hard coal with a volatile content of 26 % the value drops to 64 bar m/s. A strong correlation between the deflagration index and the volatile content is evident from this result. However, the $K_{st}$-value of WP 2 with a volatile content of 77 % is 48 bar m/s, which is even smaller than the deflagration index of hard coal. This unexpected drop in $K_{st}$-value for WP 2 is believed to be associated with a small share of fine particles in WP 2. $Q_{63}$ of WP 2 is 15 % that is two

Table 4.4: $K_{st}$-value and $ZWZ_{mod.}$ of different fuel types

| | | L-A | H | WP 2 |
|---|---|---|---|---|
| $K_{st}$-value | bar m/s | 143 | 64 | 48 |
| $ZWZ_{mod.}$ | kJ/kg °C | 14.9 | 5 | 24.2 |

times smaller than the coarsest lignite investigated here, see Table 3.2. $Q_{63}$ of Lignite A and hard coal are by 66 % and 76 %, respectively. This lack of sufficient fine fraction in WP 2 is perhaps the main reason that leads to a low $K_{st}$-value.

**Summary:**
The deflagration index shows a strong dependency on the lignite moisture content and is more susceptible to variations as the dust properties change. Lignite A and Lignite F had the largest and the smallest $K_{st}$-values among the tested dust qualities. Lignite B and Lignite G with 10 % moisture have higher $K_{st}$-values than Lignite C and Lignite D with a moisture content of 20 %. Similar to MCIT, the admixed ash reduces the $K_{st}$-value, but no clear correlation between the ash content of different lignite qualities and the $K_{st}$-value is found. In addition, volatile content and the amount of fine particles have significant influence on the $K_{st}$-value. While the volatile matter increment from hard coal to lignite increases the deflagration index, a small share of fine particle potentially reduces the $K_{st}$-value, despite an increase in the volatile content from lignite to biomass.

## 4.4 Modified ignitability characteristic number

**Ignition potential:**
Figure 4.5 shows the devolatilisation degree, $\eta_{devol}$, on the left axis and the ignition potential, $N_{Z500,\,af}$, and the calorific value of the volatiles released, $NCV_{VM}$ on the right axis. Lignites represent a devolatilisation degree in a narrow range of 60 % to 70 %, whereas this value is reduced to around 40 % for the hard coal and significantly increased to more than 90 % for WP 2. As expected, the devolatilisation degree decreases as the volatile content and coal rank drops from biomass to hard coal.
The calorific value of volatiles represents the quantity of the combustion heat that can be obtained per unit mass of volatiles. Figure 4.5 highlights that the volatiles released from Lignite A, B and C have a higher calorific value than those released from Lignite G, D and F. Compared to all lignites, the hard coal produces volatiles with the highest calorific value, while WP 2 contains volatile quality comparable to that of Lignite A. This behaviour is correlated to the fuel intrinsic characteristic and consequently, the composition and the type of volatiles formed and liberated during the pyrolysis.
The ignition potential is slightly decreased from Lignite A to Lignite B and Lignite C. In contrast, a large drop in the ignition potential is observed between Lignite C and Lignite

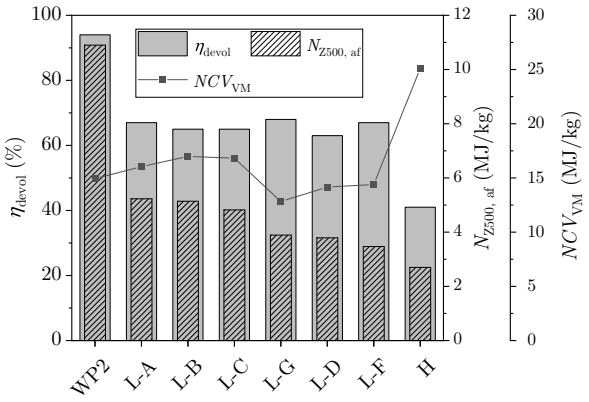


Figure 4.5: Left axis: devolatilisation degree, first right axis: ignition potential of as fired fuel, second right axis: net calorific value of released volatile matter

G, followed by slight declines towards Lignite D and Lignite F. Since all lignites represent comparable devolatilisation degrees, this drop is related to the reductions in $NCV_{\mathrm{VM}}$ of these lignite qualities. Although the calorific value of the volatiles released during hard coal pyrolysis is considerably higher than those of lignites, a low volatile content and a low devolatilisation degree result in a small ignition potential, while for WP 2, a large devolatilisation degree corresponds to the highest ignition potential.

**$ZWZ_{\mathrm{mod.}}$ of different lignite qualities:**

The ignitability characteristic number correlates the devolatilisation behaviour of the coal to the minimum ignition temperature. Figure 4.6 displays the modified ignitability characteristic numbers of lignites in descending order. Here again, Lignite A and Lignite F demonstrate the largest and smallest $ZWZ_{\mathrm{mod.}}$ of around 15 kJ/kg °C and 7.5 kJ/kg °C, respectively. As the moisture content and the median particle size are increased from Lignite A to Lignite B, the $ZWZ_{\mathrm{mod.}}$ significantly decreases to 11.7 kJ/kg°C.

Excluding Lignite A, Figure 4.6 exhibits no correlation between the $ZWZ_{\mathrm{mod.}}$ and the median particle size. The reason is attributed to the fact that neither numerator nor denominator term demonstrate a strong relationship to the particle diameter. As discussed in section 4.2, MCIT does not change considerably as the median particle size varies within a narrow range of coarse particle sizes. Moreover, the ignition potential is determined under steady-state conditions with a gradual increase in the pyrolysis temperature. Consequently, the influence of the particle size on the devolatilisation degree is less relevant, as all particle sizes have sufficient time to undergo the devolatilisation process. As the moisture content increases by 5 % from Lignite B to Lignite C, a slight reduction is observed in the $ZWZ_{\mathrm{mod.}}$. Although the ignition potential of Lignite B is higher than that of Lignite C, a higher MCIT obtained by Lignite B results in only a negligibly lower $ZWZ_{\mathrm{mod.}}$ number.

Despite a reduction in the moisture content from Lignite C to Lignite G, the $ZWZ_{\mathrm{mod.}}$ falls

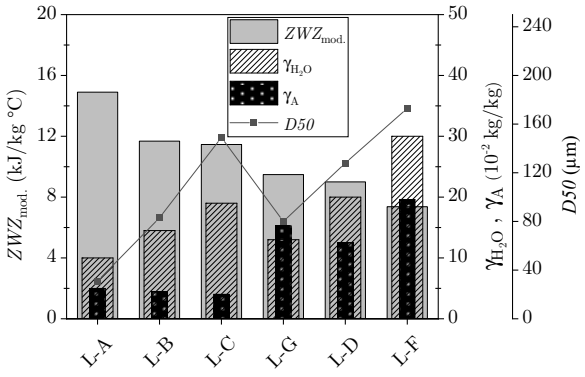


Figure 4.6: The modified ignitability characteristic number in descending order, first right axis: moisture and ash content, second right axis: median particle size

to around 9.5 kJ/kg °C, which is related to the difference in the quality of volatile matter, as discussed earlier. The $ZWZ_{\text{mod.}}$ reduces slightly to 9 kJ/kg °C when the moisture content rises to 20 % in lignite D. Considering Lignite B and C in one group and Lignite G and D in another, the decrement in $ZWZ_{\text{mod.}}$ within each group, related to a higher moisture content, is insignificant compared to the decrement in $ZWZ_{\text{mod.}}$ from one group to the other, associated with a higher ash content and lower quality volatiles. As explained in Figure 4.5, Lignite B and Lignite C release volatiles with higher calorific values compared to lignite G and Lignite D. As a consequence, smaller $ZWZ_{\text{mod.}}$ numbers associated with lower calorific volatiles are obtained for the latter group.

**$ZWZ_{\text{mod.}}$ of different fuel types:**

A low ignition potential and a high MCIT for the hard coal result in a $ZWZ_{\text{mod.}}$ of 5 kJ/kg °C, see Table 4.4, suggesting insignificant ignitability. Whereas, a large ignition potential for biomass leads to a significantly high $ZWZ_{\text{mod.}}$ of 24 kJ/kg °C compared with around 15 kJ/kg°C for the fine lignite dust, Lignite A.

Here, a large ignition potential, related to the volatile content, in the numerator has a more significant influence on $ZWZ_{\text{mod.}}$ than decremented MCIT in the denominator, associated with a low share of fine particles for the biomass. Hence, contrary to the $K_{\text{st}}$-value parameter that is more strongly governed by the particle size in case of biomass, the modified ignitability number minimizes this effect.

**Summary:**

The modified ignitability characteristic number correlates the released energy during the pyrolysis to the ignition temperature. This parameter contains the devolatilisation degree and the calorific value of the released volatiles. The results show that Lignite A, Lignite B and Lignite C produce volatile matter with higher calorific values than Lignite D, Lignite

G and Lignite F. The $ZWZ_{\text{mod.}}$ reduces from Lignite A to Lignite B and Lignite C as the moisture content increases. Further reductions in $ZWZ_{\text{mod.}}$ were observed in Lignite G, Lignite D and Lignite F, as the moisture and ash content increases. An evident trend is observed in $ZWZ_{\text{mod.}}$ with the fuel type. The $ZWZ_{\text{mod.}}$ number increases notably as the volatile content of the fuel increases and it has less sensitivity to the sample particle size. This parameter shows susceptibility to volatile matter, moisture content and ash content of fuels.

## 4.5 Conclusion

Among the investigated parameters, MIE, MCIT and $p_{\max}$ are identified as non-representative parameters to differentiate the ignition behaviour of the fuel qualities investigated. This is because the MIE is limited to the values of below 1000 mJ, which was detectable for only two fuel qualities. The MCIT is also more relevant for comparisons of fuels with distinct volatile contents and therefore did not show high sensitivity to the changes in water and ash content of various lignite qualities. The variations of $p_{\max}$ occurred within a small range with no clear trend towards the fuel properties.
$K_{\text{st}}$-value and $ZWZ_{\text{mod.}}$ both show promising results with regard to the fuel quality. Both parameters clearly demonstrate dependency on the volatile and moisture content. Therefore both parameters will be later compared in section 5.6 to explore any correlation between the theoretical ignition parameters and the ignition behaviour in practical applications. It is aimed to use the lab-scale ignition parameters as indicators to predict the fuel ignition behaviour in the plasma-assisted ignition system under the investigated boundary conditions.

# 5 Investigations of the plasma ignition system for cold start-ups

## 5.1 Interpretation of the ignition process and system validation

### 5.1.1 Ignition and flame formation process in the plasma ignition system

Figure 5.1 illustrates the process of plasma-assisted solid fuel ignition and combustion. The fuel particles which come into contact with the plasma jet are ignited and consequently form an enlarged flame around the plasma jet that keeps expanding, as more particles are ignited in the vicinity of the flame. The ignition is presumably initiated with fine particles, which are prone to a homo-heterogeneous ignition mechanism when experiencing high heating rates. Since the plasma jet temperature is extremely high, the fine particles, that are in direct contact with it, undergo mainly heterogeneous ignition. In addition, single or groups of particles which receive heat from the plasma-coal flame can be locally devolatilised and be ignited within the dust cloud, when a sufficient amount of volatiles is available at the ignition temperature, producing heat- and volatile-rich zones within the unburned dust cloud. Under these circumstances, the ignition is mainly governed by a homogeneous or mixed ignition mechanism, as it is associated with lower heating rates and a range of particle sizes. A coherent flame is formed in the dust cloud, as the plasma-coal flame proceeds to a volatile-rich atmosphere. A detailed assessment of the formation of flame cloud from single particles is, however, out of the scope of this work.

To evaluate the ignition behaviour of different fuels, it is necessary to outline the ignition and combustion process at each CC. CC 1 and CC 2 show that particles are ignited via the plasma jet, but a coherent flame is not formed. Under CC 1, only sparks and single particle

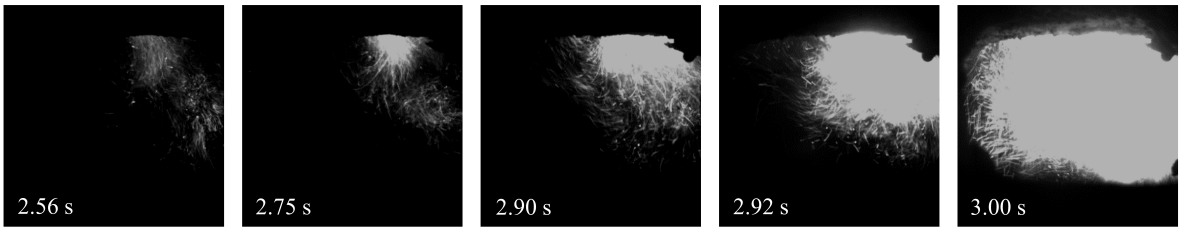


Figure 5.1: Ignition and flame formation with Lignite B with plasma-assisted ignition at 38 % thermal load and the air ratio of 1.1

ignition are observed, while CC 2 is associated with higher degrees of devolatilisation and local ignition of groups of particles, where no coherent flame is formed, i.e. local formation and extinction of flame. This can be related to both burner aerodynamic characteristics, such as flow velocity, flow swirling, etc. and burner operational parameters, such as thermal load, air ratio and plasma power.

Given the burner operational parameters, at low dust concentrations, the ignition of single particles does not produce a sufficient quantity of heat and volatiles to form a flame envelope. As the particle mass flow rate, and subsequently fine particles, increases, the heat generation and the volatiles concentration grow, and once the ignition requirements are reached, a stable flame envelope is formed. When the external ignition source in a cold environment is removed, in the absence of an additional heat source, the extent of combustion reactions and correspondingly the heat production rate and devolatilisation rate will reduce, which leads to flame extinction or reduced flame propagation velocity. Flame blowout after plasma turn-off, indicated by CC 3, is related to one or more of the following conditions: 1) the heat available from the combustion process, without an external ignition source, does not suffice to sustain the burning process, this can depend on either low fuel quantity, e.g. low thermal load or a high degree of heat loss, 2) the concentration of volatiles released is not adequate for proceeding the chain combustion reactions, 3) the flow velocity is significantly higher than the flame velocity and therefore the flame cannot be stabilised. Once a sufficient amount of heat and volatiles are available after the plasma turn-off and there is no significant difference between the flame propagation velocity and the flow velocity, a self-sustained flame is formed.

The location of the self-sustained flame in the combustion chamber mainly depends on the ratio of these two velocities. In this application, the flame lift-off occurs potentially due to a reduced flame velocity. As the flow velocity becomes larger than the flame velocity at every point of the flame, the flame is detached from the burner and is stabilised downstream within the swirl recirculation zone, where a reduced flow velocity matches the flame velocity [81], which is indicated by CC 5. When the flow velocity becomes considerably higher than

the flame propagation velocity and no point within the swirl zone is found where the flame velocity and the flow velocity match, the flame is dragged from the burner outlet until it blows out. This condition is specified by CC 4, where the flame extinguishes shortly after the plasma turn-off. In a fully-optimised burner configuration, the self-sustained flame stays anchored at the burner outlet, which is indicated by CC 6.
It should be highlighted that CC not only defines the flame status but is also an indication of the fuel's applicability for cold start-up ignition and self-sustained flame formation. CC 1 to CC 3 that indicate the occurrence of ignition and stable flame formation, assess the applicability of plasma-assisted ignition for the dedicated fuel quality. CC 4 to CC 6 describe potential of the fuel quality for the formation of a self-sustained flame under short-time plasma-supported combustion.

### 5.1.2 System validation

The plasma ignition system, which was designed and developed in IFK, was first validated using Lignite A and WP 1. Figure 5.2 compares the CC obtained at several thermal loads over the air ratios operated. Lignite A ignites and develops a coherent flame at the thermal load of 25 %, corresponding to 100 kW, indicated by CC 3. At this thermal load, as the air ratio is increased to 1.4, the CC further improves to CC 5. Once the thermal load goes to 38 %, combustion reaches CC 5 and CC 6. A further increase to 50 % thermal load results in CC 6 for air ratios of 0.9 and 1.1. For the settings operated, the CC improves when the thermal load is increased, as the amount of heat available for the ignition increases. Besides, a positive influence of the air ratio on the CC is observed for each thermal load.

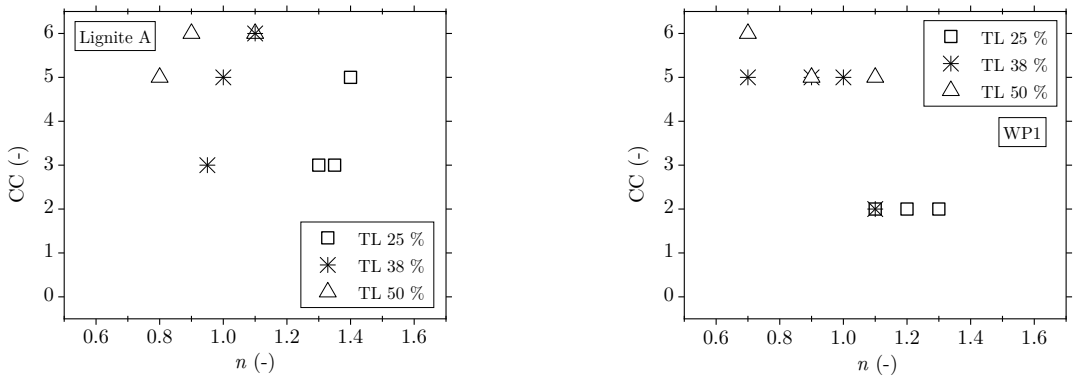


(a) (b)

Figure 5.2: CC versus air ratio at different thermal loads (TL) using 4.2 kW plasma power for (a) Lignite A and (b) WP 1

The improvement in ignition stability with the thermal load was also observed by other researchers [90, 116].
Ignition with WP 1 is achieved at the thermal load of 38 % with CC 5. A self-sustained flame attached to the burner is formed at the thermal load of 50 % and the air ratio of 0.7. For WP 1, the air ratio does not show any impact on the CC at 25 % and 38 % loads, while at the thermal load of 50 % the flame is detached from the burner as the air ratio is increased to 0.9 and 1.1.
The results of ignition tests using Lignite A and WP 1 conclude that these fuel qualities are ignitable using the developed plasma ignition system and can form an attached self-sustained flame with short-time plasma support under cold start-up conditions and the standard burner configuration. Therefore the system is validated for this application and can be further investigated for the applicability of other fuel qualities.

## 5.2 Investigations of lignite qualities

All seven lignite qualities are tested under cold start-up conditions. In the first section, the ignition behaviours with respect to CC are analysed. In the second section, the CD values achieved with these lignites are evaluated. The equivalent flue gas temperature is also assessed for selected lignite qualities to investigate any correlation between the ignition performance and the theoretical flame temperature. The investigation is performed at several thermal loads and various air ratios to monitor the behaviour of different fuels with respect to these parameters. The experimental settings corresponding to the results shown in this section are adjusted after a series of screening tests to find the most suitable configuration for these fuel qualities. The experiments for all lignites, except Lignite C, are performed at plasma position 0. Also Nozzle 1 is used as the reference nozzle for all the experiments unless otherwise mentioned. For Lignite G and Lignite H, the results with 7 kW plasma power are shown, while for the rest of lignites the results are related to the experiments performed with 4.2 kW plasma power. Moreover, the primary air flow rate of 40 $m^3$/h ($STP$) for Lignite B, Lignite C and Lignite E is reduced to 30 $m^3$/h ($STP$) for Lignite D, Lignite F, Lignite G and Lignite H.

### 5.2.1 The effect of the thermal load and air ratio on the ignition behaviour

Figure 5.3a shows that Lignite B is ignited at 25 % thermal load with CC 3. As the thermal load is increased to 38 % and 50 %, the CC improves to CC 5 and CC 6, respectively. A self-sustained flame is obtained over a wide operational range from substoichiometric to overstoichiometric conditions, under an air ratio range from 0.8 to 1.2, for the thermal loads above 38 %. Although CC 6 is only obtained at an increased air ratio at 50 % thermal load, no clear relation between the CC and the air ratio is observed for Lignite B.
The ignition tests of Lignite C were performed at a retracted plasma position inside the burner, see Figure 5.3b. As can be seen, Lignite C cannot be ignited at 25 % thermal load and as the load is increased to 38 %, coherent flames at CC 4 and CC 5 are formed. A further increase in the thermal load to 50 %, results in similar CC 4 and CC 5. When the thermal

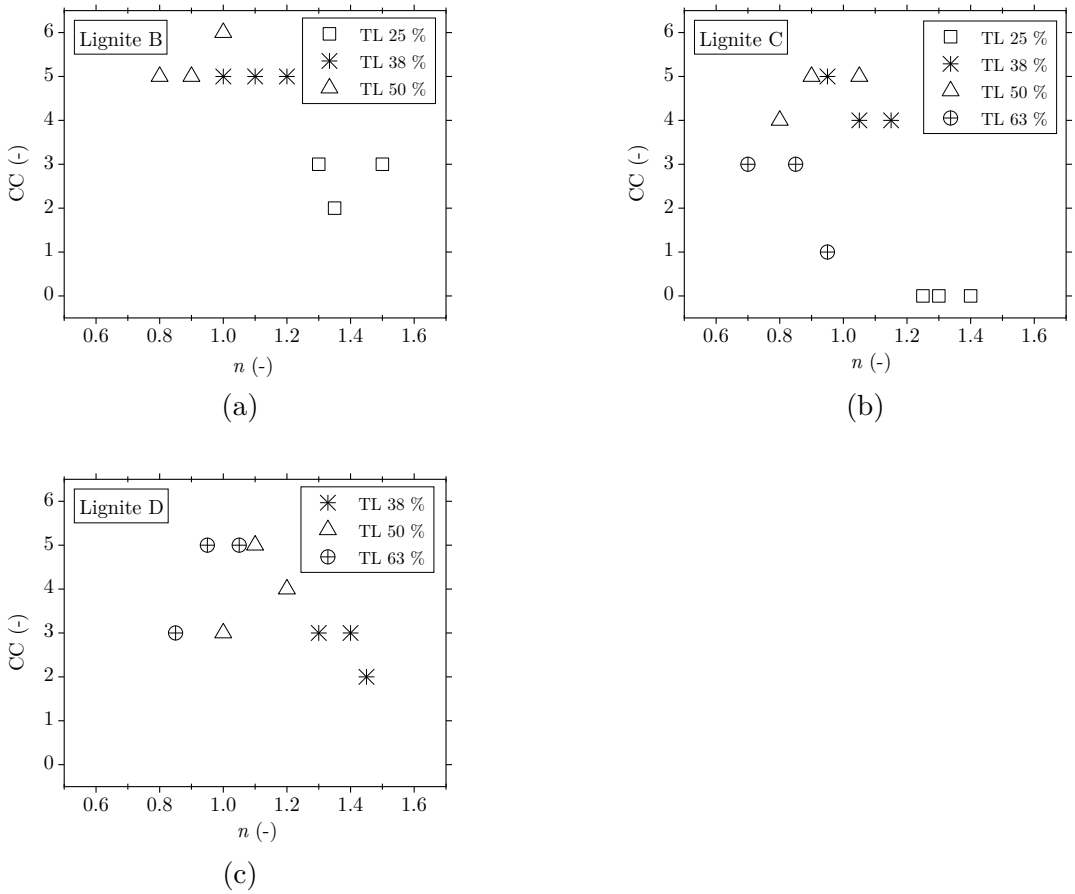


Figure 5.3: CC versus air ratio for (a) Lignite B, (b) Lignite C (ignition tests for Lignite C are performed at plasma position -40) and (c) Lignite D at different thermal loads

load is raised to a higher value of 63 %, the CC conversely drops to CC 3 and subsequently to CC 1, when the air ratio is increased from substoichiometric to the stoichiometric condition. The results of Lignite C suggest that self-sustained flames are obtained over specific thermal loads, 38 % and 50 %, and air ratios from 0.9 to 1.05. The CC at each thermal load behaves differently in relation to the air ratio. An increased air ratio has a beneficial influence on CC at the thermal load of 50 %, whereas it has negative effects on it at thermal loads of 38 % and 63 %.

Figure 5.3c illustrates that Lignite D, similar to Lignite C, reaches ignition at the thermal load of 38 %. Further increase of the thermal load to 50 % and 63 % results in the formation of self-sustained flames under specific air ratios. Increasing the air ratio shows a positive impact on the CC for the thermal load of 63 % with an air ratio range of 0.85 to 1.05. At 50 % thermal load, the CC first increases and then decreases, as the air ratio is increased from 1.0 to 1.2. At the lowest thermal load of 38 %, the ignition and formation of a coherent flame are hindered when the air ratio is increased to 1.45.

For both Lignite C and Lignite D, a self-sustained flame is obtained within a narrow operational range. Similar to the observations by others [109, 117], this behaviour highlights that fuel qualities with lower ignitability, are more sensitive to the burner boundary conditions and, thereby, optimised operational settings need to be identified through a series of experiments.

Figure 5.4a shows that CC 3 is achieved for Lignite E at 25 % thermal load, when the air ratio is reduced from 1.45 to 1.3. As the thermal load is increased to 38 %, 50 % and 63 %, still CC 3 is obtained under almost all operated air ratios from 0.7 to 1.1. The trend suggests that further increases in the thermal load, i.e. dust concentration, do not improve the combustion process to create a self-sustained flame for Lignite E, once the minimum thermal load required to form a coherent flame with plasma-supported ignition is reached. At the low thermal load of 25 %, where high air ratios are applied, the lowest operated air ratio of 1.3 is the key parameter to reach CC 3. At higher thermal loads, where the value changes from 0.7 to 1.1, the air ratio does not notably influence the ignition status.

Similar behaviour is observed for Lignite F, see Figure 5.4b. Ignition and flame formation is achieved at 50 % thermal load under substoichiometric conditions and increasing the thermal load to 63 % does not demonstrate any effect on CC. Given the operating air ratios, ignition is mainly favoured under highly fuel-rich conditions at the air ratios of below 0.7.

Figure 5.4c and 5.4d illustrate the results of ignition tests for Lignite G and Lignite H when 7 kW plasma power is used. These fuels cannot be ignited with 4.2 kW plasma and hence the plasma power is increased to provide larger ignition energy. Lignite G is ignited at the thermal load of 38 %, while a higher thermal load of 50 % was required for Lignite H to reach CC 3. Once the minimum thermal load for ignition is reached, increasing the thermal power and correspondingly the fuel quantity does not improve the CC to values higher than

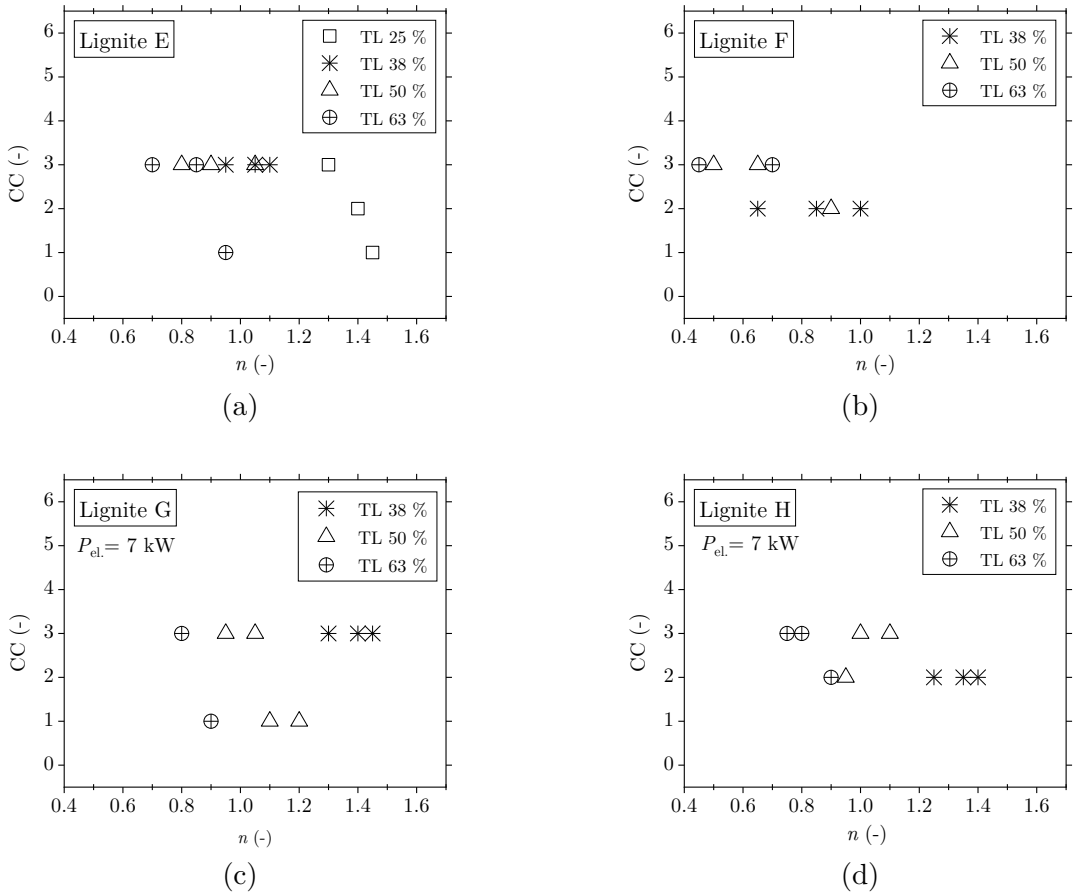


Figure 5.4: CC versus air ratio for (a) Lignite E, (b) Lignite F, (c) Lignite G and (d) Lignite H at different thermal loads, lignite G and Lignite H are ignited with a 7 kW plasma torch

3. Lignite G is ignitable over a broad air ratio range from substoichiometric to overstoichiometric up to the air ratio of 1.45, where at each thermal load operated a lower air ratio at the respective range was beneficial for ignition. Nevertheless, Lignite H does not suggest any clear relationship between the air ratio and the CC.

### 5.2.2 The effect of the thermal load and air ratio on the combustion behaviour

The ignition and self-sustained flame formation are characterised and interpreted with the help of CD and the calculated flue gas temperature. These parameters provide information on the combustion performance and the heat availability, which allow a comparative evaluation on the behaviour of lignite qualities in the plasma ignition system during the early stage

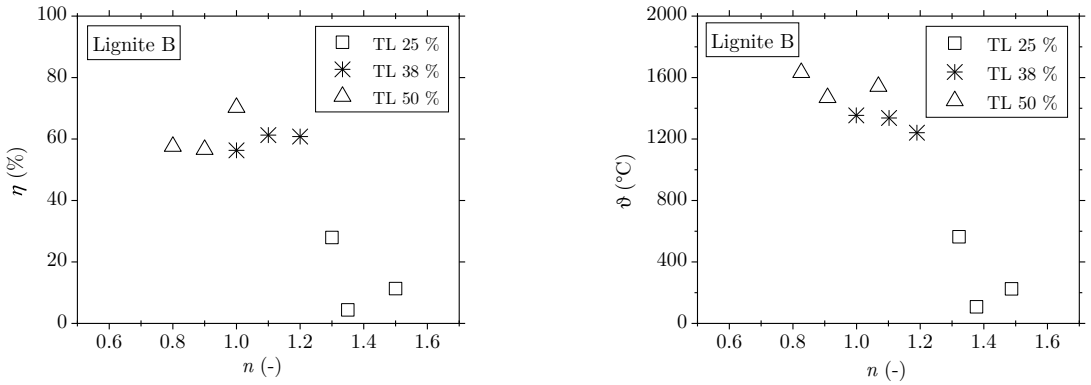


Figure 5.5: (a) CD and (b) equivalent flue gas temperature versus air ratio for Lignite B at different thermal loads

of ignition. The following evaluation also aims to identify the underlying reasons related to flame blow-out and self-sustained flame formation in the system.

Figure 5.5a compares the corresponding CD obtained at each ignition test for Lignite B. At the thermal load of 25 %, a CD of around 30 % is reached, when the CC is 3, see Figure 5.3a. The CD increases with the thermal load, which is in agreement with the behaviour of CC. As the thermal load increases, the dust concentration grows accordingly, which consequently enhances the combustion process. The highest CD value of 70 % is obtained at the thermal load of 50 % and the air ratio of 1.0 that corresponds to CC 6. An improvement in the combustion efficiency of plasma ignition with the thermal load and the air ratio was also reported by others [108].

As the air ratio at the thermal load of 25 % is increased, the CD reduces. However, a different trend is observed for higher thermal loads of 38 % and 50 %, where increasing the air ratio either enhances the CD or does not change it notably. This behaviour is associated with the heat demand required for the ignition. When a low amount of heat is produced within the early stage of combustion at the low thermal load of 25 %, increasing the air ratio, and correspondingly the secondary air enlarges the required heat demand and inhibits the ignition. Under low thermal loads, where mainly overstoichiometric air ratios are applied and a limited amount of heat is produced by ignition, increasing the secondary air serves only as a heat sink source. Nevertheless, as the thermal load is increased to 38 % and 50 %, the CD is significantly enhanced to values above 50 %, which means a considerable quantity of heat is available from the combustion process. Thus, an increased air ratio under substoichiometric and overstoichiometric conditions that yields an elevated amount of oxygen for combustion, facilitates the combustion reactions and eliminates local oxygen depletion. Once the effect of improved oxygen availability for the combustion reaction overcomes the heat loss effect, the combustion process is enhanced and consequently, a higher CD is achieved. Besides,

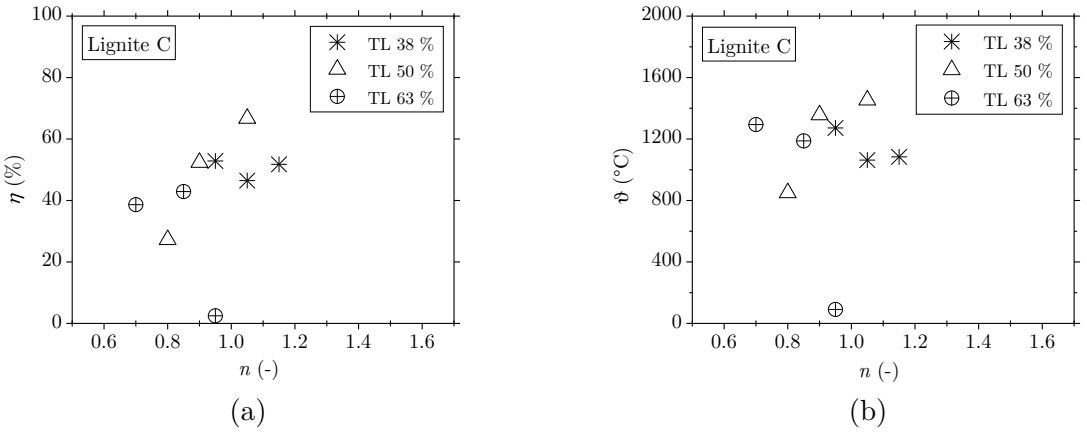


Figure 5.6: (a) CD and (b) equivalent flue gas temperature versus air ratio for Lignite C at different thermal loads

taking into account the aerodynamic boundary conditions of the burner, the formation of swirl recirculation zone can be hindered at low load operations under substoichiometric conditions. Hence, an increased secondary air also ensures a sufficient mixing of the hot flue gas products with the fresh fuel stream and the combustion air.

Figure 5.5b illustrates the effect of air ratio on the calculated flue gas temperature. Under all tested thermal loads, increasing the air ratio, even at substoichiometric conditions, tends to reduce the flue gas temperature. This highlights that, under these conditions, the improvements in the reaction kinetics resulting from an oxygen-richer environment are limited and the effect of enhancement in the rate of heat production is lower than the effect of heat loss, as the air ratio increases. Consequently, this can lead to flame blowout and ignition inhibition at excessive air ratios.

Figure 5.6a shows that CD of Lignite C is improved as the thermal load is increased from 38 % to 50 %, while a reduction in CD values is observed for 63 % thermal load, related to the reduced CC obtained at this configuration. At the minimum thermal load required for ignition, high CD values of around 50 % are obtained, thus, increasing the air ratio does not have an adverse effect on the CD. At the thermal load of 50 %, increasing the air ratio favours the CD values from around 30 % to 70 %, indicating high degrees of combustion and devolatilisation. The CD drops to around 40 %, at the thermal load of 63 %. It is assumed that a long ignition delay time and a high secondary air velocity are the associated reasons for this behaviour. This assumption is validated by comparing the calculated flue gas temperature and CD at different thermal loads.

Figure 5.6b indicates that similar flue gas temperatures at thermal loads of 50 % and 63 % are obtained. This implies that the flame blowout at 63 % thermal load is not related to insufficient heat for the continuation of the combustion reaction. The results indicate that a CD of around 30 % at the thermal load of 50 % produces an overall volatile concentration

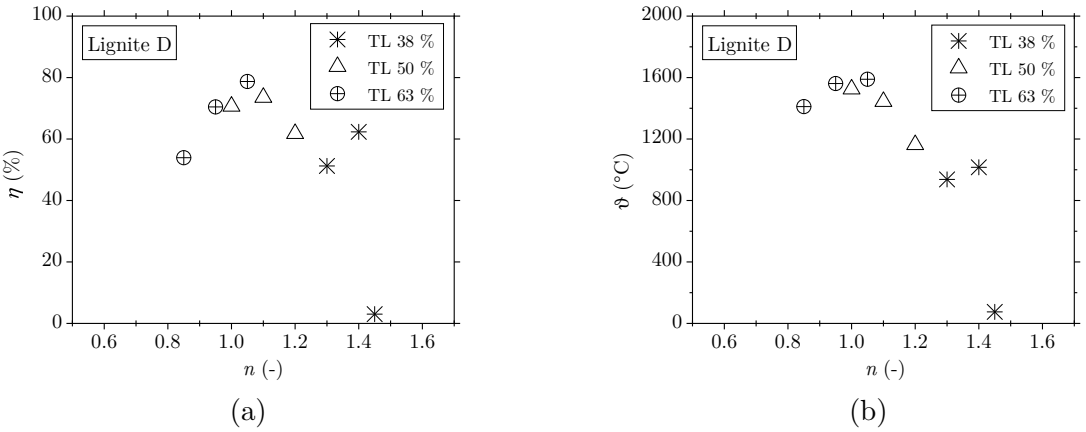


Figure 5.7: (a) CD and (b) equivalent flue gas temperature versus air ratio for Lignite D at different thermal loads

sufficient to reach CC 4 (see Figure 5.3b). Accordingly, it is unlikely that under a similar air ratio and a higher CD of around 40 % at an elevated thermal load of 63 %, the flame blowout is related to an insufficient volatile concentration. It can be concluded that the flame blowout at this configuration is most likely related to a high ratio of flow velocity to the flame velocity, which hinders the combustion reaction and eventually blows the flame out. In addition, it can be seen that similar to the CD the temperature is increasing at the thermal load of 50 % over the air ratios of 0.8 to 1.1. Under these conditions, the cooling effect of a higher air ratio is compensated by a high rate of heat production. The results of Lignite C also indicate that although there is a relation between the CC and CD, a higher CC is not always associated with a higher CD. Once the minimum amount of heat and volatiles for forming a self-sustained flame after plasma turn-off is reached, the ratio of flame velocity to the flow velocity defines the resulting CC of 4, 5, and 6. Since CC 5 and CC 6 are associated with enhanced combustion, they mainly show high CD values. However, a threshold value of CD for self-sustained flames cannot be identified.

The CD values of Lignite D are compared in Figure 5.7a. Similar to Lignite B and Lignite C, increasing the thermal load improves the CD. The influence of the air ratio on the CD for Lignite D is similar to the trends observed for Lignite C. The heat production from the improved combustion, owing to a higher oxygen availability and potentially stronger swirl intensity at higher air ratios, competes the heat loss associated with a larger heat demand and the net effect influence the CD and the flue gas temperature. At the minimum thermal load of 38 %, where CC 3 is obtained, a CD of 50 % at the air ratio of 1.3 is obtained which represents considerable heat production. A further increase in the air ratio to 1.4 and 1.45 first increases the CD to about 60 % and then decreases the CD to zero. At the thermal load of 50 %, the CD changes within a range of 60 % to 74 %. It is slightly improved, as the air ratio is increased from 1.0 to 1.1 and by a further increase to the air ratio of 1.2, a higher heat

demand associated with a larger quantity of secondary air overcomes the beneficial effect of a higher oxygen availability and consequently, the flame is cooled down and CD reduces by about 10 %. At the thermal load of 63 %, the CD value continuously increases from 54 % to about 80 %, as the air ratio changes from 0.85 to 1.05. Under this thermal load, at the air ratio of 0.85 no self-sustained flame is formed (see Figure 5.3c), but as the air ratio is increased, enhancements in the CD results in the formation of self-sustained flames within the CD values of above 70 %.

Figure 5.7b indicates that the flue gas temperature is constantly reduced at 50 % thermal load as the air ratio increases. At the highest thermal load of 63 %, the effect of enhancement in the combustion reaction overcomes the increased heat loss and hence CD and the temperature increase as the air ratio is raised from 0.85 to 1.05. The results indicate that as the CD increases considerably, the impact of enhanced combustion can dominate the heat loss. This suggests that when CD is improved at a higher thermal load, a broader range of air ratios can be applied for ignition initiation.

Figure 5.8a shows that the CD values of Lignite E slightly improve, as the thermal load is increased from 25 % to 38 % and 50 %, whereas no improvement is observed when the thermal load is further increased to 63 %. It should be emphasised that the improvements in the CD are limited to a narrow range with the minimum and maximum values of 10 % and 30 %, respectively. This behaviour postulates that the devolatilisation for this lignite quality is limited during the ignition and initial combustion, where an increased dust concentration does not have any significant impact on enhancing the combustion process. It is, therefore, considered that a low concentration of volatiles is the main parameter associated with flame blow-out when the plasma system is turned off.

An increased air ratio improves the CD values at 38 % and 50 % thermal loads, while it impairs the combustion process at the lowest and highest thermal loads of 25 % and 63 %. Since combustion cannot be rather improved at the thermal load of 63 %, the heat loss associated with the secondary air mainly dominates the heat production by the combustion process and inhibits the ignition when the air ratio is increased to near stoichiometric conditions.

Figure 5.8b demonstrates that the CD values obtained by Lignite F are not influenced by the thermal load and the values stay below 10 % within the thermal loads of 38 % to 63 %. The devolatilisation is not pronounced for this fuel quality and achieving an ignition with CC 3 at higher thermal loads is perhaps mainly associated with extended char combustion around the plasma jet due to a large fuel concentration. Given low CD values, the effect of air ratio cannot be clearly identified for Lignite F.

Figure 5.8c represents the CD of Lignite G obtained using 7 kW plasma power. The CD does not show any correlation to the thermal load and the values vary within the range of 8 % to 18 %, indicating very low degrees of devolatilisation. The air ratio has a negative influence on the CD for the thermal loads of 50 % and 63 %, while it does not notably affect the CD

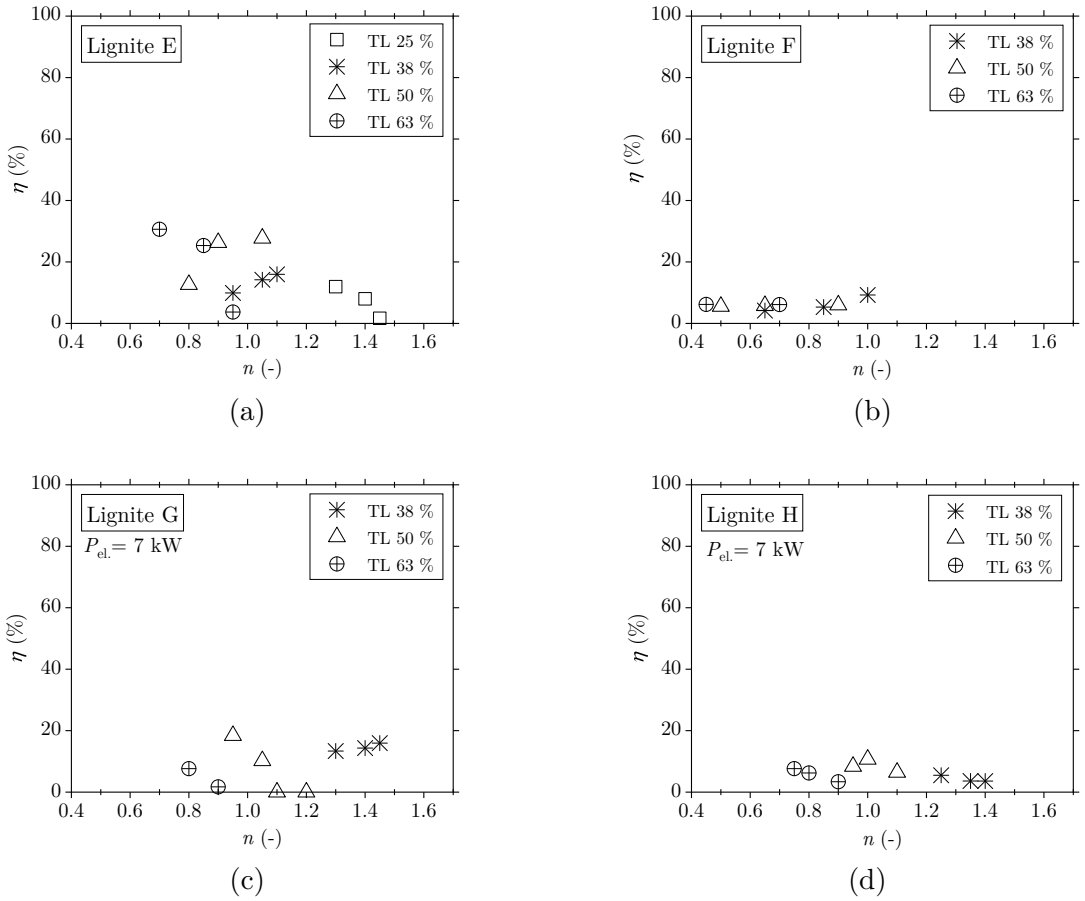


Figure 5.8: CD versus air ratio for (a) Lignite E, (b) Lignite F, (c) Lignite G and (d) Lignite H at different thermal loads

at the thermal load of 38 %. Due to extremely low CD values obtained by Lignite G, a lower air ratio to minimize the heat loss is beneficial for ignition.
The results of CD of Lignite H also show no dependency on the thermal load and the values stay below 10 %, highlighting no contribution of volatile matter in ignition and the flame formation, see Figure 5.8d. Under the thermal loads operated, the air ratio represents no progressive impact on the CD.

### 5.2.3 Characterisation of the performance of lignites in the plasma ignition system

The results of ignition testes performed for eight pre-dried lignite qualities outlines the behaviour of these fuels for the purpose of short-time plasma supported ignition under cold start-up conditions. The behaviour of these fuels with regard to ignition, devolatilisation

and self-sustained flame formation can be classified in several categories. The fuels that form an attached self-sustained flame, Lignite A and Lignite B, belong to "very high ignitability" category and lignites with detached self-sustained flame, Lignite C and lignite D, fit to the "high ignitability" category. These fuels reach high CD values which indicate good degree of volatilisation and high potential for the formation of a self-sustained flame. While CC 5 and CC 6 are obtained over a wide operational range for fuels within "very high ignitability" category, optimisation of burner parameters becomes particularly crucial when the ignitability is reduced at the "high ignitability" category. The category of "moderate ignitability" describes the fuel that are ignited with short-time plasma-support but do not form a self-sustained flame, including Lignite E and Lignite F. The CC does not improve or only slightly improves with the thermal load, once the minimum thermal load required for ignition is reached. Low CD values at high thermal loads highlight the incapability of these fuels to produce a highly-volatilised and consequently a self-sustained flame with short-time plasma support. The category of "low ignitability" includes Lignite G and Lignite H, where ignition initiation is accomplished with a higher plasma power of 7 kW. These lignites have the lowest ignitability among the tested samples, where ignition could not be accomplished with 4.2 kW plasma power. Regardless of the thermal load, very low CD values are obtained which show these fuels cannot be largely devolatilised by short-time plasma support and only a small portion of the fuel stream is combusted. These classification are summarised as follows:

**Very high ignitability (Lignite A and Lignite B)**

- Attached self-sustained flames (CC 6) are formed.
- As the thermal load increases, the ignition is improved from no ignition to the formation of self-sustained flames over a broad operational range.
- CD is improved by the thermal load, **high degrees of devolatilisation** are observed.
- Air ratio shows principally positive influence on CC and CD. Still the effect of secondary air cooling can lead to deterioration of the flame.

**High ignitability (Lignite C and Lignite D)**

- Detached self-sustained flames (CC 5) are formed.
- As the thermal load increases, the ignition is improved from no ignition to the formation of detached self-sustained flames over a limited operational range.
- CD is improved by the thermal load, **high degrees of devolatilisation** are observed,.

- Strong influence of the heat production and heat loss where CC and CD can increase, decrease or stay unchanged. An optimised air ratio is necessary to reach self-sustained flames

**Moderate ignitability (Lignite E and Lignite F)**

- Ignition and flame formation with plasma support (CC 3).
- Once the minimum thermal load for CC 3 is reached, further increase of the thermal load does not influence the CC.
- Low CD values and minor improvements by the thermal load, **low degrees of devolatilisation**.
- A lower air ratio is beneficial for ignition initiation, slight improvements in the CD are observed by the air ratio.

**Low ignitability (Lignite G and Lignite H)**

- Ignition and flame formation with plasma support (CC 3) using 7 kW plasma power.
- Once the minimum thermal load for CC 3 is reached, further increase of the thermal load does not influence the CC.
- Low CD values and no improvements by the thermal load, **low degrees of devolatilisation**.
- A lower air ratio is beneficial for ignition initiation, no improvements in the CD are also observed by the air ratio.

This characterisation provides a general overview of the ignition performance for cold start-ups in the plasma-assisted ignition system and highlights the applicability of the dedicated lignite quality to be used for this purpose. In section 5.6 the performance of these fuels are correlated to their chemical and physical properties to provide preliminary predictions on evaluating the potential of dedicated fuel qualities for this application.

## 5.3 The role of the plasma torch

To have a better understanding of the role of the plasma torch in plasma-assisted ignition, several lignites are used to investigate the influence of the plasma power and the plasma system. It is aimed to identify the effect of plasma power and different plasma systems on the ignition and the formation of a self-sustained flame as well as flame stability. The ignition and combustion processes are evaluated using the CC and CD criteria, respectively. To analyse flame stability, the flame brightness and brightness fluctuation are compared. Investigations of plasma power allow to more precisely define the required boundary conditions for ignition and development of a self-sustained flame, while concurrently optimizing system operation, where necessary plasma power with regard to the lignite quality is determined. PS I and PS II are compared at a constant power, however as explained in section 3.3.3, they generate plasma jet with different sizes. Hence, the results are expected to shed some light on the importance of the plasma jet size and the plasma power. This optimisation is of high relevance for the economic aspects of the technology when plasma power and correspondingly the operating costs can be reduced to minimum.

### 5.3.1 The effect of the plasma power

To identify the effect of plasma power on lignites with different ignition characteristics, Lignite B, Lignite C, Lignite D, Lignite E and Lignite G are used for this study. In the following, Lignite B, Lignite C and Lignite E are selected for studying the effect of plasma power on flame stability.

**The effect of the plasma power on ignition and combustion:**
Figure 5.9 shows the CC and CD obtained with Lignite B using 4.2 kW and 7 kW plasma power. As can be seen, the same CC values are obtained under all four operational settings. For Lignite B, no improvement in CC can be observed using a higher plasma power under both 25 % and 38 % thermal loads. Figure 5.9b illustrates that at the thermal load of 25 % and the air ratio of 1.5, the CD obtained with 7 kW plasma power is around 10 % higher compared to 4.2 kW power. Under the other three configurations, plasma power of 4.2 kW showed slight to large improvements in the CD values compared to 7 kW. The findings indicate that although an enhancement in CD is observed under one setting with 7 kW plasma power, a higher plasma power does not necessarily enhance the combustion process, rather, it is possible that combustion is deteriorated. Lower CD values observed for tests with 7 kW

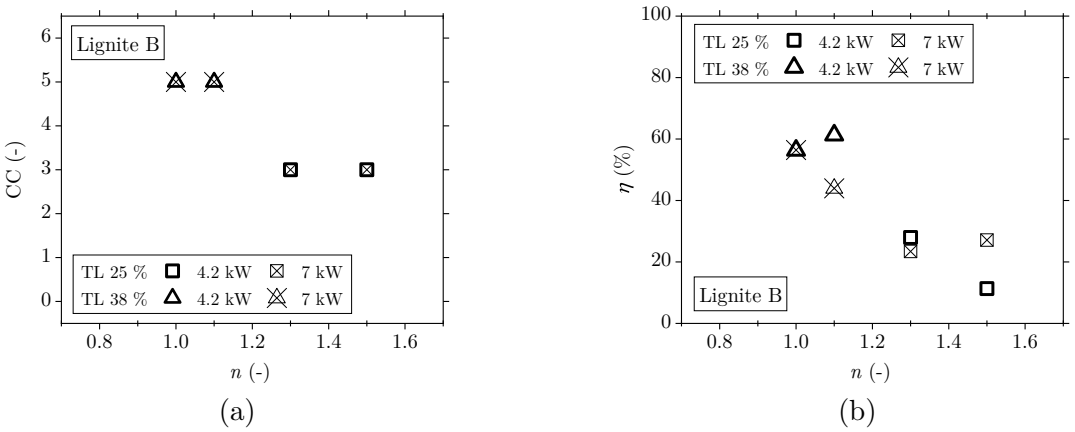


Figure 5.9: (a) CC and (b) CD for Lignite B for 4.2 kW and 7 kW plasma power

plasma power are assumed to be related to a higher velocity of the plasma working gas. This difference in the velocity enlarges considerably when the gas is ionised at a temperature range of 10 000 °C. As a result, the plasma jet formed with 7 kW power has a higher velocity than that of 4.2 kW and therefore coal particles are transported faster within the plasma jet zone. This effect can have a negative impact on the extent of combustion within the flame, resulting in a lower CD value under a higher plasma power.

Figure 5.10 illustrates the CC and CD for Lignite C and Lignite D using 4.2 kW and 7 kW power. The results of CC for both fuels show similar behaviour, see Figure 5.10a and 5.10c. The ignition is improved from CC 0 and CC 2 to CC 3 at the lowest thermal load for Lignite C at 25 % and for Lignite D at 38 %. The effect of higher plasma power compensates the insufficient ignition boundary condition, related to a low dust loading, and enhances the ignition to form a stable flame with plasma support at the lowest thermal load for each fuel. However, as the load is increased above the minimum thermal load, CC values achieved with 4.2 kW power are either higher or similar to those obtained with 7 kW. Higher plasma power does not improve the CC, once the necessary dust loading is available and the ignition is consequently initiated. For both fuels, plasma power of 4.2 kW reaches CC 5 under dedicated operational conditions, whereas no self-sustained flame (CC above 5) is obtained using 7 kW. From 15 operational settings investigated for both fuels, 7 kW plasma power reaches CC 4 at only two settings, whereas 4.2 kW plasma power achieves CC values of 4 and 5 under seven settings. This behaviour is similarly considered to be related to a higher velocity if the plasma working gas for 7 kW power, where the formation of a self-sustained flame is deteriorated. After the plasma turn-off, the cold gas stream still flows from the plasma torch nozzle in the centre of the flame. This cold flow with a higher velocity increases the probability of local flame extinction and perhaps is the main reason that no self-sustained flame is formed at a higher plasma power of 7 kW. This effect, however, is not observed for Lignite B. Lignite B, which belongs to the “very high ignitability” category, showed a stable

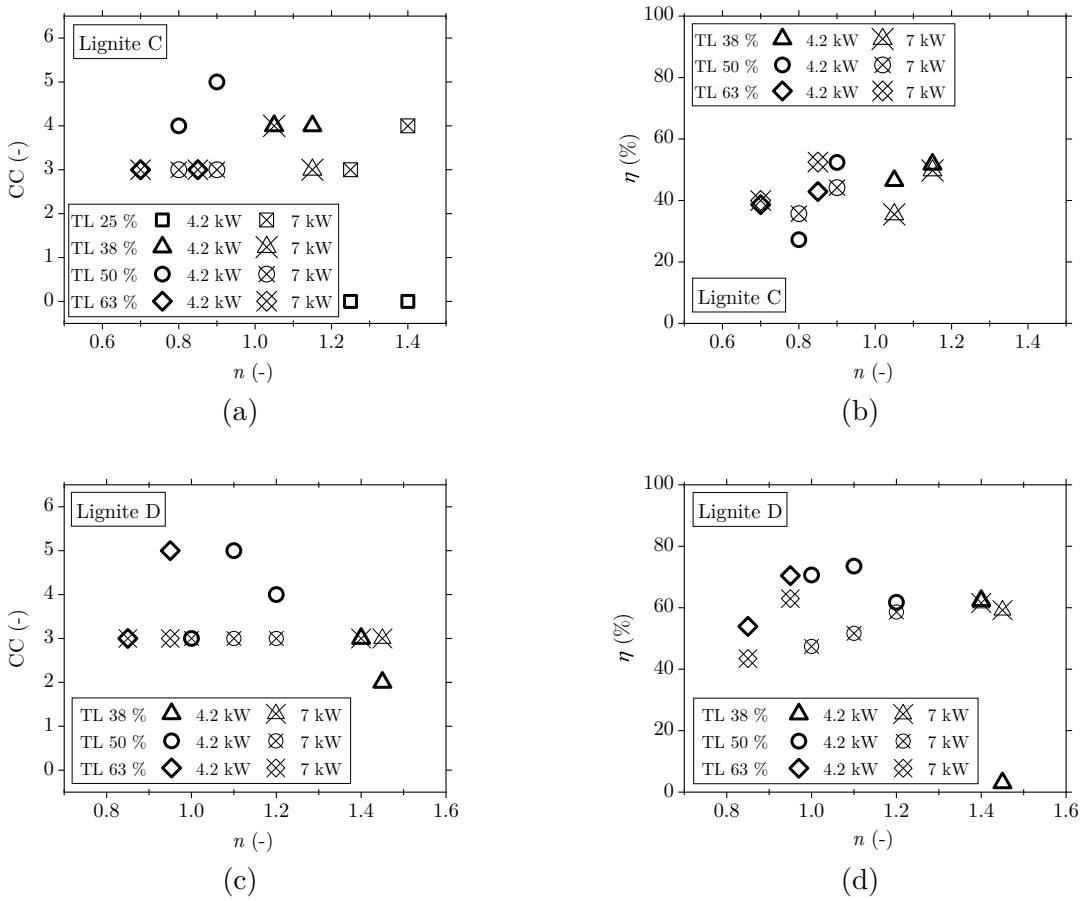


Figure 5.10: (a) CC and (b) CD for Lignite C, (c) CC and (d) CD for Lignite D with 4.2 kW and 7 kW plasma power

performance over a wide operational range. The fuels within this category are less sensitive to the undesired boundary conditions, whereas the performance of fuels within the "high ignitability" category can be more readily influenced.

Figures 5.10b compares the CD values obtained with Lignite C using different plasma powers, excluding the lowest thermal load of 25 %. Similar or slightly higher CD values are observed with 4.2 kW in four out of six settings. Similar to the results obtained with Lignite B, no significant improvement in the combustion process is shown at the plasma power of 7 kW compared to 4.2 kW. Figure 5.10d shows the CD values of Lignite D for both plasma power values. The results confirm the trend observed for Lignite B and Lignite C, where the higher plasma power does not improve the combustion process once the ignition is initiated. The fuels investigated above (Lignite B, Lignite C and Lignite D) belong to the "very high ignitability" and "high ignitability" categories. These categories are associated with a high degree of devolatilisation. Hence, the flame produced is a highly-volatile flame and correspondingly volatile combustion controls the combustion process. Under such circumstances, the role of the plasma jet is only to initiate the ignition and afterwards, the volatile combus-

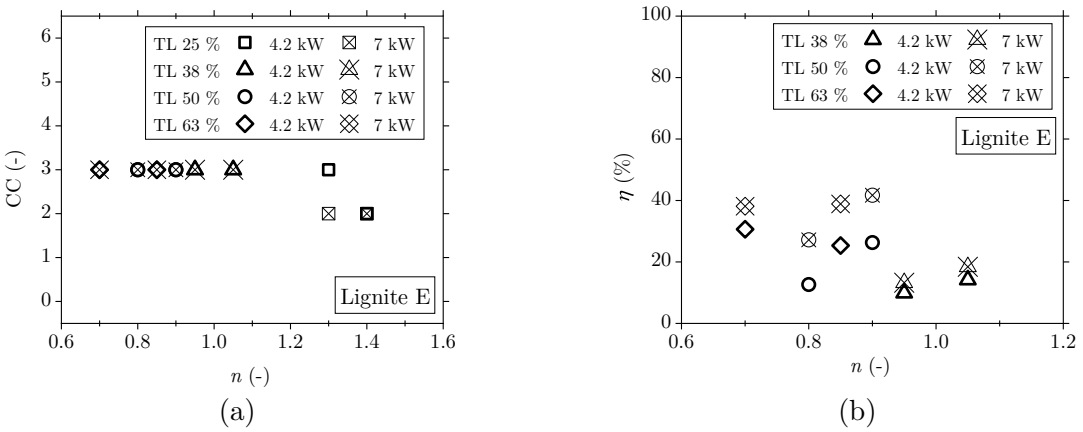


Figure 5.11: (a) CC and (b) CD for Lignite E with 4.2 kW and 7 kW plasma power

tion governs the process. As explained earlier, a lower CD value with a higher plasma power can possibly be related to a higher plasma gas velocity and consequently a shorter residence time of a part of coal particles within the flame area.

Figure 5.11a shows the CC values obtained for Lignite E using 4.2 kW and 7 kW plasma power. For this fuel, higher plasma power cannot improve the CC values at any of the operated thermal loads. Apart from the lowest thermal load of 25 %, CC 3 is achieved under both plasma powers for all the settings investigated. Figure 5.11b represents the CD values of Lignite E. For this fuel at the thermal loads of 50 % and 63 %, 7 kW plasma power produces flames with considerably higher CD values compared to 4.2 kW power. This trend contradicts the results observed by fuels within the "very high ignitability" and "high ignitability" categories. A possible explanation for this behaviour can be the controlling combustion regime. Lignite E, within the "moderate ignitability" category, is associated with a low degree of devolatilisation. This means the flame, to a large extent, propagates by char combustion and volatiles in the close vicinity of the plasma jet. For this fuel, plasma

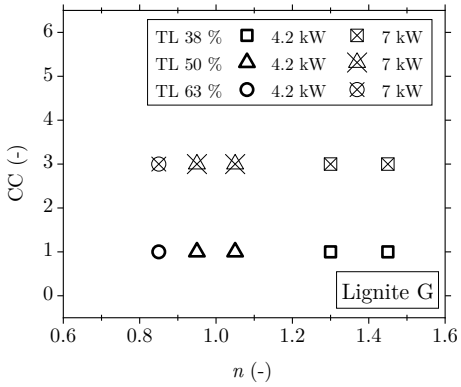


Figure 5.12: CC for Lignite G with 4.2 kW and 7 kW plasma power

jet works not only as an ignition initiator but also as a continuous source of heat for flame propagation. Therefore, the plasma power can significantly contribute to the combustion process and as observed a higher plasma power can improve the CD values by around 10 % within the CD range of 10 % to 30 %.
Figure 5.12 shows that Lignite G cannot be ignited under any thermal power using 4.2 kW plasma power. To initiate the ignition and to form a stable flame 7 kW plasma power is required. A higher plasma power increases the heating rate of the particles and realizes the ignition. For fuels within the "low ignitability" category, ignition cannot be accomplished with 4.2 kW and higher power of 7 kW is required.

**The effect of the plasma power on flame stability:**
The influence of the plasma power on flame brightness and stability for Lignite B, Lignite C and Lignite E using 4.2 kW and 7 kW are illustrated in Figure 5.13. Here, flame brightness indicates the area covered by the flame root within the captured frame. In the cases that the flame completely covered the investigated area, saturations in the brightness values are observed, for example at thermal loads of 50 % and 63 % for Lignite C and Lignite E with 7 kW plasma power, see Figure 5.13c and 5.13e. However, a clear effect can be seen in flame brightness by different plasma powers. From Figures 5.13a, 5.13c and 5.13e, it can be seen that flames formed with 7 kW plasma power have higher flame brightness under all investigated settings. The effect is not visible for Lignite E at the thermal load of 50 % and 63 %, due to the explained saturation effect, where similar flame brightness values are obtained under both plasma powers. This shows that 7 kW plasma produces flames with a more stable root zone, which is probably due to faster particle ignition and a reduced ignition delay time.
The effect of plasma power on the flame brightness fluctuation represents a similar trend for all three lignites investigated. Figure 5.13b shows that the flame fluctuation under both thermal loads are reduced as plasma power is increased from 4.2 kW to 7 kW. The fluctuations are also influenced by the thermal load. An increase in the thermal load decreases the fluctuation under both plasma powers, indicating the formation of more stable flames at higher thermal loads. Similarly, Figure 5.13d illustrates that the flame fluctuations for 7 kW power stay below 8 %, whereas they rise from 8.3 % to 20 % for the plasma power of 4.2 kW. For Lignite E, the improvements in flame stability by a higher plasma power can only be observed at the thermal load of 30 %, see Figure 5.13f. At higher thermal power the flames with 4.2 kW show comparable fluctuation in the low range of 0.6 % to 1.6 %. This shows high flame stability for flames with 4.2 kW. However, the results can be influenced by the brightness saturation effect, where the fluctuation cannot be precisely captured.

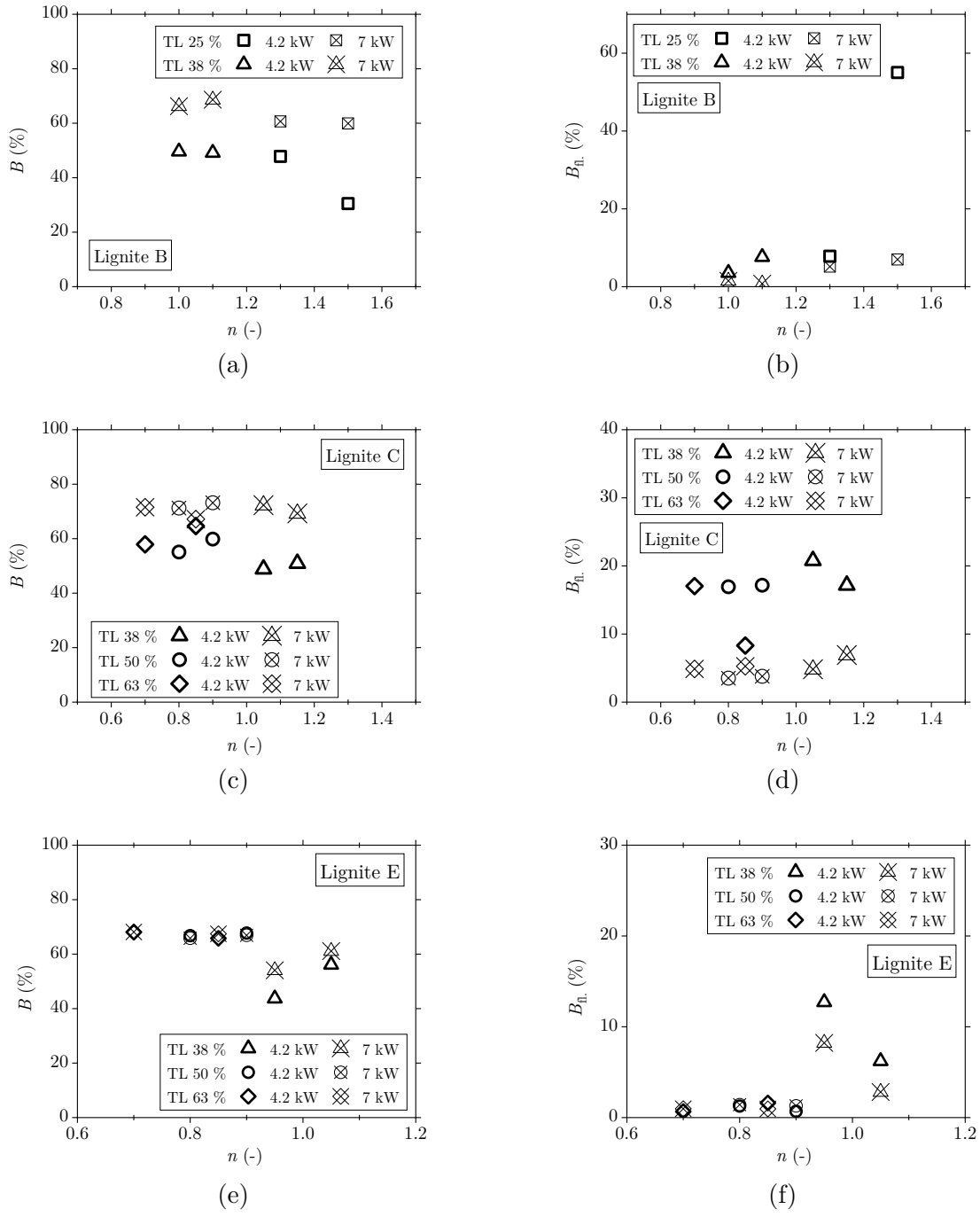


Figure 5.13: Flame brightness for (a) Lignite B, (c) Lignite C and (e) Lignite E, brightness fluctuation for (b) Lignite B, (d) Lignite C and (f) Lignite E with 4.2 kW and 7 kW plasma power (aperture of f/16 for all three lignites)

**Summary:**

The results of investigations of the effect of plasma power on ignition and combustion show that for fuels within the top two ignitability categories, plasma jet works as the primary source only for the ignition initiation. Since these fuels can be ignited relatively easily and produce a highly-volatile flame, higher plasma power just showed beneficial effects at the

minimum thermal load, where ignition boundaries are extended using this higher plasma power. As the fuel ignitability reduces, the power of the plasma jet becomes more important for ignition and combustion, where a higher plasma power improves the combustion process and enables the ignition for fuels within the "low ignitability" category. However, for none of the investigated fuels, higher plasma power could improve the CC from a stable flame with plasma support (CC 3) to the formation of a self-sustained flame (CC 5 and CC 6) in the absence of plasma. This conclusion is, however, only limited to the investigated plasma power of 4.2 kW and 7 kW. The effects observed by a power increase in this small margin can differ when the plasma power is increased by a larger factor of 3 to 5. This is more relevant when burner upscaling is of interest. To validate this hypothesis, experiments at industrial or large scales are required, where the plasma power is changed within a range of 20 kW to more than 100 kW. Investigations of flame brightness and brightness fluctuation show that increasing the plasma power from 4.2 kW to 7 kW improves flame stability, as the flame brightness increases and the fluctuation decreases. The enhancement in the flame stability is observed for lignites within different ignitability groups from "very high ignitability" to "moderate ignitability". Hence, it can be deduced that increasing the plasma power although does not enhance the CC and CD, can clearly improve flame stability in the root region regardless of the fuel ignitability category.

### 5.3.2 The effect of the plasma system

The reference PS I is compared with another DC plasma system, PS II, to investigate how the ignition is influenced by different plasma torches. The ignition tests are compared at constant 7 kW electrical power. The plasma jets produced with these two systems differ in the size and the velocity of the working gas. As mentioned earlier due to a different torch nozzle design and operating parameters, PS II produces a plasma jet less volumetric than PS I. The 7 kW plasma jet of PS I is formed with a working gas velocity two times faster than that of PS II. Although PS II produces a smaller plasma jet, which is considered a drawback for it, a lower working gas velocity, while producing the same power as that of PS I, can to some degree compensate for this disadvantage. In the following, Lignite D, Lignite E, Lignite G and Lignite H are used to compare the performance of these systems with regard to ignition initiation and combustion enhancement. Lignite D and Lignite E are further used to investigate the influence of the systems on flame stability.

**The effect of the plasma system on ignition and combustion:**
Figure 5.14a and 5.14b illustrate the CC and CD obtained for Lignite D using PS I and PS

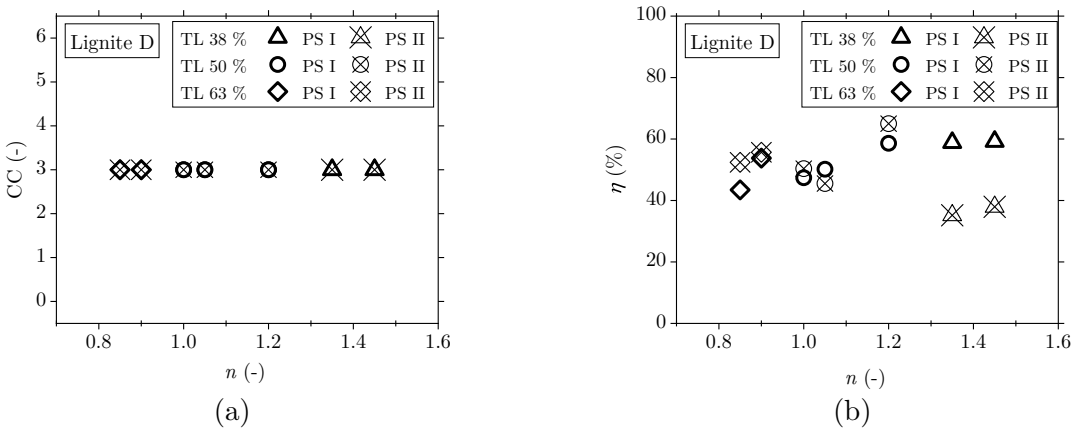


Figure 5.14: (a) CC and (b) CD for Lignite D with PS I and PS II

II. As can be seen, both systems are successful in igniting and forming a stable flame at the thermal load of 38 %. Similar CC of 3 is obtained using both systems under the settings investigated. PS I shows considerably larger CD values at the lowest thermal load of 38 %, while as the thermal load is increased, slightly higher values are obtained by PS II. This behaviour can be possibly explained by the differences in the plasma jet characteristics of each system. At the thermal load of 38 %, combustion is more influenced by a smaller plasma jet, because the dust concentration is not sufficiently high to form a highly-volatile flame independent of the plasma jet. PS I, with a larger plasma jet, benefits from an improved particle-plasma interaction, which leads to enhancements in the combustion process. At this thermal load, the influence of the plasma jet on the combustion process is more pronounced. As the thermal load and, correspondingly, the dust loading is increased, the probability of the particle passage through the plasma jet is higher. Therefore, there is sufficient contact between the plasma and particles to form a coal flame that mainly controls the rate of combustion. Once the flame is established and the combustion process is mainly governed by the volatile combustion, no significant difference is observed between the two systems. A slower plasma jet of PS II is assumed to be the reason for slightly higher CD values at the thermal loads of 50 % and 63 %.

Figure 5.15a shows that at the lowest thermal load investigated (25 %), CC 2 is achieved with PS I for Lignite E, whereas the fuel stream is not ignited by PS II. This is similarly related to a smaller plasma jet, when the dust loading is low. An increased dust concentration at higher thermal power compensates the insufficient plasma-particle interaction for the PS II jet and except one point, similar CC of 3 is obtained by both systems. Figure 5.15b displays that for Lignite E, PS I achieves either similar or higher CD values compared with PS II, excluding one measurement point at the air ratio of 1.05. The higher CD values with PS I is obtained at each thermal load under the larger air ratio. A smaller plasma jet demonstrates slightly less effective combustion when higher heat losses are experienced at the larger air ratios.

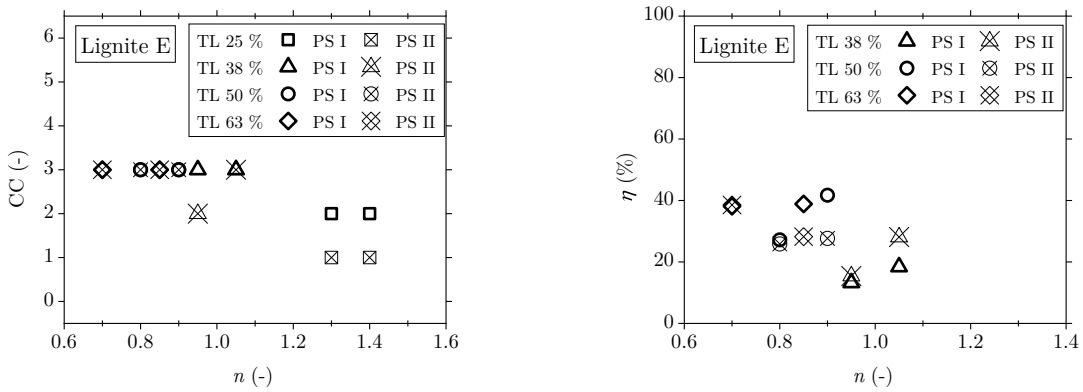


Figure 5.15: (a) CC and (b) CD for Lignite E with PS I and PS II

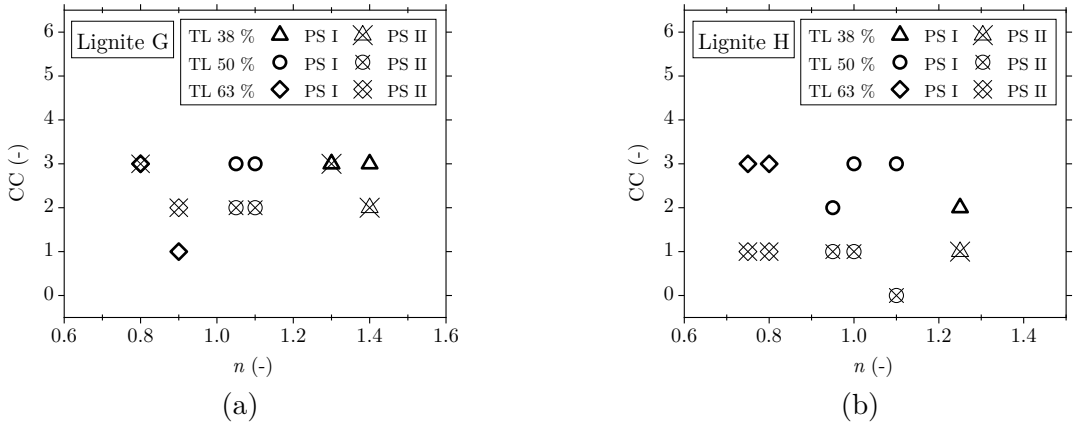


Figure 5.16: CC for (a) Lignite G and (b) Lignite H with PS I and PS II

Figure 5.16a represents that PS I is more effective in igniting Lignite G compared with PS II. From six ignition tests evaluated, PS II reaches CC 3 in only two settings compared with five settings for PS I. The advantage of a larger plasma jet is more evident for Lignite H. Figure 5.16b shows that PS II is not capable of initiating the ignition for Lignite H. PS II achieves CC 0 and CC 1, whereas PS I reaches CC 2 and CC 3. From the six investigated points, PS I successfully ignites Lignite H under four operational settings.

**The effect of the plasma system on flame stability:**

Figure 5.17 displays the flame brightness and brightness fluctuation using PS I and PS II for Lignite D and Lignite E. First, it has to be mentioned that due to specific camera settings used for each fuel quality, the values should not be compared between different fuels. The camera settings are adjusted specifically for each dedicated fuel quality, which allow comparisons between different configurations performed. Figure 5.17a and 5.17c show that the flame brightness values with PS I are, under all tested thermal loads and air ratios, above

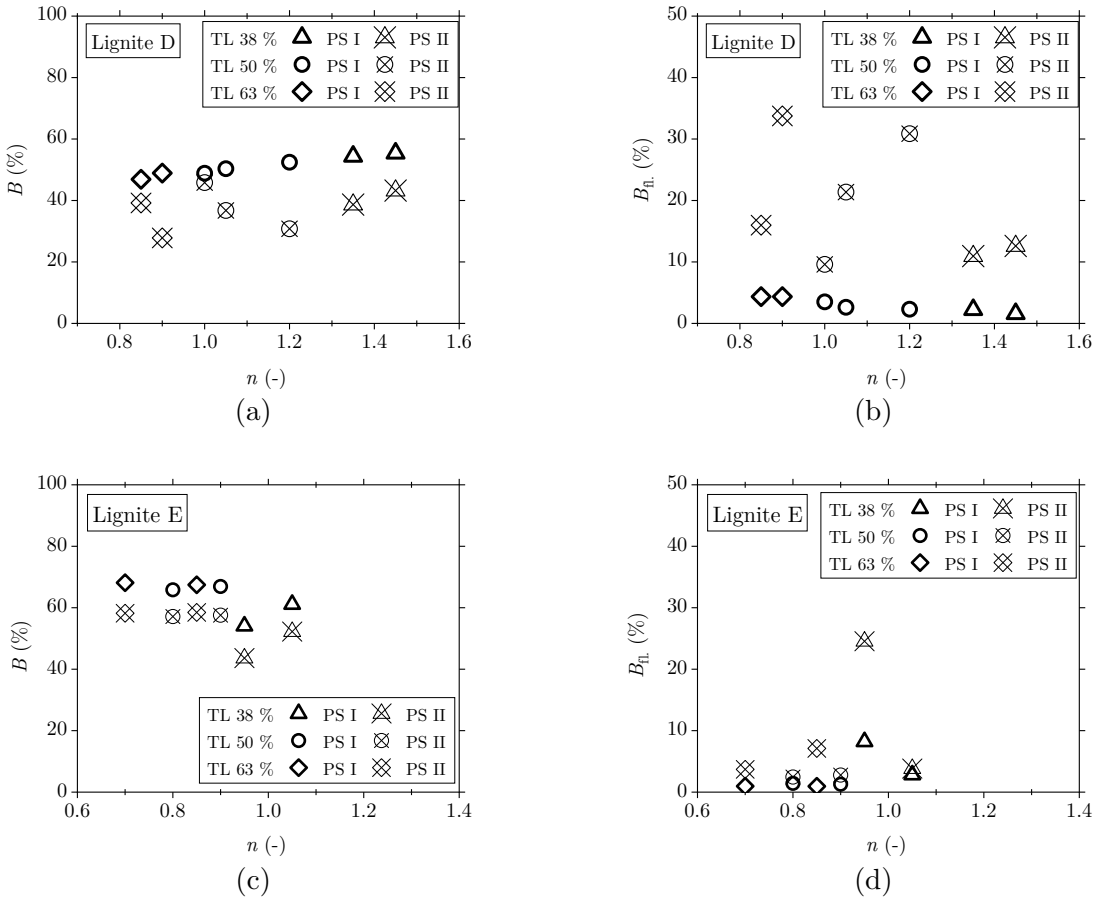


Figure 5.17: Flame brightness for (a) Lignite D and (c) Lignite E, brightness fluctuation for (b) Lignite D and (d) Lignite E with PS I and PS II (aperture of f/16 for Lignite E and f/22 for Lignite D)

those obtained by PS II for both Lignite D and Lignite E. This indicates that PS I system is capable of producing flames with a larger root region for Lignite D and Lignite E compared with PS II.

The brightness fluctuation for Lignite D are compared in Figure 5.17b. As can be seen, the flame fluctuation stays below 5 % with PS I, while the flames produced by PS II fluctuates between 10 % to 35 %. Brightness fluctuations indicate that PS I produces flames with considerably higher stability compared with PS II. Figure 5.17d does not show considerable variations in the brightness fluctuation between the systems, except at two operational settings. PS II shows a high fluctuation of above 20 %, which is related to an unstable flame with CC 2. Under other settings investigated both systems demonstrate a low fluctuation of below 10 %, though, the values for PS I were still below those of PS II.

**Summary:**

Investigations of two plasma systems with same electrical power highlight the importance

of sufficient contact between the plasma jet and fuel particles. This parameter becomes essentially critical, when the fuel ignitability is reduced. For fuels within the "high ignitability" category no notable difference is observed between the performance of the systems with regard to ignition and flame formation. As the ignitability of the fuel is reduced to the "moderate ignitability" group, the system with the smaller plasma jet is still competent for ignition initiation and flame formation. However, as the ignition boundary conditions are worsened, e.g. a low dust loading or a higher air ratio, the smaller plasma jet shows less effectiveness under several configurations. Once the fuel quality is reduced to the "low ignitability" category, where ignition is only possible with a 7 kW plasma torch, the smaller plasma jet fails to reach the same CC values as the other system. Lignite H that has the least ignitability, cannot be ignited using the system with the smaller plasma jet. It is believed that the size of the plasma jet is one of the decisive parameters that defines the applicability of the system. In particular, for the fuels within the "very high ignitability", "high ignitability" and "moderate ignitability" categories, a larger plasma jet is expected to be a potent measure to reduce the minimum thermal load required for ignition. For fuels within the "moderate ignitability" category, the plasma jet plays a role not only as an ignition source but also as an essential support to sustain the flame. As a result, the extent of plasma-particle contact during plasma-assisted combustion influences the degree of combustion enhancement. For the fuels of "moderate ignitability" category, it is expected that a considerably larger plasma jet is beneficial to enlarge the coal flame and, therefore, can be considered as a potential factor to support the formation of a self-sustained flame. For fuels within the "low ignitability category", by a rough comparison, similar results are observed with the smaller plasma jet (PS II) and 4.2 kW power of PS I. It is believed that the size of the plasma jet, i.e. plasma-particle contact, is as important as the plasma power for ignition of difficult fuels. A possible approach that is expected to be effective can be enlarging the size of the plasma jet, for example via a new nozzle design or a change in the flow rate of the plasma working gas, instead of increasing the plasma power. Further experimental investigations are required to prove this statement. Investigations of flame brightness and brightness fluctuation reveal additional information with regard to flame stability by the two plasma systems. Although a comparable performance is observed for fuels within "high ignitability" and "moderate ignitability" categories, flames produced with PS I show higher brightness levels and smaller fluctuations. This highlights that a larger plasma jet can notably improve the flame size and stability in the root region even for fuels that form a high-volatile flame.

## 5.4 Investigations of the burner design and aerodynamics

Within this section, the influence of burner flow profiles and the burner design on plasma-assisted ignition will be investigated. The effect of the secondary air swirling and primary air swirling at different plasma positions will be first assessed using Lignite B. The evaluation is supported by isothermal CFD simulations of the primary air flow and fuel particles to gain a better understanding of the influence of particle trajectories on the ignition probability. Subsequently, the impact of the plasma position in the burner is investigated using lignites from different ignitability groups, Lignite B, Lignite D, Lignite E and Lignite G. In the following, two alternative primary air nozzle designs are tested to investigate any improvement potentials using toothed or baffle ring nozzles, where the investigation is only limited to one lignite quality for each comparison. Last but not least, a reduced primary air velocity is tested for WP 1 and Lignite G.

### 5.4.1 The effect of swirling

The influence of flow swirling on ignition and the flame formation is investigated using Lignite B. This fuel, due to its high ignitability is expected to be less sensitive to the changes in the system boundary conditions. Therefore, when an effect is observed by this fuel quality, the effect can be certainly expanded even to a larger extent to the fuels with a lower ignitability. In section 5.4.1.1 the influence of the secondary air swirling on CC and CD is studied, where the swirl number is changed from 0.9 to 0. Section 5.4.1.2 evaluates the impact of primary air swirling at plasma position 0 as well as position -40 and -80. The axial velocity field and approximate particle trajectories are illustrated at different plasma positions and discussions are made with regard to the boundary conditions required for ignition and self-sustained flame formation. Afterwards, the experimental results on the effect of primary air swirling are analysed and discussions are made with regard to the findings of the particles flow trajectories and the velocity profiles in the critical zone of the plasma jet.

#### 5.4.1.1 The effect of secondary air swirling

Figure 5.18 shows the CC and CD values obtained with Lignite B versus the theoretical swirl number at plasma position 0 and -40. It can be seen that at position 0 the CC drops from CC 5 to CC 3 as the swirl number is decreased from 0.9 to 0.5. Further reductions in the swirl number to 0.27, 0.1 and 0 lead to unsuccessful ignition indicated by CC 1. A similar trend is evident at plasma position -40, where no ignition is observed at the swirl numbers of below 0.5. However, a reduction in the swirl number from 0.9 to 0.5 does not impact the CC at this plasma position. A lower flow velocity at plasma position -40 compared with position 0 is probably the underlying reason for a self-sustained flame at this configuration. Figure 5.18b shows that the decrease from CC 5 to CC 3 at plasma position 0 is associated with a notable fall in the CD from around 56 % to 30 %. Deterioration in the combustion process by reducing the swirl number to 0.5 is also observed at the position -40, where despite a constant CC, the CD is slightly reduced from 55 % to around 48 %. The results further highlight the role of swirl not only in flame stabilisation, but its necessity to initiate the ignition under cold plasma-assisted ignition conditions. At very low swirl numbers the particles have a large axial velocity and therefore do not have a sufficient residence time within the plasma zone. As a result, the critical ignition conditions with regard to volatile concentration and heat are not fulfilled. For weak swirl at below 0.4 swirl number, no recirculation zone is formed and the swirling only enlarges the flow width and increases the velocity decay as well as the entrainment. From the swirl number of proximately 0.6, a strong swirl is formed which is associated with the appearance of the recirculation bubbles, where the downstream gas is recirculated back to the burner outlet zone [77–79]. This recirculation supports the plasma-assisted ignition in two ways, first, it increases the residence time of the particles in the critical ignition zone in the surrounding of the plasma jet and second, it recirculates the released volatiles back to the ignition zone, increasing the concentration of volatiles and the probability of ignition. For the swirl burner used, it is expected that the recirculation bubbles are already formed at the swirl number of 0.5, where ignition is observed. The formation of toroidal bubbles is likely the main reason for successful ignition. The results also indicate the necessity of a certain swirl degree to reach self-sustained flame. Flame blowout after plasma shut-down is related to low CD and most probably a high primary air momentum. As the swirl degree is increased and recirculation bubbles expand, a larger amount of hot flue gas products are brought back to the flame zone and the primary air is more entrained to secondary air and correspondingly the axial velocity is further reduced. This condition improves combustion efficiency and correspondingly flame stability, where self-sustained flames are formed under both plasma positions. The swirl number of 0.9 was the maximum swirl degree achievable in the investigated burner. It is expected that a higher swirl number has the potentials for further enhancements in flame stability and can be used

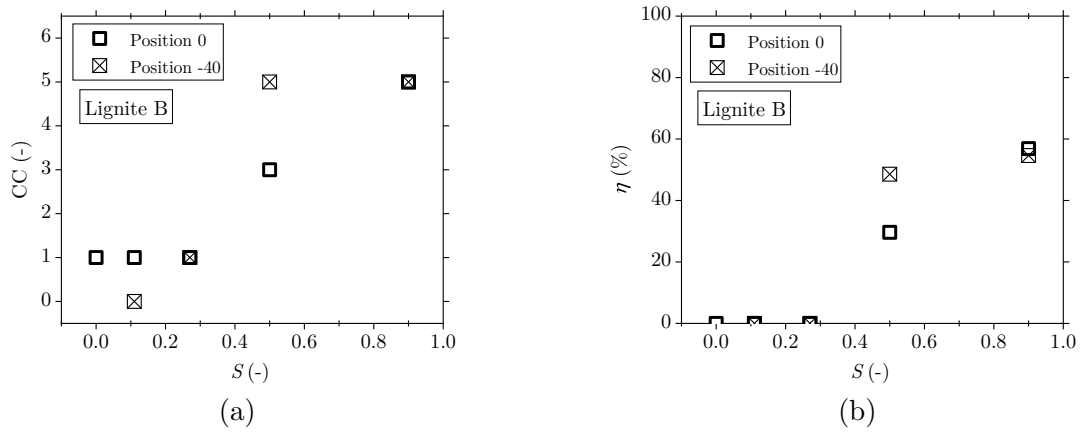


Figure 5.18: (a) CC and (b) CD for Lignite B versus secondary air swirl number at the thermal load of 38 % and the air ratio of 1

as a measure to shift a detached flame closer to the burner outlet, aiming to reach CC 6. However, special attention needs to be given to the high turbulence intensity and too early mixing resulting in local flame extinction when very high swirl numbers are applied.

#### 5.4.1.2 The effect of primary air swirling at different plasma positions

The impact of primary air swirling on ignition and the flame formation shows a strong relation to the burner configuration, in particular the plasma position. The swirling of primary air is expected to considerably change the particle transport and trajectories inside the burner as well as at the burner outlet. These swirling particles interact differently with the plasma jet depending on the position of the plasma within the burner. Therefore, the influence of primary air swirling is investigated at three plasma positions, position 0, position -40 and position -80. The velocity field and particle trajectories are illustrated to provide a better understanding of the flow field and plasma-particle interaction at different configurations.

**Particle trajectories and velocity fields:**

Figure 5.19 shows the velocity field with swirling and non-swirling primary air at different plasma positions. At position 0, swirling results in the formation of a recirculation zone at the burner outlet characterised by negative axial velocities. The flow recirculation is associated with a longer residence time within the critical ignition zone around the plasma jet. A strong decay in the axial velocity at the longitudinal direction from the burner outlet is notably detected for the swirling primary air. After the burner throat, the maximum axial velocity at the radial distance is slightly shifted towards the centre, where the plasma jet

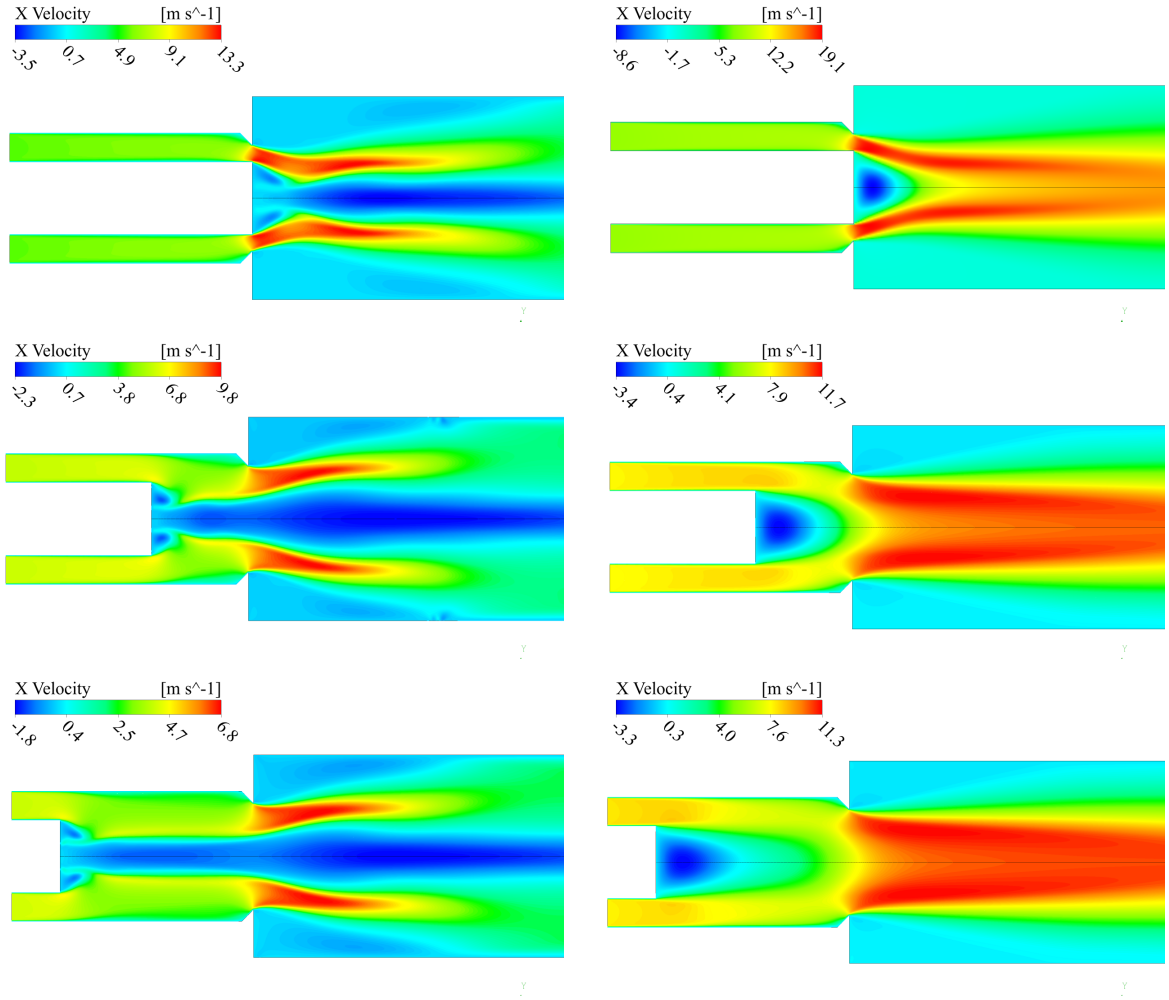


Figure 5.19: Axial velocity fields for (left) swirling primary air and (right) non-swirling primary air at plasma positions from top to bottom 0, -40 and -80

is located, due to a contracted nozzle outlet, but afterwards the maximum axial velocity is slightly moved outwards because of a high swirl velocity. Accordingly, the swirl velocity component produces a wide flow field, which is expected to considerably improve the mixing of the fuel stream with the secondary air.

The non-swirling primary air has a maximum axial velocity of 19 m/s at the burner outlet, which is relatively higher than that for the swirling flow with 13 m/s. The flow is deflected towards the centre and decays in axial velocities are not observed for the non-swirling flow close to the burner zone. A small recirculation zone is formed behind the plasma lance, which stems from a pressure drop at this position. This phenomenon is similar to the recirculation formed by bluff bodies. However, as the recirculation zone is very small in the size, it is not expected to contribute to the flame stabilisation.

As the plasma lance is retracted inside the burner by 40 mm, the axial velocity in the area of the plasma jet is lower than that at position 0. The maximum axial velocity of the swirling flow reduces in the pre-combustion zone inside the burner and increases afterwards at the

contracted burner outlet to the maximum velocity of 10 m/s. A small recirculation zone is formed inside the burner, behind the plasma lance, which is followed by a larger recirculation zone at the burner outlet. A similar behaviour in the longitudinal velocity profile is observed for the non-swirling flow, where the maximum velocity reduces in the pre-combustion section and increases at the burner outlet. For the non-swirling flow, the maximum velocity of around 12 m/s is slightly higher than the maximum velocity of the swirling flow. At position -40, the residence time within the critical ignition zone is still considerably longer for the swirling flow, because of the lower axial velocity and flow recirculation, compared with the non-swirling flow.

As the plasma lance is retracted to plasma position -80, the maximum flow velocity at the burner outlet is further reduced to approximately 7 m/s, due to a larger axial velocity decay of the swirling flow up to the burner outlet. For this plasma position, the initial plasma-particle interaction mostly takes place inside the burner. Although the flow velocity within the plasma jet area is lower than other configurations, which results in a longer plasma-particle contact time in a once-through flow, a narrow recirculation zone inside the burner is associated with less recirculation at this plasma position. For the non-swirling flow, plasma position -80 creates the lowest axial velocity profile within the critical ignition zone among the other plasma positions, as the plasma-particle interaction occurs inside the pre-combustion chamber and before the velocity rise at the burner outlet. For plasma position -80 at the burner outlet, a maximum velocity of around 11 m/s, similar to the one achieved with position -40, is calculated.

Figure 5.20 illustrates the predicted particle trajectories and an imaginary plasma jet at different positions for the swirling and non-swirling primary air. As can be seen, for the swirling flow under all three plasma positions, a large portion of the particles is thrown towards the inner circumference of the primary air nozzle. The accumulation of particles at the nozzle wall reduces the particle concentration at the radial distance from the plasma jet which in consequence lowers the probability of contact between the particles and the plasma jet. The particle radial distribution profile in the swirling flow depends on the particle size and the swirl degree. The bigger particles, due to a larger swirl momentum, are expected to be accumulated at the nozzle wall and the very fine particles are carried by the flow. Hence, although the particle concentration in the surrounding of the plasma jet is reduced, there are still fine particles following the gas flow. For the non-swirling flow, the particles are governed by the axial velocity component. The non-swirling flow creates a relatively uniform particle concentration over the cross section.

The inclined nozzle design at the burner outlet deflects the particles for both swirling and non-swirling flows towards the plasma jet in the centre. The non-swirling flow at plasma position 0 shows a large degree of contact between the plasma jet and the particles. At the deflector, few particles lose their axial velocity component and are thrown radially towards

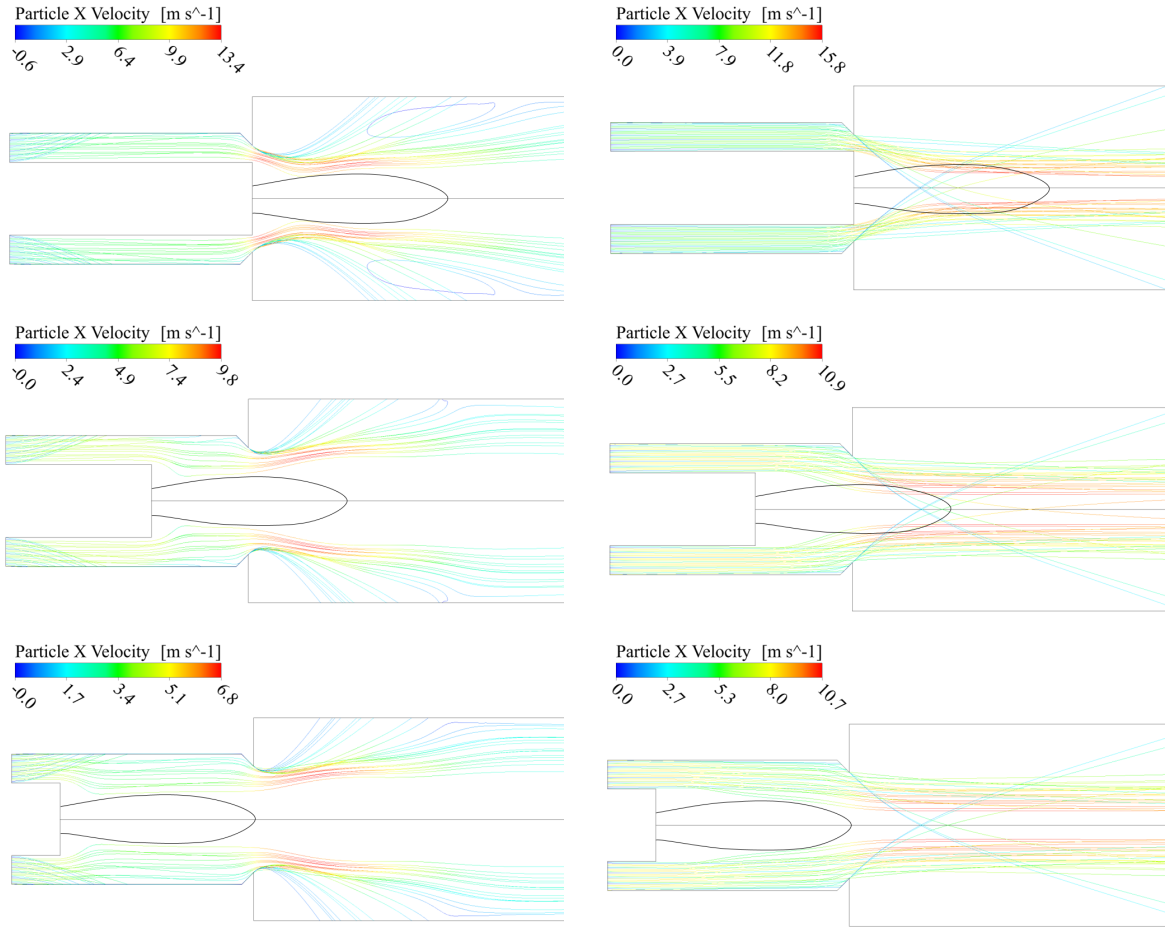


Figure 5.20: Particle trajectories for (left) swirling primary air and (right) non-swirling primary air at plasma positions from top to bottom 0, -40 and -80

the plasma jet. Nevertheless, the non-swirling particles are transported downwards with a relatively high axial velocity. For the swirling flow at plasma position 0, the smaller particles mainly follow the primary air, where they are first drawn inwards to the plasma jet and then outwards. The larger particles that are accumulated at the outer wall fly away to the surrounding after the burner outlet. The distribution of swirling particles in the furnace cross section investigated experimentally also showed a higher particle concentration at a radial distance further away from the centre compared with the non-swirling particles [179]. Although the smaller particles that follow the air flow are expected to be recirculated within the recirculation bubbles [180], this behaviour could not be predicted by the particle trajectories simulations. Compared to the non-swirling primary air, not only a much smaller portion of particles are transported by the flow but also the flow field has hindered the contact probability. It is important to highlight that although the swirling particles have impaired contact with the plasma jet compared with the non-swirling particles, they have notably a lower axial velocity and correspondingly a longer residence time within the plasma jet. Moreover, it should be also considered that the size of the plasma jet starts to enlarge

after the initial contact with the surrounding coal particles, which then results in a wider jet with an increased plasma-particle contact probability.
At plasma position -40, a part of the plasma jet is out of the burner throat and a part is located inside the burner. The initial plasma-particle contact is then expected to take place inside the burner, within the pre-combustion zone. The swirling particles are slightly distributed along the nozzle cross section due to the expansion in the surface area between the plasma lance and the burner outlet. As the swirling particles have a low velocity, they are stretched towards the plasma jet shortly after the expansion. At the contracted burner outlet the probability of contact is further improved but then the particles are dragged outwards. Thus, it is expected that most of the contact takes place within the first part of the plasma jet, inside the burner. The non-swirling particles are transported downwards with the flow after the expansion and are stretched towards the plasma jet shortly before the burner outlet. At the inclined burner outlet, they pass through the plasma jet with a higher velocity.
As the plasma lance is further retracted inside the burner to position -80, the entire plasma jet is located inside the burner. Hence, the inclined burner outlet does not play a significant role in improving the plasma-particle contact. At this plasma position, the contact is only accomplished through flow expansion inside the burner. Although the non-swirling particles have a lower contact probability at plasma position -80 compared with other positions, they have relatively longer residence time in the plasma jet. Similarly, for the swirling particles, the probability of contact is reduced but once the particles meet the plasma jet, they pose a longer contact time as they are carried along the entire plasma length with a lower velocity. The velocity field and particle trajectories comparison at different plasma positions with swirling and non-swirling primary air show benefits and drawbacks for each configuration. The swirling flow, on one hand, produces a recirculation zone with lower axial velocity and large velocity decays and, on the other hand, lowers the probability of contact between the particles and the plasma jet. By retracting the plasma position inside the burner, the plasma-particle contact probability is reduced, as a part or all of the interaction occurs inside the burner before the contraction at the burner outlet, but concurrently, the particles experience a longer residence time within the plasma jet thanks to a lower velocity. The net effect of these benefits and drawbacks determine the ignition and combustion performance that is investigated in the following.

**Ignition and flame characteristics:**
**The effect of primary air swirling on ignition and flame stability:** The ignition and combustion performance, as well as the flame stability and fluctuation, are compared for non-swirling ($S$ 0) and swirling primary air ($S$ 0.9) at two thermal loads, see Figures 5.21 and 5.22. Figure 5.21a shows that at the thermal load of 25 %, ignition and flame formation

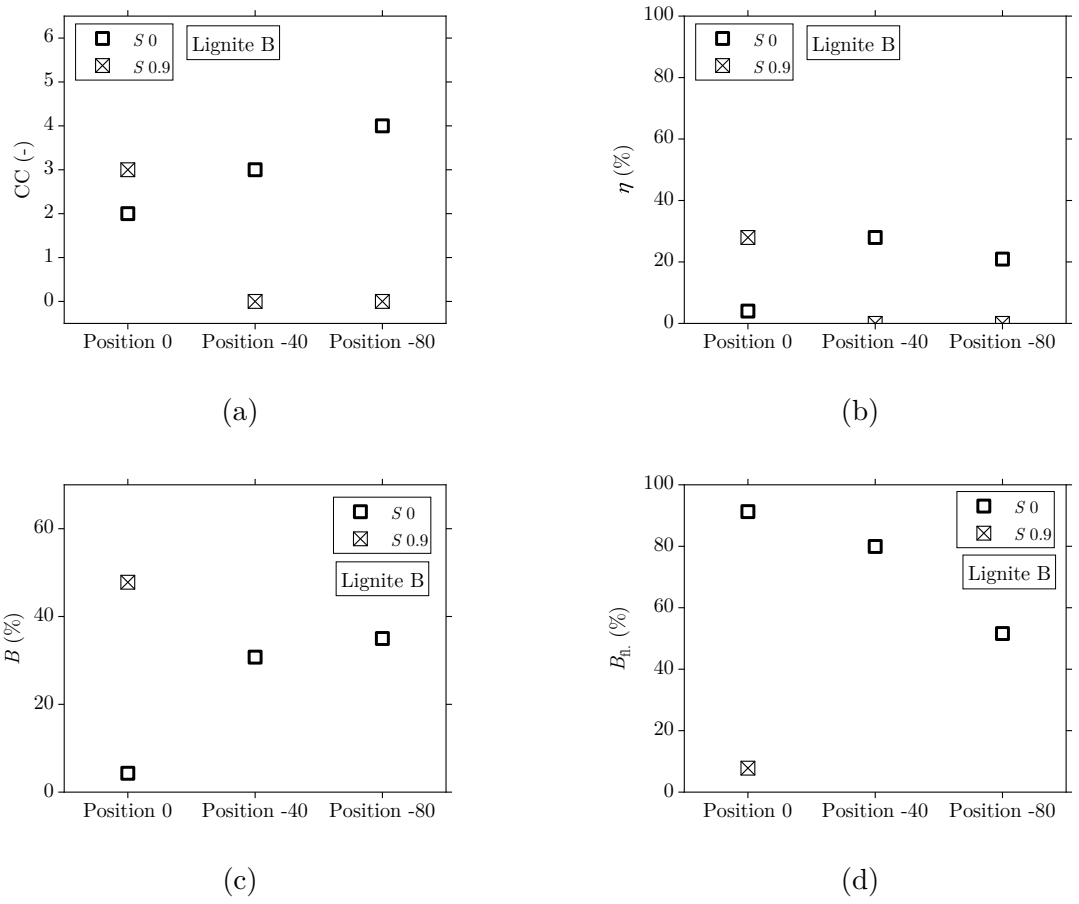


Figure 5.21: (a) CC, (b) CD, (c) flame brightness and (d) brightness fluctuation for swirling ($S$ 0.9) and non-swirling ($S$ 0) primary air with Lignite B at the thermal load of 25 % (aperture of f/16)

for the swirling primary air is only achieved at position 0 with CC 3, whereas for the non-swirling flow, a flame cannot be formed at position 0 but CC 3 and CC 4 are reached as the plasma is retracted to position -40 and -80, respectively. Figure 5.21b presents comparable CD values for the swirling flow at position 0 and the non-swirling flow at position -40, with a slight decrease in the CD as the lance is shifted to position -80. Figure 5.21c shows that the flame formed at plasma position 0 with the swirling primary air demonstrates the highest flame brightness and the lowest fluctuation in the range of 10 %. For the non-swirling flow, unsuccessful ignition with CC 2 is characterised by close to zero flame brightness and fluctuation of around 90 %. Moreover, the flames formed at position -40 and -80 have lower brightness levels than the swirling flow's flame and they show high fluctuations and poor stability, see Figure 5.21d. Nonetheless, the brightness fluctuation is reduced from 80 % to 50 %, as the plasma is further retracted inside from position -40 to -80. A lower fluctuation at position -80 compared with -40 indicates that for a non-swirling flow this position has the most favoured condition, owing to an increased residence time. Even though CC 4 is

obtained with the non-swirling flow at position -80, flame stability for the swirling flow with CC 3 is notably higher.

A similar comparison is made at the higher thermal load of 38 %, where an increased dust loading is expected to improve the ignition. Figure 5.22a displays a self-sustained flame formation with CC 5 under position 0 and position -40 for the swirling flow. The increased dust loading was also beneficial for the non-swirling flow, where CC 4 is achieved at position 0 and retracting the plasma position improves the ignition to CC 5 at both plasma positions of -40 and -80. Figure 5.22b suggests that all the flames formed have comparable CD values of around 50 %, with a slightly higher value for the swirling flow at plasma position 0. The flame brightness and fluctuation in Figure 5.22c and 5.22d show a clear trend for the swirling and non-swirling flow as the plasma is retracted inside the burner. In case of non-swirling flow, the brightness is increased when the plasma is moved from position 0 to position -40 and -80. In contrast, in case of swirling flow, position 0 shows a flame brightness higher than the one achieved by position -40. The brightness fluctuations indicate the formation of a flame with low stability at position 0 for the non-swirling flow and a significant improvement in flame stability at positions -40 and -80, where fluctuations of less than 5 % are detected. For the swirling flow, high flame stability is observed at plasma position 0 with around 5 % brightness fluctuation, while the value grows to around 25 %, as the position is changed to -40.

The results indicate that for a swirling flow, plasma position 0 and a non-swirling flow, plasma position -80 represent the best performance. Plasma position -40 also shows a comparable performance, like position -80, in a non-swirling flow and also satisfactory results under non-swirling primary air, in case of sufficient dust concentration. For the swirling flow, the probability of plasma-particle contact is improved at the contracted nozzle outlet. The inclination of nozzle outlet seems to be a crucial parameter, which greatly influences the plasma-particle contact for the swirling flow. At position 0, the particles have a velocity that provides sufficient residence time for the particle heating. A lower velocity at plasma positions -40 and -80 does not have a positive effect on the particle ignition, as the contact between the swirling particles and the plasma jet is hindered at retracted positions. Furthermore, the swirling primary air creates a recirculation zone which additionally improves the ignition boundary conditions by recirculating the released volatiles back to the critical ignition zone. At position 0 and -40, further recirculation by secondary air swirling provides additional heat, volatiles and even partly volatilised coal particles to the critical ignition zone, in the surrounding of the plasma jet. When the plasma is retracted completely inside the burner, the plasma-particle contact takes place in the absence of these recirculation bubbles and it is not improved by the nozzle contraction, which leads to unsuccessful ignition at position -80.

For the non-swirling flow, contraction at the burner nozzle accelerates the particles substan-

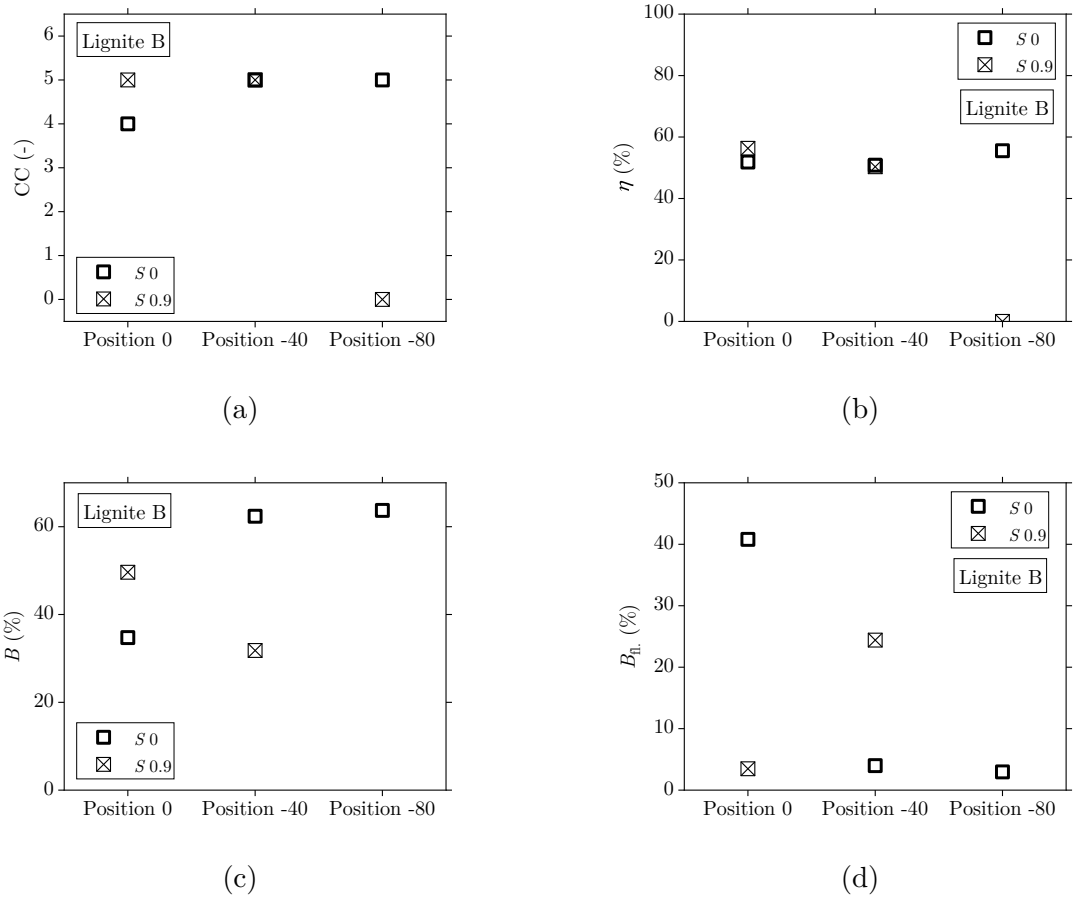


Figure 5.22: (a) CC, (b) CD, (c) flame brightness and (d) brightness fluctuation for swirling ($S$ 0.9) and non-swirling ($S$ 0) primary air with Lignite B at the thermal load of 38 % (aperture of f/16)

tially, leading to a low residence time within the plasma jet. Although the contact is less effective before the nozzle contraction, the non-swirling particles are evenly dispersed at the cross section of the pre-combustion chamber. Thus, when a sufficient dust loading is reached, the retracted plasma positions offer a lower velocity and longer residence time within the plasma jet, which shows a beneficial influence on ignition. In addition, at positions -40 and -80, the contact takes place at a lower air ratio which further supports the initial ignition.

**The effect of primary air swirling on the flame shape:** Figure 5.23 shows the flame shape for the swirling and non-swirling primary air. The flame formed with the non-swirling flow has a longer flame length, while the flame with swirling primary air shows a wider and shorter flame formation at the burner mouth. This flame shape is observed for the non-swirling flow under all three plasma positions. Due to high particle inertia in the non-swirling flow at position 0, the coal particles penetrate in the internal recirculation zone, created by the swirling secondary air, forming a penetration flame. This penetration in the

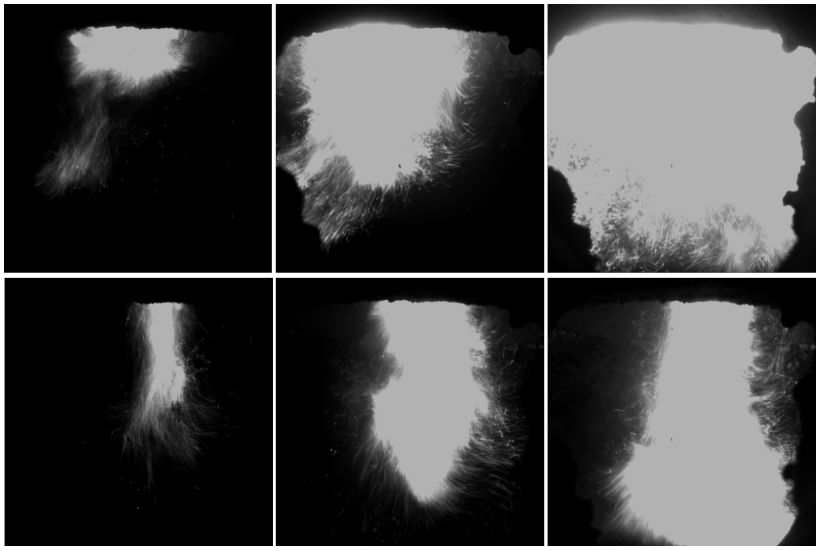

Figure 5.23: Flame shape (top row) swirling primary air (bottom row) non-swirling primary air at 38 % thermal load and position 0

CTRZ hinders the recirculation of downstream products, containing released volatiles at the ignition stage and hot flue gas products at the combustion stage in the central zone. The particles are then ignited under an air-staged condition, which is limited by oxygen availability [84, 92]. It is expected that this particle penetration is lessened as the plasma lance is retracted to positions -40 and -80, where the particle axial momentum is reduced. On the contrary, the swirling particles are dragged outwards and are assumably ignited on the mixing boundary layer of the secondary air and the CTRZ and consequently forming a wide and short flame. Hence, igniting and devolatilisation occur under air-rich conditions [84].

**Summary:**
Ignition and stable flame formation require effective plasma-particle interaction and an appropriate particle velocity to provide a sufficient residence time within the plasma jet. The swirling particles are associated with a less effective plasma-particle contact and the non-swirling particles have a high velocity and a low residence time in the plasma jet zone. The retraction of plasma lance inside the burner further hinders the plasma-particle interaction for the swirling flow as the contact cannot be improved by the burner nozzle contraction, whereas this parameter seems less relevant for the non-swirling flow and instead, a reduced gas velocity, as a results of expansion at the pre-combustion chamber, and potentially an air-lean environment represent positive impacts on the ignition boundary conditions. The flow recirculation associated with the swirling primary air have additional benefits for ignition and formation of a stable flame at position 0 and -40. This leads to the formation of a shorter and wider flame which is preferred for a pulverised fuel burner. The findings suggest that for the burner investigated, the swirling primary air at plasma position 0 rep-

resents the most promising configuration, since a flame with high stability, even at a low dust loading, is formed. Once the dust concentration is increased, the non-swirling flow also creates stable flames with low fluctuations at retracted plasma positions. Though, longer and narrower flames are formed. For the burner investigated, the highest secondary air swirl number of 0.9 seems to be insufficient to form a wide and short flame when the primary air is not swirled. For burner optimisation, it is recommended to design a burner with a higher secondary air swirling degree to create larger recirculation bubbles and to shorten the flame length. In return, a non-swirling primary air or primary air with a lower swirling degree offers an appropriate plasma-particle contact. Under these circumstances, plasma position -80 or even further retraction inside the burner is crucial to have a sufficient particle residence time within the plasma jet.

## 5.4.2 The effect of the plasma position

Based on the results obtained from section 5.4.1.2, plasma position -80 is unfavoured when the primary air is swirled. Therefore, only position 0 and -40 are further investigated using other quality lignites. The impact of the plasma position on ignition, combustion and flame brightness and stability is investigated using lignites from different ignitability groups, Lignite B, Lignite D and Lignite E. The data presented for Lignite B and E are obtained with 4.2 kW plasma power and for Lignite D, they are related to 7 kW plasma power. The impact of the plasma position on the ignition is also investigated using Lignite G with 7 kW plasma power. The investigation aims to determine the most suitable plasma position considering different fuel qualities and burner operational parameters. Since the impairment in the contact between the plasma jet and the swirling particles is expected to be compensated by a high dust concentration, as previously shown and discussed in Figure 5.21 and 5.22, in this section, the performance at higher thermal loads is more of interest.

**The effect of the plasma position on ignition and combustion:**
Figure 5.24 shows CC and CD for the three lignites investigated. Plasma position -40 leads to no ignition for Lignite B at the lowest tested thermal load of 25 %, see Figure 5.24a. As the thermal load is increased to 38 %, similar CC 5 are achieved at the air ratios of 1 and 1.1 under both plasma positions, while further increase in the air ratio to 1.2 leads to no ignition under plasma position -40. At a higher load of 50 %, a contrary trend is observed. Plasma position -40 showed similar or higher CC values. At the air ratio of 0.9, a detached self-sustained flame is anchored at the burner mouth, as the plasma lance is retracted inside the burner from position 0 to -40. Figure 5.24b shows CD values of 10 % to 30 % for

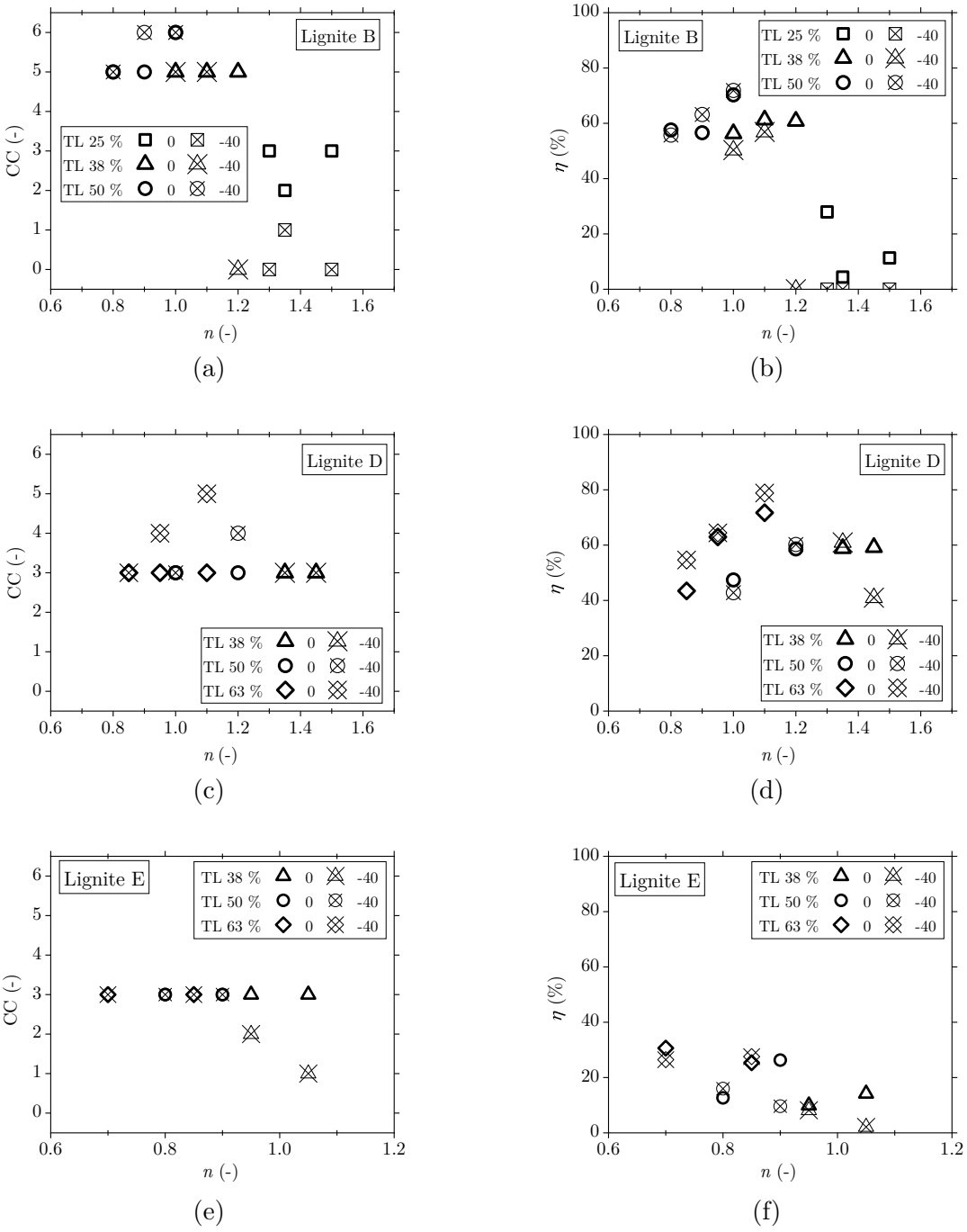


Figure 5.24: (a) CC and (b) CD for Lignite B, (c) CC and (d) CD for Lignite D (7 kW plasma power), (e) CC and (f) CD for Lignite E at plasma positions 0 and -40

position 0 at the lowest thermal load of 25 % for Lignite B, while no ignition is detected for the position -40. Around 5 % enhancement in CD values for position 0 compared with position -40 are also obtained at the thermal load of 38 %, where both positions produced detached self-sustained flames. At the highest thermal load of 50 %, similar CD values at both positions are observed at the air ratios with CC 5, while position -40 shows a slightly

improved CD related to its higher CC 6.

Figure 5.24c illustrates that at the lowest thermal load investigated for Lignite D both positions reach the same CC values. At the higher thermal load of 50 % and 63 %, plasma position 0 reaches CC 3 under all tested air ratios, while position -40 reaches CC 4 and CC 5 under three configurations. The CD values of Lignite D at position 0 and -40 do not show a clear correlation, see Figure 5.24d. At the thermal load of 38 %, position 0 showed a higher CD at the air ratio of 1.45 and a similar one at the air ratio of 1.35. For the thermal load of 50 % comparable CD values are obtained under both positions. As the thermal load is further increased to 63 %, moderate improvements of 7 % to 10 % in CD values at position -40 under two air ratios are observed.

Figure 5.24e shows that for Lignite E, differences in the CC resulted from two plasma positions are just observed at the lowest thermal load of 38 %, where ignition is only reached at position 0. At higher thermal loads, both positions reached CC 3 under the investigated configurations. Accordingly, Figure 5.24f indicates larger or comparable CD values with position 0.

The influence of retracted plasma position on the ignition and combustion shows a corresponding behaviour for the three lignites investigated. At lower thermal loads, where the dust concentration is small, the impairment in the plasma-particle interaction at position -40 is evident, as observed for Lignite B and Lignite E. The value of the critical dust concentration may vary, as for lignite B with higher ignitability, this trend is observed at 25 %, while it is shifted to a higher thermal load of 38 % as the ignitability is reduced for Lignite E. This behaviour is, however, not observed for Lignite D. The reason can be related to a higher dust concentration for this fuel due to its lower calorific value. At the thermal load of 38 %, Lignite D has a dust flow rate of 34 kg/h compared with 29 kg/h for Lignite E. As the dust concentration increases, it compensates the imperfect plasma-particle contact at position -40, which results in a similar or even enhanced ignition and combustion performance when the concentration is further enlarged. This enhancement by position -40 was only related to

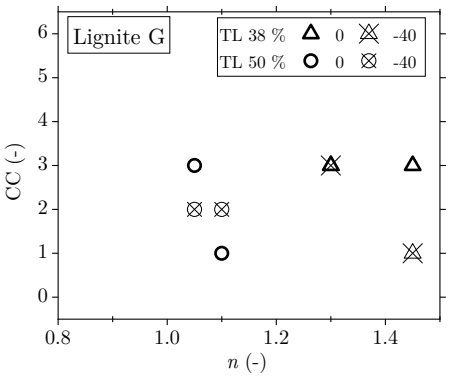


Figure 5.25: CC for Lignite G at plasma positions 0 and -40

flames with CC values above 3. Once the sufficient dust concentration is reached and the ignition is accomplished at position -40 (38 % for Lignite B and D), by a further increase in the dust concentration, the flame can benefit from a lower particle velocity at this position, when the plasma is turned off. A lower particle velocity supports the formation and stabilisation of the self-sustained flame, where under specific settings improvements within CC 4 to CC 6 are observed for Lignite B and D, relating to the "very high ignitability" and "high ignitability" groups. For Lignite E in the "moderate ignitability" group, this improvement is not observed, as this lignite does not have the required boundary conditions to form a self-sustained flame, and hence, a lower particle velocity does not bring additional benefits. Figure 5.25 displays that for Lignite G, three cases with CC 3 at position 0 are reduced to one at position -40. The ignition initiation is hampered at position -40 and this position does not bring any advantage for Lignite G within the "low ignitability" group. This effect was also observed for Lignite H that position -40 leads to no successful ignition. As ignition at position -40 is not favoured, this setting is not suitable for fuels with "low ignitability".

**The effect of the plasma position on flame stability:**

Figure 5.26 shows the flame brightness and brightness fluctuation at position 0 and -40 for Lignite B, Lignite D and Lignite E. For Lignite B and Lignite E, the flame brightness values under almost all tested configurations are considerably higher at position 0 than position -40, see Figures 5.26a and 5.26e. This difference is in the range of (15 to 25) % for Lignite B and (15 to 45) % for Lignite E. It should be noted that the brightness value of below 20 % indicates no flame formation and therefore those values are not counted. It is interesting to see that for Lignite E, the difference in the brightness values of two plasma positions reduces as the dust concentration increases at the highest thermal load of 63 %. An exception is observed for Lignite B at the air ratio of 0.9, where the flame at position -40 reached around 4 % higher flame brightness. This point is associated with CC 6 for position -40 compared with CC 5 for position 0.

Accordingly, Figure 5.26b and 5.26f represent that the brightness fluctuation values of the flames at plasma position 0 stay almost below 10 %, which is significantly lower than that at position -40, with 11 % to 35 % fluctuation for Lignite B and 12 % to 52 % for Lignite E. These findings indicate that the flames formed at plasma position 0 are noticeably more stable than the ones formed at position -40, at close to the burner zone.

Figure 5.26c and 5.26d illustrate that position 0 is featured with higher brightness values in the range of (2 to 20) % and accordingly lower fluctuations. At only two air ratios, position -40 reaches approximately 6 % higher brightness values than position 0 and correspondingly, these two points are associated with lower brightness fluctuations. The reason why, contrary to the trends observed for Lignite B and Lignite E, Lignite D at position -40, reaches lower brightness fluctuations at two air ratios and also shows less deviation in brightness values

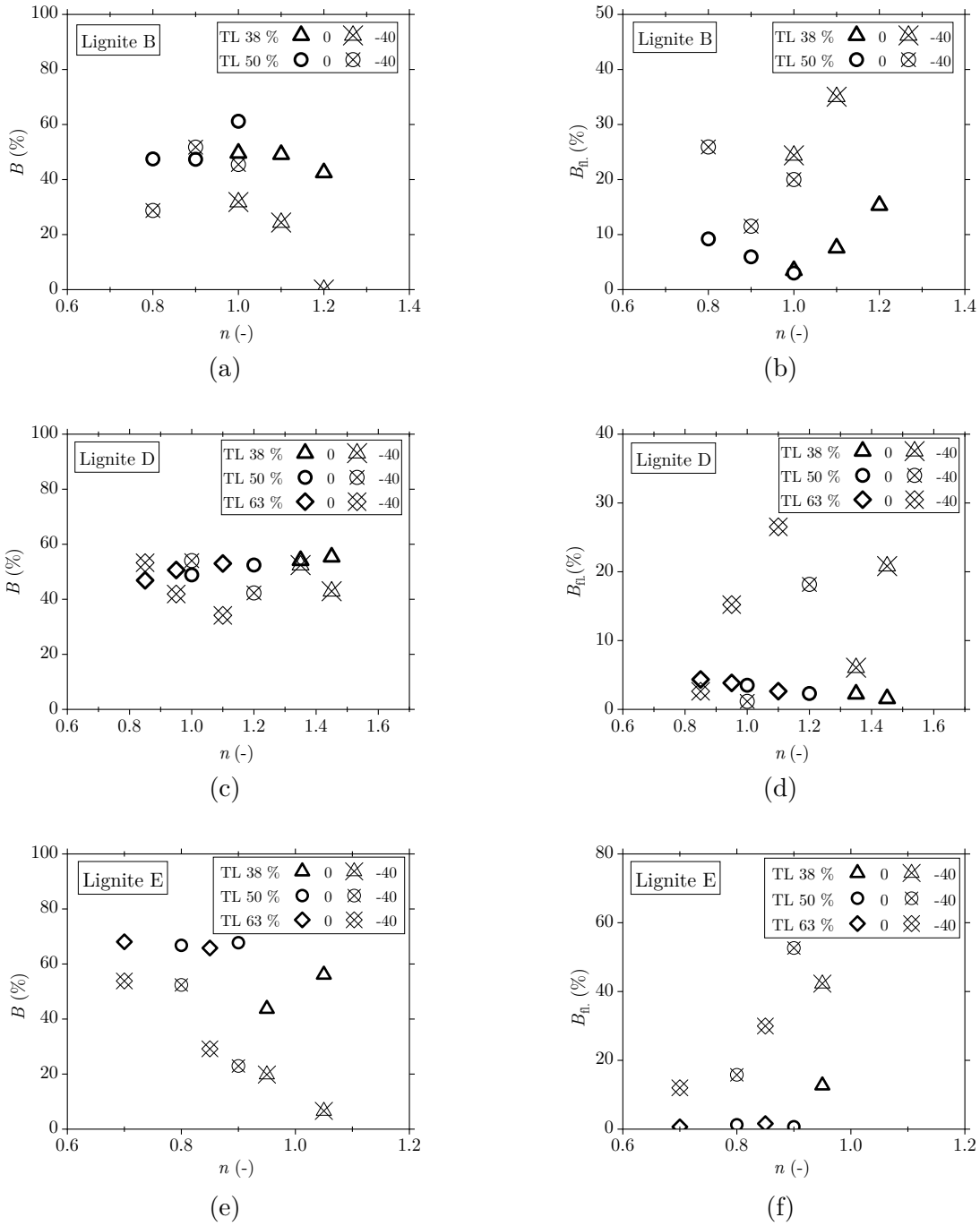


Figure 5.26: (a) flame brightness and (b) brightness fluctuation for Lignite B (aperture f/16), (c) flame brightness and (d) brightness fluctuations for Lignite D (aperture f/22), (e) flame brightness and (f) brightness fluctuation for Lignite E (aperture f/16) at plasma positions 0 and -40

than those at position 0, by a maximum of 20 %, can be related to its higher dust concentration. Comparing to the other two lignites, Lignite D has a higher dust concentration at each corresponding thermal load, which alleviates the impaired plasma-particle contact to some degree. However, the overall behaviour of the plasma position on the brightness

fluctuation for Lignite D agrees with the behaviours observed for Lignite B and Lignite E that in general, plasma position 0 results in flames with lower fluctuation levels compared with position -40.

It is worth highlighting that for Lignite D, the flame brightness at position 0 has a larger deviation from the values at position -40 under the larger air ratios at each thermal load, see Figure 5.26c. It seems that the flame brightness and correspondingly the brightness fluctuations at position -40 are influenced by the air ratio, where the brightness drops as the air ratio is increased at each thermal load and the fluctuation values increase accordingly. This effect is not detected at position 0, where comparable brightness values are attained at each thermal load for varied air ratios. The same behaviour is observed for Lignite E, where the flame brightness decreases and the fluctuation increases with the air ratio under the respective thermal load at position -40. As this behaviour is not observed for CD, this increased instability shows no direct impact on the combustion process.

Two hypotheses can be suggested to explain this behaviour. As discussed in section 5.4.1.2, the particle trajectories alter with the plasma position. While the primary air at position 0 concentrates the particles more towards the centre, the particles are more distributed outwards at position -40. These different particle paths not only impact the plasma-particle contact, but also the flame shape and the combustion regime of the resulting flame. At position -40, the particles have lower axial momentum, as a result of lower velocity at the burner outlet, which consequently leads to a larger degree of mixing with the secondary air at closer to the burner zone. Therefore, the particles are found in an air-richer atmosphere, which is associated with an increase in the heat demand at the initial stage of ignition. On the contrary, for position 0, the particles with larger axial momentum penetrate further in the internal recirculation zone, where a lower substoichiometric condition applies. The heat demand for the ignition and the flame stabilisation is hence smoothened. Under these circumstances, an increased air ratio has a larger impact on the ignition boundary conditions of particles with plasma position -40, since the initial ignition takes place under an air-richer mixture and with a high degree of turbulence, but the influence of an increased air ratio on the stoichiometric condition in the central zone is, in comparison, smaller. Thus, flame stability at plasma position -40 is impacted more severely than at plasma position 0, as the air ratio is increased.

This hypothesis can be further supported with the flame images, see Figure 5.27. At the initial stage of the ignition process (first two pictures at the left), a wider reaction zone is formed at position -40 for the three lignites investigated. Furthermore, instabilities in the size of the reaction zone are observed for Lignite B and D, which is the underlying reason of smaller brightness and larger fluctuation values. For Lignite E, the difference between the flames formed at position 0 and -40 is more related to the length of the flame, since a shorter flame is observed at position -40, where the flame front lies within the camera optical access.

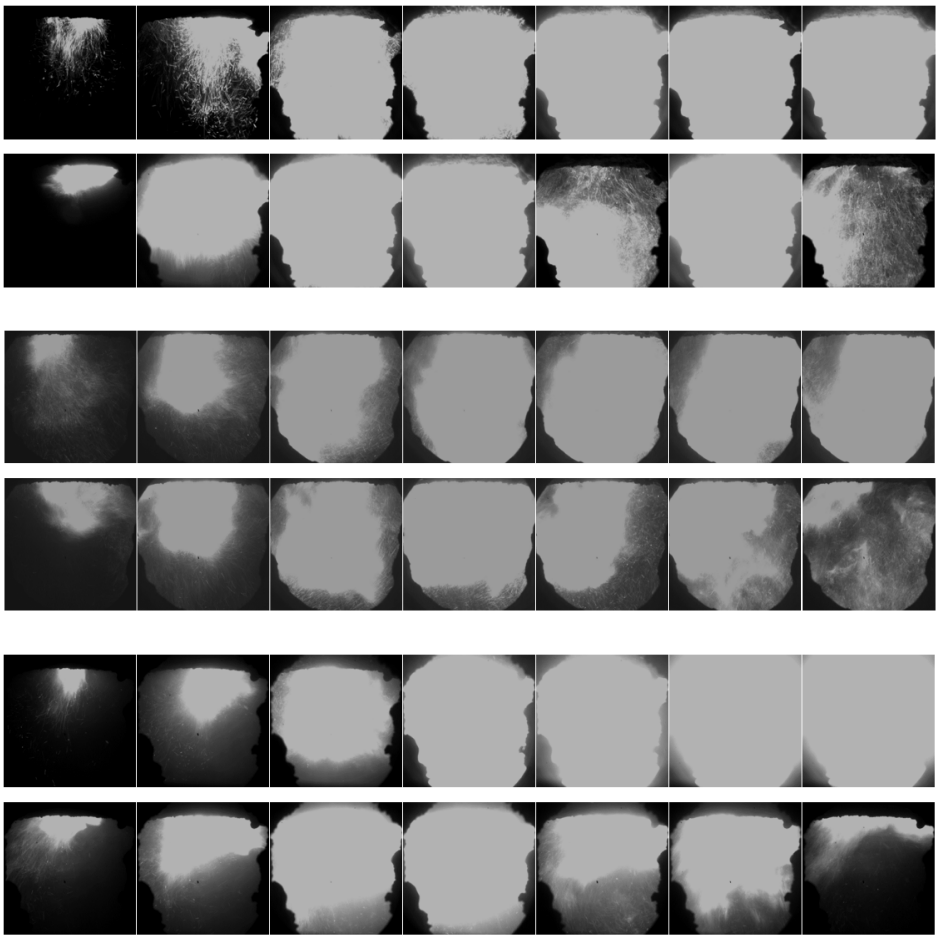

Figure 5.27: Flame evolution over 20 s at position 0 (upper line) and -40 (lower line) for Lignite B at TL = 50 % and $n = 1.0$ (top row), Lignite D at TL = 50 % and $n = 1.2$ (middle row) and Lignite E at TL = 50 % and $n = 0.9$ (bottom row)

The second hypothesis relates the instabilities to the impaired plasma-particle interaction. Although it is believed that this impaired contact is to some degree compensated at higher thermal loads and the ignition and flame formation is accomplished at plasma position -40, this imperfect plasma-particle interaction is not completely diminished. As a consequence, even after ignition initiation and flame formation, the core of the flame, which is responsible to sustain the flame, has considerable fluctuations, related to the stochastic behaviour of plasma-particle contact. This unstable flame core leads to local flame extinction and fluctuations in the envelope flame. However, since the core of the flame around the plasma jet is located inside the burner plate quarl that is out of the optical access, this hypothesis cannot be further investigated and it remains speculative.

It is important to highlight that this lower flame stability close to the burner zone does not necessarily influence the CC and CD of the flame at position -40. However, it stays unclear if a lower flow velocity, an improved oxygen availability despite ignition under an air-richer environment, ignition initiation under a substoichiometric condition in the pre-combustion zone or a combination of these factors are the associated reasons.

**Summary:**
Retracting the plasma lance inside the burner by 40 mm shows deterioration in the ignition due to ineffective plasma-particle interaction. For fuels within "very high ignitability" to "moderate ignitability" groups this effect is only observed at the low thermal loads, whereas for the fuels within the "low ignitability" group, the effect is also evident at higher thermal loads. The imperfect plasma-particle contact is, to some degree, alleviated at higher dust concentrations. Once the flame is formed, similar CC and CD values are obtained for both positions, under most of the operational settings. Plasma position -40 shows a tendency to improve flame stabilisation after the plasma turn-off by reaching higher CC at individual settings. However, the brightness fluctuation values suggest less stable flames at position -40 compared with position 0 under most of the operational settings for the three lignites investigated, which is perhaps related to different particle trajectories and ignition regimes under the two positions. Plasma position -40 is not practical for fuels which are difficult to ignite and for easy to medium ignitable fuels, the results do not highlight any substantial improvement in the performance at position -40, under the current burner configuration with a swirling primary air. Since primary air swirling considerably governs the particle ignition boundary conditions, potential advantages related to the ignition in the air-lean pre-combustion section and a reduced particle velocity could not be significantly recognised.

### 5.4.3 The effect of the primary air nozzle design

The default nozzle (Nozzle 1) with a 45° contraction at the nozzle outlet is compared with the toothed nozzle design (Nozzle 3) using Lignite B and the baffle ring design (Nozzle 2) using Lignite E. Ignition, combustion process, flame brightness and fluctuation are compared to find the optimised primary air nozzle design.

**Nozzle with the baffle ring:**
Figure 5.28a shows the same CC values for Nozzle 1 and Nozzle 2 under all tested thermal loads of 25 % to 50 %. The change of the 45° contraction with 90°, neither has any impact on the minimum thermal load of ignition nor on the highest CC value for Lignite E. Correspondingly, similar CD values are obtained using Nozzle 1 and Nozzle 2 and only under air ratios of 0.8 and 0.95, slight improvements are observed when Nozzle 2 is used, see Figure 5.28b.
Similarly, Figure 5.28c shows that the flame brightness for Nozzle 1 and Nozzle 2 under thermal loads of 38 % and 50 % are comparable, with a small rise for Nozzle 2 at the air ratio of 0.95. The brightness fluctuations for both nozzles stay below 10 % and comparable

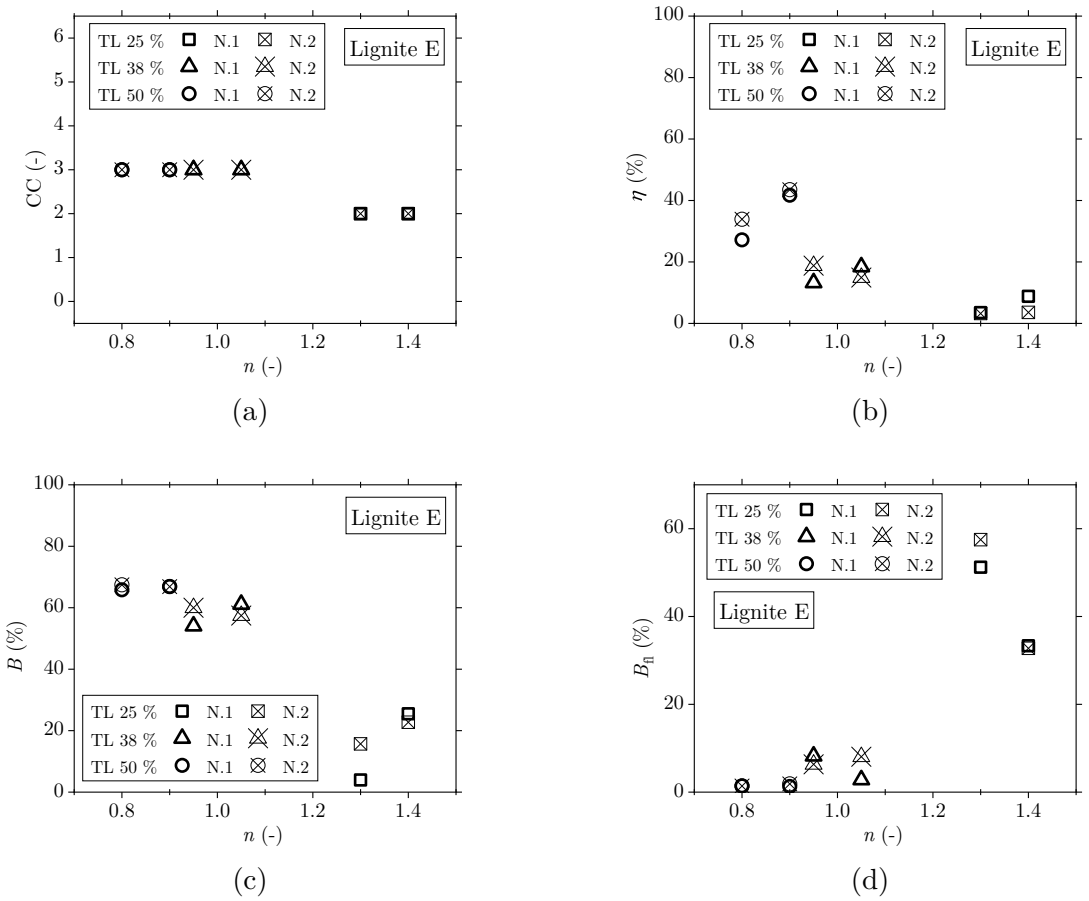


Figure 5.28: (a) CC, (b) CD, (c) flame brightness and (d) brightness fluctuation for Lignite E for Nozzle 1 (N.1) and Nozzle 2 (N.2)

values are observed with a deviation of zero to 5 %.

To conclude, no notable difference between the ignition performance and flame stability by Nozzle 1 and Nozzle 2 is detected. The results suggest that the nozzle contraction at the burner outlet enables adequate contact between particles and the plasma jet. The inclination angle of the ring does not show any significant impact on the overall performance. However, to draw a solid conclusion, the results need to be validated with lignites from other ignitability groups.

**Toothed nozzle design:**

Figure 5.29a shows pronounced improvements in CC from CC 5 to CC 6 when Nozzle 1 is replaced with Nozzle 3. At the thermal load of 25 % and the air ratio of 1.5, Nozzle 3 reaches only CC 2, while a flame with CC 3 is formed with Nozzle 1. As the thermal load is increased to 38 %, under all operated air ratios, Nozzle 3 forms flames that are attached to the burner outlet, whereas flame detachment is observed with Nozzle 1 at this thermal load. Flames with CC 6 have also relatively higher CD values by (5 to 10) %, see Figure

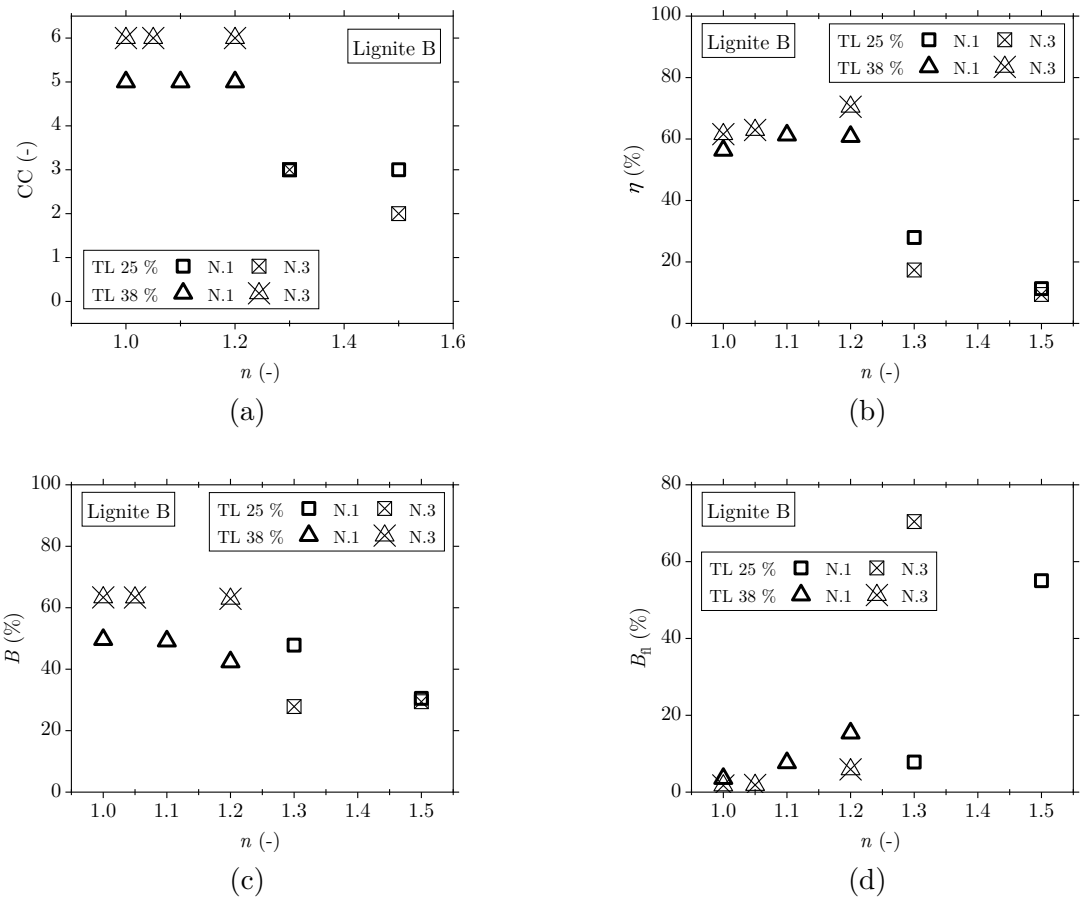


Figure 5.29: (a) CC, (b) CD, (c) flame brightness and (d) brightness fluctuation for Lignite B for Nozzle 1 (N.1) and Nozzle 3 (N.3)

5.29b. But, deteriorations in CD are observed with Nozzle 3 at the lower thermal load of 25 %, compared with Nozzle 1.

Similar trends like the ones in Figure 5.29b are observed for flame brightness in Figure 5.29c. Nozzle 3, in comparison with Nozzle 1, produces flame with lower brightness levels at the thermal load of 25 %, while larger values are observed at the higher thermal load of 38 %, which is related to flames with CC 6. In Figure 5.29d, the increase in the flame brightness at the thermal load of 38 % is correspondingly associated with lower brightness fluctuation, (1.5 to 5) % for Nozzle 3 compared with (3.5 to 15.5) % for Nozzle 1. In contrast, the brightness fluctuation for Nozzle 3 at the thermal load of 25 % rises drastically to 70 % compared with 8 % for Nozzle 1. The results imply that the toothed nozzle design has a significant influence on flame stability and flame stabilisation at the burner outlet, once a fully envelope flame is formed. This is in agreement with the practical experiences, where this improvement is related to an increase in the particle residence time within the critical ignition zone, due to particle deacceleration at the toothed ring and an increased mixing [86]. Under low thermal loads, where high overstoichiometric air ratios and a low dust loading apply, the ignition

happens under lower ignition limits, where an increased mixing and turbulence intensity worsens the ignition boundary conditions via local extinction. Accordingly, one can expect that the toothed nozzle design is not a suitable option for fuels with low ignitability. For fuels with high ignitability, it is shown that the design can greatly improve the CC by anchoring the detached flame to the burner and improving the flame stability.

### 5.4.4 The effect of the primary air velocity

The influence of the primary air velocity on ignition and combustion is investigated using wood pellets (WP 1) and Lignite G. The velocity is reduced from 15.5 m/s to 11.5 m/s by lowering the volumetric flow rate of the primary air.
For WP 1, Figure 5.30a shows that at the thermal load of 38 % and the high velocity, CC 3 is obtained under substoichiometric conditions, where the values drop to CC 2 with the shift to stoichiometric and overstoichiometric conditions. By a decrease in the fuel transport velocity to 11.5 m/s, CC is enhanced from CC 3 to CC 5 at under-stoichiometric conditions. The improvement is also observed at the air ratio of 1, where by reducing the primary air velocity an unsuccessful ignition is changed to a self-sustained flame. However, at the higher air ratio of 1.1, excessive heat loss prevents the flame formation even at a lower velocity. A reduced primary air velocity also does not show any influence on the CC at the lower thermal load of 25 %.
Figure 5.30b reveals that at the air ratio of 0.8, a CD of around 35 % is achieved by both velocities. This implies that an approximately comparable amount of heat and volatiles is available at the time of plasma turn-off, and therefore, a high primary air velocity is responsible for the flame blowout. When the air ratio and consequently, the heat demand

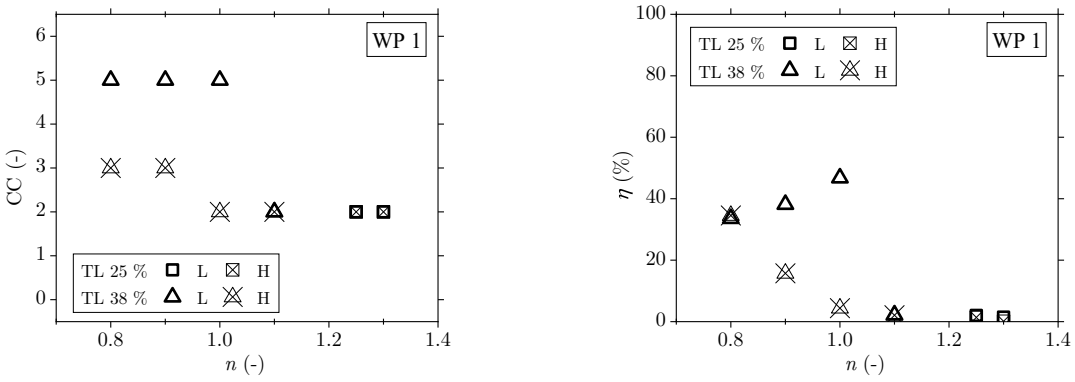


(a) (b)

Figure 5.30: (a) CC, (b) CD for WP 1 for 15.5 m/s (H) and 11.5 m/s (L) primary air velocity

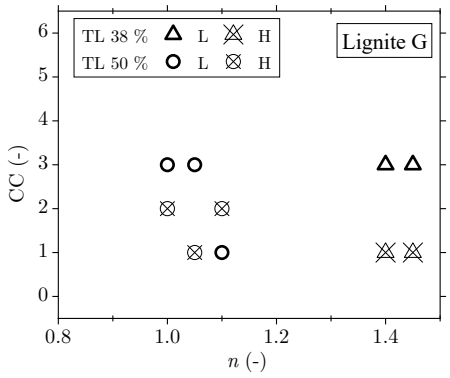


Figure 5.31: CC for Lignite G with 15.5 m/s (H) and 11.5 m/s (L) primary air velocity

for combustion as well as the velocity of secondary air are increased, the deviation in the CD values between the high and low velocity rises. The CD for the high velocity falls below 20 % at the air ratio of 0.9, compared with 40 % at the low velocity. The results indicate that a proper primary air velocity is necessary to ensure sufficient mixing and particle residence time for devolatilisation and ignition within the critical ignition zone.
Figure 5.31 shows that ignition for Lignite G is only accomplished when the primary air velocity is reduced from 15.5 m/s to 11.5 m/s. At the low velocity, CC 3 is obtained under both thermal loads of 38 % and 50 %, while only CC 1 and CC 2 are reached at the high velocity.
Deteriorations in ignition and combustion are observed with the higher primary air velocity. The extent of this deterioration depends on the fuel ignitability. For WP with a large degree of devolatilisation, a high primary air velocity is mainly preventing the formation of a self-sustained flame and for Lignite G with a low ignitability the effect is largely reflected on the ignition.

## 5.5 Investigations of the influence of particle size using milled wood pellet

Wood as the standard substitute for coal in thermal power plants is a great alternative to be employed for plasma cold start-up, as it has a high volatile content. The milling of woody biomass is limited by the low grindability of material due to their fibrous structure [181]. Given the high reactivity of biomass and to reduce the fuel preparation costs, the wood pellets are not finely milled. The PSD of industrially used wood pellets are relatively large [182]. Nevertheless, the main requirements to initiate the ignition under cold furnace conditions

is the presence of sufficient amount of fine particles. As these particles have a large surface to volume ratio, they are devolatilised quickly and create a combustible mixture. However, it is not clear which particle sizes are the most critical share and how much of these fine particles are essential to create a combustible mixture under the dedicated burner condition. The following section aims to determine the minimum amount of fine fraction necessary for plasma-assisted cold start-up ignition and to identify the impact of the fine particles on the ignition and combustion process for milled wood pellets. The results will provide information on the PSD of a wood sample that is suitable for this application, where the milling cost is optimised.

### 5.5.1 Ignition boundary conditions

WP 2 is used to investigate the effect of particle size on the ignition boundary conditions and the combustion process. The information related to the PSD of the samples and preparation methods can be found in section 3.1.2.1.

Table 5.1 summarizes the ignition boundary conditions, where TL indicates the smallest thermal load at which ignition occurred, the corresponding air ratio, $n$, and the CC achieved. $DL_{63}$, $DL_{90}$ and $DL_{200}$ represent the dust loading of particles below 63 µm, 90 µm and 200 µm, respectively, at the corresponding thermal load.

For M3, the finest PSD with a *D50* of 283 µm (see Table 3.3), ignition is accomplished with

Table 5.1: Ignition boundary conditions for different milled wood particle size distributions

| Sample | TL | CC | $n$ | $DL_{63}$ | $DL_{90}$ | $DL_{200}$ |
|---|---|---|---|---|---|---|
| | % | (-) | | g/kg | | |
| M3 | 25 | 4 | 0.7 | 43 | 80 | 183 |
| M2 | 31 | 4 | 0.6 | 50 | 101 | 198 |
| M1 | 31 | 3 | 0.6 | 50 | 86 | 176 |
| WP 2 | 31 | 3 | 0.6 | 29 | 51 | 138 |
| S1 | 75 | 3 | 0.5 | 28 | 71 | 289 |
| S2 | 75 | 2 | 0.5 | 7 | 23 | 209 |
| S3 | 75 | 1 | 0.5 | 2 | 5 | 54 |

CC 4 at the thermal load of 25 %. For M2, M1 and the original milled WP 2, ignition is reached at the thermal load of 31 %, where M2 reaches CC 4 and M1 and WP 2 reach CC 3. For S1 sample, sieved with 100 µm, ignition is obtained at 75 % thermal load with CC 3. For S2 and S3, no ignition and only CC 1 and CC 2 are obtained at the highest tested thermal load of 75 %. The values of the dust loading for particles below the given particle size shows that WP 2 reached ignition at a $DL_{63}$ of 29 g/kg, $DL_{90}$ of 51 g/kg and $DL_{200}$ of 138 g/kg. Considering these values as the ignition limit, M1, M2 and M3 represent higher dust loadings at their initial ignition points and therefore the values related to WP 2 can be considered as the ignition limit values.
Further shifting to coarser PSD, it can be seen that ignition initiation at CC 3 is reached for S1 at the thermal load of 75 %. To determine which particle fraction is critical for the ignition initiation, the S1 dust loadings at different size fraction are compared with the defined limit values. It can be seen that at TL 75 %, S1 represents a $DL_{63}$ of 28 g/kg (close to the limit values), while the dust loading of particles below 90 µm and 200 µm are far above their limit values. These limit values of $DL_{90}$ and $DL_{200}$ are reached at smaller thermal loads of 63 % and 38 %, respectively, though no ignition is obtained. This highlights the relevance of the fine particle fraction of below 63 µm for an ignition initiation. For S2 and S3 no ignition is obtained at the highest tested thermal load of 75 %. Similarly, these samples have a relatively low $DL_{63}$ and $DL_{90}$ below the identified limit.
It should be noted that for M2 and M1, the critical $DL_{63}$ and $DL_{90}$ are also obtained at the lower thermal load of 25 %, but no ignition occurs. This can be related to a weak or almost no formation of a swirl recirculation zone at the burner outlet under substoichiometric conditions for the low thermal load of 25 %.
These findings indicate that the particles smaller than 63 µm are the critical share for ignition and even when a considerable amount of particles between 63 µm and 90 µm are available, the ignition is not obtained until the required amount of $DL_{63}$ is reached.

## 5.5.2 Ignition and combustion behaviour

To investigate the impact of different particle fractions on combustion and flame formation M3, M2, M1 and WP 2 are tested at different thermal loads under substoichiometric and overstoichiometric conditions. Figure 5.32 and 5.33 show the CC and CD of different WP size distributions at the air ratios of 0.5 (0.6), 0.7, 0.9 an 1.1 over the thermal loads of 25 % to 63 %.
At the air ratio of 0.6, Figure 5.32a, no distribution reaches ignition at the thermal load of 25 %. As the thermal load is increased, all four distributions represent ignition, though M3

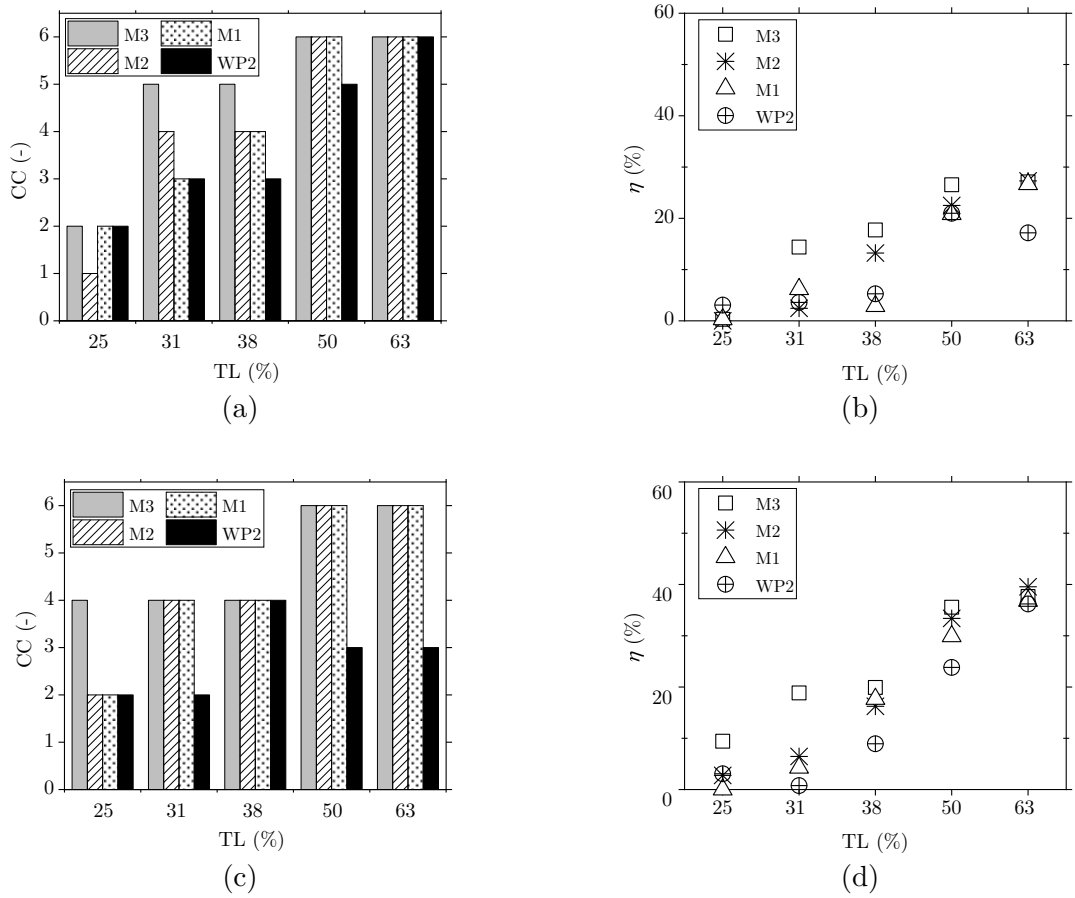


Figure 5.32: (a) CC and (b) CD for different size distributions at the air ratio of 0.6 for the thermal loads of 25 % and 31 % and the air ratio of 0.5 from thermal loads above 38 % (c) CC and (d) CD for different size distributions at the air ratio of 0.7

with CC 5 demonstrates a better performance than M2 (CC 4), M1 and WP 2 (CC 3). By a further increase to 38 % thermal load at the air ratio of 0.5, M3, M2 and WP 2 do not show any improvement, but CC achieved for M1 is enhanced to CC 4 and reach the same value as that of M2. At the thermal load of 50 %, all M-distributions produce a self-sustained flame anchored at the burner outlet, while WP 2 creates a detached self-sustained flame. As the dust loading is considerably increased at the thermal load of 63 %, all distributions form attached self-sustained flames (CC 6).

Figure 5.32b shows the largest CD values for M3 at the lower thermal loads (31 % and 38 %), among the M-distributions, and comparable values at higher thermal loads (50 % and 63 %). These results indicate that the variations in CC and CD related to different size distributions get smaller with the thermal load. As the sample fineness increases, the improved performance is more evident at lower thermal loads, e.g. lower dust loadings, when compared with coarser distributions.

At the air ratio of 0.7, see Figure 5.32c, improved CC for M3 compared with M2 and M1

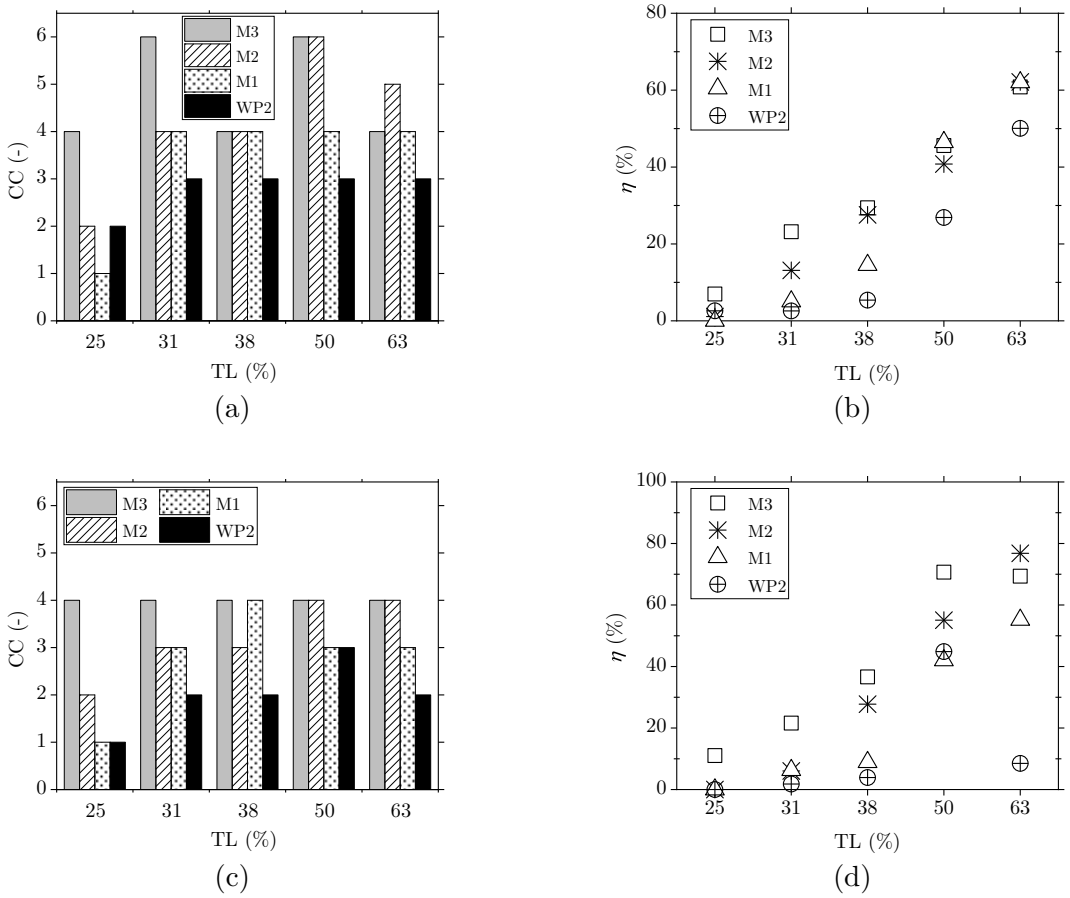


Figure 5.33: (a) CC and (b) CD for different size distributions at the air ratio of 0.9 (c) CC and (d) CD for different size distributions at the air ratio of 1.1

is only observed at the lowest thermal load of 25 %, where M3 has CC 4, whereas M1 and M2 show unsuccessful ignition at CC 2. For the thermal loads higher than 31 %, all M-distributions (M3, M2 and M1) represent identical CC values, where they reach attached self-sustained flames at the thermal loads of 50 % and 63 %. But, WP 2 shows comparably worse performance, where the ignition is first achieved at the thermal load of 38 % with CC 4 and as the thermal load increases, it drops to CC 3.

The CD values in Figure 5.32d do not fully correspond to the CC trends observed in Figure 5.32c. Despite similar CC, M3 shows a relatively higher CD value than M2 and M1 at the thermal load of 31 %. From TL 38 % to TL 63 %, comparable CD values are observed for the M-distributions, which is also in agreement with their corresponding CC achieved. Regardless of CC, WP 2 reaches lower CD values compared with the M-distributions, except the highest thermal load of 63 %, owing to a large dust loading.

Similar to the behaviour observed in Figure 5.32a and Figure 5.32c, at the air ratio of 0.9, ignition at the thermal load of 25 % is only achieved for M3, see Figure 5.33a. Under all thermal loads investigated, WP 2 represents a lower CC compared with the M-distributions.

At this increased air ratio of 0.9, only M3 and M2 produce attached self-sustained flames and M1 reaches maximum CC 4. Figure 5.33b agrees with the trends previously observed that M3 has higher CD values at the low thermal loads (25 % and 31 %) and CD values become comparable for the M-distributions at the higher thermal loads (50 % and 63 %). M2 reaches a similar CD level to M3 even at the thermal load of 38 %.
The importance of fine particles in ignition and flame stabilisation is more pronounced at the overstoichiometric condition. Figure 5.33c shows that none of the distributions create a self-sustained flame at the air ratio of 1.1. M3 reaches maximum CC 4 under all tested thermal loads and WP 2 shows unsuccessful ignition with CC 2 under all thermal loads except one ignition at the load of 50 %. As expected, M3 has better performance than M2 and M1 at thermal loads below 38 %, whereas M2 reaches similar CC at 50 % and 63 % loads. Enhanced combustion associated with M3 is evident up to the thermal load of 50 %, see Figure 5.33d. Since the ignition boundary conditions are worsened at the overstoichiometric ratio, enhanced CD for M3 compared with M2 and M1 shifts to higher thermal loads, where M2 reaches a slightly higher CD value only at the highest thermal load of 63 %.

**Summary:**
The results highlight significant improvement in the CC and CD over all thermal loads, as WP 2 is enriched with fine particles below 100 µm to form M1, by a slight increase of only 5 % in $Q_{90}$, corresponding to a 3 % increase in $Q_{63}$. By further enriching the sample with the particle sizes between 100 µm and 212 µm (M2), the performance enhancement in ignition and the flame stabilisation (higher CC), compared with M1, is observed at the air ratios of 0.9 and 1.1 and only thermal loads above 50 %, while comparable CC values are obtained at lower air ratios of 0.7 and 0.5 over the entire thermal loads tested. These particle shares also show improvements in CD values at the air ratio of 0.9 and 1.1 under most of the thermal loads. When the sample is further enriched with the particles between 212 µm and 315 µm (M3), CC improves at lower thermal loads of 25 % and 31 % almost under all air ratios investigated from 0.5 to 1.1. At substoichiometric conditions, the difference in CD between M-distributions is mainly observed at lower thermal loads, while at the overstoichiometric condition this difference extends also to higher thermal loads.
When cost optimisation with regard to biomass milling is concerned, a PSD equivalent to M2 can be potentially suggested as a trade-off between the performance and the cost. Although, the ignition is shifted to larger thermal loads, the highest CC achieved with this quality is similar to M3, where CC 6 is reached at the maximum air ratio of 0.9. When improvements in the ignition performance are concerned, it is recommended to enlarge the share of fine particles below 100 µm, in particular below 63 µm, as improvement in CC between WP 2 and M1 is evident under all air ratios and thermal loads.

## 5.6 Theoretical and experimental considerations on plasma-assisted ignition

Within this section, overall performance of the lignites tested is correlated to their properties to identify the range of operation for this system with regard to the fuel quality. As an indication for the overall performance, the highest CC achieved with each fuel over the entire experimental matrix, when 4.2 kW plasma power was applied, will be used in this section. It should be noted that for all the fuels investigated, this highest CC, represented here, has been observed under more than one test condition.

### 5.6.1 Correlation to fuel properties

To correlate the chemical characteristics of lignites to the ignition performance in the plasma ignition system and consequently to identify the suitable fuel qualities for this application, the volatile, moisture and ash contents of fuels are correlated to CC. Figure 5.34 illustrates the chemical and physical properties of the lignites, where the colour of each lignite indicates the highest CC obtained using 4.2 kW plasma power.

In Figure 5.34a, the volatile content of lignites is plotted versus the median particle size. The volatile content of fuels, except Lignite F and Lignite H, stays in a narrow range of 41 % to 49 %. It can be seen that the fuels within the "very high ignitability" category have the highest volatile content and the smallest median particle size. These lignites have a median particle size smaller than approximately 450 µm. As the median particle size increases to above 500 µm, no correlation between the volatile content and the ignitability can be found. This finding again highlights the importance of particle size when rapid devolatilisation is concerned. For this configuration, where the flame produced in the surrounding of the plasma jet is the only heat source for the devolatilisation and ignition, the particles need to be sufficiently fine to release volatiles within a short residence time in order to expand the flame and reach an adequately high CD and consequently a self-sustained flame.

A clear correlation between the moisture content and the ignitability of lignites can be seen in Figure 5.34b. The fuels within the "very high ignitability" category have a moisture content between 10 % to 15 %, as the moisture is increased to 20 %, the lignites fall to the "high ignitability" category. Although a higher moisture content and larger particle sizes contribute to curbing the ignitability, an increase in the moisture from 10 % to 15 % and the median particle size from 50 µm to around 320 µm does not alter the ignitability category of Lignite B. However, aggravations in the performance between Lignite A and Lignite B

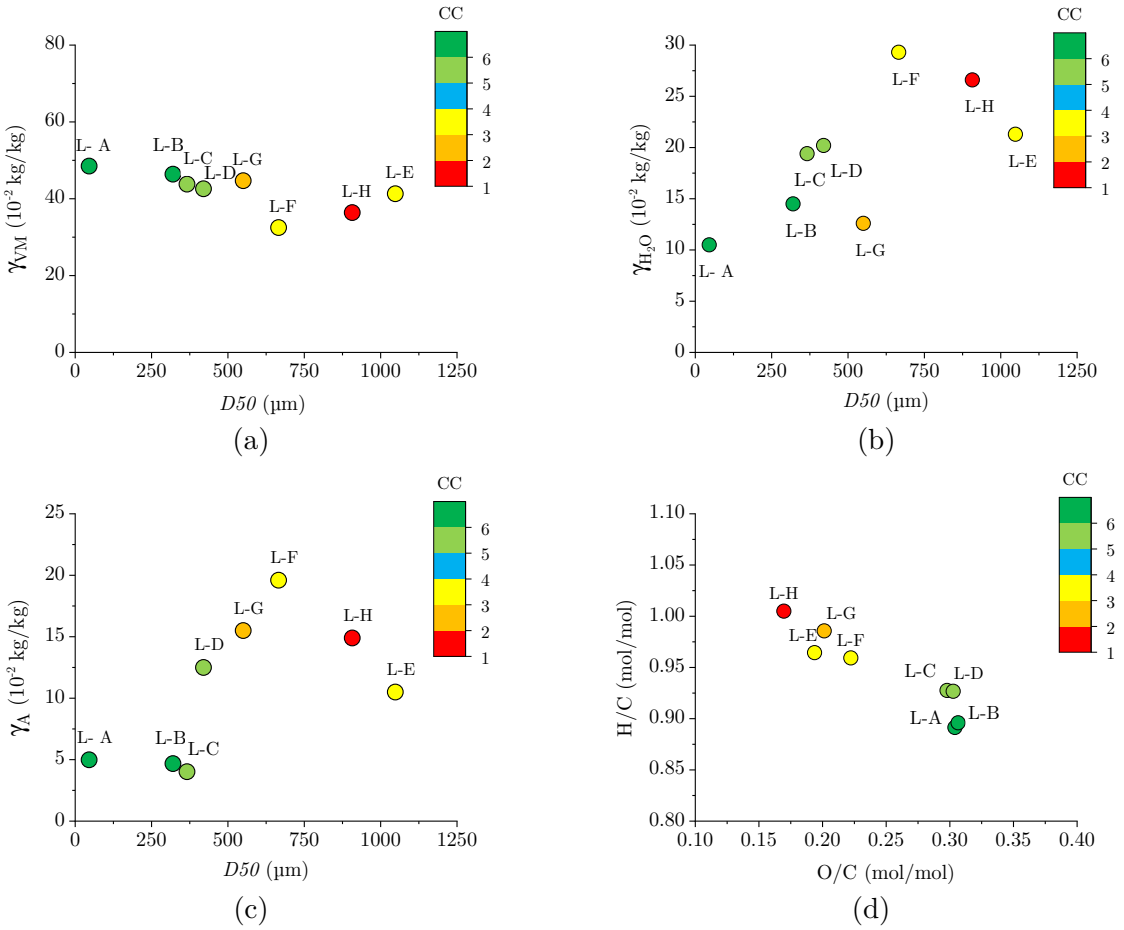


Figure 5.34: (a) Fuel volatile content, (b) moisture content, (c) ash content versus median particle size of the samples sieved below 2 mm, (d) molar O/H/C diagram, the colour of each point represents the highest CC obtained with 4.2 kW plasma power within the tested experimental matrix

is pronounced as depicted in Figure 5.2a and Figure 5.3a. CC 6 for Lignite B is obtained at defined boundary conditions, whereas Lignite A produces attached flames over a wider range of operational parameters. A further increase in the moisture content from 15 % to 20 % lowers the ignitability category to the "high ignitability". Flame detachment within this category is most likely related to an increased ignition delay time associated with higher moisture content in fuel. Similar effects of moisture on ignition delay and the combustion performance are observed by others [183, 184].

Figure 5.34c outlines the ash content of the tested lignites and suggests that although Lignite A, B, and C have a low ash content of 5 %, a self-sustained flame is also formed with Lignite D containing 12 % ash. Even though it is expected that ash, as an inert material, reduces the ignitability of fuel, no significant discrepancy in the ignition and self-sustained flame performance of Lignite D compared with Lignite C is observed. However, since the aerodynamic parameters of the burner slightly differ for experiments performed with Lignite C and Lignite D (a different primary air velocity and a different plasma position), any conclusion

should be drawn with caution.

Given the differences in the moisture and ash content, it can be highlighted that moisture has a relatively high inhibiting effect on ignition and the formation of self-sustained flame. A 5 %-variation in the moisture notably impacts the fuel performance in the plasma ignition system, whereas an increase of about 8 % in ash content does not considerably influence the ignition and flame stabilisation. This finding agrees well with other publications on the effect of moisture and ash on the ignition behaviour [61, 68] and what have been observed in Chapter 4 with respect to $K_{\mathrm{st}}$-value and $ZWZ_{\mathrm{mod.}}$ parameters. As previously explained, this is related first to the higher heat sink effect by moisture compared with ash and second to other ignition inhibition mechanisms of moisture such as agglomeration and reducing oxygen diffusion and partial pressure in the boundary layer of particles [61, 66–68].

Given the lignites with a median particle size of below 450 µm, qualities with a moisture content of up to 20 % and ash contents up to 12 % show satisfactory performance with regard to the formation of a self-sustained flame. Observation by other authors that the particle size is a determining factor in the performance of plasma-assisted cold start-up [117] is also confirmed in this work. However, the increase of median particle size from 45 µm in Lignite A up to 450 µm when sufficient fine fraction for the initial ignition is available[1] showed an unproblematic performance, while exceeding this particle size does not provide promising results. The performance of fuels within the "moderate ignitability" and the "low ignitability" groups cannot be directly correlated to the moisture content and ash content, as very coarse particle size hinders the ignition and therefore their performance is not governed by their chemical properties.

Figure 5.34d illustrates the properties of different lignite qualities within the Van-Krevelen diagram. It is important to mention, that when interpreting this diagram, one should keep in mind that the axis range of Van-Krevelen diagram covers a much wider range and here the axis values are adjusted for better data visualisation. The molar O/C ratio for fuels within "very high ignitability" and "high ignitability" categories is around 0.3, which according to Van-Krevelen diagram belongs to the soft brown coal category. As the O/C ratio decreases, the quality of lignite shifts to the hard brown coal category within the Van-Krevelen diagram, where qualities of lignites belonging to "moderate ignitability" and "low ignitability" categories are located. A higher O/C ratio facilities the ignition process by an early release of molecules with O-H bond [29] and by a higher CO yield during devolatilisation [185], which produces an easily ignitable mixture. The results suggest that a higher O/C ratio and a lower H/C ratio tend to improve the ignitability category of the investigated lignites from "low ignitability" to "very high ignitability" regarding their performance in the plasma ignition system.

[1] For these fuels $Q_{63}$ is above 16 %

## 5.6.2 Correlation to ignitability parameters

Figure 5.35 shows the $ZWZ_{\text{mod.}}$ number and $K_{\text{st}}$-value of the fuels investigated in Chapter 4, where similarly the colour of each fuel addresses the highest CC obtained with 4.2 kW plasma power. The parameters are plotted versus the median particle size of the 2 mm-sieved samples used for the pilot-scale testing. Figure 5.35a shows that Lignite A, Lignite B and WP 2 with $ZWZ_{\text{mod.}}$ above approximately 12 kJ/kg °C reach CC 6. However, very high $ZWZ_{\text{mod.}}$ for WP 2 compared with Lignite A was not projected from the observations of the pilot-scale testing , most likely due to large particle sizes of WP 2. For Lignite C and Lignite D with CC 5, $ZWZ_{\text{mod.}}$ is found to be between (9 to 12) kJ/kg °C. The deterioration in the ignition performance for Lignite F with CC 3, containing high ash and moisture contents, is also highlighted by a lower $ZWZ_{\text{mod.}}$ number of below 8 kJ/kg °C. The $ZWZ_{\text{mod.}}$ of Lignite G is in the range of fuels within the "high ignitability", nonetheless its performance during pilot-scale testing corresponds to the "low ignitability". This is perhaps related to the coarse particle size distribution of Lignite G sample used for the pilot-scale tests. Not only, the $ZWZ_{\text{mod.}}$ parameter showed low sensitivity to the particle size within the tested samples, as explained previously, but also there is a large deviation between the particle sizes of the sample used for the dust explosion tests and the one from pilot-scale tests. *D50* of Lignite G used for the dust explosion test is 80 µm, whereas for the pilot-scale test the median diameter is around 550 µm. Nevertheless, more experiments need to be carried out to validate this hypothesis and it remains tentative why Lignite G shows poor performance.

It can be concluded that when the ignition performance is inhibited mainly due to large particle sizes, the $ZWZ_{\text{mod.}}$ number is not representative. Since as observed in 5.6.1, the ignition performance during pilot-scale testing is not influenced by the fuel chemical properties when the fuels have a broad particle size distribution with *D50* of above 500 µm, for these fuels $ZWZ_{\text{mod.}}$ is unable to give any indication to which category ("moderate ignitability" or "low ignitability") they belong. However, for fuels within the "very high ignitability" and "high ignitability" categories the $ZWZ_{\text{mod.}}$ numbers represent promising results and can be used as a potential indicator for assessing the fuel ignitability within the top two categories.

Figure 5.35b similarly shows the $K_{\text{st}}$-values, where for Lignite A and Lignite B in the "very high ignitability" category the values stays above approximately 110 bar m/s. With the deterioration in the performance from CC 6 to CC 5, the $K_{\text{st}}$-value reduces to (80 to 90) bar m/s for Lignite C and Lignite D. Lignite G has a $K_{\text{st}}$-value of around 100 bar m/s that contradicts with its performance represented by "low ignitability" category. Similar to the trend observed by $ZWZ_{\text{mod.}}$, a coarse particle size distribution in the pilot-scale investigation is expected to be the underlying reason for this behaviour. Surprisingly for WP 2 with CC 6, the $K_{\text{st}}$-value drops to around 50 bar m/s. As explained in section 4.3.3, a small fraction of particles below 63 µm is considered responsible for this low value, which also here does not

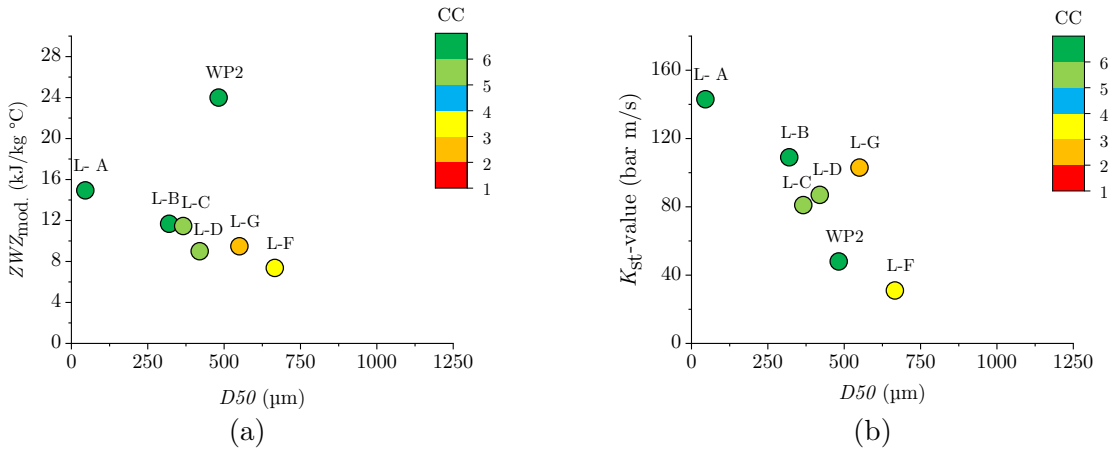


Figure 5.35: (a) Modified ignitability characteristic number and (b) deflagration index versus median particle size, the colour of each point represents the highest CC obtained with 4.2 kW plasma power within the tested experimental matrix

represent its performance with CC 6. For Lignite F, the $K_{st}$-value of around 30 bar m/s also addresses the low ignitability of this fuel.

Given both parameters, it can be speculated that the performance of Lignite G can be potentially enhanced by increasing the fineness, whereas for Lignite F with the worst ignition characteristics among the fuels tested, it is not clear how much the performance can be improved by reducing the fuel particle size.

To conclude, the $ZWZ_{mod.}$ number is more relevant for characterizing ignition based on their devolatilisation behaviour. At the same time, $K_{st}$-value is also a representative parameter that is influenced largely by the share of fine particles of the tested sample and therefore to reach more conclusive results the deviation in the particle samples needs to be minimised. For WP 2, $ZWZ_{mod.}$ slightly overestimates its performance, while $K_{st}$-value underestimates it. Overall, both parameters predict the ignitability of dust samples to a good degree when the median particle size stays below 450 µm and they can be used as indications to estimate the ignition performance for plasma-assisted pulverised fuel ignition.

## 5.7 Some remarks on burner design parameters

Self-sustained flame formation under cold start-up conditions with fuels reaching CC 5 and CC 6 is achieved under specific operational conditions when short-time plasma-assisted ignition was applied. Variations in the boundary conditions show a range of the operational

parameters that represent the most promising results. These values are summarised in Table 5.2, where the subscript of $n$ indicates the parameter, with respect to that, the air ratio is calculated, $w$ denotes the velocity magnitude at the burner outlet and $R$ is the ratio of primary air momentum to the secondary air momentum.

Within the investigated concept that plasma is responsible to initiate the ignition and following the high-volatile flame sustains the combustion after short-time plasma support, the power of plasma torch can be minimised and concurrent efforts need to be focused on enlarging the size of the plasma jet in order to maximize the plasma-particle contact and to increase the probability of ignition. In this 400 kW burner, the self-sustained flame formation is achieved at minimum thermal load between 38 % to 50 % equivalent to a dust loading of 0.5 to 0.75 for Lignite B and Lignite C and 0.8 and 1.2 dust loadings for WP 1 and Lignite D, respectively. The increased values for the latter two fuels is related to a reduction in the primary air quantity. These thermal loads correspond to a plasma-to-coal power ratio of 2.1 % to 2.8 %, considering 4.2 kW plasma power. However, due to the scale of the pilot burner and limitations in reducing the power of the plasma system, this ratio is well above the values that need to be considered for a large-scale burner. The value is expected to reduce significantly, when the burner is up-scaled, which was also observed by similar studies, where a 3 kW plasma torch was implemented for a 400 kW test burner and also a 30 MW industrial-size burner [14, 15, 116].

For Lignite B and WP 1 with high ignitability, the range of operated air ratio is larger than Lignite C and Lignite D, see Table 5.2. Considering the local air ratio with respect to the primary air, the values are in the range of 0.1 to 0.3. The air ratio with respect to volatile matter (calculated by assuming the stoichiometric air required for the combustion of H, S and volatile C, derived from $C_{total}$ subtracted by $C_{fix}$) stays within a range of 2.0 to 3.0 for lignites and 1.1 to 1.7 for WP 1 and correspondingly with respect to the primary air the ranges drop to 0.25 to 0.75. To ensure successful ignition and high combustion efficiency, it is recommended to initiate the ignition at a low air ratio and gradually increase the amount of secondary air until the upper limit to ultimately promote combustion and increase the CD. Another study by the author proved that this method brings about satisfactory results in stabilizing the flame at an air ratio that otherwise flame blowout is observed [20].

It should be noted that by comparing to commercial-scale burners, the given velocity magnitudes may stay below the typical design values. A primary air velocity of 11.5 m/s is even more favourable than 15.5 m/s, while both values stay below the typical primary air velocities of above 20 m/s. The lower velocity of around 8 m/s for Lignite C is related to the velocity at the burner outlet when plasma position -40 is employed. It should be mentioned that Lignite C is transported with a similar velocity as Lignite B up to the burner outlet.

Moreover, one should consider that the typical design values address the nominal numbers for a full load operation with an air ratio of 1.15 to 1.35, whereas in this work the con-

Table 5.2: Burner parameters

| Parameter | unit | Lignite B | Lignite C [1] | Lignite D | WP 1 |
|---|---|---|---|---|---|
| TL | % | 38-50 | 50 | 50-63 | 38-50 |
| $DL$ | kg/kg | 0.5-0.7 | 0.75 | 1.2-1.5 | 0.8-1.1 |
| $n$ | - | 0.8-1.2 | 0.9-1.05 | 0.95-1.1 | 0.7-1.1 |
| $n_{\mathrm{VM}}$ | - | 2.1-3.05 | 2.15-2.5 | 2-2.35 | 1.1-1.7 |
| $n_{\mathrm{PA}}$ | - | 0.2-0.3 | 0.2 | 0.1-0.15 | 0.15-0.2 |
| $n_{\mathrm{PA,VM}}$ | - | 0.55-0.75 | 0.5 | 0.25-0.3 | 0.25-0.3 |
| $w_{\mathrm{SA}}$ | m/s | 9-14 | 11.5-14.5 | 16-21 | 8-19.5 |
| $w_{\mathrm{PA}}$ [2] | m/s | 15.5 | 8.3 | 11.5 | 11.5 |
| $w_{\mathrm{SA}}/w_{\mathrm{PA}}$ | - | 0.6-1.0 | 1.4-1.7 | 1.5-1.9 | 0.7-1.7 |
| $R$ | - | 0.25-0.7 | 0.15-0.2 | 0.07-0.1 | 0.08-0.5 |

ditions are all related to minimum and part load configurations covering substoichiometric conditions from an air ratio of 0.7 up to maximum 1.2. Also, the velocities in the 400 kW pilot-scale burner are considerably lower than those in large-scale facilities since the velocities are restricted by the time required for complete combustion in the 7 m test furnace. In addition, concepts can be developed within which the velocity of the fuel particle is reduced at the burner outlet. One example that showed promising results is the toothed primary air nozzle design, which is similar to the DS® burners [86, 165] of the Company Mitsubishi Power. The ratio of primary air to secondary air momentum resulting from these velocity ranges is also characterised for each fuel quality.

A retracted plasma position can be beneficial when combined with a non-swirling primary air. When primary air is swirled and the plasma system is adjusted coaxially in the central fuel channel, the design has to consider reflecting the particles towards the plasma jet, which in this study was achieved via a contracted nozzle outlet at the burner.

[1] At plasma position -40

[2] Velocity at the nozzle outlet

# 6 Investigations of plasma-assisted combustion during part-load operation

## 6.1 Part-load operation with plasma-assisted combustion

To investigate potential and applicability of the plasma ignition system, as a supporting burner, with the aim of improving the combustion performance during part-load operation, hard coal combustion at several thermal loads under standard combustion and plasma-assisted combustion conditions are carried out. To protect the plasma torch head from the prolonged heat exposure in the furnace, the plasma position of -40 was selected for these experiments. During standard combustion, the plasma is only turned off and the torch positioning in the burner stays at -40 mm. An air ratio of 1.17 to 1.2 and plasma torch position of -40 were employed as the default setting for the part-load operation from 75 % to 38 %. At the thermal load of 25 %, due to operational limitations, the air ratio was increased to 1.3. In return, to alleviate any detrimental impact of a larger air ratio, plasma position 0 was adjusted for 25 % thermal load. In-flame measurements of gas emissions and temperature as well as flue gas emissions at the furnace end are evaluated in the following.

### 6.1.1 In-flame measurements

Figure 6.1 demonstrates the centreline flame temperature and oxygen volume fraction measured at three distances from the burner outlet, where the thermal load is changed from 75 % to 38 %. Since 25 % thermal load had a different operational setting, the in-flame mea-

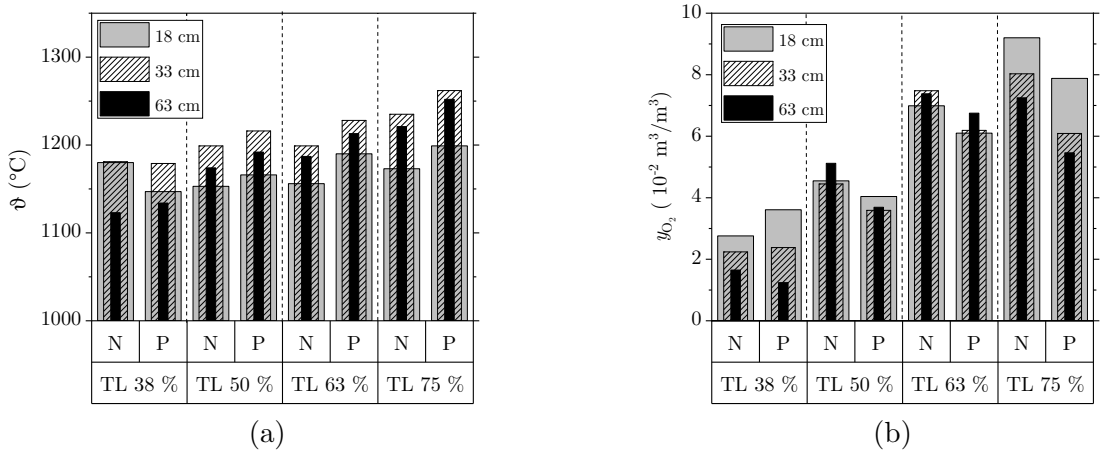


Figure 6.1: Furnace centreline in-flame measurements of (a) temperature and (b) $O_2$ volume fraction at several thermal loads under plasma-assisted combustion (P) and standard combustion (N) at three distances from the burner outlet (18 cm, 33 cm and 63 cm)

surements close to the burner zone are not compared directly with other cases.

Figure 6.1a shows a consistent temperature regime at the thermal loads of 75 % to 50 %, where flame has the highest temperature at 33 cm from the burner, followed by 63 cm and 18 cm. This behaviour is similar for both standard and plasma-assisted combustion conditions, which implies that the main combustion zone is intensified from 33 cm from the burner and plasma-assisted combustion does not have a notable influence on the centreline temperature regime, as no change in the temperature profile trend is observed during plasma-assisted combustion. However, at the thermal load of 38 %, neither under standard combustion nor plasma-assisted combustion, this temperature profile is found. This altered temperature profile may indicate a shift in the reaction zone and perhaps its size.

Comparing the plasma-assisted and standard combustion conditions, at each thermal load between 75 % to 50 %, plasma-assisted combustion has slightly higher temperatures. This trend is valid for all three distances from the burner outlet. At the thermal load of 75 % and 63 %, this temperature increase is in the range of 25 °C to 35 °C. As the thermal load is reduced to 50 %, the centreline temperature difference between standard and plasma-assisted combustion is lowered to around 15 °C. Further reduction in the thermal load to 38 % shows a higher flame temperature at 18 cm distance and a similar temperature at 33 cm distance from the burner outlet during standard conditions compared with plasma-assisted combustion. Moving further downstream from the burner outlet by 63 cm, a 10 °C increase is observed during plasma-assisted combustion.

This effect can be explained by the furnace wall temperature, see Table 6.1. As the thermal load is reduced, the furnace is cooled down consequently as the result of the heat loss. At low thermal loads the radiation heat loss from the particles overcomes the heat produced by the

Table 6.1: Furnace wall temperature at 33 cm from the burner during part-load operation

| | TL 38 % | TL 50 % | TL 63 % | TL 75 % |
|---|---|---|---|---|
| | °C | | | |
| N | 1032 | 1053 | 1095 | 1291 |
| P | 1024 | 1051 | 1095 | 1315 |

combustion reactions, which results in cooling of the CTRZ [90]. Reducing the thermal load from 75 % to 63 % leads to a drop of around 200 °C in the furnace wall temperature followed by a small reduction of 40 °C, as the thermal load is down to 50 %. Nevertheless, comparable wall temperatures are measured during the standard and plasma-assisted combustion for the thermal loads of 75 % to 50 %, which suggests a stable operation during the part load. As the load is reduced to 38 %, the combustion becomes unstable, where the furnace temperature does not remain constant. A higher furnace wall temperature during standard combustion is because these experiments are performed prior to plasma-assisted experiments.

It can be concluded that plasma assistance marginally increases the flame temperature, as long as the combustion is steady-state and when at low loads the furnace temperature is not stable over time, plasma-assisted combustion is also ineffective in maintaining the flame and furnace temperature. This effect was more prominently observed at the thermal load of 25 %, where the flame temperature difference between standard combustion and plasma-assisted combustion is 100 °C and 50 °C at the distance of 18 cm and 33 cm, respectively. This temperature drop occurred within only 30 min operation time.

Similar to the wall temperature, as the thermal load is reduced, the flame temperature falls under both standard and plasma-assisted combustion conditions. Under standard combustion conditions, temperatures that are measured at three distances from the burner centreline, drop with a large gap from 75 % to 63 % thermal load, while they remain relatively unchanged, with a maximum reduction of 10 °C, as the load is further reduced to 50 %, followed by a larger drop when the load is reduced to 38 %. Under plasma-assisted combustion conditions, the flame temperature drops almost steadily with the thermal load. The temperature drops more steeply, as the distance from the burner outlet increases. This trend is observed for both standard combustion and plasma-assisted combustion conditions, which can be related to a more pronounced impact on the main reaction zone, here at 63 cm and 33 cm, as the thermal load is reduced.

Figure 6.1b shows the $O_2$ volume fraction at the centreline. For thermal loads of 75 % and 38 %, $y_{O_2}$ drops with the distance from the burner under both standard and plasma-assisted combustion condition. However, no evident trend is found for the thermal loads of 63 % and 50 %.

For all three distances from the burner outlet, plasma-assisted combustion leads to lower

$y_{O_2}$ values, for the thermal loads of 75 % to 50 %. At the thermal load of 38 %, a larger $y_{O_2}$ is observed for plasma-assisted combustion at 18 cm from the burner and as the distance increases comparable and lower values are obtained, respectively. The behaviour of $y_{O_2}$ during standard and plasma-assisted combustion is in agreement with the temperatures in Figure 6.1a. A higher temperature during plasma-assisted combustion corresponds to a lower $y_{O_2}$ and a lower temperature at the thermal load of 38 % is associated with a higher $y_{O_2}$. This highlights that plasma-assisted combustion results in enhanced ignition and perhaps devolatilisation and consequently improved combustion close to the burner zone for the stable thermal loads of above 50 %.

Moreover, there is a descending trend of $y_{O_2}$, under both plasma-assisted and standard combustion conditions by lowering the thermal load. This effect can be related to the burner aerodynamics, where the secondary air axial (forward) and swirl momentum reduce and correspondingly the ratio of primary air to secondary air momentum increases, as the thermal load is lowered. This means that the secondary air swirling strength correspondingly falls with the thermal load, resulting in less effective mixing of fuel and secondary air.

At high thermal loads, i.e. 75 %, a large secondary air swirl momentum strongly diverts the primary air and fuel particles to the secondary air and a large axial momentum carries the fuel particles with a high velocity. Consequently, the particles are presumably combusted at a mixing layer between the internal recirculation zone and the secondary air in an oxygen-rich environment, further away from the centreline. By reducing the thermal load and correspondingly the secondary air volume flow, the swirling intensity of the secondary air reduces and as a consequence the extend to which particles are dragged outwards to the secondary air is lowered. Under these circumstances, ignition may be initiated at a radial distance nearer to the centreline. Besides, the burning particles have a longer residence time within the near burner zone, which accordingly can shift the main reaction zone closer to the burner. This is why the oxygen uptake is increased at specific distances from the burner outlet as the thermal load reduces.

Figure 6.2a illustrates that the $NO_x$ formation, under both standard combustion and plasma-assisted combustion, is promoted at the burner outlet, where the values fall with the distance from the burner. However, for the thermal load of 75 %, this drop is not observed, which again, can be related to a short particle residence time and a shift in the zone where $NO_x$ is mainly formed.

Figure 6.2a displays a significant rise in the $y_{NO_x}$ values associated with the plasma-assisted combustion under all thermal loads. An increase in the $NO_x$ level during plasma-assisted combustion was also observed by others [108]. For the thermal loads of 75 % to 50 %, $y_{NO_x}$ increases from a range of (500 to 600) $10^{-6}\,m^3/m^3$ to a range of (700 to 880) $10^{-6}\,m^3/m^3$ under plasma-assisted combustion. Since the flame temperature is below 1300 °C, the contribution of thermal $NO_x$ from the coal flame in the total emission is negligible. Thus, fuel nitrogen is

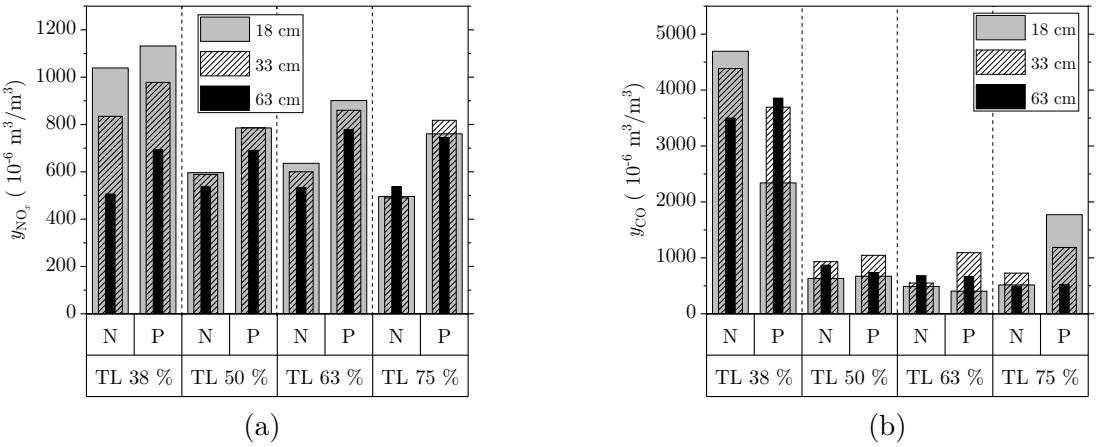


Figure 6.2: Furnace centreline in-flame measurements of (a) $NO_x$ and (b) CO at several thermal loads under plasma-assisted combustion (P) and standard combustion (N) at three distances from the burner outlet (18 cm, 33 cm and 63 cm)

assumed as the main source of $NO_x$ formation during standard combustion. This is equivalent to 30 % to 40 % fuel nitrogen conversion. During the plasma-assisted combustion, the higher $NO_x$ level can be associated with either an extended conversion of fuel nitrogen to $NO_x$ or by NO production related to thermal plasma. A significant jump in $y_{NO_x}$ during plasma-assisted combustion is most likely resulted from the latter hypothesis. NO is produced via the Zeldovich mechanism in thermal plasmas with a maximum NO production at a temperature of 3300 K. The reaction of nitrogen molecules with abundant atomic oxygen in plasma, is the main reason for NO formation by thermal plasmas [186]. This NO synthesis is related not only to the plasma carrier gas but also to the combustion air in the vicinity of the plasma jet. Investigations on the $NO_x$ production by plasma, in the absence of coal flame, showed values of (230 to 250) $10^{-6}\,m^3/m^3$, where the values demonstrated an increasing trend with the secondary air. The variations of the plasma carrier gas also represented a dramatic increase of $150 \cdot 10^{-6}\,m^3/m^3$ when the plasma carrier gas was slightly raised by 4 l/min. Moreover, although the flame temperature measured during the plasma-assisted combustion is just slightly increased and still stays below 1300 °C, no measurements could be performed in the burner quarl at the vicinity of the plasma jet. It is expected that local high temperature spots are also formed in the coal flame at the close vicinity of the plasma jet, further contributing in thermal $NO_x$ production. It is worth mentioning that as the load reduces from 75 % to 38 %, during plasma-assisted combustion compared with standard combustion, the rate of increase in $y_{NO_x}$ at close to the burner zone decreases from an average of nearly 50 % to approximately 20 %. This further implies that the thermal NO formation during plasma-assisted combustion is proportional to the quantity of the combustion air.
The trends of $NO_x$ emissions with the thermal load at different distances from the burner are discrete. At 18 cm and 33 cm from the burner under both standard and plasma-assisted

combustion, $y_{NO_x}$ increases in the range of (50 to 145) $10^{-6}\,m^3/m^3$, as the load is reduced from 75 % to 63 %. However, by further reducing the load to 50 %, $y_{NO_x}$ goes down during plasma-assisted combustion and stays relatively constant under the standard combustion condition. This results in a maximum increase of nearly $100 \cdot 10^{-6}\,m^3/m^3$ during standard combustion and almost similar $y_{NO_x}$ levels for plasma-assisted combustion compared with the values at 75 % thermal load. As the load is reduced to 38 %, the $NO_x$ levels go up considerably under both standard and plasma-assisted combustion conditions. These changes of $y_{NO_x}$ are more prominent at 18 cm from the burner, in the range of (340 to 440) $10^{-6}\,m^3/m^3$, compared with the values at 33 cm from the burner, in the range of (200 to 250) $10^{-6}\,m^3/m^3$. Nonetheless, for both standard and plasma-assisted combustion, the $NO_x$ levels at 63 cm from the burner stay relatively constant during load changes.

The $NO_x$ profiles at the centreline indicate that reducing the thermal load of the burner does not have a significant impact on the local $NO_x$ levels, as long as the combustion is mostly stable at the burner outlet. A considerable rise in $y_{NO_x}$ at the burner area is most likely related to an impaired recirculation zone at the thermal load of 38 %. At this load, the *Re* number of the secondary air, calculated based on the velocity and temperature of the secondary air at the burner outlet, falls below the lower limit of 18000 that is required for sustaining a stable recirculation zone. The oxygen-lean atmosphere within the internal recirculation zone disappears, which subsequently leads to inhibit the $NO_x$ reduction mechanisms close to the burner zone. However, as the distance increases from the burner, further progress in the combustion and reduction mechanisms brings about similar $NO_x$ levels at 63 cm distance for different thermal loads.

This hypothesis agrees with the $y_{CO}$ values shown in Figure 6.2b. Significantly higher CO values at the thermal load of 38 % compared with other thermal loads suggest incomplete combustion reactions, resulting from poor mixing of fuel and secondary air and an indication that the main reaction zone is located nearer to the centreline. Comparing the CO levels between standard and plasma-assisted combustion demonstrates no evident trend. Hence, no concrete conclusion can be drawn on the effect of plasma-assisted combustion at near burner CO values.

### 6.1.2 Flue gas emissions

Figure 6.3 depicts the $O_2$ volume fraction at the furnace outlet for different thermal loads. Plasma-assisted combustion shows no significant impact on $y_{O_2}$ in the flue gas. For the thermal loads of 38 %, 50 % and 63 % the $O_2$ level is lower during the plasma-assisted combustion, where a contrary trend is observed for the thermal loads of 75 % and 25 %. The average $y_{O_2}$

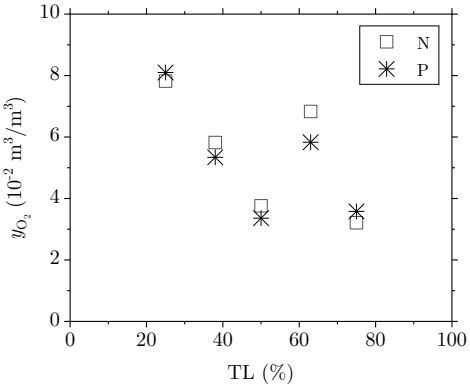


Figure 6.3: The average $O_2$ volume fraction in furnace end flue gas at several thermal loads under plasma-assisted combustion (P) and standard combustion (N)

stays at around $3 \cdot 10^{-2}\,\mathrm{m^3/m^3}$, for the thermal load of 50 % and 75 %, while it increases to about $5 \cdot 10^{-2}\,\mathrm{m^3/m^3}$ at the lower load of 38 % and further to around $8 \cdot 10^{-2}\,\mathrm{m^3/m^3}$ at the thermal load of 25 %. The results validate that the combustion performance stays relatively stable until the thermal load of 50 % and it reduces at the loads below 38 %, where plasma-assisted combustion does not show considerable improvements. It should be mentioned that the sudden rise in $y_{O_2}$ at the thermal load of 63 % is possibly connected to false air leakage at this configuration, though, it stays tentative why this jump is observed.

Figure 6.4 represents the emissions of $NO_x$ and CO at the furnace end. The $NO_x$ emissions during plasma-assisted combustion increase by around (215 to 260) mg/m$^3$ due to thermal NO formation by plasma. When the increase in the amount of flue gas by the thermal load is considered, it is seen that the difference in $NO_x$ production between plasma assisted combustion and standard combustion is increased from 28 g/h at 25 % thermal load to 70 g/h

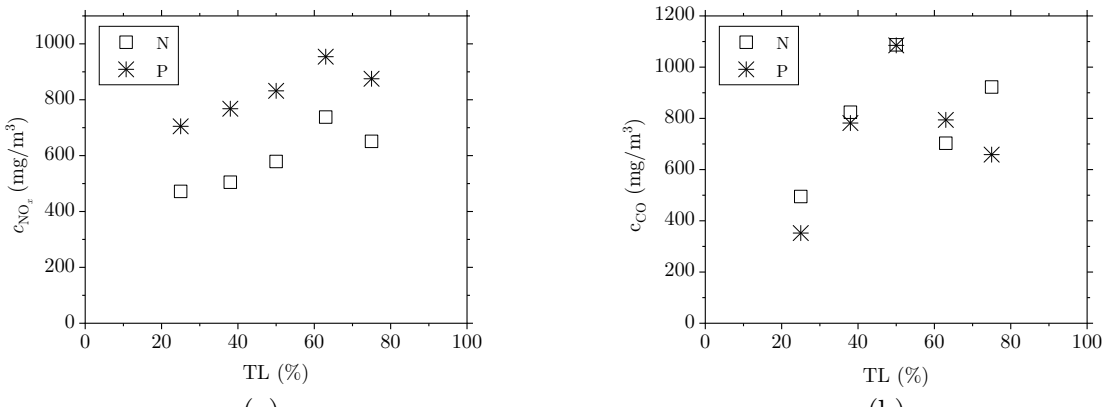


Figure 6.4: Emissions of (a) $NO_x$ and (b) CO corrected for $y_{O_2} = 6 \cdot 10^{-2}\,\mathrm{m^3/m^3}$ at several thermal loads under plasma-assisted combustion (P) and standard combustion (N)

at 75 % thermal load. The net incremented $NO_x$ production goes with the thermal load up, which fully agrees with the $NO_x$ emissions trends at the burner area. The results validate a correlation between the thermal NO production by plasma and the amount of secondary air.

There is a gradual rise in the $NO_x$ emissions with the thermal load, from 470 mg/m$^3$ at 25 % load to 650 mg/m$^3$ at 75 % load. The jump of the $NO_x$ level at 63 % thermal load is directly contributed to a higher $O_2$ level at this thermal load, which also corresponds to a lower CO emission level.

CO emissions at the furnace end do not indicate any specific trend neither towards the thermal load nor the plasma-assisted combustion. At the thermal load of 25 %, the low CO level does not necessarily indicate a good burnout, though on the contrary, poor carbon conversion which is also evident from $O_2$ values at the furnace outlet. For the thermal load of 38 % to 75 %, the CO emissions vary between 660 mg/m$^3$ and 1080 mg/m$^3$. During plasma-assisted combustion, a considerable drop in the CO emission is found for the thermal loads of 75 % and 25 %, while for other loads only a slight improvement or deterioration is observed. Although a firm conclusion regarding the CO emissions during part-load operation with plasma-assisted combustion cannot be given, a propensity to a lower CO emission is observed by plasma-assisted combustion.

## 6.2 The impact of the plasma position on plasma-assisted combustion

The influence of plasma position on in-flame measurements close to the burner zone is investigated at 50 % thermal load. Figure 6.5a shows that centreline flame temperatures at plasma position 0 are slightly lower than those at position -40 and almost similar to the temperatures obtained under standard combustion.

At 18 cm from the burner, $y_{O_2}$ at position 0 and -40 show the highest and lowest level, respectively, see Figure 6.5b. However, at farther distances from the burner, i.e. 33 cm and 63 cm, $y_{O_2}$ for plasma position 0 is lower than that under standard combustion and still higher compared with plasma position -40. Since the primary air velocity increases at plasma position 0, the residence time reduces compared with standard and plasma position -40 configurations. Therefore, it is postulated that the oxygen uptake at the area closer to the burner, i.e. 18 cm, reduces. Nevertheless, at 33 cm and 63 cm, farther from the burner outlet, the enhanced combustion resulting from the plasma-supported combustion compensates the short residence time leading to a lower $y_{O_2}$ compared with the standard combustion. It

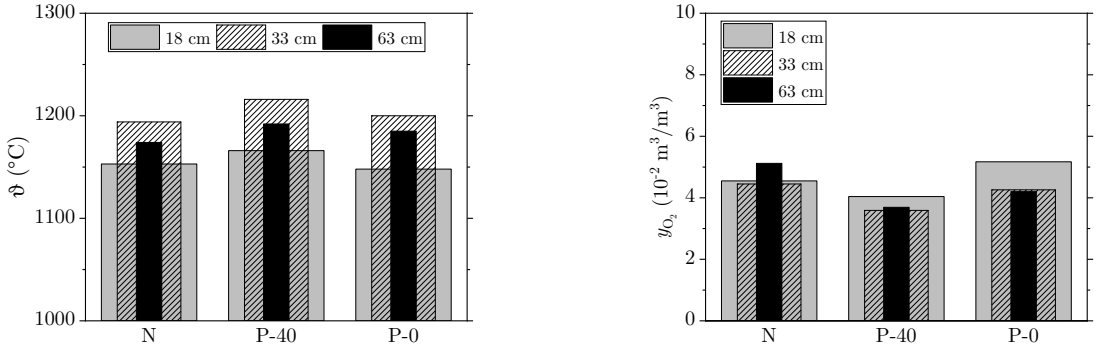


(a) (b)

Figure 6.5: Furnace centreline in-flame measurements of (a) temperature and (b) $O_2$ volume fraction for standard combustion (N), plasma position -40 (P-40) and plasma position 0 (P-0) at three distances from the burner outlet (18 cm, 33 cm and 63 cm)

should be mentioned that all these variations are in range of maximum $1 \cdot 10^{-2}\,\mathrm{m^3/m^3}$ and the changes in $y_{O_2}$ can also be partly related to the fluctuations in the combustion process. Figure 6.6a illustrates that at plasma position 0, the $NO_x$ emissions are lower compared with plasma-assisted combustion at position -40. It is believed that owing to a higher primary air momentum at plasma position 0 the fuel particles are carried, to a larger extent than other two settings, within the internal recirculation zone, where an air-lean atmosphere promotes the NO reduction pathways. The contribution of thermal NO formation within the plasma jet still results in a slightly higher $NO_x$ level, about $50 \cdot 10^{-6}\,\mathrm{m^3/m^3}$, than the standard combustion operation.

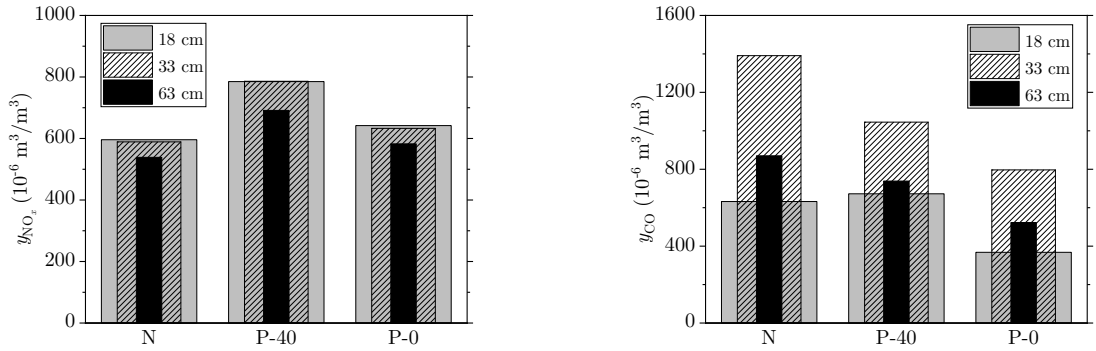


(a) (b)

Figure 6.6: Furnace centreline in-flame measurements of (a) $NO_x$ and (b) CO under standard combustion (N), plasma position -40 (P-40) and plasma position 0 (P-0) at three distances from the burner outlet (18 cm, 33 cm and 63 cm)

Figure 6.6b shows a considerable reduction in CO levels at all distances from the burner with plasma position 0 compared with standard combustion and plasma-assisted combustion at position -40. This can be potentially corresponded to a shorter residence time at the burner area and consequently a lower degree of devolatilisation and gasification at specific distance from the burner outlet.
To conclude, plasma position 0 shows improvements in reducing the $NO_x$ emission compared with plasma position -40. The $NO_x$ values at position 0 are still slightly higher than the standard operation. This behaviour shows that the additional NO produced with plasma can to a large extent be converted to $N_2$ by optimizing the near burner flow profile. Reductions in the CO concentration and a slight increase in the $O_2$ level at the burner zone under plasma position 0 are most probably associated with a higher primary air velocity which can potentially lead to a shift in the main combustion zone during part-load operation. With regard to the flame temperature, slight decrease in the values compared with plasma position -40 is observed, nonetheless, no evident impact of plasma position on the centreline flame temperature is found.

## 6.3 The impact of the air ratio on plasma-assisted combustion

The influence of air ratio during part-load operation and plasma-assisted combustion is investigated at 50 % thermal load and plasma position -40. Air staging with an air ratio of 0.8 at the burner is performed to evaluate potential of a substoichiometric atmosphere for reducing the $NO_x$ emissions during plasma-assisted combustion. The overall air ratio of 1.15 at the furnace outlet was adjusted during air-staging. At each air ratio, the performance under standard and plasma-assisted combustion at position -40 is compared.
Figure 6.7a depicts that the centreline flame temperatures at all three distances from the burner drops considerably by (40 to 60) °C, as the air ratio is increased to 1.3, while they stay relatively constant within the burner air ratio of 0.8 to 1.2. This indicates deteriorations in the combustion performance at the air ratio of 1.3 due to excessive heat sink by the secondary air.
Under all settings, the temperature profile remains unaltered, where the highest temperature is obtained at 33 cm from the burner, followed by 63 cm and 18 cm. Thus, it can be assumed that the location of the main reaction zone is not dramatically influenced by the stoichiometric condition, since identical profiles are measured under the standard and plasma-assisted combustion regardless of the air ratio.

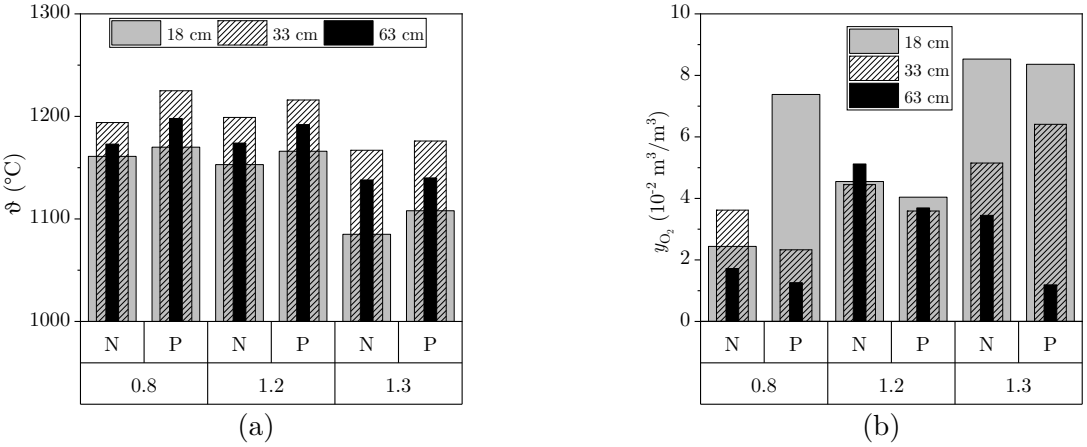


Figure 6.7: Furnace centreline in-flame measurements of (a) temperature and (b) $O_2$ volume fraction versus burner air ratio under plasma-assisted combustion (P) and standard combustion (N) at three distances from the burner outlet

Figure 6.7b illustrates that, in general, the $O_2$ volume fraction close to the burner zone increases with the air ratio, as the oxygen availability at the burner zone rises. The profile of $y_{O_2}$ does not show any clear trend with the distance from the burner under various configurations. However, in most cases, the oxygen drops with the distance from the burner.
Under each air ratio, plasma-assisted combustion, when compared with standard combustion, shows a drop in the $O_2$ level at the farthest distance measured from the burner, i.e. 63 cm, while at other distances an evident behaviour cannot be concluded. This behaviour is in agreement with the trends observed in Figure 6.1b and validates that plasma assistance is eventually prone to enhance combustion close to the burner zone.
In a similar manner, Figure 6.8a depicts an elevated $NO_x$ level during plasma-assisted com-

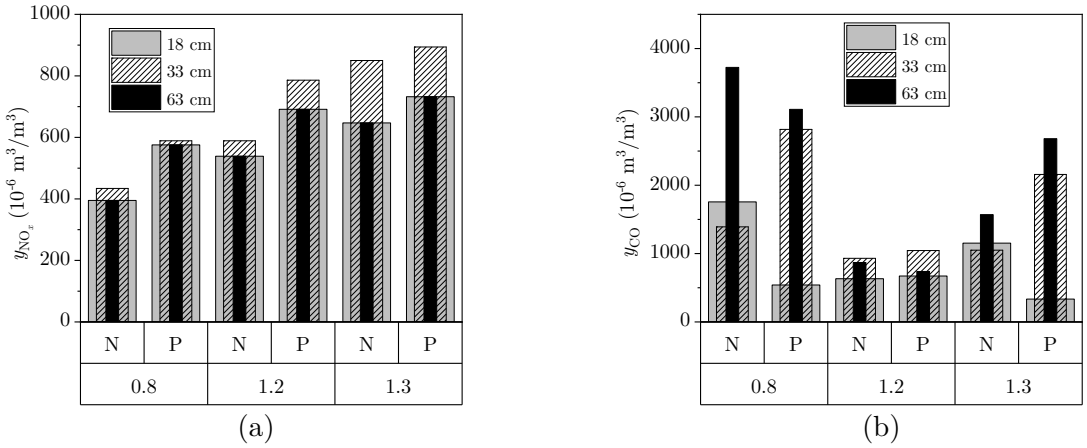


Figure 6.8: Furnace centreline in-flame measurements of (a) $NO_x$ and (b) CO versus burner air ratio under plasma-assisted combustion (P) and standard combustion (N) at three distances from the burner outlet

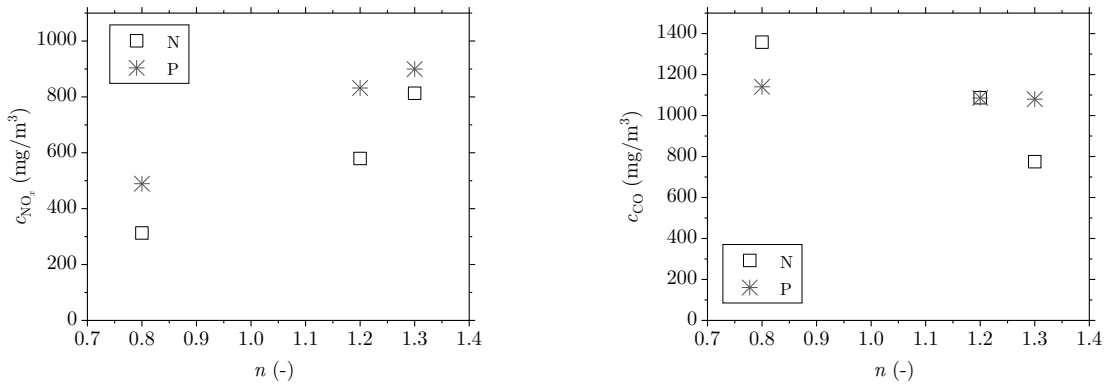


Figure 6.9: Emissions of (a) $NO_x$ and (b) CO corrected for $y_{O_2} = 6 \cdot 10^{-2}\,m^3/m^3$ versus burner air ratio under plasma-assisted combustion (P) and standard combustion (N)

bustion. Moreover, it distinctly shows a rise in the $NO_x$ level with the air ratio under both standard and plasma-assisted combustion at all distances from the burner. This leads to almost similar $NO_x$ values during plasma-assisted combustion under air-staging, e.g. a burner air ratio of 0.8, and standard combustion with an air ratio of 1.2 and even reductions in the $NO_x$ level when compared with standard combustion at an air ratio of 1.3. These findings validate the observations by others [11, 12], that replacing unstaged coal burners with two-stage plasma-coal burners leads to reductions in the $NO_x$ levels as the results of volatile combustion under substoichiometric conditions.

The $NO_x$ emissions at the end of the furnace illustrates an identical trend, where the $NO_x$ level increases with the air ratio, see Figure 6.9a. It should be also mentioned that the $NO_x$ increment rate with the air ratio is larger at the overstoichiometric condition compared with the increment rate between the air ratio of 0.8 and 1.2. This trend is more pronounced under the standard combustion, while the $NO_x$ values grow almost constantly under plasma-assisted combustion.

Figure 6.8b does not signify any trends for the CO levels at the burner area under different air ratios. During plasma-assisted combustion, higher and lower CO values than those during standard combustion are observed at various distances from the burner. The CO emission at the end of the furnace reduces with the air ratio during the standard combustion, whereas it does not change considerably during plasma-assisted combustion, see Figure 6.9b. This results in lower and higher CO emissions during plasma-assisted combustion compared with the standard combustion at the burner air ratio of 0.8 and 1.3, respectively.

To sum up, plasma-assisted combustion during air-staging is a viable approach to reduce the $NO_x$ emissions mainly related to thermal NO formation with plasma and concurrently support the combustion process close to the burner zone. Moreover, it should be also highlighted

that this increased $NO_x$ level during plasma-assisted combustion is limited by the amount of plasma carrier gas and the combustion air in the vicinity of the hot temperature zones. Therefore, considering an up-scaled burner, the quantity of the $NO_x$ produced via thermal plasma can in comparison to the total fuel $NO_x$ be much smaller than what is observed in the 400 kW burner. This dilution effect may to a large degree alleviate the incremented $NO_x$ level.

# 7 Conclusion and outlook

Within the existing and future energy system scenarios, fossil fuel power plants are still responsible to supply the residual load required to cover the gap between the production by renewable sources and the energy demand. This is, in particular, relevant for pulverised fuel power stations to support the residual load, which requires flexible operation. The need to increase the flexibility of pulverised fuel power plants demands cost and energy-efficient solutions for start-ups and the minimum load operation. Plasma-assisted solid fuel ignition and combustion is an alternative technology for the plant start-up and also supporting firing. Direct ignition of pulverised fuel particles in a high-temperature plasma jet allows ignition initiation under cold furnace conditions without a need for auxiliary start-up fuels. This work investigated the applicability of this technology for a broad range of fuel qualities and operational parameters to gain a better understanding of the process under extreme boundary conditions. To increase the system robustness and reducing the associated costs of the plasma system, the concept in which plasma is used only as an ignition source with short-time support was of interest. The application of short-time plasma-assisted ignition under cold furnace conditions was studied using ten fuel qualities. Lab-scale analysis on the ignition properties of fuels was performed to give some insight into the fuel ignition behaviour. Parametric studies were carried out in a pilot-scale facility, evaluating several operational parameters such as plasma power, swirl, plasma position, primary air nozzle and particle size distribution. In addition, plasma-assisted combustion experiments were performed to identify the potential as a supporting burner during part-load operation.

Lab-scale tests on fuel ignition properties performed for selected fuels showed that dust explosibility screening and minimum ignition energy may give some hints on the ignitability of fuels but both parameters are insufficient to be used as indications for this purpose. Minimum cloud ignition temperature was found to be the most susceptible to fuel volatile content and the particle size when the median diameter is reduced from a range of (80 to 150) µm to 45 µm and increased to a median diameter of 230 µm between different fuels. The ignition temperature was, however, not representative of a variation in the moisture and ash content of different fuel qualities within a narrow range of (5 to 10) %. Nevertheless, an evident ignition inhibition effect was observed by the addition of inert ash material to a lignite quality.

The determination of maximum explosion pressure showed only slight variations between different fuel qualities without any correlation to their properties. But deflagration index that indicates the rate of heat release, represented a strong dependency on the moisture content, where the $K_{\mathrm{st}}$-values drop with the moisture content. A decrease in the volatile content and also a small share of fine particles also reduced the $K_{\mathrm{st}}$-value. $ZWZ_{\mathrm{mod.}}$ was another parameter used to characterise the ignitability of fuels, which correlated the energy released during the devolatilisation to the ignition temperature. $ZWZ_{\mathrm{mod.}}$ increases with the volatile content and reduces with the moisture and ash content for the investigated lignites. It also showed less sensitivity to the particle size. Among the tested lignites, Lignite A and Lignite B were determined as the most ignitable qualities, respectively and Lignite F was specified as the least ignitable lignite quality with respect to both $K_{\mathrm{st}}$-value and $ZWZ_{\mathrm{mod.}}$. For Lignite C, Lignite D and Lignite G and also WP 2 and hard coal discrepancies in the ignition properties were observed between these criteria.

The developed plasma ignition system was first validated using two high-volatile fuels, where ignition as well as flame stabilisation with short-time plasma support were proved plausible. To analyse the ignition tests, qualitative and quantitative evaluation methods were developed. Based on the visual measurements and observations, Combustion Class (CC) parameter was developed to characterise the status of ignition and flame formation. CC 3 indicates the formation of a stable flame with the support of plasma, values below CC 3 indicate unsuccessful ignition, whereas CC 5 (detached flame) and CC 6 (attached flame) are related to self-sustained flames with short-time plasma support. Ignition tests performed over a wide range of thermal loads and air ratios showed distinctive behaviour by the investigated lignite qualities. Attached self-sustained flames were obtained only by Lignite A and Lignite B. The performance deteriorated for Lignite C and Lignite D, where only under specific operational conditions detached self-sustained flames were formed. Other lignite qualities could not reach a performance higher than CC 3. Lignite E and Lignite F demonstrated a low degree of devolatilisation and flames were only formed with the support of plasma. For Lignite G and Lignite H ignition was obtained by an increase in the plasma power from 4.2 kW to 7 kW. Within the first two groups specified as “very high ignitability” and “high ignitability”, CC and combustion degree (CD) were improved with the thermal load, whereas for other fuels in the “moderate ignitability” and “low ignitability” increasing the thermal load above the minimum load required for ignition did not bring any benefit with respect to CC. Moreover, smaller air ratios (substoichiometric) favoured the ignition initiation, while an increase in the air ratio was required to enhance the combustion process. A higher air ratio, on one hand, increases the heat demand for the ignition initiation and on the other hand improves the oxygen availability and consequently the heat production by combustion.

Increasing the plasma power from 4.2 kW to 7 kW showed that the lower ignition limits, e.g.

the minimum thermal load at which ignition occurs, can be extended for fuels from "high ignitability" to "moderate ignitability" categories. A higher plasma power was essential for the ignition initiation in the "low ignitability" category. At larger thermal loads, no improvements in the combustion process by a higher plasma power was observed for fuels within "very high ignitability" and "high ignitability" categories, whereas for Lignite E within the "moderate ignitability" group higher CD values were observed. This behaviour was associated with the different types of flames formed by fuels in different ignitability groups. Lignite B, Lignite C and Lignite D created flames with high CD values, suggesting that flame propagation is controlled more by a high degree of devolatilisation, whereas low CD values for Lignite E indicated that the flame is more influenced by plasma as the ignition source and therefore increasing the plasma power enhanced the combustion process. However, regardless of CC and CD, all the flames formed by 7 kW plasma showed lower fluctuations and higher stability at the flame root region. This demonstrated that although increasing the plasma power can not play any role in the formation of self-sustained flames, it still enhances the flame stability at the near burner region for fuels from different ignitability categories.
Deployment of another plasma system with a less volumetric plasma jet highlighted the importance of plasma-particle contact, in particular, for fuels within the "low ignitability" categories. Ignition did not accomplish with the smaller plasma jet for Lignite G and Lignite H. Deteriorations in the CD compared with the reference plasma system were observed for Lignite E and Lignite D under the configurations that the ignition condition was exacerbated such as low thermal loads or high air ratios. Although for Lignite D and Lignite E, within the "high ignitability" and "moderate ignitability" groups, no significant difference was observed between the CC obtained by the two systems, the stability of flames that were formed with the smaller plasma jet was evidently reduced. These findings suggested that the importance of plasma-particle contact can be as dominant as plasma power. This conclusion can support the future system design where instead of increasing the plasma power and accordingly the cost of the system, designs should focus on enlarging the size of the plasma jet.
Investigations of the burner aerodynamics focused on the effect of swirl, plasma positioning in the burner and the primary air nozzle and velocity. Reducing the theoretical secondary air swirl number from 0.9 to 0.5 deteriorated the CC from CC 5 to CC 3 at plasma position 0 and further reducing the swirl number to 0.3 resulted in complete ignition inhibition. The formation of the central recirculation zone showed significant influence not only on flame stabilisation but also on ignition initiation. Investigations of the effect of primary air and particle swirling on ignition and the plasma-particle contact were performed at different plasma positions. The most promising results were obtained under primary air swirling at plasma position 0. Experiments with non-swirling primary air showed on the contrary better performances at plasma position -40 and -80. This behaviour was correlated to the degree of plasma-particle contact and the velocity of particles. Due to the centrifugal force,

swirling particles were accumulated at the circumference of the primary air nozzle and did not have sufficient contact with the plasma jet before the contracted nozzle outlet. On the contrary, non-swirling particles are distributed evenly at the nozzle cross-section and a retracted plasma position provided a longer contact due to a lower particle velocity before the contracted nozzle outlet. Moreover, non-swirling primary air created a longer and thinner flame compared with the swirling primary air, forming a shorter and wider flame.
The effect of plasma position -40 on cold start-up ignition tests was further investigated using more fuel qualities under a broad range of operational parameters. For fuels within the "very high ignitability" to "moderate ignitability", the imperfect plasma-particle contact at position -40 was compensated with a larger amount of dust as the thermal load increased and similar performances were observed under both positions. For fuels that reach self-sustained flames, plasma position -40 even showed improvements in the CC at few individual settings, which was presumably related to a lower particle velocity. However, plasma position -40 was not effective for the fuels within the "low ignitability" category, where deterioration in the plasma-particle contact could not be overcome by a larger dust quantity. Furthermore, evaluations on the flame stability identified flames at plasma position 0 with higher stability and fewer fluctuations at the near burner region. It was concluded that under the investigated burner boundary conditions, plasma position -40 did not bring any significant benefit for the plasma ignition system.
A toothed nozzle design instead of an inclined edge with 45° showed improvements in stabilizing the flame at the burner outlet by reaching CC 6, but deteriorations were observed with this nozzle at lower thermal loads. The reason was attributed to an increased turbulence effect under undesired ignition conditions. Comparisons with another nozzle outlet, a baffle ring with 90°, showed no effect on the ignition performance compared with the standard nozzle. Also, reduced primary air velocity of 11.5 m/s instead of 15.5 m/s was beneficial for the ignition performance.
The influence of particle size on the ignition behaviour was assessed using several size distributions of a wood pellet quality. Increasing the share of fine particles below 90 µm by only 5 % to reach 13 % considerably improved the ignition and combustion performance. Ignition at the minimum thermal load was achieved over a wider range of air ratios and the CC was improved over the entire thermal loads and air ratios. Further enriching with particles below 200 µm resulted in enhancement of CC at the air ratios of 0.9 and 1.1 and thermal loads of above 50 %, while similar results were obtained at air ratios of 0.5 and 0.7 and also lower thermal loads. Enriching the pulverised wood pellet with particles below 300 µm extended the ignition boundaries towards a lower thermal load and also resulted in reaching a higher CC at low loads.
The lignites from "very high ignitability" and "high ignitability" categories, forming attached and detached self-sustained flames, were considered suitable qualities for the application of

cold start-up plasma-assisted ignition. These qualities had a particle size below 450 µm, a moisture content of below 20 % and an ash content of below 12 %. The performance was evidently reduced (from CC 6 to CC 5) by increasing the moisture content, as the lignites within the "very high ignitability" had a moisture content of below 15 %. The flame lift-off could be further enhanced by improving the burner design such as reducing the primary air velocity, applying proper nozzle geometries and potentially controlling the swirling degree of the combustion air. The effect of the ash content on the ignition performance and the ignitability category was not as pronounced as that of moisture. The performance of lignites within the "moderate ignitability" and "low ignitability" categories with a relatively large median size of above 500 µm could not be correlated to their moisture and ash content.

The comparison of theoretical numbers, which indicate the ignition characteristics of solid fuels, with the cold start-up plasma-assisted ignition performance showed promising results with respect to the lignites within the "very high ignitability" and "high ignitability" categories. The $ZWZ_{\mathrm{mod.}}$ and $K_{\mathrm{st}}$-value, identified previously as most representative parameters, drop as the ignition performance reduces from Lignite A to Lignite D. These parameters can be used in future works to estimate the fuel ignition performance as long as the particle size are comparable in the studies.

Further investigations on the influence of plasma-assisted combustion on combustion and emission behaviour during part-load operation showed an improved combustion performance during plasma assistance, where the near-burner temperature increased and the oxygen fraction dropped. However, this improvement was only observed during the loads at which combustion was established stable, and 4.2 kW plasma could not notably stabilise the flame at low loads at which the combustion was unstable and the furnace temperature was dropping constantly. A surge in the $NO_x$ values not only at the near-burner zone but also at the furnace end flue gas was observed during plasma-assisted combustion. This rise was correlated to the thermal $NO_x$ formation by the plasma jet. Part-load operation in the investigated burner was stable with no rise in the near burner $NO_x$ and CO emissions until the burner load of 50 %, while a further reduction in the burner load to 38 % led to a considerable increase in the near-burner emissions. Nevertheless, this trend was not observed for $NO_x$ and CO emissions at the furnace outlet. Increasing the thermal load resulted in a gradual rise in the end-of-furnace $NO_x$ emissions and no evident trend for CO emissions. Moreover, reducing the secondary air altered the flow profile and the swirling intensity at close to the burner zone which correspondingly influenced the oxygen profile at the burner outlet.

The comparison between the emission behaviour at plasma position 0 and -40 showed a slight increase and decrease in the $O_2$ volume fraction and the temperature, respectively. This was perhaps associated with a higher primary air velocity at position 0 compared with that at position -40. The experiments at plasma position 0 showed a lower $NO_x$ level than that at position -40, which was similarly correlated to the delayed mixing of fuel stream and sec-

ondary air at plasma position 0. The finding highlighted that the near-burner aerodynamics can be deployed to reduce the $NO_x$ emissions resulting from the thermal plasma.
Furthermore, increasing the air ratio from 1.2 to 1.3 increases the $NO_x$ levels under both standard and the plasma-assisted condition, whereas air-staging demonstrated a considerable contribution in reducing the $NO_x$ levels at both near-burner and furnace end. The $NO_x$ levels during air-staged plasma-assisted combustion were similar to those during standard combustion at the air ratio of 1.2. Additionally, the rise in the air ratio to 1.3 decreased the flame temperature considerably compared with the values at the air ratio of 1.2. The effect was evident under both standard and plasma-assisted combustion.

Based on the observations and results obtained during this work it is recommended to further pursue research in this topic with a special focus on the following aspects:

- This study was performed at a 500 kW pilot-scale facility. To increase the maturity of this technology and to further investigate the effect of scaling on the plasma-assisted ignition process, development of plasma-ignition systems at larger scales should be considered. With a special focus on biomass-fired power plants as an important element of a carbon-neutral energy system, the technology readiness level for the short-time plasma-assisted ignition process needs to be increased via demonstration activities.
- Investigating the ignition performance of lignites from "moderate ignitability" and "low ignitability" groups with a finer particle size distribution to identify the range of suitable qualities with less variation of parameters. It is not clear why Lignite G and Lignite H required a higher plasma power to be ignited. A broad particle size distribution for these fuels did not allow to find any correlation with respect to fuel properties. An investigation with fewer variables can largely contribute to specify the underlying reasons.
- Low devolatilisation degrees and lack of sufficient heat to proceed with the devolatilisation and combustion reactions during the early stage of the ignition were identified as the main parameters inhibiting the formation of self-sustained flames in lower ignitability groups. Preliminary tests with prolonged plasma assisted ignition instead of short-time plasma-assisted ignition showed satisfactory results for fuels that could not form self-sustained flames. For fuels within "moderate ignitability" and "low ignitability" prolonged plasma-assisted ignition and/or preheating the combustion air can be investigated as possible measures to establish self-sustained flames.
- Within this work the applicability of short-time plasma-assisted combustion for ignition and flame formation is studied. However, deteriorations in the flame stability even for fuels within the "high ignitability" category was observed after the plasma

shut-down. The ignition boundary conditions and burner design parameters need to be improved to reach more stable flames after short-time plasma-assisted ignition. Further optimizations are required to increase the flame stability and reducing the lift-off distance in self-sustained flames.

- The development and validation of models for CFD simulations of plasma-assisted ignition under cold start-up conditions using the experimental data produced in this work are suggested. The simulation needs to evaluate the effect of plasma power and plasma jet size identified here, which can greatly contribute in the design of future plasma systems, where the plasma power is minimized and the plasma jet size is maximised.
- The knowledge and know-how of plasma-assisted ignition and combustion for pulverized fuel obtained from this work should also be disseminated in other industrial firing applications to not only reduce the consumption of auxiliary fossil fuels but also to promote and facilitate the electrification of the power and industry sectors. Experiments are required to determine the system requirements and boundary conditions for other industrial firing technologies.

# References


[1] United Nation, Framework Convention on Climate Change: Paris Agreement, www.unfccc.int, (accessed on 05.02.2021) (2015).

[2] European Commission, Communication from the commission to the European parliament, the European Council, the Council, the European Economic and Social Committee and the Committee of the Regions, The European Green Deal, www.ec.europa.eu, (accessed on 16.11.2021) (2019).

[3] European Commission, 2030 Framework for Climate and Energy, www.ec.europa.eu, (accessed on 12.01.2021) (2020).

[4] IEA, Policies database, www.iea.org, (accessed on 05.02.2021), all rights reserved (2020).

[5] Statistisches Bundesamt, Gross electricity production in Germany, www.destatics.de, (accessed on 20.11.2022) (2022).

[6] VGB PowerTech e. V., Flexibility Toolbox, Compilation of Measures for the Flexible Operation of Coal-Fired Power Plants, March 2018.

[7] IEA Clean Coal Center, C. Henderson, Increasing the flexibility of coal-fired power plants, www.iea-coal.org, (accessed on 18.09.2020), all rights reserved (2014).

[8] IEA, Technology Roadmap: Delivering Sustainable Bioenergy, www.iea.org, (accessed on 10.05.2019), all rights reserved (2017).

[9] A. Purkus, E. Gawel, N. Szarka, M. Lauer, V. Lenz, A. Ortwein, P. Tafarte, M. Eichhorn, D. Thrän, Contributions of flexible power generation from biomass to a secure and cost-effective electricity supply–a review of potentials, incentives and obstacles in Germany, Energy, Sustainability and Society 8 (1) (2018) 18. doi:10.1186/s13705-018-0157-0.

[10] E. I. Karpenko, Y. E. Karpenko, V. E. Messerle, A. B. Ustimenko, Use of plasma fuel systems at thermal power plants in Russia, Kazakhstan, China, and Turkey, High Energy Chemistry 43 (3) (2009) 224–228. doi:10.1134/S0018143909030114.

[11] A. S. Askarova, E. I. Karpenko, V. E. Messerle, A. B. Ustimenko, Plasma enhancement of combustion of solid fuels, High Energy Chemistry 40 (2) (2006) 111–118. doi:10.1134/S0018143906020081.

[12] M. A. Gorokhovski, Z. Jankoski, F. C. Lockwood, E. I. Karpenko, V. Messerle, A. B. Ustimenko, Enhancement of Pulverised Coal Combustion by Plasma Technology, Combustion Science and Technology 179 (10) (2007) 2065–2090. doi:10.1080/00102200701386115.

[13] H.-C. Schröder, F. Guoqing, Plasma ignition system for the oil-free power plant Zetes in Turkey and its advantages for the changed circumstance of the energy market, VGB PowerTech 7 (2017) 77–81.

[14] G. Heimann, Erfolgreiche Installation und Inbetriebnahme einer Zünd- und Stützfeuerung mittels Trockenbraunkohlebrenner mit Plasmazündung, VGB PowerTech 7 (2016) 40–44.

[15] G. Heimann, Flexibilitätssteigerung von Braunkohlekraftwerken, VGB PowerTech 4 (2015) 47–51.

[16] U. Burchhardt, N. Jentsch, Forschungsverbundvorhaben Entwicklung eines Stützfeuerungssystems auf Basis von Trockenbraunkohle zur Erhöhung der Flexibilität bestehender Dampfkraftwerke, Lausitz Energie Kraftwerke AG (2017).

[17] R. Youssefi, J. Maier, S. Merli, G. Scheffknecht, Evaluation of the Ignition and Combustion Behavior of Solid Fuels with the Support of a Plasma Torch, in: 50. Kraftwerkstechnisches Kolloquium, Dresden, Germany, 2018.

[18] R. Youssefi, J. Maier, G. Scheffknecht, Experimental Investigations on Plasma Assisted Solid Fuel Ignition and Combustion, in: 12th European Conference on Industrial Furnaces and Boilers, Online, 2020.

[19] R. Youssefi, J. Maier, G. Scheffknecht, Experimental Investigations on Biomass Ignition with the Support of a Plasma Torch, in: 29. Deutsche Flammentag, Bochum, Germany, 2019.

[20] R. Youssefi, J. Maier, G. Scheffknecht, Experimental investigations on plasma-assisted wood pellet ignition for the start-up of biomass-fired power stations, Renewable and Sustainable Energy Reviews 138 (2021) 110522. doi:10.1016/j.rser.2020.110522.

[21] T. Segers, F. Norman, R. Youssefi, J. Maier, F. Verplaetsen, The Influence of Sieving on the Dust Explosion Characteristics of a Lignite Coal, Chemical Engineering Transactions 77 (2019) 475–480. doi:10.3303/CET1977080.

[22] R. Youssefi, J. Maier, G. Scheffknecht, Pilot-Scale Experiences on a Plasma Ignition System for Pulverized Fuels, Energies 14 (16) (2021) 4726. doi:10.3390/en14164726.

[23] R. Youssefi, T. Segers, F. Norman, J. Maier, G. Scheffknecht, Experimental Investigations of the Ignitability of Several Coal Dust Qualities, Energies 14 (19) (2021) 6323. doi:10.3390/en14196323.

[24] M. H. Baig, Determination of ignition and combustion boundaries in a pilot pul-verized fuel burner (Master thesis), University of Stuttgart, Institute of Combustion and Power Plant Technology (2018).

[25] P. Reich, Application of an electrical ignition system for cold start up using two types of lignite (Student research project), University of Stuttgart, Institute of Combustion and Power Plant Technology (2018).

[26] S. K. Nunna, Simulation of fluid flows for a fuel air nozzle using Ansys Fluent (Student research project), University of Stuttgart, Institute of Combustion and Power Plant Technology (2019).

[27] P. A. Kasmirski de Moura, Investigations on the Influence of particle size of wood pellets on plasma-assisted ignition (Master thesis), University of Stuttgart, Institute of Combustion and Power Plant Technology (2020).

[28] H. Spliethoff, Power generation from solid fuels, Springer, Heidelberg, 2010.

[29] J. Zelkowski, Kohlecharakterisierung und Kohleverbrennung: Kohle als Brennstoff, Physik und Theorie der Kohleverbrennung, Technik, VGB PowerTech Service GmbH, Essen, 2004.

[30] P. R. Solomon, M. B. Colket, Coal devolatilization, Symposium (International) on Combustion 17 (1) (1979) 131–143. doi:10.1016/S0082-0784(79)80016-8.

[31] D. B. Anthony, J. B. Howard, Coal devolatilization and hydrogasification, AIChE Journal 22 (4) (1976) 625–656. doi:10.1002/aic.690220403.

[32] H.-Y. Cai, A. J. Güell, I. N. Chatzakis, J.-Y. Lim, D. R. Dugwell, R. Kandiyoti, Combustion reactivity and morphological change in coal chars: Effect of pyrolysis temperature, heating rate and pressure, Fuel 75 (1) (1996) 15–24. doi:10.1016/0016-2361(94)00192-8.

[33] H. Kobayashi, J. B. Howard, A. F. Sarofim, Coal devolatilization at high temperatures, Symposium (International) on Combustion 16 (1) (1977) 411–425. doi:10.1016/S0082-0784(77)80341-X.

[34] P. R. Solomon, D. G. Hamblen, R. M. Carangelo, M. A. Serio, G. V. Deshpande, General model of coal devolatilization, Energy & Fuels 2 (4) (1988) 405–422. doi:10.1021/ef00010a006.

[35] J. B. Howard, R. H. Essenhigh, Pyrolysis of Coal Particles in Pulverized Fuel Flames, Industrial & Engineering Chemistry Process Design and Development 6 (1) (1967) 74–84. doi:10.1021/i260021a013.

[36] D. B. Anthony, J. B. Howard, H. C. Hottel, H. P. Meissner, Rapid devolatilization of pulverized coal, Symposium (International) on Combustion 15 (1) (1975) 1303–1317. doi:10.1016/S0082-0784(75)80392-4.

[37] H. Rezaei, S. Sokhansanj, X. Bi, C. J. Lim, A. Lau, A numerical and experimental study on fast pyrolysis of single woody biomass particles, Applied Energy 198 (2017) 320–331. doi:10.1016/j.apenergy.2016.11.032.

[38] H. Lu, E. Ip, J. Scott, P. Foster, M. Vickers, L. L. Baxter, Effects of particle shape

and size on devolatilization of biomass particle, Fuel 89 (5) (2010) 1156–1168. doi:10.1016/j.fuel.2008.10.023.

[39] R. Dolezal, Dampferzeugung, Verbrennung, Feuerung, Dampferzeuger, Springer-Verlag, 1990.

[40] H. H. Katalambula, K. Kitano, K. Ikeda, T. Chiba, Mechanism of ignition of single coal particle: Effect of heating rate on particle size dependence of ignition temperature: Effect of heating rate on particle-size dependence of ignition temperature, J. Chem. Eng. Japan 29 (3) (1996) 523–530. doi:10.1252/jcej.29.523.

[41] R. Khatami, C. Stivers, Y. A. Levendis, Ignition characteristics of single coal particles from three different ranks in O2/N2 and O2/CO2 atmospheres, Combustion and Flame 159 (12) (2012) 3554–3568. doi:10.1016/j.combustflame.2012.06.019.

[42] J. B. Howard, R. H. Essenhigh, Mechanism of solid-partical combustion with simultaneous gas-phase volatiles combustion, Symposium (International) on Combustion 11 (1) (1967) 399–408. doi:10.1016/S0082-0784(67)80164-4.

[43] H. Jüntgen, K. H. van Heek, An update of german non-isothermal coal pyrolysis work, Fuel Processing Technology 2 (4) (1979) 261–293. doi:10.1016/0378-3820(79)90018-3.

[44] R. H. Essenhigh, M. K. Misra, D. W. Shaw, Ignition of coal particles: A review, Combustion and Flame 77 (1) (1989) 3–30. doi:10.1016/0010-2180(89)90101-6.

[45] K. Strauß, Kraftwerkstechnik: Zur Nutzung fossiler, nuklearer und regenerativer Energiequellen, VDI-Buch, Springer, Berlin, Heidelberg, 2009.

[46] D. W. Pershing, J. Wendt, Pulverized coal combustion: The influence of flame temperature and coal composition on thermal and fuel NOx, Symposium (International) on Combustion 16 (1) (1977) 389–399. doi:10.1016/S0082-0784(77)80339-1.

[47] J. H. Pohl, A. F. Sarofim, Devolatilization and oxidation of coal nitrogen, Symposium (International) on Combustion 16 (1) (1977) 491–501. doi:10.1016/S0082-0784(77)80346-9.

[48] J. O. L. Wendt, Mechanisms Governing the Formation and Destruction of NOx and

Other Nitrogenous Species in Low NOx Coal Combustion Systems, Combustion Science and Technology 108 (4-6) (1995) 323–344. doi:10.1080/00102209508960405.

[49] C. P. Fenimore, Formation of nitric oxide in premixed hydrocarbon flames, Symposium (International) on Combustion 13 (1) (1971) 373–380. doi:10.1016/S0082-0784(71)80040-1.

[50] T. Abbasi, S. A. Abbasi, Dust explosions-cases, causes, consequences, and control, Journal of hazardous materials 140 (1-2) (2007) 7–44. doi:10.1016/j.jhazmat.2006.11.007.

[51] J. Cheng, X. Wang, T. Si, F. Zhou, J. Zhou, K. Cen, Ignition temperature and activation energy of power coal blends predicted with back-propagation neural network models, Fuel 173 (2016) 230–238. doi:10.1016/j.fuel.2016.01.043.

[52] M. J. Ajrash, J. Zanganeh, B. Moghtaderi, The effects of coal dust concentrations and particle sizes on the minimum auto-ignition temperature of a coal dust cloud, Fire and Materials 41 (7) (2017) 908–915. doi:10.1002/fam.2437.

[53] D. O. Glushkov, G. V. Kuznetsov, D. A. Chebochakova, O. E. Lyakhovskaya, N. E. Shlegel, I. S. Anufriev, E. Yu. Shadrin, Experimental study of coal dust ignition characteristics at oil-free start-up of coal-fired boilers, Applied Thermal Engineering 142 (2018) 371–379. doi:10.1016/j.applthermaleng.2018.07.010.

[54] W. Cao, L. Huang, J. Zhang, S. Xu, S. Qiu, F. Pan, Research on Characteristic Parameters of Coal-dust Explosion, Procedia Engineering 45 (2012) 442–447. doi:10.1016/j.proeng.2012.08.183.

[55] H. Yu, C. Wang, L. Pang, Y. Cui, D. Chen, Inhibiting effect of coal fly ash on minimum ignition temperature of coal dust clouds, Journal of Loss Prevention in the Process Industries 61 (2019) 24–29. doi:10.1016/j.jlp.2019.05.018.

[56] N. Fernandez-Anez, D. J. Slatter, M. A. Saeed, H. N. Phylaktou, G. E. Andrews, J. Garcia-Torrent, Ignition sensitivity of solid fuel mixtures, Fuel 223 (2018) 451–461. doi:10.1016/j.fuel.2018.02.106.

[57] D. Wu, F. Norman, F. Verplaetsen, E. van den Bulck, Experimental study on the minimum ignition temperature of coal dust clouds in oxy-fuel combustion atmospheres,

Journal of hazardous materials 307 (2016) 274–280. doi:10.1016/j.jhazmat.2015.12.051.

[58] L. Tognotti, A. Malotti, L. Petarca, S. Zanelli, Measurement of Ignition Temperature of Coal Particles Using a Thermogravimetric Technique, Combustion Science and Technology 44 (1-2) (2007) 15–28. doi:10.1080/00102208508960290.

[59] W. Moroń, W. Rybak, Ignition behaviour and flame stability of different ranks coals in oxy fuel atmosphere, Fuel 161 (2015) 174–181. doi:10.1016/j.fuel.2015.08.065.

[60] R. Siwek, C. Cesana, Ignition behavior of dusts: Meaning and interpretation, Process Safety Progress 14 (2) (1995) 107–119. doi:10.1002/prs.680140205.

[61] J. Yuan, W. Wei, W. Huang, B. Du, L. Liu, J. Zhu, Experimental investigations on the roles of moisture in coal dust explosion, Journal of the Taiwan Institute of Chemical Engineers 45 (5) (2014) 2325–2333. doi:10.1016/j.jtice.2014.05.022.

[62] K. L. Cashdollar, Coal dust explosibility, Journal of Loss Prevention in the Process Industries 9 (1) (1996) 65–76. doi:10.1016/0950-4230(95)00050-X.

[63] K. L. Cashdollar, Overview of dust explosibility characteristics, Journal of Loss Prevention in the Process Industries 13 (3-5) (2000) 183–199. doi:10.1016/S0950-4230(99)00039-X.

[64] C. Huéscar Medina, B. MacCoitir, H. Sattar, D. J. Slatter, H. N. Phylaktou, G. E. Andrews, B. M. Gibbs, Comparison of the explosion characteristics and flame speeds of pulverised coals and biomass in the ISO standard 1m3 dust explosion equipment, Fuel 151 (2015) 91–101. doi:10.1016/j.fuel.2015.01.009.

[65] M. Mittal, Study of explosibility data of coal dust for designing explosion safety measures, Int J Adv Engg Tech 4 (3) (2013) 82–91.

[66] R. K. Eckhoff, Influence of dispersibility and coagulation on the dust explosion risk presented by powders consisting of nm-particles, Powder Technology 239 (2013) 223–230. doi:10.1016/j.powtec.2013.02.007.

[67] M. Traoré, O. Dufaud, L. Perrin, S. Chazelet, D. Thomas, Dust explosions: How should

the influence of humidity be taken into account?, Process Safety and Environmental Protection 87 (1) (2009) 14–20. doi:10.1016/j.psep.2008.08.001.

[68] B. Du, W. Huang, N. Kuai, J. Yuan, Z. Li, Y. Gan, Experimental Investigation on Inerting Mechanism of Dust Explosion, Procedia Engineering 43 (2012) 338–342. doi:10.1016/j.proeng.2012.08.058.

[69] P. R. Amyotte, Solid inertants and their use in dust explosion prevention and mitigation, Journal of Loss Prevention in the Process Industries 19 (2-3) (2006) 161–173. doi:10.1016/j.jlp.2005.05.008.

[70] A. G. Dastidar, P. R. Amyotte, M. J. Pegg, Factors influencing the suppression of coal dust explosions, Fuel 76 (7) (1997) 663–670. doi:10.1016/S0016-2361(97)00039-2.

[71] J. G. Torrent, I. S. Armada, R. A. Pedreira, A correlation between composition and explosibility index for coal dust, Fuel 67 (12) (1988) 1629–1632. doi:10.1016/0016-2361(88)90206-2.

[72] J. García-Torrent, J. Cantalapiedra-Fuchs, J. Montes-Villalón, R. Alcántara-Pedreira, Improvement in the correlation between the composition index and the explosibility index for coal dust, Fuel 70 (9) (1991) 1099–1101. doi:10.1016/0016-2361(91)90266-D.

[73] A. Ramírez, J. García-Torrent, A. Tascón, Experimental determination of self-heating and self-ignition risks associated with the dusts of agricultural materials commonly stored in silos, Journal of hazardous materials 175 (1-3) (2010) 920–927. doi:10.1016/j.jhazmat.2009.10.096.

[74] J. Garcia-Torrent, N. Fernandez-Anez, L. Medic-Pejic, A. Blandon-Montes, J. M. Molina-Escobar, Ignition and explosion parameters of Colombian coals, Journal of Loss Prevention in the Process Industries 43 (2016) 706–713. doi:10.1016/j.jlp.2016.06.007.

[75] J. García Torrent, Á. Ramírez-Gómez, N. Fernandez-Anez, L. Medic Pejic, A. Tascón, Influence of the composition of solid biomass in the flammability and susceptibility to spontaneous combustion, Fuel 184 (2016) 503–511. doi:10.1016/j.fuel.2016.07.045.

[76] F. F. Ling, P. Basu, C. Kefa, L. Jestin, Boilers and Burners, Springer New York, New York, NY, 2000.

[77] A. K. Gupta, D. G. Lilley, N. Syred, Swirl Flows, Abacus Press, 1984.

[78] D. G. Lilley, Swirl Flows in Combustion: A Review, AIAA Journal 15 (8) (1977) 1063–1078. doi:10.2514/3.60756.

[79] J. M. Beér, N. A. Chigier, Combustion Aerodynamics, Fuel and energy science series, Applied Science Publ, London, 1972.

[80] S. R. Turns, An introduction to combustion: Concepts and applications, 3rd Edition, McGraw-Hill, Boston, 2011.

[81] L. Vanquickenborne, A. van Tiggelen, The stabilization mechanism of lifted diffusion flames, Combustion and Flame 10 (1) (1966) 59–69. doi:10.1016/0010-2180(66)90028-9.

[82] J. E. Broadwell, W. J. Dahm, M. G. Mungal, Blowout of turbulent diffusion flames, Symposium (International) on Combustion 20 (1) (1985) 303–310. doi:10.1016/S0082-0784(85)80515-4.

[83] J. P. Smart, K. J. Knill, B. M. Visser, R. Weber, Reduction of NOx emissions in a swirled coal flame by particle injection into the internal recirculation zone, Symposium (International) on Combustion 22 (1) (1989) 1117–1125. doi:10.1016/S0082-0784(89)80122-5.

[84] J. P. Smart, D. J. Morgan, Exploring the Effects of Employing Different Scaling Criteria on Swirl Stabilised Pulverised Coal Burner Performance, Combustion Science and Technology 100 (1-6) (1994) 331–343. doi:10.1080/00102209408935459.

[85] T. Abbas, P. Costen, M. A. Hassan, F. C. Lockwood, The Effect of the Near Burner Aerodynamics on Pollution, Stability and Combustion in a PF-Fired Furnace, Combustion Science and Technology 93 (1) (1993) 73–90. doi:10.1080/00102209308935283.

[86] A. Leisse, D. Lasthaus, New Experiences Gained from Operating DS (Swirl Stage) Burners, VGB PowerTech (11) (2008) 43–49.

[87] Y. Sung, G. Choi, Effectiveness between swirl intensity and air staging on NOx emissions and burnout characteristics in a pulverized coal fired furnace, Fuel Processing Technology 139 (2015) 15–24. doi:10.1016/j.fuproc.2015.07.026.

[88] M. Gu, M. Zhang, W. Fan, L. Wang, F. Tian, The effect of the mixing characters of primary and secondary air on NO formation in a swirling pulverized coal flame, Fuel 84 (16) (2005) 2093–2101. doi:10.1016/j.fuel.2005.04.019.

[89] C. Katzer, F. Schierack, S. Tappe, J. Krautz, Ergebnisse der Untersuchung zur Betriebsstabilität und des Emissionsverhaltens der TBK-Feuerung im Labor und an einem Großdampferzeuger, in: 49. Kraftwerkstechnisches Kolloquium, Dresden, Germany, 2017.

[90] S. Godoy, K. Hirji, R. C. Lockwood, J. Miller, Stability Limits of Pulverised Coal Burners, Combustion Science and Technology 44 (5-6) (1986) 319–335. doi:10.1080/00102208608960311.

[91] K. Hein, W. Leuckel, Further studies on the effect of swirl on pulverised coal flames, Trials C-14: Document Nr. F 32/a/40, International Flame Reserach Foundation, IJmuiden, Netherlands (1969).

[92] F. C. Lockwood, T. Mahmud, Short Communication, Combustion Science and Technology 66 (4-6) (1989) 319–328. doi:10.1080/00102208908947156.

[93] R. Jeschke, B. Henning, W. Schreier, Flexibility through highly-efficient technology, VGB PowerTech 5 (2012) 64–68.

[94] G. Bonizzoni, E. Vassallo, Plasma physics and technology; industrial applications, Vacuum 64 (3-4) (2002) 327–336. doi:10.1016/S0042-207X(01)00341-4.

[95] F. Fabry, C. Rehmet, V. Rohani, L. Fulcheri, Waste Gasification by Thermal Plasma: A Review, Waste and Biomass Valorization 4 (3) (2013) 421–439. doi:10.1007/s12649-013-9201-7.

[96] Y. Ju, W. Sun, Plasma assisted combustion: Dynamics and chemistry, Progress in Energy and Combustion Science 48 (2015) 21–83. doi:10.1016/j.pecs.2014.12.002.

[97] Y. Ju, W. Sun, Plasma assisted combustion: Progress, challenges, and opportunities,

Combustion and Flame 162 (3) (2015) 529–532. doi:10.1016/j.combustflame.2015.01.017.

[98] G. T. Kim, B. H. Seo, W. J. Lee, J. Park, M. K. Kim, S. M. Lee, Effects of applying non-thermal plasma on combustion stability and emissions of NOx and CO in a model gas turbine combustor, Fuel 194 (2017) 321–328. doi:10.1016/j.fuel.2017.01.033.

[99] D. A. Lacoste, J. P. Moeck, D. Durox, C. O. Laux, T. Schuller, Effect of Nanosecond Repetitively Pulsed Discharges on the Dynamics of a Swirl-Stabilized Lean Premixed Flame, Journal of Engineering for Gas Turbines and Power 135 (10) (2013). doi:10.1115/1.4024961.

[100] D. H. Lee, K.-T. Kim, H. S. Kang, Y.-H. Song, J. E. Park, Plasma-assisted combustion technology for NOx reduction in industrial burners, Environmental science & technology 47 (19) (2013) 10964–10970. doi:10.1021/es401513t.

[101] A. Starikovskiy, N. Aleksandrov, Plasma-assisted ignition and combustion, Progress in Energy and Combustion Science 39 (1) (2013) 61–110. doi:10.1016/j.pecs.2012.05.003.

[102] M. I. Boulos, P. L. Fauchais, E. Pfender, Handbook of Thermal Plasmas, Springer International Publishing, 2017.

[103] F. Zhao, S. Li, Y. Ren, Q. Yao, Y. Yuan, Investigation of mechanisms in plasma-assisted ignition of dispersed coal particle streams, Fuel 186 (2016) 518–524. doi:10.1016/j.fuel.2016.08.078.

[104] R. A. Kalinenko, A. P. Kuznetsov, A. A. Levitsky, V. E. Messerle, Y. A. Mirokhin, L. S. Polak, Z. B. Sakipov, A. B. Ustimenko, Pulverized coal plasma gasification, Plasma Chemistry and Plasma Processing 13 (1) (1993) 141–167. doi:10.1007/BF01447176.

[105] I. B. Matveev, V. E. Messerle, A. B. Ustimenko, Plasma Gasification of Coal in Different Oxidants, IEEE Transactions on Plasma Science 36 (6) (2008) 2947–2954. doi:10.1109/TPS.2008.2007643.

[106] V. E. Messerle, A. B. Ustimenko, O. A. Lavrichshev, Comparative study of coal plasma gasification: Simulation and experiment, Fuel 164 (2016) 172–179. doi:10.1016/j.fuel.2015.09.095.

[107] Y. Pang, L. Bahr, P. Fendt, L. Zigan, S. Will, T. Hammer, M. Baldauf, R. Fleck, D. Müller, J. Karl, Plasma-Assisted Biomass Gasification with Focus on Carbon Conversion and Reaction Kinetics Compared to Thermal Gasification, Energies 11 (5) (2018) 1302. doi:10.3390/en11051302.

[108] P. Kanilo, V. Kazantsev, N. Rasyuk, K. Schünemann, D. Vavriv, Microwave plasma combustion of coal, Fuel 82 (2) (2003) 187–193. doi:10.1016/S0016-2361(02)00201-6.

[109] M. Sugimoto, K. Maruta, K. Takeda, O. P. Solonenko, M. Sakashita, M. Nakamura, Stabilization of pulverized coal combustion by plasma assist, Thin Solid Films 407 (1-2) (2002) 186–191. doi:10.1016/S0040-6090(02)00035-4.

[110] M. Gorokhovski, E. I. Karpenko, F. C. Lockwood, V. E. Messerle, B. G. Trusov, A. B. Ustimenko, Plasma technologies for solid fuels: experiment and theory, Journal of the Energy Institute 78 (4) (2005) 157–171. doi:10.1179/174602205X68261.

[111] V. E. Messerle, A. B. Ustimenko, A. S. Askarova, A. O. Nagibin, Pulverized coal torch combustion in a furnace with plasma-coal system, Thermophysics and Aeromechanics 17 (3) (2010) 435–444. doi:10.1134/S0869864310030145.

[112] V. E. Messerle, E. I. Karpenko, A. B. Ustimenko, O. A. Lavrichshev, Plasma preparation of coal to combustion in power boilers, Fuel Processing Technology 107 (2013) 93–98. doi:10.1016/j.fuproc.2012.07.001.

[113] S. Bian, J. w. Wang, Z. y. Qian, The Combustion Situation of Pulverized Coal in Plasma Ignition Burner, in: Asia-Pacific Power and Energy Engineering Conference (APPEEC 2010), Chengdu, China, 2010. doi:10.1109/APPEEC.2010.5448819.

[114] Q. Chen, M. Liu, W. Xia, Study on Coal Plasma Ignition and Combustion in a Primary Combustor: 2009 Asia-Pacific Power and Energy Engineering Conference, in: Asia-Pacific Power and Energy Engineering Conference (APPEEC 2009), Wuhan, China, 2009. doi:10.1109/APPEEC.2009.4918809.

[115] S. Belosevic, M. Sijercic, P. Stefanovic, A numerical study of pulverized coal ignition by means of plasma torches in air–coal dust mixture ducts of utility boiler furnaces, International Journal of Heat and Mass Transfer 51 (7-8) (2008) 1970–1978. doi:10.1016/j.ijheatmasstransfer.2007.06.003.

[116] C. Katzer, M. Klatt, A. Lisk, H. J. Krautz, Experimentelle Untersuchung zur Entwicklung eines elektrisch zündenden Kohlestaubbrenners, in: 48. Kraftwerktechnisches Kolloquium, Dresden, Germany, 2016.

[117] C. Katzer, Bedarf an Verbrennungsforschung für Braunkohlekraftwerke-Am Beispiel des LS kraftwerkstechnik der BTU Cottbus-Senftenberg, VGB PowerTech 8 (2018) 58–64.

[118] H. Krautz, C. Katzer, M. Klatt, Forschungsverbundvorhaben Entwicklung eines Stützfeuerungssystems auf Basis von Trockenbraunkohle zur Erhöhung der Flexibilität bestehender Dampfkraftwerke., Brandenburgische Technische Universität Cottbus - Senftberg, Fakultät 3 - Lehrstuhl Kraftwerkstechnik (2017).

[119] A. P. Burdukov, E. B. Butakov, G. V. Chernova, Experimental studies of ignition of a 5 MW semi-industrial installation in Ekibastuz coal using electrochemical activation technology, Journal of Physics: Conference Series 1261 (2019) 012006. doi:10.1088/1742-6596/1261/1/012006.

[120] Agora Energiewende, Flexibility in thermal power plants-with a focus on existing coal-fired power plants, www.agora-energiewende.de, (accessed on 24.07.2019) (2017).

[121] J. B. Kitto, S. C. Stultz, Steam, its generation and use, 41st Edition, Babcock & Wilcox, Barberton, Ohio, 2005.

[122] Mitsubishi Hitachi Power Systems Europe GmbH, Schlussbericht FlexIgnite: Erhöhung der Flexibilität durch elektrische Zündung von Kraftwerksbrennern (FlexIgnite), Teilthema: Auslegung, Optimierung und Untersuchung elektrischer Zündsysteme zur Zündung fester Brennstoffe (2020).

[123] F. Kluger, D. Ristic, R. Daniel, Plasma Supported Combustion for an Extension of Coal fired Power Station Flexible Operation Capability, in: 50. Kraftwerkstechnisches Kolloquium, Dresden, 2018.

[124] V. E. Messerle, A. B. Ustimenko, and O. A. Lavrichshev, Plasma-assisted ignition and combustion of pulverized coal at thermal power plants of Kazakhstan, in: International Conference on Power Systems, Energy, Environment, 2014.

[125] T. Mączka, H. Pawlak-Kruczek, L. Niedzwiecki, E. Ziaja, A. Chorążyczewski, Plasma

Assisted Combustion as a Cost-Effective Way for Balancing of Intermittent Sources: Techno-Economic Assessment for 200 MWel Power Unit, Energies 13 (19) (2020) 50–56. doi:10.3390/en13195056.

[126] V. E. Messerle, A. B. Ustimenko, Y. E. Karpenko, M. Y. Chernetskiy, A. A. Dekterev, S. A. Filimonov, Modeling and full-scale tests of vortex plasma-fuel systems for igniting high-ash power plant coal, Thermal Engineering 62 (6) (2015) 442–451. doi:10.1134/S0040601515060063.

[127] E. I. Karpenko, Y. E. Karpenko, V. E. Messerle, A. B. Ustimenko, Using plasma-fuel systems at Eurasian coal-fired thermal power stations, Thermal Engineering 56 (6) (2009) 456–461. doi:10.1134/S0040601509060020.

[128] E. I. Karpenko, V. E. Messerle, A. B. Ustimenko, Plasma-aided solid fuel combustion, Proceedings of the Combustion Institute 31 (2) (2007) 3353–3360. doi:10.1016/j.proci.2006.07.038.

[129] V. E. Messerle, E. I. Karpenko, A. B. Ustimenko, Plasma assisted power coal combustion in the furnace of utility boiler: Numerical modeling and full-scale test, Fuel 126 (2014) 294–300. doi:10.1016/j.fuel.2014.02.047.

[130] V. E. Messerle, A. B. Ustimenko, Plasma-Aided Coal Ignition and Combustion: Modeling and Full-Scale Trials, IEEE Transactions on Plasma Science 42 (12) (2014) 3716–3721. doi:10.1109/TPS.2014.2345871.

[131] V. S. Peregudov, The thermal engineering characteristics of plasma-assisted ignition of coal, Thermal Engineering 57 (6) (2010) 476–481. doi:10.1134/S0040601510060030.

[132] H. Brüggemann, F. Kluger, G. Schmidt, Innovative Konzepte zur Flexibilisierung des Kraftwekseinsatzes, VGB PowerTech 4 (2017) 52–56.

[133] C.-S. Wong, R. Mongkolnavin, Elements of plasma technology, SpringerBriefs in applied sciences and technology, 2191-530X, Springer, Singapore, 2016.

[134] V. Rohani, S. Takali, G. Gérard, F. Fabry, F. Cauneau, L. Fulcheri, A New Plasma Electro-Burner Concept for Biomass and Waste Combustion, Waste and Biomass Valorization 8 (2017) 2791–2805. doi:10.1007/s12649-017-9829-9.

[135] H. S. Uhm, Y. C. Hong, D. H. Shin, A microwave plasma torch and its applications, Plasma Sources Science and Technology 15 (2) (2006) 26–34. doi:10.1088/0963-0252/15/2/S04.

[136] L. Fulcheri, F. Fabry, S. Takali, V. Rohani, Three-Phase AC Arc Plasma Systems: A Review, Plasma Chemistry and Plasma Processing 35 (4) (2015) 565–585. doi:10.1007/s11090-015-9619-8.

[137] S. Takali, F. Fabry, V. Rohani, F. Cauneau, L. Fulcheri, Development of a 100 kW plasma torch for plasma assisted combustion of low heating value fuels, Journal of Physics: Conference Series 550 (1) (2014) 012018. doi:10.1088/1742-6596/550/1/012018.

[138] J. Kopecki, D. Kiesler, M. Leins, A. Schulz, M. Walker, M. Kaiser, H. Muegge, U. Stroth, Investigations of a high volume atmospheric plasma torch at 915MHz, Surface and Coatings Technology 205 (2011) S342–S346. doi:10.1016/j.surfcoat.2011.04.031.

[139] B. Greiner, M. Kaiser, R. Böcher, Mikrowellen-Plasma-Zündsystem im Leistungsbereich 1 kW bis 3 kW zum Betrieb an Staubverbrennungssystemen für unterschiedliche Brennstoffarten, in: 49. Kraftwerkstechnisches Kolloquium, Dresden, Germany, 2017.

[140] International Organization for Standardization, ISO 17225-2:2020 - Solid biofuels - Fuel specifications and classes - Part 2: Graded wood pellets (2020).

[141] DIN Deutsches Institut für Normung e. V., DIN 51718:2002-06 - Testing of solid fuels - Determination of the water content and the analysis moisture (2002).

[142] DIN Deutsches Institut für Normung e. V., DIN 51720:2001-03 - Testing of solid fuels - Determination of the content of volatile components (2001).

[143] DIN Deutsches Institut für Normung e. V., DIN 51719:1997-07 - Testing of solid fuels - Determination of the ash content (1997).

[144] DIN Deutsches Institut für Normung e. V., DIN 51734:2008-12 - Testing of solid fuels - Immediate analysis and calculation of the fixed carbon (2008).

[145] DIN Deutsches Institut für Normung e. V., DIN 51732:2014-07 - Testing of solid fuels

- Determination of the total content of carbon, hydrogen and nitrogen - Instrumental methodsInstrumentelle Methoden (2014).

[146] DIN Deutsches Institut für Normung e. V., DIN 51724-1:2019-10 - Testing of solid fuels - Determination of the sulfur content - Part 1: Total sulfur (2019).

[147] DIN Deutsches Institut für Normung e. V., DIN 51900-1:2000-04 - Testing of solid and liquid fuels - Determination of the calorific value with the bomb calorimeter and calculation of the calorific value - Part 1: General information, basic devices, basic methods (2000).

[148] International Organization for Standardization, ISO 18134-3:2015 - Solid biofuels - Determination of moisture content - Part 3: Moisture in general analysis sample (2015).

[149] International Organization for Standardization, ISO 18123:2015 - Solid biofuels - Determination of the content of volatile matter (2015).

[150] International Organization for Standardization, ISO 18122:2015 - Solid biofuels - Determination of ash content (2015).

[151] International Organization for Standardization, ISO 16948:2015 - Solid biofuels - Determination of total content of carbon, hydrogen and nitrogen (2015).

[152] International Organization for Standardization, ISO 16994:2016 - Solid biofuels - Determination of total content of sulfur and chlorine (2016).

[153] International Organization for Standardization, ISO 18125:2017 - Solid biofuels - Determination of calorific value (2017).

[154] Malvern Instruments Ltd., Mastersizer 3000 User Manual (Issue 1.0) (October 2011).

[155] International Organization for Standardization, ISO 13320:2020 - Particle size analysis - Laser diffraction methods.

[156] DIN Deutsches Institut für Normung e. V., DIN ISO 9277 - Determination of the specific surface area of solids by gas adsorption - BET method (ISO 9277:2010) (2010).

[157] International Organization for Standardization, ISO 17827-2:2016 - Solid biofuels -

Determination of particle size distribution for uncompressed fuels - Part 2: Vibrating screen method using sieves with aperture of 3,15 mm and below (2016).

[158] DIN Deutsches Institut für Normung e. V., DIN EN ISO/IEC 80079-20-2:2016-12 - Explosive atmospheres - Part 20-2: Material characteristics – Combustible dusts test methods.

[159] VDI Verein Deutscher Ingenieure e.V., VDI 2263:2003-05 - Dust Fires and Dust Explosions Hazards - Assessment -Protective Measures - Part 1: Test Methods for the Determination of the Safety Characteristic of Dusts (May 1990).

[160] Kühner AG, Device Manual, Modified Hatmann Appartus - Dust Explosion Test.

[161] DIN Deutsches Institut für Normung e. V., DIN EN 13821:2002 - Determination of minimum ignition energy of dust/air mixtures.

[162] DIN Deutsches Institut für Normung e. V., DIN EN 14034-1:2011-04 -Determination of explosion characteristics of dust clouds - Part 1: Determination of the maximum explosion pressure pmax of dust clouds.

[163] DIN Deutsches Institut für Normung e. V., DIN EN 14034-2:2011-04 - Determination of explosion characteristics of dust clouds – Part 2: Determination of the maximum rate of explosion pressure rise (dp/dt)max of dust clouds.

[164] Endress+Hauser GmbH+Co. KG, Technical Information: Endress+Hauser Vortex Flow Measuring System: Proline Prowirl 72F, 72W, 73F, 73W, www.de.endress.com.

[165] A. Leisse, S. Rehfeldt, D. Meyer, Ignition behavior of pulverised solid fuel particles at hot surfaces, VGB PowerTech 11 (2014) 45–49.

[166] C. Schmid, J. Dugue, Movable Block Swirler Calibration, IFRF Doc. No. F 59/y/8, International Flame Reserach Foundation, IJmuiden, Netherlands (April 1990).

[167] T. J. Fudihara, L. Goldstein Jr., M. Mori, The three-dimensional numerical aerodynamics of a movable block burner, Brazilian Journal of Chemical Engineering 20 (4) (2003) 391–401. doi:10.1590/S0104-66322003000400006.

[168] A. Schulz, S. Merli, M. Walter, Schlussbericht FlexIgnite: Erhöhung der Flexibilität

durch elektrische Zündung von Kraftwerksbrennern (FlexIgnite), Teilprojekt: Detaillierte experimentelle Untersuchung von Plasmen zur Zündung fester Brennstoffe, Universität Stuttgart, Institut für Grenzflächenverfahrenstechnik und Plasmatechnologie (2019).

[169] S. Merli, R. Youssefi, J. Maier, B. Glocker, A. Schulz, M. Walker, Flexible plasma ignition in coal power plants for the energy transition, in: 19. Fachtagung für Plasmatechnologie, Cottbus, 17-19 June 2019.

[170] J. Ballester, T. García-Armingol, Diagnostic techniques for the monitoring and control of practical flames, Progress in Energy and Combustion Science 36 (4) (2010) 375–411. doi:10.1016/j.pecs.2009.11.005.

[171] Y. Yan, G. Lu, M. Colechin, Monitoring and characterisation of pulverised coal flames using digital imaging techniques, Fuel 81 (5) (2002) 647–655. doi:10.1016/S0016-2361(01)00161-2.

[172] G. Lu, Y. Yan, M. Colechin, A Digital Imaging Based Multifunctional Flame Monitoring System, IEEE Transactions on Instrumentation and Measurement 53 (4) (2004) 1152–1158. doi:10.1109/TIM.2004.830571.

[173] A. González-Cencerrado, A. Gil, B. Peña, Characterization of PF flames under different swirl conditions based on visualization systems, Fuel 113 (2013) 798–809. doi:10.1016/j.fuel.2013.05.077.

[174] C. Katzer, K. Babul, M. Klatt, H.-J. Krautz, Quantitative and qualitative relationship between swirl burner operatingconditions and pulverized coal flame length, Fuel Processing Technology 156 (2017) 138–155. doi:10.1016/j.fuproc.2016.10.013.

[175] R. Hernández, J. Ballester, Flame imaging as a diagnostic tool for industrial combustion, Combustion and Flame 155 (3) (2008) 509–528. doi:10.1016/j.combustflame.2008.06.010.

[176] A. González-Cencerrado, B. Peña, A. Gil, Coal flame characterization by means of digital image processing in a semi-industrial scale PF swirl burner, Applied Energy 94 (2012) 375–384. doi:10.1016/j.apenergy.2012.01.059.

[177] Ansys® Academic Research Mechanical, Release 2020 R2.

[178] Ansys® Academic Research Mechanical, Release 2020 R2, help System, Modeling Turbulence, Ansys, Inc.

[179] L. Zhengqi, S. Rui, C. Lizhe, W. Zhixin, W. Shaohua, Q. Yukun, Effect of primary air flow types on particle distributions in the near swirl burner region, Fuel 81 (6) (2002) 829–835. doi:10.1016/S0016-2361(01)00179-X.

[180] S. V. Apte, K. Mahesh, P. Moin, J. C. Oefelein, Large-eddy simulation of swirling particle-laden flows in a coaxial-jet combustor, International Journal of Multiphase Flow 29 (8) (2003) 1311–1331. doi:10.1016/S0301-9322(03)00104-6.

[181] S. Yu, J. Park, M. Kim, H. Kim, C. Ryu, Y. Lee, W. Yang, Y.-g. Jeong, Improving Energy Density and Grindability of Wood Pellets by Dry Torrefaction, Energy & Fuels 33 (9) (2019) 8632–8639. doi:10.1021/acs.energyfuels.9b01086.

[182] S. G. Sahu, N. Chakraborty, P. Sarkar, Coal–biomass co-combustion: An overview, Renewable and Sustainable Energy Reviews 39 (2014) 575–586. doi:10.1016/j.rser.2014.07.106.

[183] A. Tahmasebi, H. Zheng, J. Yu, The influences of moisture on particle ignition behavior of Chinese and Indonesian lignite coals in hot air flow, Fuel Processing Technology 153 (2016) 149–155. doi:10.1016/j.fuproc.2016.07.017.

[184] R. Kurose, H. Tsuji, H. Makino, Effects of moisture in coal on pulverized coal combustion characteristics, Fuel 80 (10) (2001) 1457–1465. doi:10.1016/S0016-2361(01)00019-9.

[185] H. Hu, Q. Zhou, S. Zhu, B. Meyer, S. Krzack, G. Chen, Product distribution and sulfur behavior in coal pyrolysis, Fuel Processing Technology 85 (8-10) (2004) 849–861. doi:10.1016/j.fuproc.2003.11.030.

[186] A. Fridman, Plasma Chemistry, Cambridge University Press, Cambridge, 2008.